UNIVERSITÀ DEGLI STUDI DI MILANO

DIPARTIMENTO DI CHIMICA

PhD COURSE IN CHEMISTRY, XXIX CYCLE

SYNTHESIS OF PEPTIDOMIMETIC LIGANDS TARGETING CELL-SURFACE RECEPTORS INVOLVED IN TUMOR ANGIOGENESIS

CHIM/06 Organic Chemistry

Simone ZANELLA
R10458

Tutor: Prof. Dr. Cesare GENNARI (Università degli Studi di Milano)
Co-Tutor: Prof. Dr. Umberto PIARULLI (Università degli Studi dell'Insubria)

Co-ordinator: Prof. Dr. Emanuela LICANDRO

A.Y. 2015/2016

The present work was led by:	Prof. C. Gennari, Prof. U. Piarulli	
Doctoral Final Oral Examination:	March, 17th 2017	
Examination Committee:	Chairperson:	Prof. Dr. L. Colombo Università degli Studi di Pavia (IT)
	Second Member:	Prof. Dr. P. Seneci Università degli Studi di Milano (IT)
	Third Member:	Prof. Dr. M. Resmini Queen Mary, University of London (UK)

The work herein described was performed at at Dipartimento di Chimica (Università degli Studi di Milano), in the period from January 2014 to December 2016 under the supervision of Prof. Cesare Gennari.

I sincerely acknowledge my supervisors, Prof. Gennari and Prof. Piarulli, for giving me the opportunity to work in a really interesting and multifaceted project, as well as for their tutoring activity and contribution to my experience as student.

I would like to thank all the scientists that collaborated and participated to this research work. In particular, I gratefully thank Dr. Luca Pignataro, Prof. Laura Belvisi (Università degli Studi di Milano); Dr. Daniela Arosio (CNR-ISTM); Dr. Mayra Paolillo (Università degli Studi di Pavia); Dr. Michele Caruso, Dr. Fabio Gasparri (Nerviano Medical Sciences s.r.l.); Dr. Laura Schembri, Dr. Franca Marino (Università degli Studi dell'Insubria); Dr. Marta De Zotti, Prof. Fernando Formaggio (Università degli Studi di Padova); Prof. Lorenzo Stella (Università degli Studi di Roma "Tor Vergata").

A particular mention is dedicated to all my friends with whom I shared my life in the laboratory.

I would like to dedicate the present work to my dear family, my parents Giancarlo and Giovanna, and my aunt Maria, who encouraged me in finding my way in the world of Chemistry, and to Sara, the special person that showed enough patience to support me not only as PhD student, but also as man.

TABLE OF CONTENTS

ABBREVIATIONS

Ac	Acetyl
Akt	Protein kinase B (PKB)
Aib	2-Aminoisobutyric acid
Api	4-Aminopiperidine-4-carboxylic acid
aq.	Aqueous solution
bFGF	Basic fibroblast growth factor
Bn	Benzyl
Boc	*tert*-Butyloxycarbonyl
Boc-ON	2-(Boc-oxyimino)-2-phenylacetonitrile
BSA	Bovine serum albumin
Bu	Butyl
Bz	Benzoyl
CAM	Cell adhesion molecule
Cas9	CRISPR associated-9
Cbz	Carboxybenzyl
CD	Circular dichroism
CRISPR	Clustered regularly interspaced short palindromic repeats
DBU	1,8-diazabicyclo[5.4.0]undec-7-ene
DCC	*N*,*N'*-dicyclohexylcarbodiimide
DHB	2,5-Dihydroxybenzoic acid
DIC	*N*,*N*'-Diisopropylcarbodiimide
DKP	2,5-Diketopiperazine
DMAP	4-Dimethylaminopyridine
DMF	*N*,*N*-Dimethylformamide
DMSO	Dimethyl sulfoxide
ECD	Extracellular domain
ECM	Extracellular matrix
EDC	1-Ethyl-3-(3-dimethylaminopropyl)carbodiimide
EDT	1,2-Ethanedithiol
EEDQ	*N*-Ethoxycarbonyl-2-ethoxy-1,2-dihydroquinoline
EGF	Epidermal growth factor
EGFR	Epidermal growth factor receptor
eq	Equivalents
ESI	Electrospray ionisation
Et	Ethyl
FAK	Focal adhesion kinase
FC	Flash chromatography
FDA	Food and Drug Administration
FGFR	Fibroblast growth factor receptor
Fmoc	9-Fluorenylmethoxycarbonyl
GIST	Gastrointestinal stromal tumor
HATU	O-(7-azabenzotriazol-1-yl)-tetramethyl-uronium hexafluorophosphate
HCC	Hepatocellular carcinoma
HCCA	α-Cyano-4-hydroxycinnamic acid
HMPA	Hexamethylphosphoramide
HOAt	1-Hydroxy-7-azabenzotriazole
HPLC	High performance liquid chromatography
HSPG	Heparan sulfate proteoglycans
HUVEC	Human umbilical vein endothelial cell
IC	Inhibitory capacity
IGF-I	Insulin-like growth factor 1
IL-8	Interleukin 8
*i*Pr	Isopropyl
J	Scalar coupling constants

KHMDS	Potassium bis(trimethylsilyl)amide
MALDI	Matrix-assisted laser desorption ionization
Me	Methyl
MIDAS	Metal ion-dependent adhesion site
MMP	Matrix metalloproteinase
MS	Mass spectroscopy
Mtr	4-Methoxy-2,3,6-trimethylbenzenesulphonyl
M.W.	Micro-waves
NMR	Nuclear Magnetic Resonance
NHS	*N*-Hydroxysuccinimide
PAB	4-Aminobenzyl
Pbf	2,2,4,6,7-pentamethyldihydrobenzofuran-5-sulfonyl
PBS	Phosphate-buffered saline
PDGFR	Platelet-derived growth factor receptor
PEG	Polyethylene glycol
Ph	Phenyl
PLGF	Placenta growth factor
ppm	Part per million
PTX	Paclitaxel
quant.	Quantitative
RCC	Renal cell carcinoma
R_f	Retention factor
r.t.	Room temperature
RTK	Receptor tyrosine kinase
SIN	Sinapinic acid
SMDC	Small molecule-drug conjugate
SPPS	Solid-phase peptide synthesis
SPS	Solid-phase synthesis
Src	Proto-oncogene tyrosine-protein kinase Src
*t*Bu	*tert*-Butyl
tert	Tertiary
TFA	Trifluoroacetic acid
THF	Tetrahydrofuran
TLC	Thin-layer chromatography
TMS	Tetramethylsilane
t_R	Retention time
VEGF	Vascular endothelial growth factor
VEGFR	Vascular endothelial growth factor receptor
δ	Chemical shift

Amino acid*	One-letter code	Three-letter code
Alanine	A	Ala
Arginine	R	Arg
Asparagine	N	Asn
Aspartic	D	Asp
Cysteine	C	Cys
Glutamine	Q	Gln
Glutamic acid	E	Glu
Glycine	G	Gly
Histidine	H	His
Isoleucine	I	Ile
Leucine	L	Leu
Lysine	K	Lys
Methionine	M	Met
Phenylalanine	F	Phe
Proline	P	Pro
Serine	S	Ser
Threonine	T	Thr
Tryptophan	W	Trp
Tyrosine	Y	Tyr
Valine	V	Val

* D-amino acids are described by D-Xaa in the three-letter code and with the small letter in the one-letter code.

GENERAL ASPECTS OF ANGIOGENESIS

I.1 BIOLOGICAL FEATURES OF ANGIOGENESIS

Angiogenesis is a complex biological phenomenon that results in the generation of new blood vessels starting from the pre-existing vasculature network. Since this event is related to both physiological and pathological processes, a variety of proteins are involved in angiogenesis regulation by different mechanisms in order to keep pro- and anti-angiogenic responses balanced.[1] In physiological conditions, the hierarchy of mature vasculature is structurally well-defined and organized to provide efficiently the oxygen and nutrients supply required to support cell growth and survival. On the other hand, a tumor-related angiogenic event is characterized by abnormal spread and diffusion of unarranged, undifferentiated vessels that are not capable of sustaining cancer cells progression and development.[2] Hence, the tumor mass requires a continual neovascularization, augmenting the recruitment of new vessels. In this framework, compounds able to interfere with tumor angiogenesis represent a powerful tool in chemotherapy, thus their individuation and investigation became more and more important.

In the last decade, the use of anti-angiogenic agents demonstrated to restrain cancer growth and diffusion by limiting the initiation of capillary network: tumor cells are not able to exploit the pre-existent vasculature for nutrients and oxygen supply, with a consistent delay in cancer progression and metastasis.[3] Moreover, the clearance of chemotherapeutics by tumor mass is prevented and the overall efficacy of the drug is improved. Disorder is the main feature of tumor vasculature, which is composed by a large number of vessel subtypes lacking in organization, structure and function. The first consequence is an ineffective vascularization of the tumor mass, leading to a decrease of oxygen pressure and pH: these metabolic stress conditions up-regulate specific antigens to maintain and support a pro-angiogenic state, stimulating a continuous formation of new blood vessels.[4] The transition from a quiescent to an aggressive state was named "angiogenic switch" by Hanahan and Folkman in 1996 and it results in a rapid tumor growth, progression and metastasis (FIGURE 1).[5] However, another feature contributes to tumor mass transition from a dormant to an aggressive state: oncogenic mutations.[3] Activated oncogenes are capable of increasing cell proliferation and survival by escaping cell death and apoptosis. This process is defined tumorigenesis and allows the development of large tumor masses that can

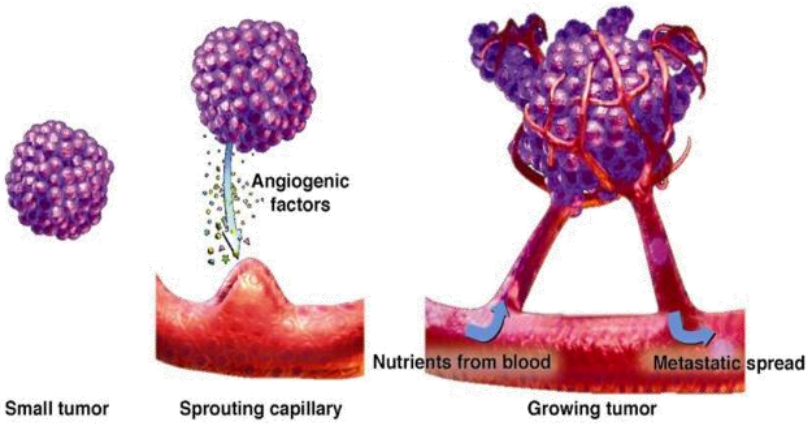

FIGURE 1. A small tumor mass is able to receive oxygen and nutrients supply by diffusion from the pre-existing vasculature. Once the angiogenic switch occurred, the up-regulation of specific angiogenic factors by cancer cells drives the formation of new blood vessels to feed more extensively the tumor, which starts expanding and shredding into metastasis.

eventually be lethal for the patient. Both tumorigenesis and angiogenesis are basic requirements for cancer progression: oncogenic transfection in tumor mass triggers angiogenic events by up-regulating vascular endothelial growth factors (VEGFs) expression; on the other hand, endothelial cell proliferation is necessary for sustaining neoplastic growth by supplying nutrients and oxygen. In conclusion, the anti-angiogenic strategy in cancer treatment relies on the ability of certain angiogenesis inhibitors to prevent and modulate new blood vessel formation, aiming at converting cancer into a chronic, steady disease.

I.2 ANGIOGENESIS INHIBITORS

The biological activity of anti-angiogenic agents relies on two main mechanisms of action: I) sequestration of certain soluble proteins; II) disruption or inhibition of protein-protein interactions. In the first case, the anti-angiogenic agent interacts selectively with a specific pro-angiogenic factor, provoking its aggregation or avoiding its interaction with the target receptor. This interference can result in a positive overall anti-cancer effect, characterized by tumor restriction, or in a negative response, with cancer cells consequently over-expressing the sequestered lacking protein. The inhibitors of a specific receptor can interact either with the extracellular or with the intracellular domains. Depending on the target cell membrane receptor, from small molecules to engineered proteins were developed and validated as anti-angiogenic agents.[3] A number of endogenous angiogenesis inhibitors are present in the blood flow and tissues environment: most of them belong to the collagen protein family. Tumstatin and endostatin are two well-known examples of collagen-related peptide fragments able to block and down-regulate the angiogenic process.[6] Apart from these natural inhibitors, a variety of synthetic agents have been prepared, some of which reached the market. Bevacizumab (Avastin®) was the first monoclonal antibody to be approved by the FDA for the treatment of colon cancer. It is a humanized anti-VEGF antibody that directly targets the VEGF-A protein: the binding of bevacizumab to VEGF-A prevents the latter from interacting with VEGF receptors (VEGFRs), thus impeding the spread of the angiogenesis signaling. Erlotinib (Tarceva®, **1** in FIGURE 2) is a small molecule drug able to inhibit the tyrosine kinase portion of epidermal growth factor receptor (EGFR), but also to block the expression of some angiogenic proteins, such as VEGF, basic fibroblast growth factor (bFGF) and transforming growth factor-α (TGF-α). Approved by the FDA, **1** is used in lung cancer treatment and the anti-tumor activity of bevacizumab is augmented when co-administered with erlotinib.[7] Caplostatin is a non-toxic HPMA (*N*-(2-hydroxypropyl)methacrylamide) copolymer decorated with the synthetic fumagillin analogue TNP-470 (**3**, FIGURE 2). The biological activity of caplostatin arises from fragment **3**, which was demonstrated to inhibit the endothelial proliferation *in vitro*. Upon conjugation to the HMPA moiety and the formation of caplostatin, the major neurotoxic side effects of **3** were suppressed, maintaining the wide anti-tumor activity shown by the parental compound fumagillin (**2**, FIGURE 2).[8]

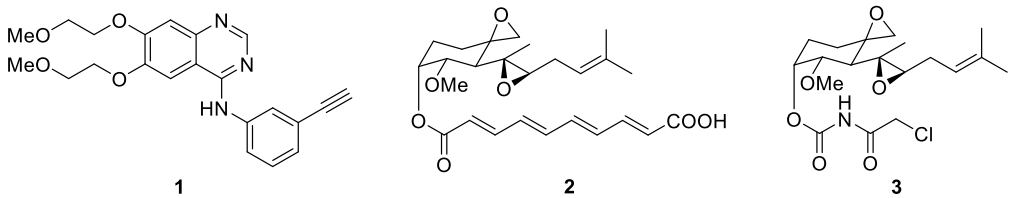

1 **2** **3**

FIGURE 2. Structures of erlotinib (**1**), fumagillin (**2**) and its derivative TNP-470 (**3**).

Clinical trials on anti-angiogenic agents validated the angiogenesis blockade as promising strategy to fight cancer progression and to understand better the biological mechanisms underlying the overall phenomena that cause the formation of new vasculature. The anti-tumor activity spectrum of the drugs reported in the literature can be expanded by co-administering different anti-angiogenic agents aiming at circumventing drug resistance, a common feature developed by aggressive cancer cells. However, against this kind of tumors angiogenesis inhibition can generate only a fleeting effect, because cancer

cells can adopt a variety of adaptive mechanisms to overcome the anti-angiogenic treatment.[9] Resistant tumors have two main weapons they can exploit when facing the therapy: I) activation and/or up-regulation of diverse angiogenic pathways; II) increase in pericyte composition of the new blood vessels. In the first case, when the activity of a certain protein is inhibited, tumor cells still have a number of other antigens on which they rely on to stimulate angiogenic processes. On the other hand, a higher pericyte density around the tumor microvasculature can protect the newly formed capillary network against anti-angiogenic therapy, thus becoming crucial for the correct establishment and maturation of the just sprouted vessels. A coherent solution may be found in impeding pericyte interaction with angiogenic proteins within the tumor environment.

Thanks to the continuous research advances, scientists are gathering more and more information about angiogenesis and the biological aspects driving tumors towards the angiogenic switch. Although the clinical application of anti-angiogenic agents decreased with respect to the initial usage, a number of these inhibitors have been developed and reported in the literature: likely, further improvements of this strategy will allow first to restrain effectively, then to cure cancer and other diseases related to angiogenesis.

PART I. TARGETING INTEGRINS

In the first part of my Thesis, I will describe the integrin receptor family.
After a brief biological introduction, the attention will be focused on the RGD recognition motif, giving a general overview of some of the integrin ligands reported in the literature and concluding with the specific class of peptidomimetics containing a 2,5-diketopiperazine (DKP) scaffold, developed in our research group.
Next, the *iso*DGR sequence will be discussed, with cyclopeptides and *cyclo*[DKP-*iso*DGR] compounds as examples of the limited number of integrin binders containing the *iso*DGR sequence described so far.
The last topic concerns the exploitation of RGD ligands in cancer therapy, where peptides and peptidomimetics targeting integrins are employed as carriers to deliver relevant payloads at the tumor site, taking advantage of integrin over-expression on the surface of cancer cells.

Part of the work described in this Chapter was published in the following article:

- Panzeri, S.; Zanella, S.; Arosio, D.; Vahdati, L.; Dal Corso, A.; Pignataro, L.; Paolillo, M.; Schinelli, S.; Belvisi, L.; Gennari, C.; Piarulli, U. *Chem. Eur. J.* **2015**, *21*, 6265.

1 INTEGRIN RECEPTORS AND LIGANDS

1.1 INTEGRIN RECEPTOR FAMILY

In the last twenty years, different cell adhesion molecules (CAMs) have been discovered and studied in order to elucidate their role in cell life and survival.[10] This wide class of molecules is composed by diverse protein families, which are responsible for physiological integrity, morphology and division of cells, but may also become involved in the pathological development of diseases and malfunctions. In particular, CAMs fulfill a central role in cell-to-cell and cell-extra-cellular matrix (ECM) relationships: many disorders can arise when the correct operation of these essential mechanisms fails, thus even leading to cancer, thrombosis, arthritis and diabetes.[11] Four protein classes compose the cell adhesion molecules: integrins, cadherins, selectins and immunoglobulins (FIGURE 3).

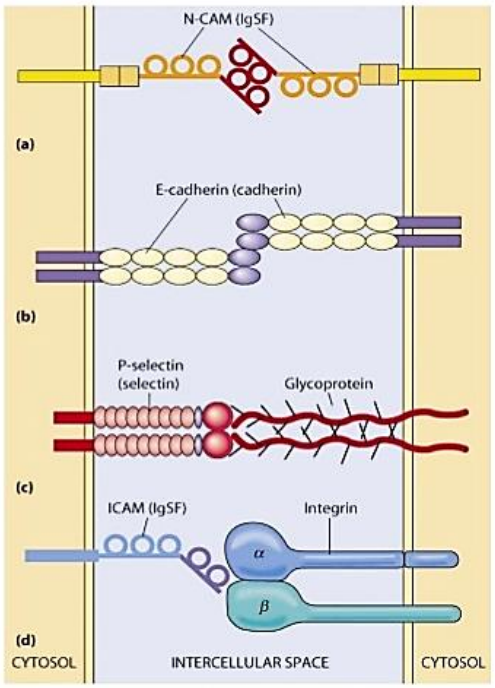

FIGURE 3. Cell Adhesion molecules families: immunoglobulins (a), cadherins (b), selectins (c), and integrins (d).

Integrins are a family of transmembrane glycoproteins, which consists of two subunits, namely α and β. 18 α-subunits and 10 β-subunits pair together in a non-covalent manner, forming 24 specific heterodimers (FIGURE 4 and FIGURE 5) that act in some essential events of the cell biology, *i.e.* cell proliferation, migration, survival, and intracellular signal transduction.[12] Particular growth factors, such as immunoglobulins and cytokines, are known to interact with integrin receptors and trigger signaling pathways by activating receptor tyrosine kinases (RTKs).[13] The interaction with extracellular ligands provokes first the formation of receptor clustering, then a conformational rearrangement in integrin subunits, resulting in the modulation of ligand affinity.[14]

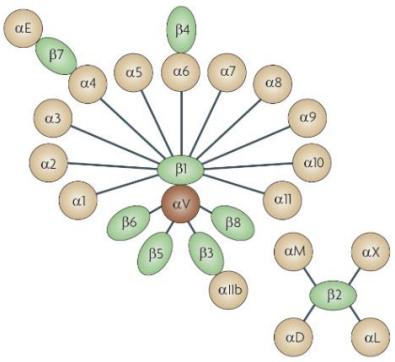

FIGURE 4. The integrin family. Adapted from ref. 12a.

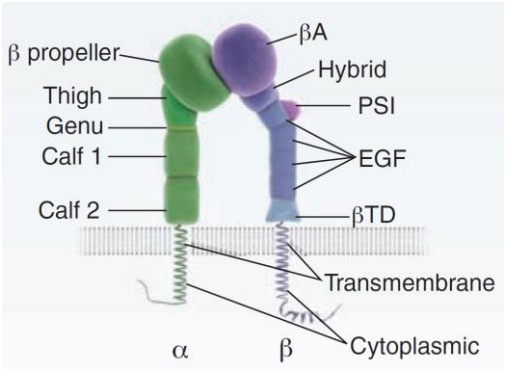

FIGURE 5. Integrin receptor representation. Adapted from ref. 12b.

Endogenous ligands presenting the tripeptide sequence arginine-glycine-aspartic acid (Arg-Gly-Asp, or RGD, FIGURE 6) can interact with a number of integrin receptors (*e.g.* $\alpha_V\beta_3$, $\alpha_V\beta_5$, $\alpha_5\beta_1$),[15] which are strictly related to cancer development, metastasis and tumor angiogenesis. Hence, integrin receptors can be exploited as target in cancer therapy. For this reason, different research groups designed and synthesized a variety of peptides and peptidomimetics displaying the RGD recognition motif to target and bind these specific integrins. In this frame, the attention will be focused on $\alpha_V\beta_3$ receptor.

1.2 INTEGRIN $\alpha_V\beta_3$ AS TARGET RECEPTOR

Among all the integrin receptors, $\alpha_V\beta_3$ is one of the most involved in angiogenesis, and participates to the subtle regulation mechanism underlying the angiogenic processes. Different interleukines and growth factors, which are over-expressed in tumor masses, are able to trigger the expression of this receptor in endothelial cells.[16] Therefore, the population of integrin $\alpha_V\beta_3$ on the membrane of cancer cells is very abundant with respect to healthy tissues, resulting in a continuous stimulation of angiogenesis.[17] The way integrin $\alpha_V\beta_3$ stimulates angiogenesis derives from its ability to interact with matrix metalloproteinase-2 (MMP-2) that degrades the collagen matrix, therefore allowing the reorganization of the ECM in order to form new blood vessels.[18] In cancer cells, the coordinated regulation system able to stop angiogenic signaling fails. A small tumor mass can grow up very quickly by enabling pro-angiogenic events related to integrin receptors with the so called "angiogenic switch", thus becoming a highly aggressive tumor, capable of spreading and shredding by metastasis. For this reason, many efforts have been devoted to discover and elucidate the rationale for the interaction of extra-cellular matrix proteins with cells. One of the most important contributions to this field is represented by the work of Ruoslahti and Pierschbacher, which in 1984 discovered the molecular basis of the ECM proteins recognition.[19] In particular, they demonstrated that fibronectin, an endogenous ligand for many integrins, was recognized by its target receptors thanks to the tripeptide sequence Arg-Gly-Asp (RGD, FIGURE 6).

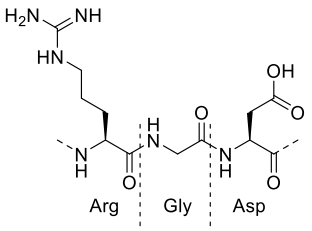

FIGURE 6. The Arg-Gly-Asp (RGD) recognition motif.

1.3 RGD INTEGRIN LIGANDS

Since the discovery of Ruoslahti, a number of different peptide and peptidomimetic libraries have been developed and, among them, a few were found to bind integrin $\alpha_V\beta_3$ with high affinity. Diverse strategies were adopted aiming at displaying the RGD motif in a proper conformation. The first approach was the inclusion of this sequence in cyclic structures, resulting in a higher rigidity of the peptide backbone and limiting the flexibility of flanking residues. Among the RGD-based binders reported in the literature, the research group of Professor Kessler developed the potent integrin ligand Cilengitide (**4**, FIGURE 7).[20] Xiong and co-workers managed to isolate the co-crystal of integrin $\alpha_V\beta_3$ complexed with Cilengitide and studied the key interactions by X-ray analysis (FIGURE 8):[21] while interacting with the receptor binding site, the RGD recognition motif turned out to adopt an extended conformation in which the C_β atoms of arginine and aspartic acid residues are distant about 9 Å. This requirement proved to be a fundamental requirement in order to achieve the ligand-protein interaction, in particular the so-called "electrostatic clamp".

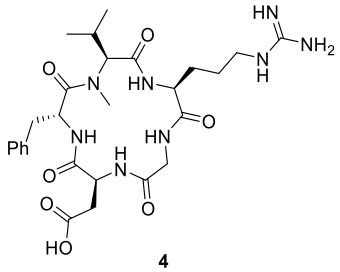

4

FIGURE 7. The potent integrin ligand Cilengitide (**4**).

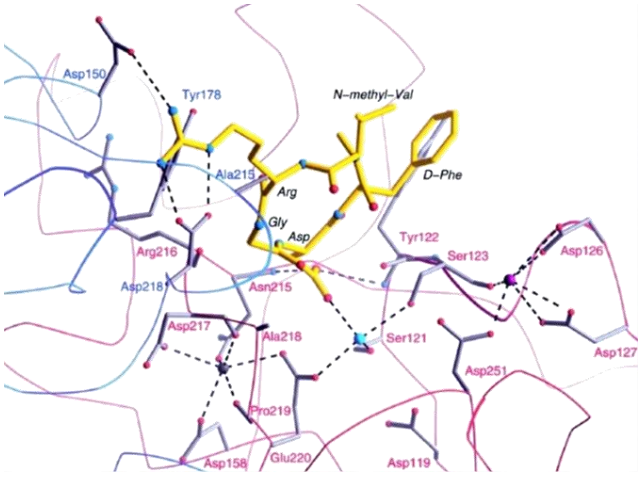

FIGURE 8. Co-crystal of integrin $\alpha_v\beta_3$ complexed with Cilengitide (**4**). Adapted from ref. 21.

The formation of this electrostatic interaction is essential and relies on the establishment of two bridge salts: one between the arginine side chain and negatively charged residues in the α subunit; the other involving the β-carboxylate moiety of aspartic and the Mn^{2+} divalent metal cation of the metal ion-dependent adhesion site (MIDAS) region in the β subunit.[20b] Different types of integrin ligands satisfying these fundamental requirements were developed as anti-angiogenic agents and showed high affinity for the target receptor.[22]

As shown in FIGURE 9, various strategies were adopted to present the RGD binding motif in a suitable conformation for the interaction with the integrin receptor. The common feature of ligands **5**-**14** is the inclusion of the RGD tripeptide sequence within a cyclic structure, in order to limit the backbone flexibility, with the aim of arranging the arginine and the aspartic side chains in a similar way to that of Cilengitide.[23]

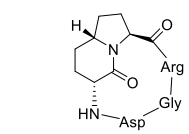

5
$\alpha_v\beta_3$ 14.3 nM
$\alpha_v\beta_5$ >10^3 nM

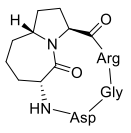

6
$\alpha_v\beta_3$ 3.8 nM
$\alpha_v\beta_5$ 1.39 nM

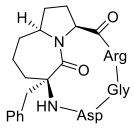

7
$\alpha_v\beta_3$ 6.4 nM
$\alpha_v\beta_5$ 7.7 nM

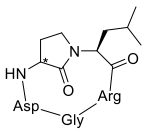

8a (*S*)
$\alpha_v\beta_3$ 40 nM
$\alpha_{IIb}\beta_3$ 2.8 μM

8b (*R*)
$\alpha_v\beta_3$ 0.8 nM
$\alpha_{IIb}\beta_3$ 0.5 nM

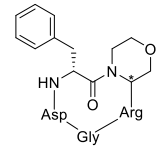

9a (*S*)
$\alpha_v\beta_3$ 157 nM
$\alpha_v\beta_5$ 15.1 nM

9b (*R*)
$\alpha_v\beta_3$ 32.6 nM
$\alpha_v\beta_5$ 21 nM

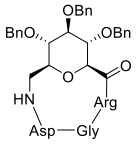

10
$\alpha_v\beta_3$ 25 nM
$\alpha_v\beta_5$ >10^4 nM

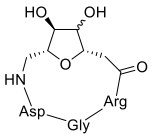

11
$\alpha_v\beta_3$ 1.49 μM
$\alpha_v\beta_5$ 0.38 μM

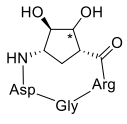

12a (*S*)
$\alpha_v\beta_3$ 51.4 nM
$\alpha_v\beta_5$ 165.5 nM

12b (*R*)
$\alpha_v\beta_3$ 44.7 nM
$\alpha_v\beta_5$ 125.4 nM

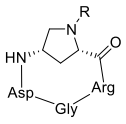

13a (R=H)
$\alpha_v\beta_3$ 4.4 nM
$\alpha_v\beta_5$ 80.2 nM

13b (R=*n*-Heptyl)
$\alpha_v\beta_3$ 2.8 nM
$\alpha_v\beta_5$ 36.1 nM

13c (R=Propionyl)
$\alpha_v\beta_3$ 5.6 nM
$\alpha_v\beta_5$ 94.0 nM

13d (R=Benzyl)
$\alpha_v\beta_3$ 5.1 nM
$\alpha_v\beta_5$ 86.6 nM

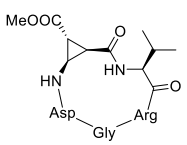

14
$\alpha_v\beta_3$ 20 nM
$\alpha_5\beta_1$ 1.5 nM

FIGURE 9. Selected examples of integrin ligands (**5**-**14**) and relative integrin affinity, expressed as IC_{50} value. See ref. 23.

Even though a variety of ligands targeting $\alpha_V\beta_3$ and $\alpha_V\beta_5$ integrin managed to enter clinical trials due to their potent activity against tumor angiogenesis, this approach in cancer treatment was unsuccessful. As a matter of fact, although Cilengitide is non-toxic and tolerated, its anti-angiogenic activity – and thus its anti-cancer efficacy – has become controversial. Indeed, in contrast with the initially reported results, in specific experimental conditions, Cilengitide was shown to act as an angiogenesis agonist.[24] Though the use of $\alpha_V\beta_3$ integrin ligands as anti-angiogenic agents was put into question, a different strategy emerged, consisting in their use as tumor targeting agents. Following the latter approach, different RGD-based small molecules have been used as carriers to deliver selectively both chemotherapeutics[25] and imaging agents[26], exploiting the over-expression of integrin $\alpha_V\beta_3$ on the membrane of tumor cells.
In 2009-2012 our research group described a new class of cyclic integrin ligands in which a 2,5-diketopiperazine (DKP1-DKP7, FIGURE 10 on the left) scaffold constrained the RGD sequence.[27] Apart from the decreased flexibility of the peptide backbone, the DKP portion avoids metabolic cleavage of amide bonds in α-amino peptides, due to the increased constrain and conformational rigidity of the backbone. Moreover, the structure itself of the DKP ring can actively participate to the ligand-receptor interaction, owing to the presence of hydrogen bond donors and acceptors, such as amide protons and carbonyl groups, respectively. In this frame, a better matching with the biological target can be achieved by introducing diversity in the DKP ring at four positions. By varying the configuration at C3 and C6 and the substitution at N1 and N4, a small library of DKP scaffolds was synthesized (DKP1-DKP7, FIGURE 10 on the left) and used to prepare *cyclo*[DKP-RGD] peptidomimetics bearing the RGD recognition motif (**15-21**, FIGURE 10 on the right).[27a]

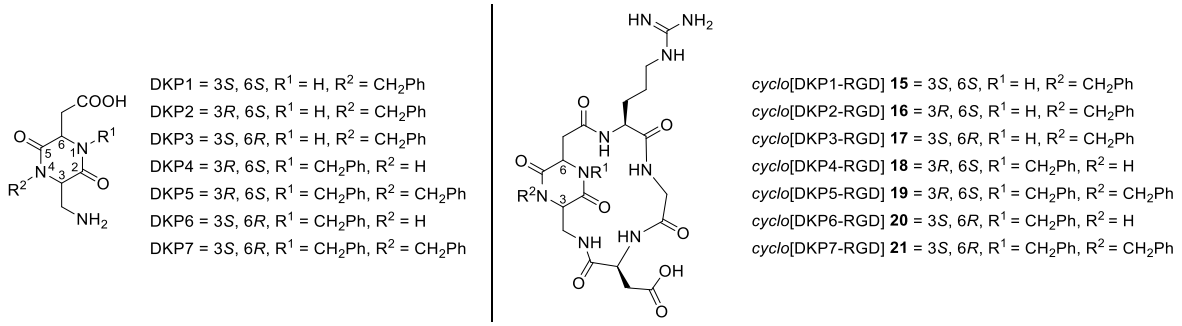

FIGURE 10. DKP1-DKP7 scaffold library and the corresponding *cyclo*[DKP-RGD] peptidomimetics (**15-21**).[27a]

In vitro binding assays on the isolated $\alpha_V\beta_3$ and $\alpha_V\beta_5$ integrin receptors qualified the synthesized peptidomimetics **16-21** as low nanomolar binders for $\alpha_V\beta_3$ (TABLE 1). In contrast to Cilengitide (**4** in FIGURE 7) reported as reference compound, these ligands showed a higher $\alpha_V\beta_3/\alpha_V\beta_5$ selectivity for integrin. Compounds **16-21** were investigated by means of NMR and MC/SD simulations, in order to elucidate their conformational preferences: the ligands possessing the best affinity for the $\alpha_V\beta_3$ receptor were distinguished by a defined, extended arrangement of the RGD tripeptide due to the presence of intramolecular hydrogen bond patterns locking the structure and limiting the backbone flexibility.
Further *in vitro* biological investigations were performed on *cyclo*[DKP3-RGD] (**17**): the tested compound efficiently inhibited angiogenesis in human umbilical vein endothelial cells (HUVECs).[28] Moreover, **17** exerted a potent biological activity either under basal conditions or in the presence of different effectors[29] (FIGURE 11): this effect was ascribed to the disruption of endothelial cell-ECM attachment upon the interaction of *cyclo*[DKP3-RGD] with integrin receptors. On the other hand, compound **17** did not affect other cellular aspects, *e.g.* cell viability and proliferation.

TABLE 1. Evaluation of the binding affinity of compounds **15**-**21** on isolated receptor.

Compound	Structure	IC_{50} (nM)[a]	
		$\alpha_V\beta_3$	$\alpha_V\beta_5$
15	*cyclo*[DKP1-RGD]	3898 ± 418	$>10^4$
16	*cyclo*[DKP2-RGD]	3.2 ± 2.7	114 ± 99
17	*cyclo*[DKP3-RGD]	4.5 ± 1.1	149 ± 25
18	*cyclo*[DKP4-RGD]	7.6 ± 4.3	216 ± 5
19	*cyclo*[DKP5-RGD]	12.2 ± 5.0	131 ± 29
20	*cyclo*[DKP6-RGD]	2.1 ± 0.6	79 ± 3
21	*cyclo*[DKP7-RGD]	0.2 ± 0.09	109 ± 15
4	Cilengitide	0.6 ± 0.1[b]	11.7 ± 1.5[b]

[a] IC_{50} values were calculated as the concentration of compound required for 50% inhibition of biotinylated vitronectin binding. Screening assays were performed by incubating the immobilized integrins $\alpha_V\beta_3$ and $\alpha_V\beta_5$ with increasing concentrations (10^{-12} – 10^{-5} M) of the RGD ligands in the presence of biotinylated vitronectin (1 mg/mL), and measuring the concentration of bound vitronectin in the presence of the competitive ligands (see ref. 27). [b] Calculated as the concentration of compound required for 50% inhibition of biotinylated vitronectin binding (see ref. 20).

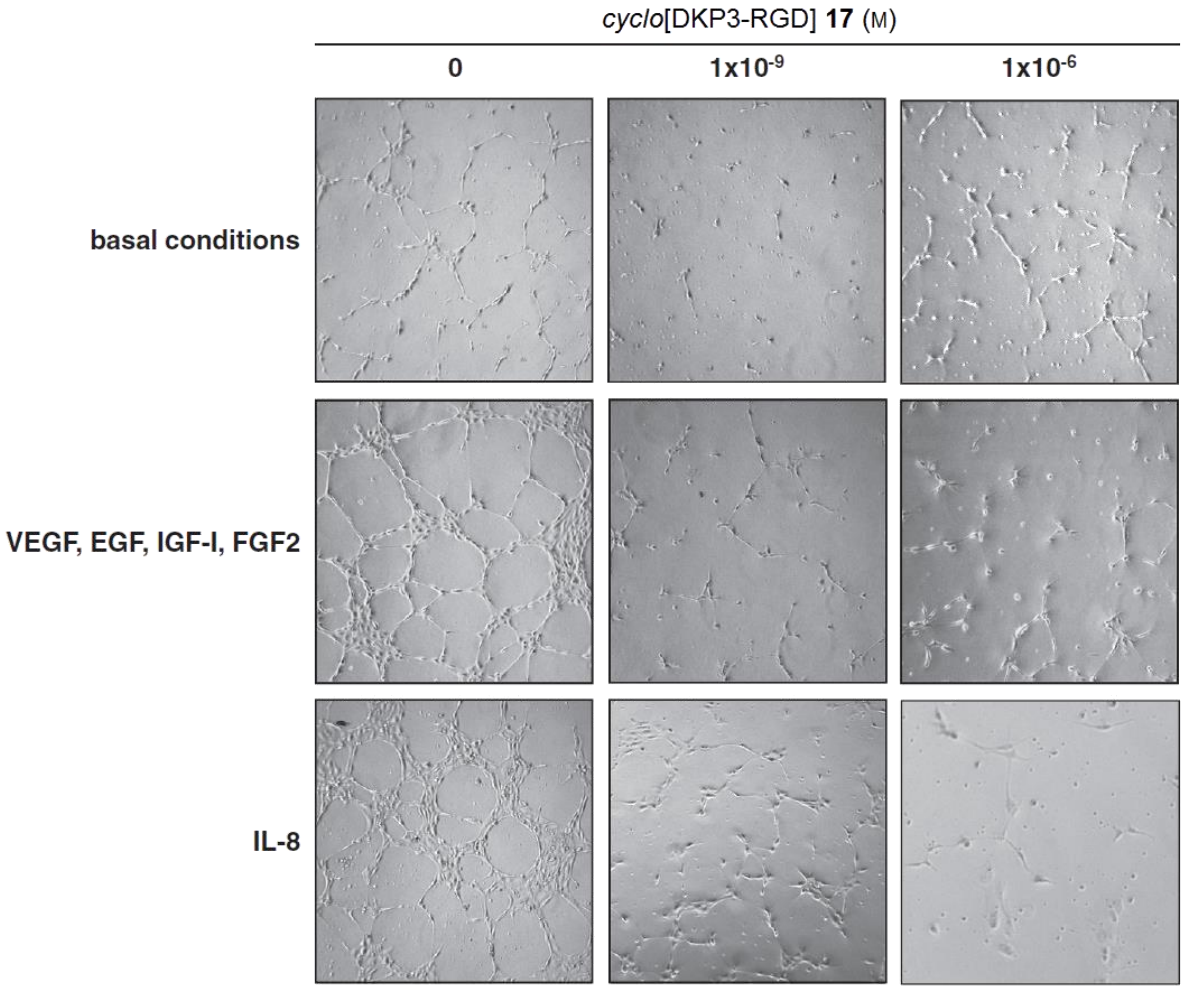

FIGURE 11. Representative phase contrast photomicrographs of HUVE cells plated on Matrigel in basal conditions or in the presence of VEGF, EGF, IGF-I, and bFGF or IL-8, without and with *cyclo*[DKP3-RGD] (**17**) at different concentrations. Adapted from ref. 28.

1.4 *iso*DGR INTEGRIN LIGANDS

In 2006, Dr. Corti and colleagues identified a new integrin binding motif while investigating the interaction of fibronectin with integrin receptors.[30] The asparagine residue in the asparagine-glycine-arginine (Asn-Gly-Arg, or NGR, FIGURE 12) sequence of fibronectin was observed to undergo spontaneous post-translational modifications with the formation of an *iso*aspartate portion, thus converting the original NGR tripeptide into the new *iso*aspartate-glycine-arginine (*iso*Asp-Gly-Arg, or *iso*DGR, FIGURE 12). The reason why this transformation occurs lies in tissue aging and the β-amino acid product *iso*Asp is not provoking a loss of function in fibronectin, a usual consequence of such modifications. Actually, the conversion of NGR into *iso*DGR enabled a stronger interaction with the integrin target receptor, resulting in an overall gain of protein function.

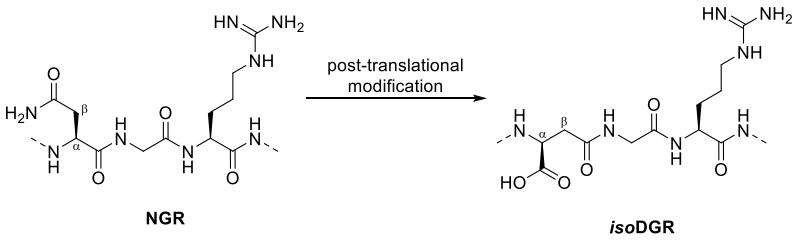

FIGURE 12. Post-translational modification converting the NGR portion into its derivative *iso*DGR.

In this frame, biochemical studies highlighted that the NGR portion in the FN-I5 region of fibronectin is involved in the deamidation of Asn263 to Asp and *iso*Asp: the conversion of the amide side chain of asparagine into the carboxylic acid fragment in aspartate or *iso*aspartate is responsible for the increased endothelial cell adhesion. This reaction occurs at physiological pH and consists in the loss of a molecule of ammonia leading to a succinimide intermediate, whose hydrolysis restores the carboxylic moiety in the side chain and forms both the DGR and *iso*DGR motifs (FIGURE 13).

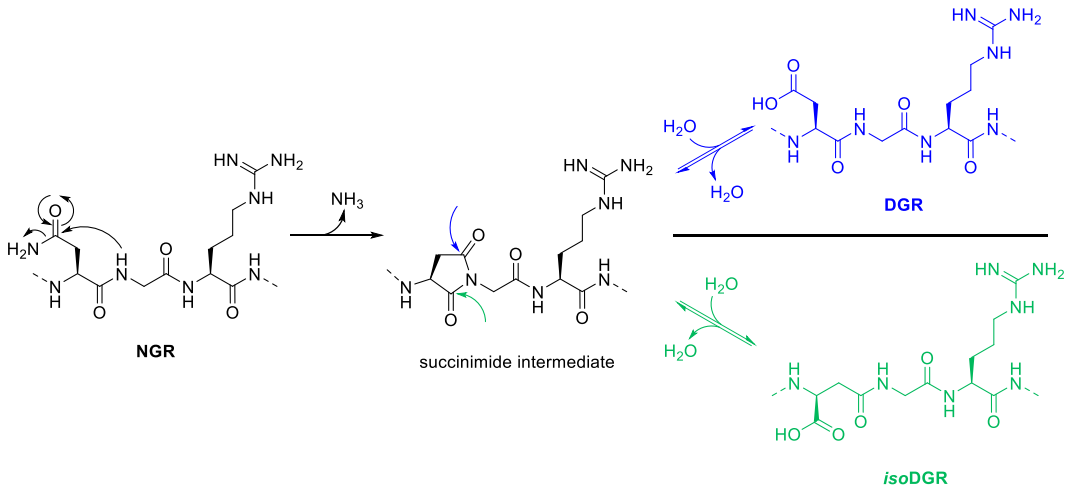

FIGURE 13. The deamidation reaction responsible for the transformation of NGR into *iso*DGR and DGR motifs in fibronectin.

At this stage, the question about which between the *iso*DGR and the DGR tripeptides was the one responsible for the activation of the integrin receptor arose. Affinity assays on a library of cyclic peptides proved that among the *iso*DGR (*iso*Asp-Gly-Arg), *iso*dGR (D-*iso*Asp-Gly-Arg) and DGR (Asp-Gly-Arg) motifs only the first one is able to bind the $\alpha_v\beta_3$ receptor with sub-micromolar affinity.[30b] Provided these findings, the group of Corti focused its attention on the molecular requirements for the interaction with the integrin receptor and compared two cyclopeptides containing the *iso*DGR or the RGD sequences, namely *iso*DGR-2C and RGD-2C (**22** and **23** respectively in FIGURE 14).

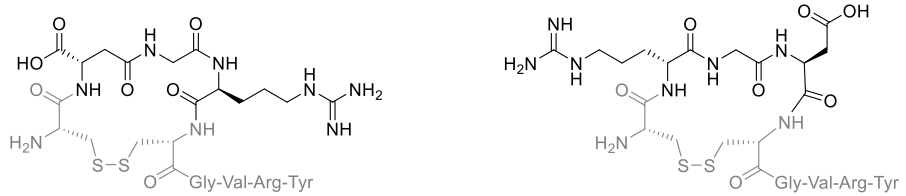

FIGURE 14. The two cyclopeptides **22** and **23** investigated by Corti and colleagues.

As consequence of the backbone structure, the *iso*DGR binding motif occupies the interaction site of $\alpha_V\beta_3$ integrin adopting a reversed orientation, but still presenting the arginine and the aspartate side chains with a suitable distance to establish the same polar interactions shown in RGD binders (FIGURE 15).[31]

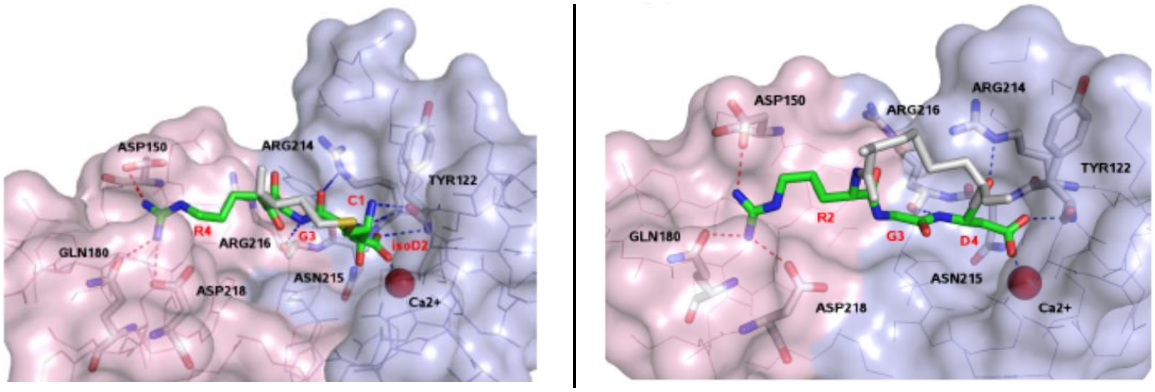

FIGURE 15. Representation of *iso*DGR-2C (**22**, on the left) and RGD-2C (**23**, on the right) interacting the $\alpha_V\beta_3$ binding pocket. The α subunit is colored in pink, the β subunit in cyan. Adapted from ref. 31.

Following NMR experiments were in agreement with the docking studies and the two tested compounds **22** and **23** showed comparable IC_{50} values in affinity binding assays on isolated $\alpha_V\beta_3$ receptor, thus reinforcing the idea of a possible competition for the same binding site. Based on these findings, many efforts have been devoted to the synthesis of potent *iso*DGR-based ligands. Keeping in mind the structural features of the strong binder Cilengitide (**4**, FIGURE 7), in 2010 Professor Kessler and co-workers prepared a library of cyclic pentapeptides containing the *iso*DGR motif.[32] However, these ligands displayed from moderate to low affinities for the isolated $\alpha_V\beta_3$ integrin, with the best binder *cyclo*[G*iso*DGRphg] (**24** in FIGURE 16) having IC_{50} = (89 ± 19) nM.

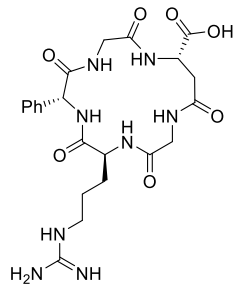

24

FIGURE 16. Structure of the integrin ligand *cyclo*[G*iso*DGRphg] (**24**).

The major difference between RGD and *iso*DGR recognition motifs was reported in 2012, when the research group of Dr. Musco demonstrated the ability of some *iso*DGR-containing compounds to inhibit $\alpha_V\beta_3$ integrin activation by interacting with the binding site in the inactive form, thus qualifying them as true integrin antagonists.[33] The inhibition of this conformational change is crucial for stopping the integrin intracellular signaling, therefore preventing the pathological events related to tumor exploitation of integrin receptors. For this reason, the development of potent *iso*DGR binders became very attractive, with the possibility to exploit them as lone-standing anti-angiogenic agents or as carrier to effect active drug targeting to tumor site.

In 2013, our research group employed the well-established DKP scaffold system in the synthesis of two constrained peptidomimetic ligands containing the *iso*DGR motif (**25-26**, FIGURE 17).[34] The *in vitro*

TABLE 2. Evaluation of the binding affinity of compounds **25-26** on isolated receptor.

Compound	Structure	IC_{50} (nM)[a]	
		$\alpha_V\beta_3$	$\alpha_V\beta_5$
16	*cyclo*[DKP2-RGD]	3.2 ± 2.7	114 ± 99
17	*cyclo*[DKP3-RGD]	4.5 ± 1.1	149 ± 25
25	*cyclo*[DKP2-*iso*DGR]	46.7 ± 18.2	220 ± 84
26	*cyclo*[DKP3-*iso*DGR]	9.2 ± 1.1	312 ± 21
4	Cilengitide	0.6 ± 0.1[b]	11.7 ± 1.5[b]
24	*cyclo*[G*iso*DGRphg]	89 ± 19[c]	n.d.

[a] IC_{50} values were calculated as the concentration of compound required for 50% inhibition of biotinylated vitronectin binding. Screening assays were performed by incubating the immobilized integrins $\alpha_V\beta_3$ and $\alpha_V\beta_5$ with increasing concentrations (10^{-12} – 10^{-5} M) of the RGD or *iso*DGR ligands in the presence of biotinylated vitronectin (1 mg/mL), and measuring the concentration of bound vitronectin in the presence of the competitive ligands (see ref. 27). [b] Calculated as the concentration of compound required for 50% inhibition of biotinylated vitronectin binding (see ref. 20). [c] Determined by a solid phase binding assay using supported vitronectin, soluble $\alpha_V\beta_3$ integrin, specific primary and secondary antibodies (see ref. 32).

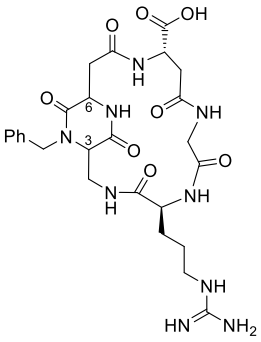

cyclo[DKP2-*iso*DGR] **25** = 3*R*, 6*S*
cyclo[DKP3-*iso*DGR] **26** = 3*S*, 6*R*

FIGURE 17. The *cyclo*[DKP-*iso*DGR] peptidomimetics **25-26** reported by our research group.

evaluation of **25** and **26** in binding assays on purified integrin $\alpha_V\beta_3$ (TABLE 2) qualified *cyclo*[DKP3-*iso*DGR] **26** as the most potent *iso*DGR-based peptidomimetic reported so far in the literature. NMR and Monte Carlo/Stochastic Dynamics (MC/SD) studies revealed a higher conformational flexibility in compound **25**, compared to **26**: due to a lower rigidity, *cyclo*[DKP2-*iso*DGR] (**25**) showed a lesser affinity for $\alpha_V\beta_3$ integrin in comparison with *cyclo*[DKP3-*iso*DGR] (**26**). Although **26** is able to adopt two different conformations, in both of them the *iso*DGR sequence is arranged in such an extended conformation that is appropriate for interacting with the target receptor (FIGURE 18, on the left). In addition, docking studies on the representative conformations from MC/SD calculations resulted in top-ranked poses of *cyclo*[DKP3-*iso*DGR] within the $\alpha_V\beta_3$ receptor binding site, while considering the integrin-Cilengitide co-crystal complex as model (FIGURE 18, on the right).

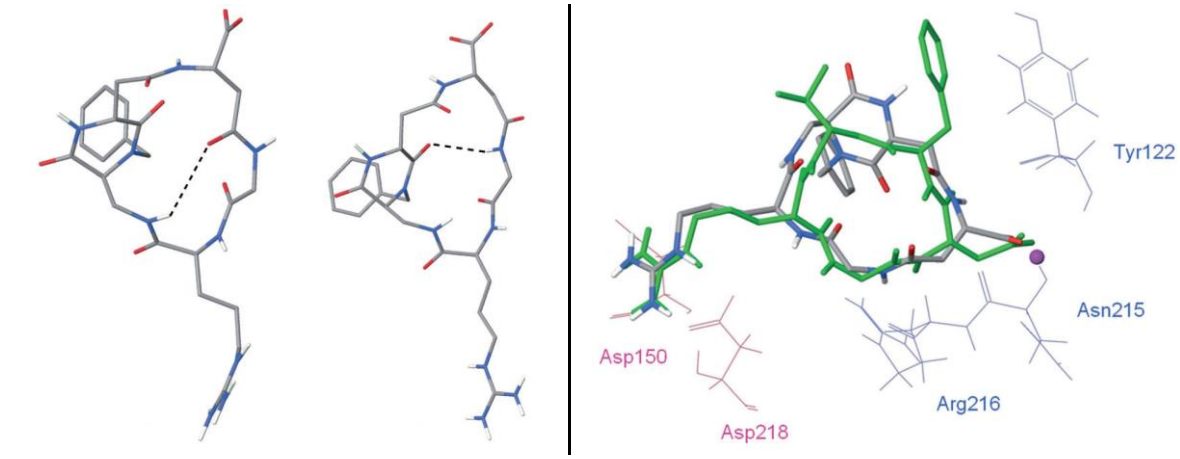

FIGURE 18. MC/SD simulations (on the left) and docking studies (on the right) on the *iso*DGR peptidomimetic **26**. Adapted from ref. 34.

1.5 RGD LIGANDS IN CANCER THERAPY

A variety of radiolabeled agents containing RGD-based ligands was synthesized and validated in cancer imaging at the clinical level.[35] On the other hand, small molecules containing this tripeptide sequence are still under investigation and far from therapeutic treatments. As mentioned before, the over-expression of integrin $\alpha_V\beta_3$ by cancer cells can be exploited for the selective delivery of therapeutics by RGD-decorated prodrugs. Integrin receptors are used to exploit different internalization-recycling cycles upon interaction with their ligands: these processes are mediated by such proteins as caveolin and

clathrin, capable of triggering receptor folding and inclusion into vesicles that are delivered to endosomes.[36] In the case of integrin $\alpha_V\beta_3$, two pathways are available: I) protein degradation by specific enzymes in endosomes or lysosomes, II) restoration to the cell membrane. Consequences of these events encompass cell migration/diffusion and activation of other receptor families by cross-talk mechanisms.[37] Among the cytotoxic agents used in chemotherapy, paclitaxel (PTX, **27**, FIGURE 19) is one of the most widely employed in the construction of RGD-containing small molecule-drug conjugates (SMDCs). Paclitaxel is usually derivatized at the 2'-hydroxy group, which is essential for the biological activity of the drug, by formation of an ester bond: this strategy increased the efficacy of paclitaxel in *in vivo* tests.[38]

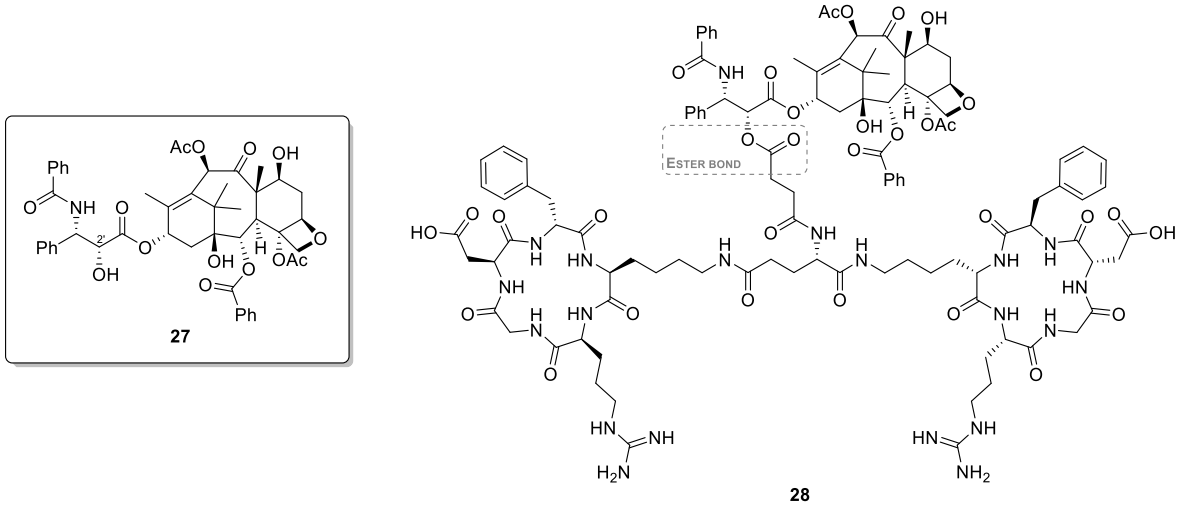

FIGURE 19. The anti-cancer agent paclitaxel (**27**) and the prodrug **28** developed by Ryppa and co-workers.

However, such PTX esters showed poor stability even in phosphate buffer and the premature release of the drug was observed, limiting the overall applicability of this kind of SMDC. As representative example of such paclitaxel conjugates, in 2009 Ryppa and co-workers synthesized prodrug **28** (FIGURE 19), a divalent RGD compound designed to improve the affinity towards the target receptor by exploiting the multi-presentation of the recognition sequence, and studied its anti-proliferative activity on HUVECs.[39] The short half-life of **28** (*ca.* 2 h in phosphate buffer solution at 37 °C) compromised the assay even after less than 1 h, frustrating the targeting ability issued by the integrin binding portions.

Having in hands peptidomimetics able to target integrin $\alpha_V\beta_3$ with high affinity (**16-21**, FIGURE 10, TABLE 1), in 2012 our research group reported the synthesis and the biological evaluation of *cyclo*[DKP3-RGD]-PTX conjugate **29** (FIGURE 20).[40] Paclitaxel was linked to the *cyclo*[DKP3-RGD]-CH_2NH_2 targeting moiety (**30**, FIGURE 20) through a succinate fragment and, despite the increased steric hindrance on the *cyclo*[DKP-RGD] portion, conjugate **29** retained a low nanomolar affinity and a very high selectivity for the target $\alpha_V\beta_3$ integrin [IC_{50} ($\alpha_V\beta_3$) = (5.2 ± 2.3) nM and IC_{50} ($\alpha_V\beta_5$) = (219 ± 124) nM]. *In vivo* tests on conjugate **29** in nude mice xenografted with IGROV-1/Pt1 cancer cells (namely, a cell line over-expressing the $\alpha_V\beta_3$ receptor) showed a better efficacy of the conjugate with respect to the free cytotoxic agent. Indeed, due to the active integrin targeting, the anti-tumor activity of **29** was superior despite the lower dose administered to the animal (FIGURE 21). Similarly to compound **28**, the drawback of this approach was the poor stability of the ester bond connecting the drug to the RGD peptidomimetic. As a matter of fact, even though prodrug **29** proved to be stable in physiological solution for at least 7 days, the release of paclitaxel took place both in human and in murine plasma, with half-lives of 143 min and 165 min respectively (FIGURE 21).

These *in vivo* experiments on **29** pointed out the benefit of using *cyclo*[DKP-RGD] integrin binders as targeting agent in site-directed anti-cancer conjugates and, at the same time, confirmed that the linker

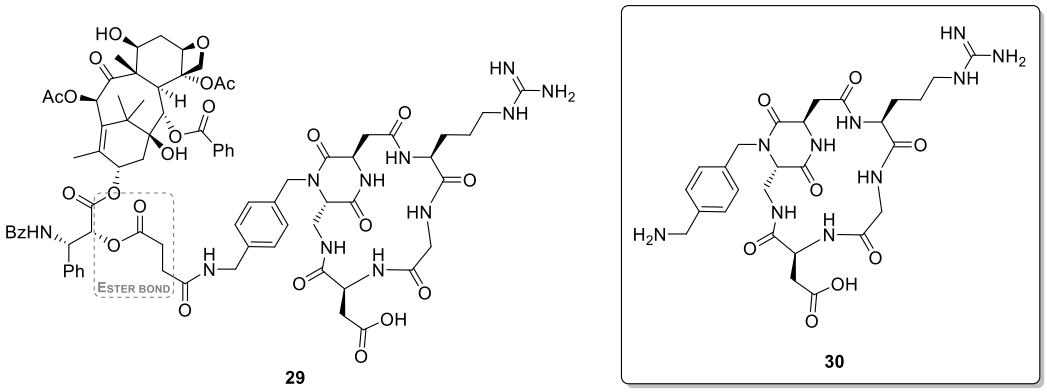

FIGURE 20. The chemical structures of *cyclo*[DKP3-RGD]-PTX conjugate **29** and of *cyclo*[DKP3-RGD]-CH_2NH_2 **30** integrin ligand.

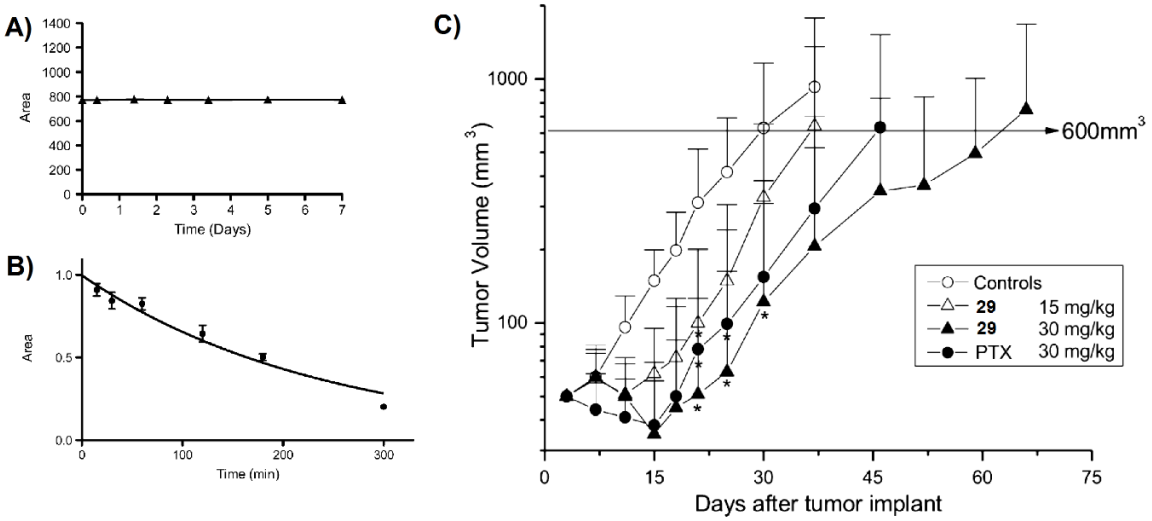

FIGURE 21. A) Stability of conjugate **29** (1.28 mM) in physiological solution; B) stability of **29** in murine plasma; C) biological evaluation of **29** *in vivo* compared to paclitaxel (PTX) on IGROV-1/Pt1 ovarian carcinoma. Adapted from ref. 40.

system represents a very critical point for the efficacy of the prodrug and its essential role in the selective release of the cytotoxic payload within the tumor site. This observation prompted the investigation and the research of different systems to link the portions of the conjugate. Generally, a small molecule-drug conjugate can be divided into at least three portions: the ligand, the drug, and the linker, as depicted in FIGURE 22.[41] Additional parts, such as spacers, can be added to improve the pharmacokinetic properties of the SMDC: the main role of these fragments is to increase the solubility and the stability in aqueous medium, as well as to enhance the drug release under specific conditions.

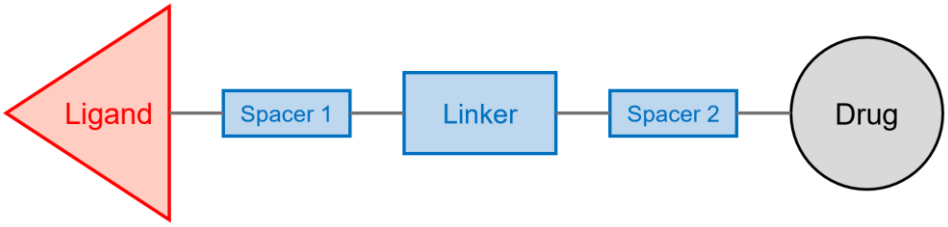

FIGURE 22. General representation of a small molecule-drug conjugate. Adapted from ref. 41.

In the literature, several examples of linker moieties, capable of being cleaved under specific conditions, have been developed. In particular, the most common strategies employed in this class of smart prodrugs consists in:

- hydrolysis of certain amide, oxime and hydrazone functional groups;
- enzymatic cleavage of a specific amide bond in substrate peptide sequences;
- reduction of disulfide bonds.

The general mode of action of internalizing small molecule-drug conjugates is shown in FIGURE 23.[42] Upon interaction with the target receptor, a series of events takes place and the formation of a vesicle including the ligand-receptor complex occurs. The fusion of this vesicle with early endosomes can allow the release of the payload from pH-dependent linker systems. Otherwise, the conjugate survives and gets in touch with proteases in lysosomes, where ester and specific amide bonds are hydrolyzed, thus releasing the drug. Passive diffusion drives the cytotoxic agent outside the corpuscle (*i.e.* endosome or lysosome) and the vesicle recycling restores the receptor on the cell surface.

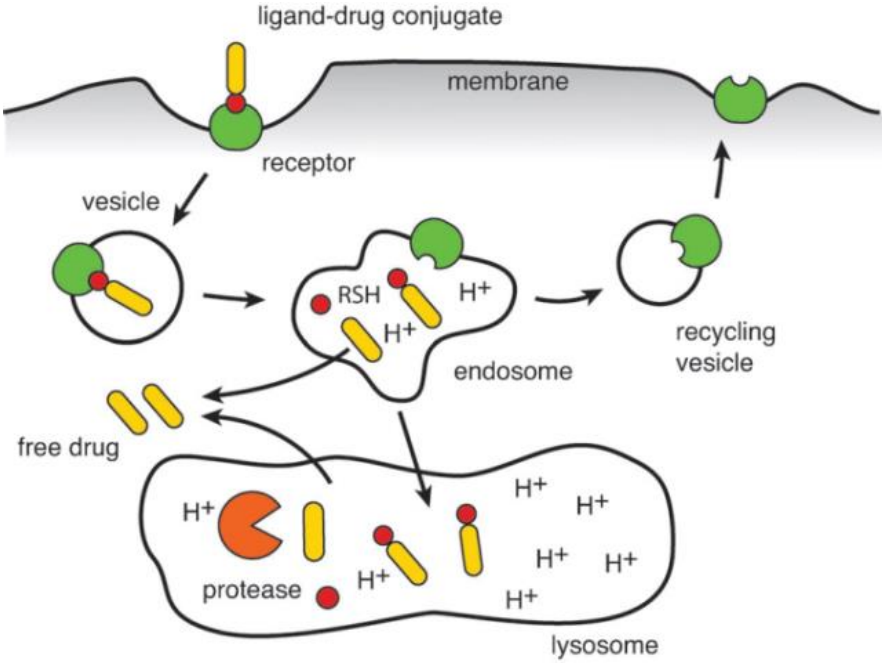

FIGURE 23. General mechanism of action of internalizing SMDCs. Adapted from ref. 42.

Thus, the logical development of compound **29** was the synthesis of conjugates in which the integrin ligand and the payload were connected through a peptide linker, eventually cleaved in the presence of some specific proteases located in endosomes and lysosomes inside the cell. For this reason, taking inspiration from the work published by Scheeren and co-workers,[43] our research group synthesized the conjugate *cyclo*[DKP3-RGD]-Val-Ala-PTX (**31**, FIGURE 24).[25a] The structure of prodrug **31** resembles the schematic representation shown in FIGURE 22 and it is possible to recognize the integrin ligand (*cyclo*[DKP3-RGD]), the cytotoxic agent (paclitaxel), the peptide linker (valine-alanine, Val-Ala) and two different spacers.

Conjugate **31** showed a high affinity for the purified $\alpha_V\beta_3$ receptor (TABLE 3) and a marked selectivity for the integrin over-expressing cell line CCRF-CEM $\alpha_V\beta_3$ with respect to the isogenic cell line CCRF-CEM non-expressing the target receptor (TABLE 4). The related conjugate *cyclo*[DKP3-RGD]-uncleavable-PTX **32** was designed to be unable to release the drug, and thus used as negative control in anti-proliferative assays. The free drug itself showed a pronounced selectivity against CCRF-CEM $\alpha_V\beta_3$ cells: the *S* value of the compound **31** was corrected taking into account the different biological activity

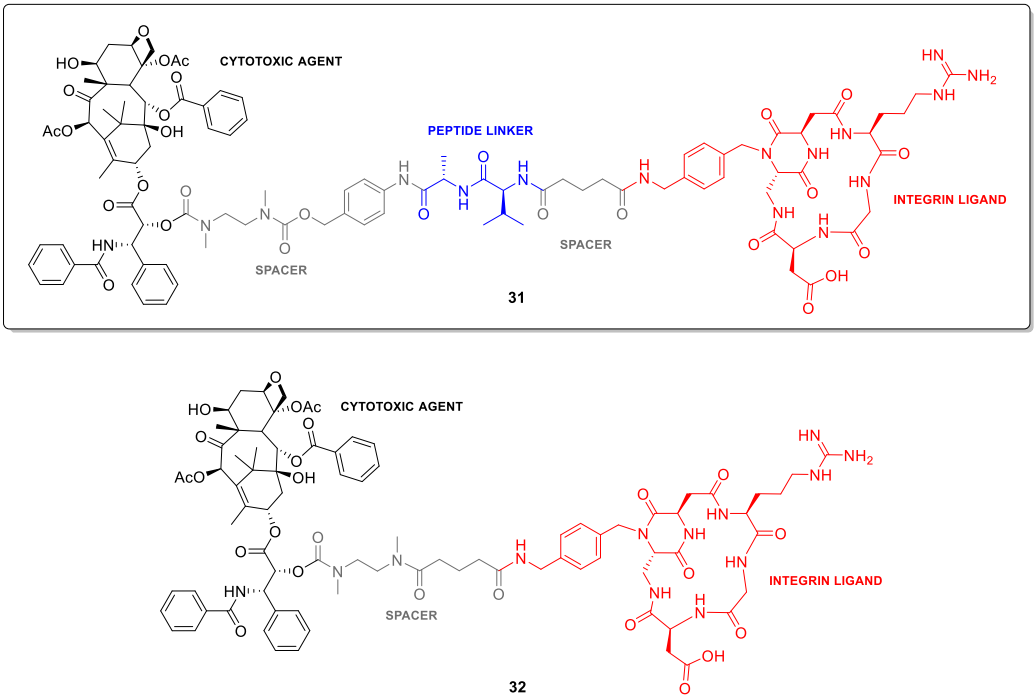

FIGURE 24. Structures of conjugates **31** and **32**.

TABLE 3. Evaluation of the binding affinity of compounds **31** and **32** on isolated receptor.

Compound	Structure	IC_{50} (nM)[a]	
		$\alpha_V\beta_3$	$\alpha_V\beta_5$
31	*cyclo*[DKP3-RGD]-Val-Ala-PTX	13.3 ± 3.6	924 ± 290
32	*cyclo*[DKP3-RGD]-uncleavable-PTX	10.8 ± 1.7	1050 ± 270
17	*cyclo*[DKP3-RGD]	4.5 ± 1.1	149 ± 25

[a] IC_{50} values were calculated as the concentration of compound required for 50% inhibition of biotinylated vitronectin binding as estimated by GraphPad Prism software. All values are the arithmetic mean the standard deviation (SD) of triplicate determinations.

TABLE 4. Evaluation of anti-tumor activity of compounds **31** and **32** *in vitro*.

Compound	Structure	IC_{50} (nM)[a]		S[b]	TI[c]
		CCRF-CEM ($\alpha_V\beta_3$ –)	CCRF-CEM $\alpha_V\beta_3$ ($\alpha_V\beta_3$ +)		
27	Paclitaxel	155 ± 55	21 ± 2	7.4	1
31	*cyclo*[DKP3-RGD]-Val-Ala-PTX	5153 ± 977	77 ± 20	66.9	9.0
32	*cyclo*[DKP3-RGD]-uncleavable-PTX	> 10000	> 10000	n.d.	n.d.

[a] IC_{50} values were calculated as the concentration of compound required for 50% inhibition of cell viability in culture, based on quantitation of the ATP present as estimated by CellTiter-GLO; cells were treated for 6 h in U-bottomed 96-well plates, then washed and incubated for 138 h in compound-free medium in 96-well flat-bottomed plates. [b] Selectivity (S): IC_{50} ($\alpha_V\beta_3$ –)/IC_{50} ($\alpha_V\beta_3$ +). [c] Targeting index (TI): selectivity/selectivity observed with free paclitaxel.

of paclitaxel on the two cell lines and the corresponding Targeting Index (TI) was calculated. This new parameter allowed the direct evaluation of the tumor-targeting ability of **31** *in vitro*.

As previously shown in FIGURE 23, the mechanism of action of conjugates **31** and **32** relies on the interaction with integrin $\alpha_V\beta_3$ and on the subsequent internalization by vesicles. After reaching the lysosomal corpuscles, specific proteases, such as cathepsin B, process the substrate dipeptide Val-Ala and hydrolyze the C-terminus of the dipeptide sequence in **31** (FIGURE 25). A fast electron cascade takes place in the aromatic aniline ring, with the release of CO_2 and the formation of the stable free amine that will slowly cyclize releasing the free paclitaxel **27** inside the tumor cell.

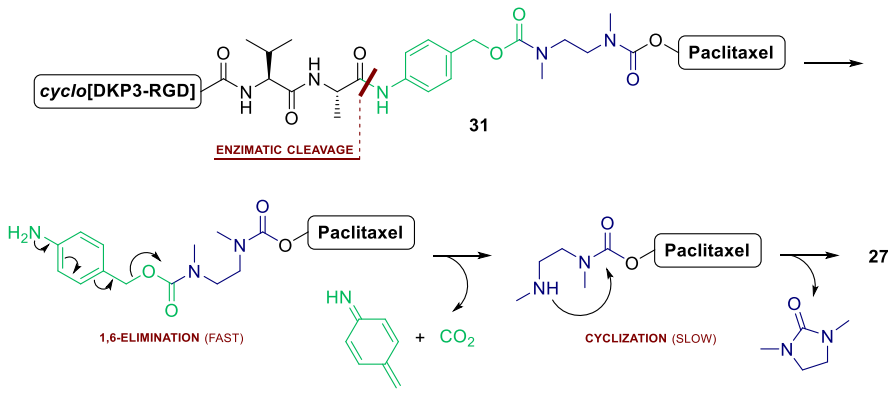

FIGURE 25. Proteolysis of conjugate **31** leading to the release of free paclitaxel **27**.

The uncleavable conjugate **32** is not susceptible to enzymatic hydrolysis, lacking any substrate peptide sequence: once entered the cell, the paclitaxel payload cannot be released and thus no biological activity against the tumor cell line is observed (see TABLE 4).

Since the literature on SMDC targeting integrin $\alpha_V\beta_3$ still lacks a lead compound, prodrug **31** and its biological studies represent a valuable reference in this field. Moreover, the targeting index (TI) of 9.0 – yet not outstanding in absolute terms – demonstrates the feasibility of combining an RGD-peptidomimetic and paclitaxel using the Val-Ala dipeptide as linker strategy. In view of these promising results, we decided to expand the library of *cyclo*[DKP-*iso*DGR] and to develop an *iso*DGR-based ligand suitable for the preparation of small molecule-drug conjugates, with the aim of comparing the targeting efficacy of the *iso*DGR motif with respect to the RGD sequence.

1.6 CHEMICAL TOOLS AS NEGATIVE CONTROL IN BIOLOGICAL INVESTIGATIONS

In order to evaluate the ability of any synthesized compound to target cancer cells, *in vitro* assays such as those mentioned above (TABLE 4) require two cell lines that differ in the expression of integrin receptors on the surface of cell membrane (see CCRF-CEM and CCRF-CEM $\alpha_V\beta_3$ in TABLE 4). We decided to use two isogenic cell lines differing only in the level of integrin $\alpha_V\beta_3$ expression. In this particular case, the native non-expressing cell line CCRF-CEM was manipulated by transfection with a DNA vector to prepare a subclone expressing integrin $\alpha_V\beta_3$. Quite unexpectedly, the CCRF-CEM $\alpha_V\beta_3$ subclone showed a slightly higher sensitivity to paclitaxel with respect to the parental CCRF-CEM: this is the reason why we introduced the targeting index and standardized the *S* value of prodrug **31**, taking into account the intrinsic selectivity shown by the cytotoxic agent itself.

The research of appropriate cell lines could not be trivial and the conditions used to grow and to store the cell cultures could affect the integrin expression on the cell surface. Therefore, the biological system has to be monitored regularly, confirming that no mutation occurred over time. A possible simplification of this scenario can be the use of a single cell line in *in vitro* assays and performing parallel experiments in the presence of a negative control. In principle, a compound unable to interact with the receptor should work as well as an integrin non-expressing cell line (such as parental CCRF-CEM) when investigating the targeting ability of integrin ligands.

In 1994, Engel and co-workers published an interesting article, in which a variety of linear and cyclic penta- and hexapeptides was examined as integrin ligands.[44] Among the compounds synthesized and studied, selected cyclopeptides **33-38** are shown in FIGURE 26. An amino acid residue with non-natural configuration was introduced systematically along the backbone to evaluate the influence on the overall conformation and, therefore, on the biological activity of the compound.

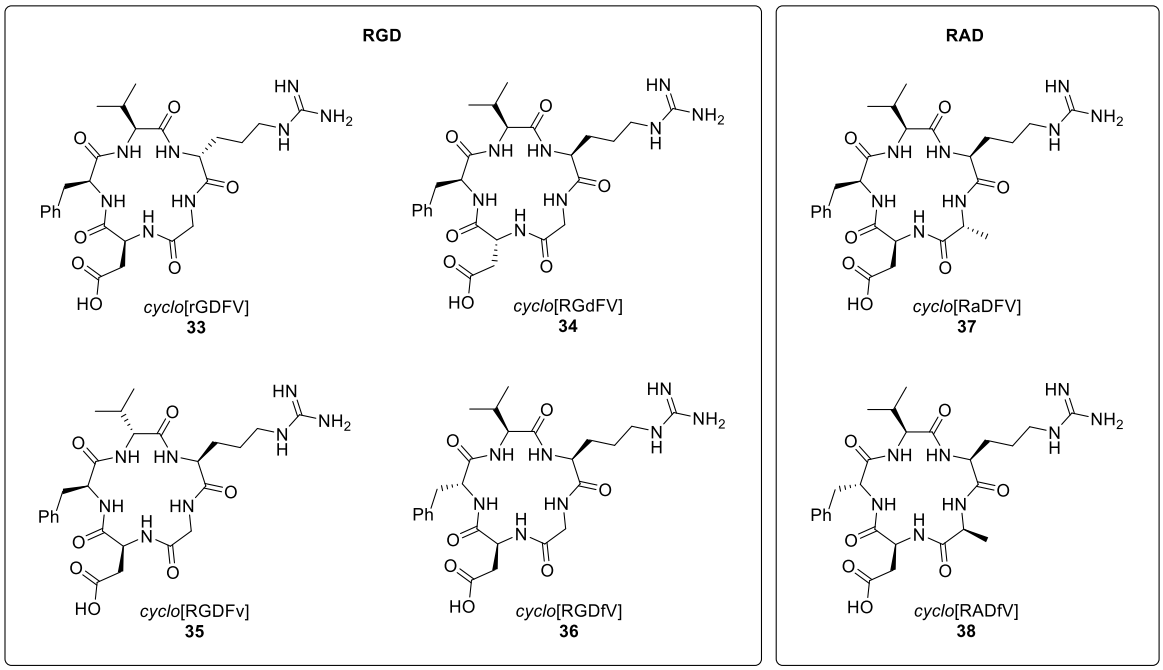

FIGURE 26. Selected cyclopeptides **33**-**38** bearing either the RGD or the RAD motif. Residues in lowercase are D-amino acids.

The ability of compounds **33-38** to inhibit the binding of vitronectin to both soluble and immobilized integrin $\alpha_V\beta_3$ was evaluated *in vitro* (TABLE 5). *Cyclo*[RGDfV] **36**, namely Bachem, was found to be a potent integrin ligand and its further optimization led to Cilengitide (**4**, FIGURE 7) by *N*-methylation of the valine residue.[20] Replacement of glycine with alanine resulted in weaker integrin binders: in particular, in comparison with the corresponding RGD peptide **35**, **38** showed a two orders of magnitude loss of affinity towards the target receptor. Similarly, **37** was the worst ligand among those synthesized and reported by the authors.

TABLE 5. Evaluation of the inhibitory activity of compounds **33-38** on isolated $\alpha_V\beta_3$.

Compound	Structure	IC_{50} (μM)	
		soluble $\alpha_V\beta_3$	immobilized $\alpha_V\beta_3$
33	*cyclo*[rGDFV]	72 ± 10.7	25 ± 4
34	*cyclo*[RGdFV]	152 ± 3.5	18.1 ± 14.8
35	*cyclo*[RGDfV]	0.049 ± 0.019	0.050 ± 0.024
36	*cyclo*[RGDFv]	11.3 ± 1.2	0.4 ± 0.1
37	*cyclo*[RaDFV]	>>240	>>240
38	*cyclo*[RADfV]	4.1 ± 1.0	8.9 ± 5.0

In the literature, compounds displaying the Arg-Ala-Asp sequence were found to be unable to bind the integrin receptor, and therefore replacement of the RGD motif with the RAD derivative has been exploited as negative control both in drug targeting and in tumor imaging.[45]

Based on these results, we concluded that the inclusion of RAD or RaD sequence into a DKP peptidomimetic may afford a weak ligand for integrin $\alpha_V\beta_3$, to be exploited in anti-proliferative assays as negative control. The first step would be the preparation of *cyclo*[DKP-RAD] and/or *cyclo*[DKP-RaD] to test in *in vitro* binding assay on isolated receptor, as previously done with both RGD and *iso*DGR compounds. Then, the motif showing the highest IC_{50} value will be used to synthesize a suitable derivative for conjugation, aiming at preparing prodrugs related to those presenting the RGD recognition motif as targeting moiety.

2 SYNTHESIS OF INTEGRIN LIGANDS

2.1 *CYCLO*[DKP-*ISO*DGR] LIGANDS

2.1.1 SYNTHESIS OF *CYCLO*[DKP-*ISO*DGR] PEPTIDOMIMETICS

Compounds **25** and **26** (FIGURE 17, see PARAGRAPH I – 1.4) were the first two *iso*DGR integrin ligands reported by our research group.[34] However, the library of *cyclo*[DKP-RGD] peptidomimetics consisted of seven members, with six of them presenting a low nanomolar affinity for integrin $\alpha_v\beta_3$ (TABLE 1, PARAGRAPH I – 1.3). Following a similar strategy to that reported for the synthesis of **25** and **26**, two more *cyclo*[DKP-*iso*DGR] compounds, namely *cyclo*[DKP5-*iso*DGR] and *cyclo*[DKP7-*iso*DGR] (**39** and **40**, respectively, in FIGURE 27) have been synthesized.[46] The new compounds **39** and **40** were synthesized starting from DKP scaffolds **41** and **42**, suitable for solid-phase peptide synthesis (SPPS). The retrosynthetic analysis of **39** and **40** is straightforward (SCHEME 1): macrocycle opening leads to linear compound **A**, which is readily accessible by solid phase synthesis using SASRIN resin, protected amino acids and azido acid scaffolds **41**-**42**, obtained by known compounds **43**-**44** (see SCHEME 3).

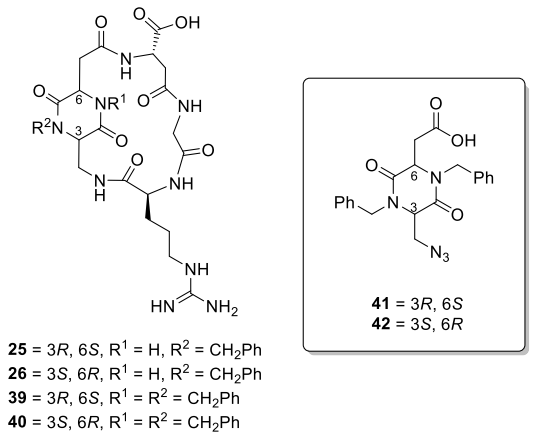

FIGURE 27. The library of *cyclo*[DKP-*iso*DGR] peptidomimetics and the DKP scaffold used in the synthesis of **33** and **34**.

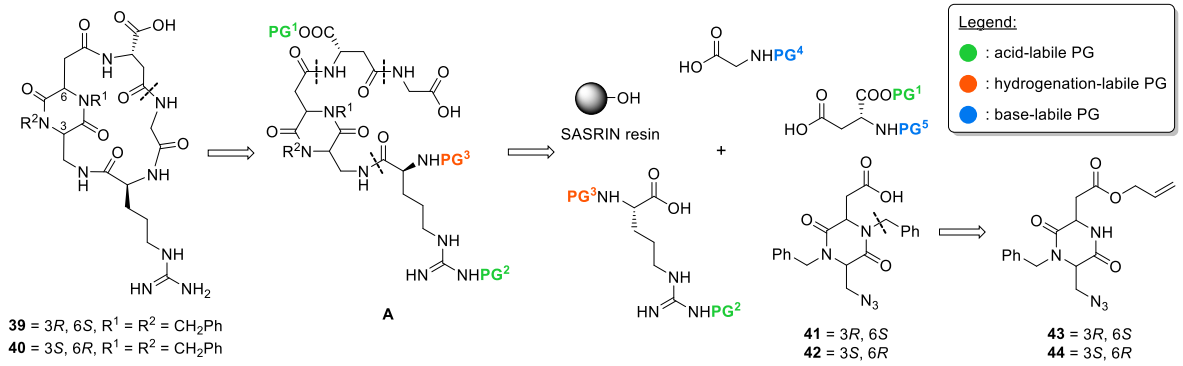

SCHEME 1. Retrosynthesis of compounds **39**-**40**.

We selected acid-labile *t*Bu and Mtr (Mtr = 4-Methoxy-2,3,6-trimethylbenzenesulphonyl) groups to protect the *iso*Asp (PG^1) and Arg (PG^2) side chains respectively, and carboxybenzyl-carbamate (Cbz) for the α-amino functionality of arginine (PG^3). Fluorenylmethyloxycarbonyl (Fmoc) was used for the base-labile PGs (PG^4 and PG^5). The synthesis of compounds **39**-**40** is shown in SCHEME 2 and started from connecting the glycine and the *iso*aspartate residues to the solid support. The carboxylic acid

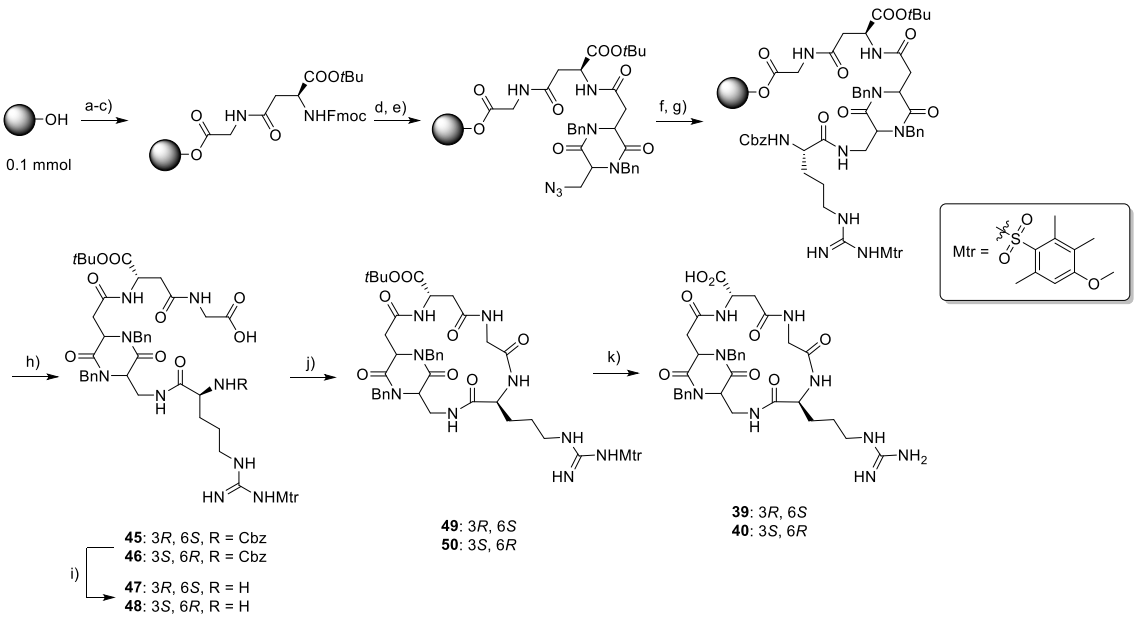

SCHEME 2. Reagents and conditions: a) Fmoc-Gly-OH, DIC, DMAP (cat.), DMF; b) 2% piperidine and 2% DBU in DMF; c) Fmoc-Asp(OH)-O*t*Bu, DIC, HOAt, DMF; d) 2% piperidine and 2% DBU in DMF; e) **41-42**, DIC, HOAt, DMF; f) PMe_3, dioxane/water 4:1, 20 min × 3 times; g) Cbz-Arg(Mtr)-OH, DIC, HOAt, DMF; h) 1% TFA in CH_2Cl_2, r.t., 5 min × 10 times, 71-81%; i) H_2, 10% Pd/C, THF/H_2O 1:1, 98%-quant.; j) HATU, HOAt, *i*Pr_2NEt, DMF (1.4 mM), 32%; k) TFA/thioanisole/EDT/anisole 90:5:3:2, 25-37%.

moiety was activated using condensing agents, such as *N,N'*-diisopropylcarbodiimide (DIC) and 1-hydroxy-7-azabenzotriazole (HOAt) in *N*,*N*-dimethylformamide (DMF). Subsequent treatment with a 2% solution of piperidine and 1,8-diazabicyclo[5.4.0]undec-7-ene (DBU) removed the Fmoc protecting group and liberated the amine moiety to couple in the next step (steps a-e). At this stage, a Staudinger reduction of the supported azide was carried out in the presence of PMe_3 (step f): the reaction completion was checked by subjecting few beads to the Kaiser test. The resulting free $–NH_2$ functionality was reacted with Cbz-Arg(Mtr)-OH (step g) and the linear compound was cleaved from the resin using 1% trifluoroacetic acid (TFA) solution in dichloromethane (step h). The very mild conditions for the cleavage reaction allowed to selectively obtain the free carboxylic acids **45-46** without deprotecting the *iso*aspartate side chain (bearing a *t*Bu ester moiety). Hydrogenolysis at room temperature on **45** and **46** (step i), catalyzed by 10% Pd/C, afforded the amino acids **47** and **48** that led to the cyclized protected compounds **49-50**, upon macrocyclization with HATU, HOAt and diisopropylethylamine in high dilution conditions (step j). At last, Mtr and *t*Bu ester protecting groups were removed in TFA using thioanisole, 1,2-ethanedithiol (EDT) and anisole as scavengers: the final peptidomimetics **39-40** were obtained as TFA salts after reverse-phase HPLC purification and freeze-drying from water. The preparation of DKP azido acids **41-42** necessary for the SPPS was carried out in two steps by further modification of the corresponding precursors **43-44**, already reported for the synthesis of *iso*DGR ligands **25-26** (SCHEME 3). The alkylation at the second nitrogen atom in the DKP ring of **43-44** was performed using benzyl bromide with potassium hexamethyldisilazide (KHMDS) as base at low temperature. The dibenzylated compounds **53-54** were treated with a catalytic amount of $[Pd(PPh_3)_4]$ in the

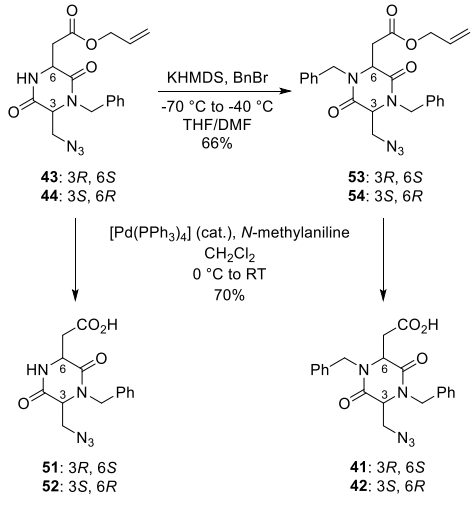

SCHEME 3. Preparation of scaffolds **41-42**.

presence of *N*-methylaniline to remove the allyl ester and to obtain the desired azido acids **41**-**42**. The choice of protecting groups and of the solid support is a key aspect of the synthesis. SASRIN resin was chosen because of such mild cleavage conditions (1% TFA in CH_2Cl_2) compatible with the presence of acid-labile protecting groups. Protection of the α-amino group of arginine with Cbz, (sensitive to catalytic hydrogenation) allowed for isolation and purification of the free carboxylic acid, after the cleavage from the beads, in order to continue the synthesis with a pure intermediate. Moreover, since the SPPS protocol relies on a large excess of reagents (up to 3-5 eq in comparison to the 1 eq of the resin), a Kaiser test should be performed after each coupling and Fmoc-removal steps, repeating the last operation whenever the test result was unsatisfactory.

2.1.2 BIOLOGICAL EVALUATION OF *CYCLO*[DKP-*ISO*DGR] PEPTIDOMIMETICS **39**-**40**

2.1.2.1 BINDING ASSAYS ON ISOLATED RECEPTOR

In collaboration with Dr. Daniela Arosio (CNR-ISTM, Milan), the new peptidomimetics **39** and **40** were tested *in vitro* to assess their affinity for isolated integrin receptors $\alpha_V\beta_3$ and $\alpha_V\beta_5$: the experimental IC_{50} values are presented in TABLE 6, where compounds **4**, **17**, **25** and **26** (entries 1-4) are reported as references.

TABLE 6. Evaluation of the binding affinity of compounds **39**-**40** on isolated receptor.

Entry	Compound	Structure	IC_{50} (nM)[a]	
			$\alpha_V\beta_3$	$\alpha_V\beta_5$
1	**4**	Cilengitide	0.6 ± 0.1[b]	11.7 ± 1.5[b]
2	**17**	*cyclo*[DKP3-RGD]	4.5 ± 1.1	149 ± 25
3	**25**	*cyclo*[DKP2-*iso*DGR]	46.7 ± 18.2	220 ± 84
4	**26**	*cyclo*[DKP3-*iso*DGR]	9.2 ± 1.1	312 ± 21
5	**39**	*cyclo*[DKP5-*iso*DGR]	490 ± 77	9100 ± 800
6	**40**	*cyclo*[DKP7-*iso*DGR]	255 ± 140	5100 ± 400

[a] IC_{50} values were calculated as the concentration of compound required for 50% inhibition of biotinylated vitronectin binding. Screening assays were performed by incubating the immobilized integrins $\alpha_V\beta_3$ and $\alpha_V\beta_5$ with increasing concentrations (10^{-12} – 10^{-5} M) of the RGD or *iso*DGR ligands in the presence of biotinylated vitronectin (1 mg/mL), and measuring the concentration of bound vitronectin in the presence of the competitive ligands, see ref. 46. [b] Calculated as the concentration of compound required for 50% inhibition of biotinylated vitronectin binding, see ref. 20.

The *iso*DGR-based peptidomimetics (entries 3-6) showed a range of affinity for target integrin receptor from low nanomolar to submicromolar concentrations: the data reported in TABLE 6 pointed out how the conformational behaviour of *cyclo*[DKP-*iso*DGR] compounds is strictly dependent on the structure of the diketopiperazine scaffold. This trend is peculiar of this class of peptidomimetics, since it was not observed with the corresponding RGD ligands (see TABLE 1, PARAGRAPH I – 1.3). In comparison with the already reported ligands **25**-**26**, the newly synthesized *cyclo*[DKP5-*iso*DGR] **39** and *cyclo*[DKP7-*iso*DGR] **40** showed lower integrin affinities.

2.1.2.2 INHIBITION OF INTEGRIN-MEDIATED SIGNALING

Among the peptidomimetics synthesized in our group, *cyclo*[DKP3-*iso*DGR] **26** represents the most potent *iso*DGR integrin binder and, for this reason, in collaboration with Dr. Mayra Paolillo (Università degli Studi di Pavia, Pavia), **26** was further investigated *in vitro*, together with the RGD ligand *cyclo*[DKP3-RGD] **17**. In this way, a direct comparison between **17** and **26**, containing the same DKP3 scaffold and possessing similar IC_{50} values on isolated $\alpha_V\beta_3$ receptor, was established by evaluating their effects on different cellular functions of U373 glioblastoma cells.

The focal adhesion kinase (FAK) is a tyrosine kinase located in the cytoplasm and plays an essential role in cell motility, survival, and proliferation exploiting a variety of mechanisms. FAK exerts its

biological ativity by associating with membrane receptors and with specific protein complexes in the nucleus. Cell binding to ECM proteins triggers the formation of integrin clusters that, in turn, promotes the activation of FAK: this phenomenon is essential for tumor growth, progression and metastasis, and leads to the association of FAK with Src (FIGURE 28).[47] This complex is responsible for the subsequent signalling cascade of Akt, an intracellular kinase related to cell survival and strictly regulated by integrin receptors.

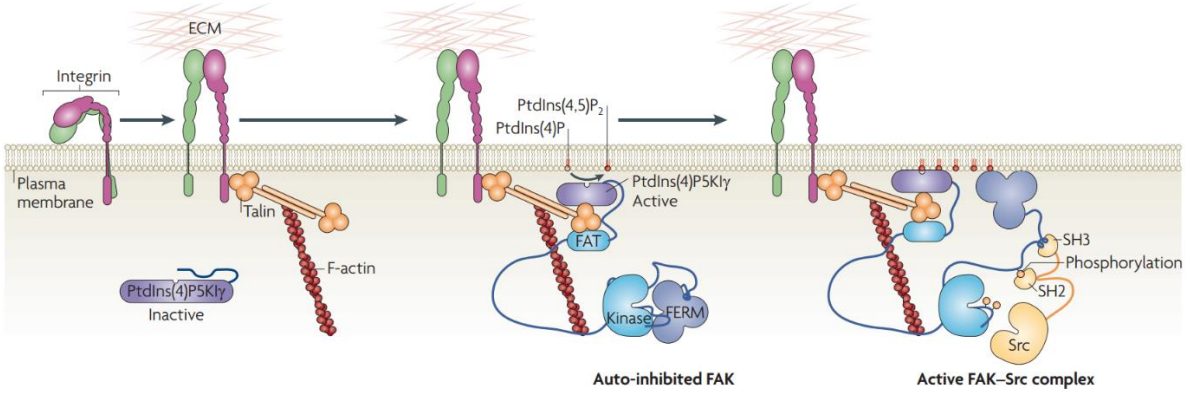

FIGURE 28. Integrin interactions with ECM recruite focal adhesion proteins, *e.g.* talin, FAK., and trigger FAK activation and FAK-Src complex formation. Adapted from ref. 47b.

For these reasons, both FAK and Akt were considered as appropriate integrin-dependent effectors in order to evaluate the acivity of *cyclo*[DKP3-RGD] (**17**) and *cyclo*[DKP3-*iso*DGR] (**26**) on the integrin transduction pathway. Notably, compounds **17** and **26** were found able to prevent the phosphorylation of FAK and Akt, displaying inhibitory effects on cell infiltration processes mediated by integrin receptors (FIGURE 29): these experimental data qualify **17** and **26** as integrin antagonists.

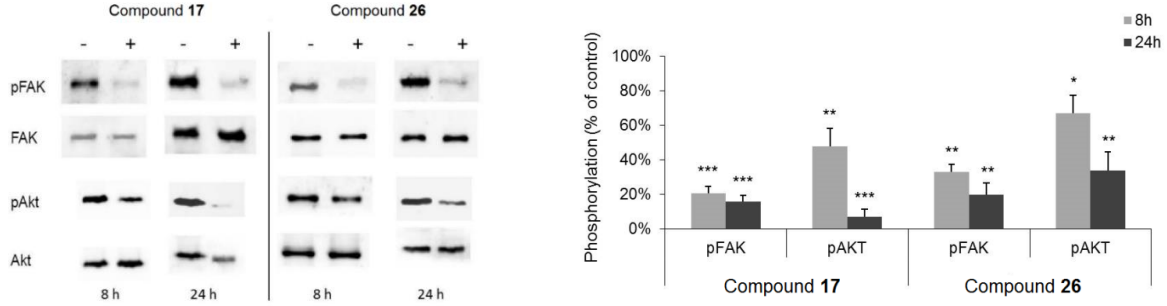

FIGURE 29. Inhibition of FAK and Akt phosphorylation upon treatment with **17** or **26** (+) for 8 and 24 hours. Adapted from ref. 46.

After 24 hours the decrease in phosphorylated protein content was clearly evident in comparison with the control experiment. Concerning *cyclo*[DKP3-RGD], these results are coherent with the remarkable anti-angiogenic activity already observed when treating HUVE cells with **17** in the presence of angiogenesis promoters.[28] As far as we know about *iso*DGR motif and related ligands, *cyclo*[DKP3-*iso*DGR] **26** represents the first compound in this field that was investigated and assessed as inhibitor of FAK/Akt signalling and of integrin-mediated infiltration processes.

2.2 *ISO*DGR-BASED SMDCS

In view of the very interesting biological results mentioned in the previous paragraph, we decided to explore further the field *iso*DGR peptidomimetics and to continue the comparison between RGD and *iso*DGR recognition motifs. In PARAGRAPH I – 1.5, it has been already shown how RGD compounds can effect drug turgeting to tumors. In particular, the SMDC *cyclo*[DKP3-RGD]-Val-Ala-PTX (**31**) was

shown to be able to deliver selectively (S = 66.9 and TI = 9.0 in TABLE 4) the cytotoxic agent paclitaxel, discriminating two cell lines expressing integrin $\alpha_V\beta_3$ at different levels. Prompted by these encouraging results, we planned to synthesize an *iso*DGR analog of **31**, namely *cyclo*[DKP3-*iso*DGR]-Val-Ala-PTX (**55**, FIGURE 30), and to investigate its biological activity.

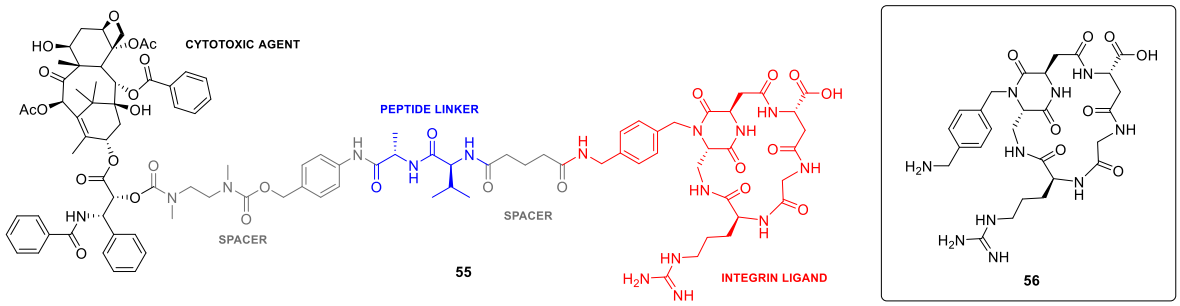

FIGURE 30. Structure of *cyclo*[DKP3-*iso*DGR]-Val-Ala-PTX **55** and of *cyclo*[DKP3-*iso*DGR]-CH_2NH_2 peptidomimetic **56**.

2.2.1 SYNTHESIS *CYCLO*[DKP-*ISO*DGR]-CH_2NH_2 PEPTIDOMIMETIC **56**

In order to conjugate paclitaxel (or any other molecular entity) to *cyclo*[DKP-*iso*DGR] ligand, we had to synthesize a peptidomimetic containing the *iso*DGR sequence and a proper handle, namely *cyclo*[DKP3-*iso*DGR]-CH_2NH_2 (**56**, FIGURE 30). Contrary to compounds **25**-**26** and **39**-**40**, we envisaged a new synthetic plan, exploiting a solution-phase approach to limit the wastefulness of valuable compounds (*e.g.* the DKP scaffold) and to pave the way for a future scale up. For this reason, we revised the retrosynthetic analysis of **56** (SCHEME 4). Compound **56** derives from intermediate **A** by removing protecting groups 1, 4 and 5 (PG^1, PG^4 and PG^5) and opening the macrocycle. In turn, **A** can be obtained following two different strategies, the retrosynthetic plans A and B shown in SCHEME 4. The pathways are straightforward and differ only in the disconnection sequence (dipeptide first, in plan A, or arginine first, in plan B). In any case, the precursors are the same and consist of glycinate ester, α,α-diprotected aspartate and an already published DKP scaffold (used as either Boc- or azide-protected amine). While reversing the retrosynthetic analyses to the corresponding synthetic schemes (SCHEME 5), the use of three classes of orthogonal protecting groups was required. In particular, acid-labile protecting groups are in green (PG^1 = *t*Bu ester, PG^4 = PG^5 = Mtr), hydrogenation-labile groups in orange (PG^2 = benzyl ester, PG^3 = Cbz) and base-labile groups in cyan (PG^6 = Fmoc).

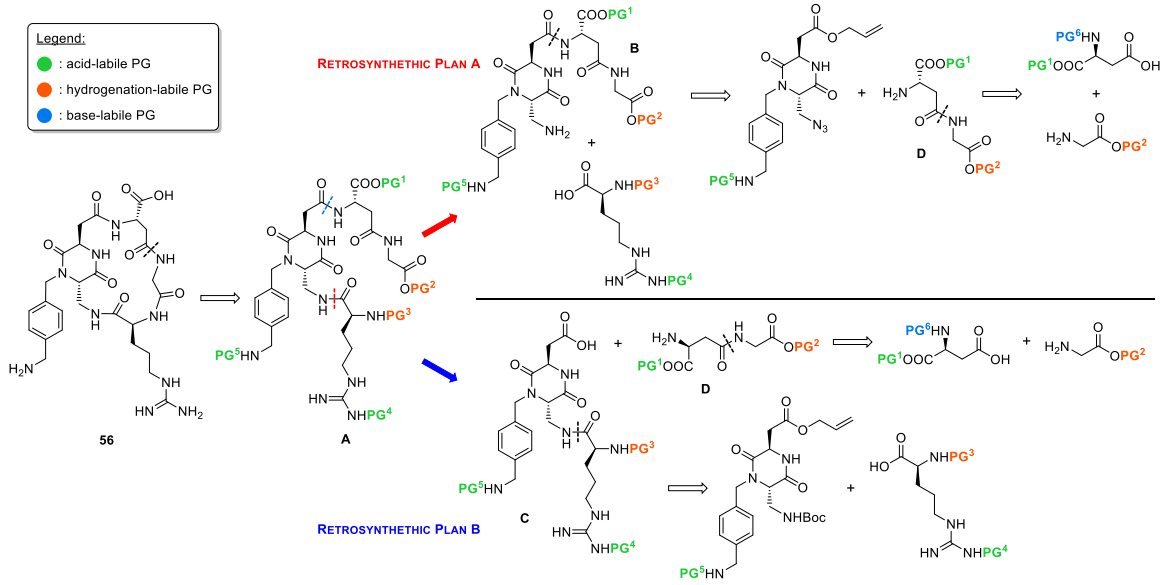

SCHEME 4. Retrosynthetic analysis of *cyclo*[DKP3-*iso*DGR]-CH_2NH_2 peptidomimetic (**56**). Protecting groups in different colors are orthogonal.

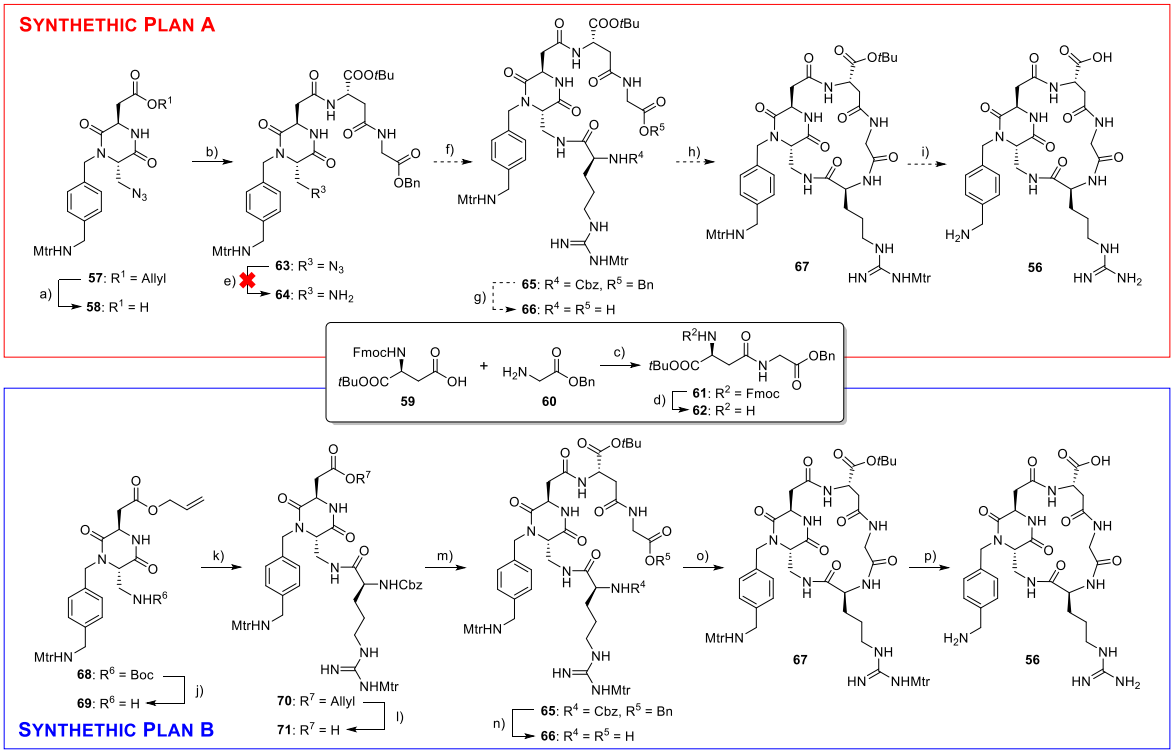

SCHEME 5. Synthesis of peptidomimetic **56**. Reagents and conditions. Synthetic plan A: a) [Pd(PPh$_3$)$_4$], *N*-Methylaniline, CH_2Cl_2, 0 °C, 1 h, 84%; b) **62**, HATU, HOAt, *i*Pr$_2$NEt, DMF, 0 °C to r.t., overnight, 67%; c) HATU, HOAt, *i*Pr$_2$NEt, DMF, 0 °C to r.t., overnight, 86%; d) piperidine, DMF, 2 h, r.t., 67%; e) PMe_3 in toluene, H_2O, THF, 5 h; f) Cbz-Arg(Mtr)-OH, HATU, HOAt, *i*Pr$_2$NEt, DMF, 0 °C to r.t., overnight; g) H_2, 10% Pd/C, THF/H_2O 1:1, overnight, r.t.; h) HATU, HOAt, *i*Pr$_2$NEt, DMF/$CH_2Cl_2$1:1 (1.4 mM), 0 °C to r.t., overnight; i) TFA/TMSBr/thioanisole/EDT/phenol 70:14:10:5:1, 2 h, r.t. Synthetic plan B: j) TFA, CH_2Cl_2, r.t., 2 h; k) Cbz-Arg(Mtr)-OH, HATU, HOAt, *i*Pr$_2$NEt, DMF, 0 °C to r.t., overnight, 94% over 2 steps; l) [Pd(PPh$_3$)$_4$], *N*-Methylaniline, CH_2Cl_2, 0 °C, 1 h, 88%; m) **62**, HATU, HOAt, *i*Pr$_2$NEt, DMF, 0 °C to r.t., overnight, 95%; n) H_2, 10% Pd/C, THF/H_2O 1:1, overnight, r.t., 95%; o) HATU, HOAt, *i*Pr$_2$NEt, DMF/CH_2Cl_2 1:1 (1.4 mM), 0 °C to r.t., overnight, 79%; p) TFA/TMSBr/thioanisole/EDT/phenol 70:14:10:5:1, 2 h, r.t., 47%.

The synthesis of *iso*DGR peptidomimetic **56** started with the preparation of amine **62** by simple coupling reaction of Fmoc-Asp(OH)-OAllyl **59** and glycine benzyl ester **60** (step c) and Fmoc-deprotection of the corresponding dipeptide **61** (step d) in the presence of piperidine in DMF. Interestingly, compound **62** was easily purified by flash chromatography (FC) on silica gel after workup of the reaction mixture with ethyl acetate/sat. aq. $NaHCO_3$. As matter of fact, the crude amine compound was tested in coupling reaction with Fmoc-Phe-OH as model carboxylic acid, without obtaining the desired amide product (results not shown). With **62** in our hands, we first investigated the feasibility of synthetic plan A and managed to obtain azide **63**: the allyl ester in **57** (synthesized according to the previously reported procedure)[40] was cleaved (step a) and the resulting carboxylic acid **58** was coupled with amine **62** (step b). However, the Staudinger reduction on **63** (step e) led to a complex mixture, in which the presence of the desired amine **64** was not detected by mass spectrometry analysis (results not shown). Catalytic hydrogenation on **63** was not considered as an alternative, as it would have removed the benzyl ester moiety on glycine residue. Hence, we decided to focus on the different synthetic plan B. The starting material **68**, as well as **57**, is an intermediate of *cyclo*[DKP3-RGD]-CH_2NH_2 (**30**) and is obtained from **57** by one pot reduction and Boc-protection using PMe_3 and 2-(Boc-oxyimino)-2-phenylacetonitrile (Boc-ON) in tetrahydrofuran (THF). The transformation of **57** into **68** was achieved in very good yields (76-88%).[40] This strategy was preferred to the direct Staudinger reduction on azide **57** because of the easy purification of protected compound **68** by flash chromatography and the quantitative yield of a reliable reaction such as the subsequent Boc-deprotection. Indeed, treating **68** with TFA in dichloromethane (step j) afforded the corresponding free amine **69** as trifluoroacetate salt that reacted with Cbz-Arg(Mtr)-OH (step k) forming compound **70** in 94% yield after two steps. A catalytic amount

of [Pd(PPh$_3$)$_4$] in the presence of an amine nucleophile, *i.e. N*-methylaniline, effected the allyl ester removal on **70** (step l), leaving the Cbz-protecting group on the α-amino functionality of arginine untouched and affording carboxylic acid **71**. The subsequent amide coupling with dipeptide **62** (step m) furnished the linear, protected compound **65** in high yields (95%). Palladium-catalyzed hydrogenation of **65** in THF/H_2O (step n) removed simultaneously both the carboxybenzyl-carbamate and the benzyl ester from arginine and glycine residues, respectively. The resulting linear amino acid **66** was treated with HATU, HOAt and *i*Pr$_2$NEt under high dilution conditions (1.4 mM in 1:1 DMF/CH_2Cl_2, step o) to favor the intramolecular macrocyclization. The final deprotection of **67** (step p) was carried out in TFA with trimethylsilylbromide (TMSBr), thioanisole, EDT and phenol as scavengers. The trifluoroacetate salt of the desired cyclic peptidomimetic **56** was obtained in modest yields (47%), after reverse-phase HPLC and freeze-drying from water. To the best of our knowledge, *cyclo*[DKP3-*iso*DGR]-CH_2NH_2 (**56**) is the first *iso*DGR peptidomimetic entirely synthesized in solution-phase.

2.2.2 SYNTHESIS *CYCLO*[DKP-*ISO*DGR]-VAL-ALA-PTX PRODRUG **55**

The next step was the conjugation of compound **56** to paclitaxel (PTX, **27**) through a smart linker system able to release the cytotoxic agent selectively at the tumor site. As depicted in FIGURE 30, we planned the synthesis of *cyclo*[DKP3-*iso*DGR]-Val-Ala-PTX **55** to establish a comparison with the corresponding RGD prodrug *cyclo*[DKP3-RGD]-Val-Ala-PTX (**31**, FIGURE 24, PARAGRAPH I – 1.5). Thus, we exploited the same retrosynthesis used for **31**: SCHEME 6 shows how **55** can be obtained starting from peptidomimetic **56**, peptide linker **A** and paclitaxel (**27**).

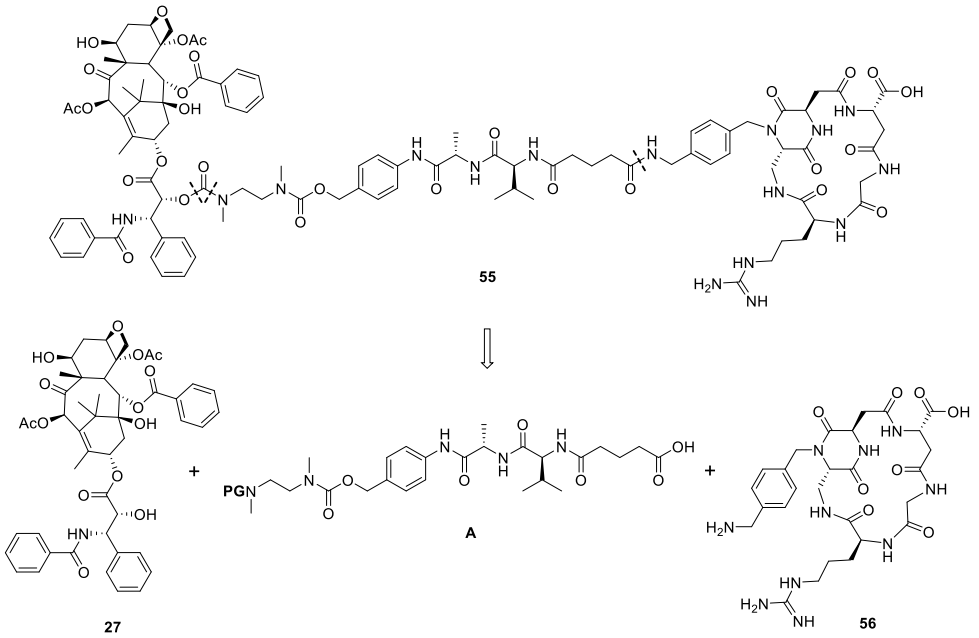

SCHEME 6. Retrosynthetic analysis of *cyclo*[DKP3-*iso*DGR]-Val-Ala-PTX prodrug (**55**).

The retrosynthesis of linker **A** is shown in SCHEME 7. The carboxylic acid **A** derives from glutaric anhydride and intermediate **B**, after removing protecting group 2 (PG^2) at the valine nitrogen atom. In turn, **B** can be cut at the carbamate level, revealing the benzyl alcohol derivative **C** and the mono-protected diamine **D**. Retro-amide coupling on **C** affords 4-aminobenzyl alcohol and dipeptide **E**, which is obtained starting from L-alanine and nitrogen-protected L-valine.

The retrosynthetic approach shown in SCHEME 7 was applied to the synthesis of peptide linker **72** (compound **A** with PG^1 = Boc, SCHEME 8).[25a] We chose Boc and Fmoc as protecting groups 1 and 2, respectively. Fmoc-valine **73** was activated with *N,N'*-dicyclohexylcarbodiimide (DCC) and *N*-hydroxysuccinimide (NHS) in THF, affording the corresponding activated ester (step a1) that was

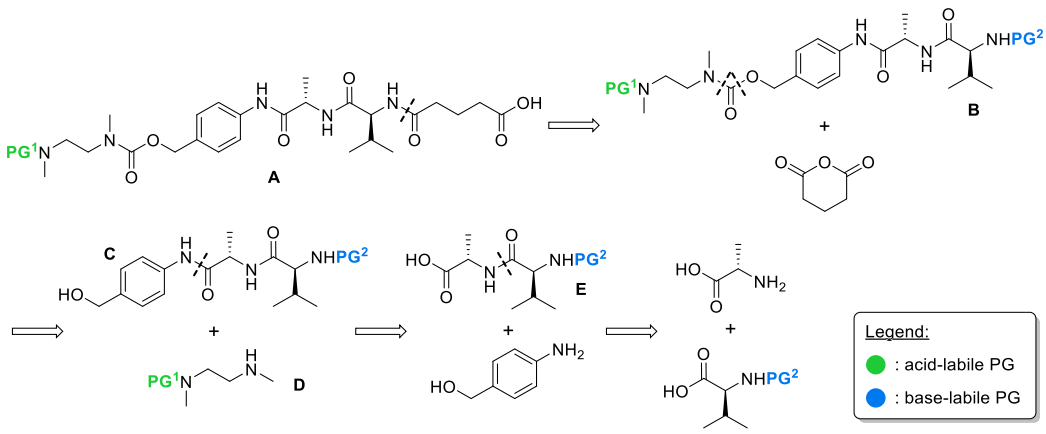

SCHEME 7. Retrosynthetic analysis of peptide linker **A**.

reacted with L-alanine in the presence of sodium hydrogencarbonate as base in THF/H_2O (step a2). In this way, dipeptide **74** was obtained in modest yields (47%): subsequent optimization of the reaction conditions, which consisted in longer reaction time, allowed the isolation of the desired product in higher yields (results not shown). The next coupling was effected pre-activating the carboxylic acid **74** with 2-ethoxy-1-ethoxycarbonyl-1,2-dihydroquinoline (EEDQ) in dichloromethane/methanol: the activated ester formed *in situ* was directly reacted with 4-aminobenzyl alcohol affording compound **75** in 65% yield (step b). Carbonate **76** was prepared by reacting benzyl alcohol **75** with 4-nitrophenylchloroformate in the presence of a base (step c). The reaction between **76** and *N*-(Boc)-*N*,*N'*-dimethylethylenediamine (**78**), which was synthesized according to previously reported procedures (step f),[48] smoothly gave the protected carbamate **79** (step d). Conversion of **79** into the corresponding amine upon treatment with piperidine (step e1) and the subsequent opening of glutaric anhydride furnished the desired peptide linker **72** (step e2).

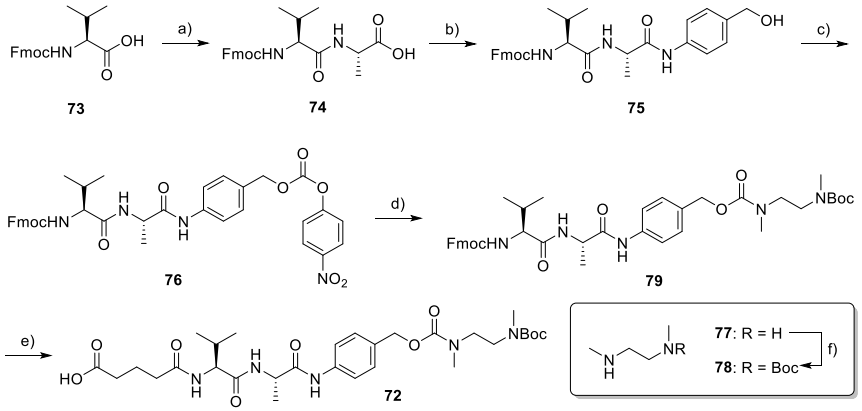

SCHEME 8. Synthesis of peptide linker **72**. Reagents and conditions. a) 1. DCC, NHS, THF, r.t.; 2. L-alanine, $NaHCO_3$, THF/H_2O (1:1), r.t., 1 h, 47%; b) 4-aminobenzyl alcohol, EEDQ, CH_2Cl_2/MeOH (2:1), r.t., overnight, 65%; c) 4-nitrophenylchloroformate, pyridine, THF, r.t., 4 h, 88%, d) **78**, *i*Pr_2NEt, THF, r.t., overnight, 91%; e) 1. piperidine, DMF, 0 °C to r.t., 2 h; 2. glutaric anhydride, DMAP, *i*Pr_2NEt, DMF, 0 °C to r.t., overnight, 77%; f) Boc_2O, CH_2Cl_2, 0 °C to r.t., overnight, 91%. The synthesis was performed according to ref. 25a.

The next step was the coupling reaction of **56** with **72** (SCHEME 9). The carboxylic acid of the linker was first activated as *N*-hydroxysuccinimidyl ester (**80**, step a), then reacted with the *iso*DGR peptidomimetic using a procedure well-established in our group (step b). The conjugation was performed in phosphate buffer solution (PBS) and acetonitrile controlling the acidity of the reaction medium: pH was set around 7.5 by addition of aliquots of sodium hydroxide over the reaction time. Indeed, in acidic conditions, the benzyl amine **56** is protonated and cannot act as nucleophile towards

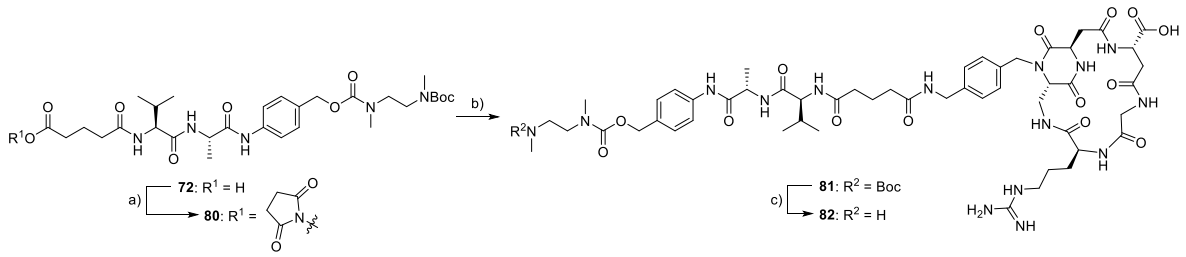

SCHEME 9. Synthesis of *iso*DGR derivative **82**. Reagents and conditions. a) NHS, EDC·HCl, DMF, 0 °C to r.t., overnight; b) **56**, PBS/CH_3CN, pH 7.5, 0 °C to r.t., overnight; c) TFA, CH_2Cl_2, r.t., 1 h, 55% over three steps.

the electrophile **80**. However, in basic conditions, the hydrolysis of the activated ester **80** becomes competitive, leading to the starting material **72** as dead end. The reaction mixture was concentrated under high vacuum, then the residue was dissolved in the minimum amount of acetonitrile and precipitated with diethyl ether: the solid precipitate was collected and identified as **72**. The crude compound **81** was directly deprotected from Boc-carbamate, affording the free amine **82** as trifluoroacetate salt after reverse-phase HPLC and freeze-drying from water.The last fragment to synthesize before starting the assembly of the final conjugate **55** was a suitable activated derivative of paclitaxel. In particular, the cytotoxic agent had to be made reactive only at the 2'-position. Indeed, the three hydroxy groups at the positions 1, 7 and 2' are different in terms of reactivity, considering, first of all, that the alcohol functionality at position 1 is tertiary and thus less reactive (SCHEME 10). Both the –OH functions at positions 7 and 2' are secondary, but the methyl group on the quaternary C8 hinders the hydroxy group on the adjacent C7. For this reason, a careful control of reaction conditions can result in a regioselective functionalization of the 2'-hydroxy moiety. To carry out the conjugation of **82** to paclitaxel, **27** was reacted with 4-nitrophenylchloroformate in the presence of pyridine in CH_2Cl_2 at low temperature, affording carbonate **83** (SCHEME 10).

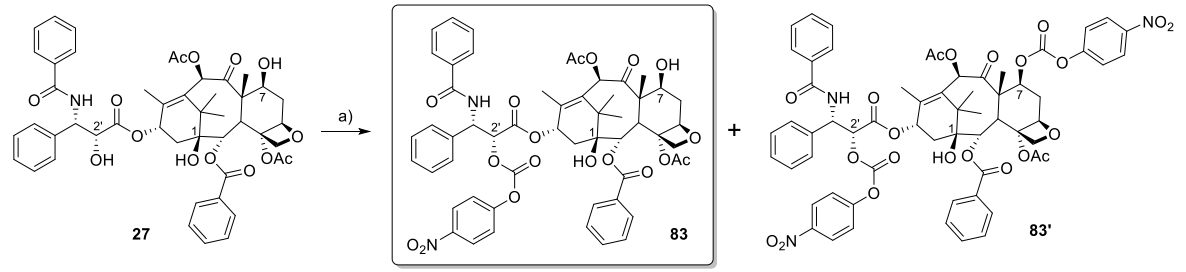

SCHEME 10. Synthesis of paclitaxel derivative **83**. Reagents and conditions. a) 4-nitrophenylchloroformate, pyridine, CH_2Cl_2, -50 °C to -20 °C, 4 h, 84% based on recovered starting material. The synthesis was performed according to ref. 25a.

The activation reaction was checked by thin-layer chromatography (TLC), monitoring the formation of the product: since we did not manage to achieve full conversion of paclitaxel into the desired carbonate, we tried to perform the reaction at -20 °C for times longer than 4 hours. However, already after 2 hours, a third spot appeared on the TLC: this compound was less polar and bearing a larger chromophore system, since it had a higher retention factor (R_f) and it was more UV visible. These observations suggested the formation of byproduct **83'**, deriving from the double activation of paclitaxel on both 2'- and 7-position. This hypothesis was coherent with the fact that, when treated with ceric ammonium molibdate solution, this compound was stained to a smaller extent with respect to the spot of the desired product **83** (*i.e.* more hydroxyl groups were available in **83**). A simple flash chromatography on silica gel allowed the isolation of the byproduct **83'** (identified by MS, data not shown), the desired product **83**, and the unreacted starting material **27**, which was subsequently recycled to prepare a new batch of activated paclitaxel. The final conjugation step of **82** to paclitaxel derivative **83** was performed in DMF

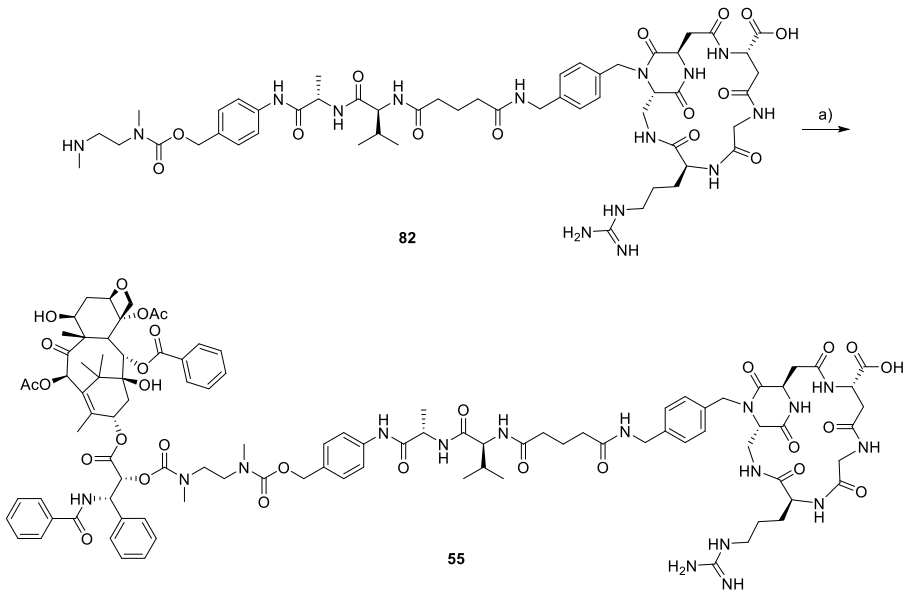

SCHEME 11. Synthesis of conjugate **55**. Reagents and conditions. a) **83**, *i*Pr$_2$NEt, DMF, 0 °C to r.t., overnight, 52%.

with diisopropylethylamine as base to deprotonate the trifluoroacetate salt (SCHEME 11, step a). Over the time, the reaction mixture changed from colorless and transparent to bright yellow due to the release of 4-nitrophenol, an evidence that reaction was taking place. The work-up was straightforward and consisted in solvent evaporation, dissolution of the crude residue with water/acetonitrile and centrifugation to remove the precipitate: the supernatant was purified using reverse-phase HPLC. The desired conjugate **55** was identified by MS analysis, isolated and freeze-dried from water as trifluoroacetate salt. It is worth to mention that **55** represents the first *iso*DGR peptidomimetic-drug conjugate, especially because of the aforementioned difficulty in synthesizing *iso*DGR-containing ligands possessing low IC_{50} values towards integrin receptors.

2.2.3 BIOLOGICAL EVALUATION OF *CYCLO*[DKP-*ISO*DGR]-VAL-ALA-PTX PRODRUG **55**

2.2.3.1 BINDING ASSAYS ON ISOLATED RECEPTOR

As preliminary evaluation of the activity of conjugate **55**, *in vitro* binding assays on purified integrin $\alpha_V\beta_3$ (TABLE 7) were run in house by Dr. Arosio. The simple ligands *cyclo*[DKP3-RGD] **17** and *cyclo*[DKP3-*iso*DGR] **26**, as well as the RGD conjugate analog **31** are reported as reference compounds. Despite the increased hindrance around the *iso*DGR portion, *cyclo*[DKP-*iso*DGR]-Val-Ala-PTX **55** maintained a remarkable ability to target the integrin receptor, comparable to those both of the parental *iso*DGR ligand (entry 2) and of the related RGD-conjugate (entry 3).

TABLE 7. Evaluation of the binding affinity of compound **55** on isolated receptor.

Entry	Compound	Structure	IC_{50} (nM)[a]	
			$\alpha_V\beta_3$	$\alpha_V\beta_5$
1	**17**	*cyclo*[DKP3-RGD]	4.5 ± 1.1	149 ± 25
2	**26**	*cyclo*[DKP3-*iso*DGR]	9.2 ± 1.1	312 ± 21
3	**31**	*cyclo*[DKP3-RGD]-Val-Ala-PTX	13.3 ± 3.6[b]	924 ± 290[b]
4	**55**	*cyclo*[DKP3-*iso*DGR]-Val-Ala-PTX	11.0 ± 0.2	n.d.

[a] IC_{50} values were calculated as the concentration of compound required for 50% inhibition of biotinylated vitronectin binding. Screening assays were performed by incubating the immobilized integrins $\alpha_V\beta_3$ and $\alpha_V\beta_5$ with increasing concentrations (10^{-12} – 10^{-5} M) of the RGD or *iso*DGR ligands in the presence of biotinylated vitronectin (1 mg/mL), and measuring the concentration of bound vitronectin in the presence of the competitive ligands. [b] See ref. 25a.

This experimental evidence stimulated us to investigate further the biological activity of the newly synthesized prodrug and, in particular, to determine its ability to deliver selectively the payload to cancer

cells. For this reason, in collaboration with Nerviano Medical Science (NMS, Nerviano) we subjected **55** to a number of different *in vitro* tests: in the next paragraph, preliminary results of anti-proliferation analysis are reported, while lysosome extract digestion and stability assays are currently ongoing. These biological characterizations will allow to establish a direct comparison between the RGD and the *iso*DGR ability to target tumors, adding further data to those shown in PARAGRAPH I – 2.1.2.

2.2.3.2 ANTI-PROLIFERATIVE ASSAYS

In collaboration with Dr. Fabio Gasparri (Nerviano Medical Sciences s.r.l., Nerviano), the targeting ability of the newly synthesized *cyclo*[DKP3-*iso*DGR]-Val-Ala-PTX conjugate (**55**) was assessed by *in vitro* anti-proliferative assays. In order to carry out this test, U87 human glioblastoma cells were first selected as integrin $\alpha_V\beta_3$-expressing cell line, then used to generate the corresponding clone U87 β_3-KO, in which the expression of the gene encoding for the β_3 integrin subunit was deleted using CRISPR-Cas9 gene editing technology.[49] Immunofluorescence studies on this set of cell lines are shown in FIGURE 31 and demonstrated the complete knock-out of β_3 integrins in U87 β_3-KO. Moreover, the presence of integrin $\alpha_V\beta_5$ was checked, confirming that the CRISP-Cas9 technique selectively silenced only the target β_3 gene, without affecting the expression of other α_V integrins.

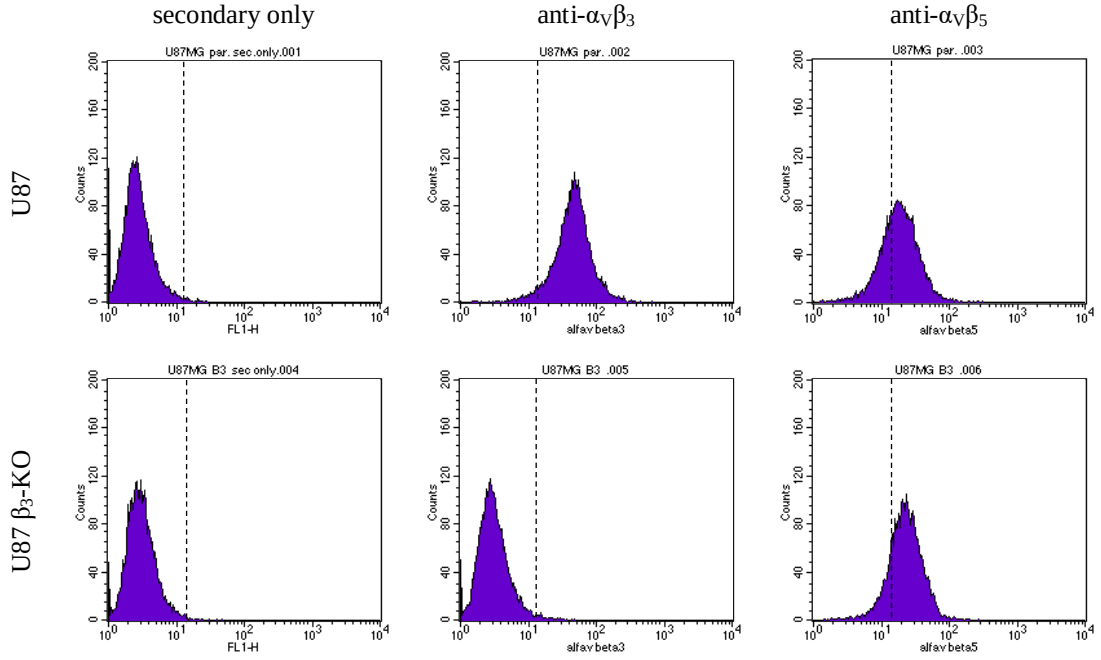

FIGURE 31. Immunofluorescence experiments on U87 and U87 β_3-KO cells to assess the different $\alpha_V\beta_3$ integrin expression.

With this cellular model in our hands, we proceeded evaluating the biological activity of prodrug **55**. Cells were incubated with increasing doses of *cyclo*[DKP3-*iso*DGR]-Val-Ala-PTX for 144 h (TABLE 8), before measuring the cell viability in the culture. Parallel experiments were performed following the same protocol and testing either the reference compound *cyclo*[DKP3-RGD]-Val-Ala-PTX (**31**) or the free drug paclitaxel (**27**). As previously observed (see TABLE 4, ref. 25a), paclitaxel itself showed a remarkable intrinsic selectivity towards, in this case, the non $\alpha_V\beta_3$-expressing clone U87 β_3-KO: for this reason, the *S* values of both the tested conjugates **31** and **55** were normalized and the experimental TI were obtained. Unexpectedly, the reference prodrug **31** proved not to work properly with the current biological system (TI = 0.3), but, on the other hand, compound **55** was able to target the parental U87 cell line ($\alpha_V\beta_3$ +) *ca.* 26 times more efficiently (TI = 8.0) than **31**.

TABLE 8. Evaluation of anti-proliferative activity of compound **55** *in vitro*.

Compound	Structure	IC_{50} (nM)[a]		*S*[b]	TI[c]
		U87 β_3-KO ($\alpha_V\beta_3$ –)	U87 ($\alpha_V\beta_3$ +)		
27	Paclitaxel	2.5 ± 0.3	39.5 ± 7.1	0.06	1
31	*cyclo*[DKP3-RGD]-Val-Ala-PTX	184.9 ± 176.3	9416.3 ± 655.6	0.02	0.3
55	*cyclo*[DKP3-*iso*DGR]-Val-Ala-PTX	409.5 ± 68.4	861.7 ± 215.2	0.48	8.0

[a] IC_{50} values were calculated as the concentration of compound required for 50% inhibition of cell viability in culture, based on quantitation of the ATP present as estimated by CellTiter-GLO; cells were treated for 144 h in U-bottomed 96-well plates. [b] Selectivity (*S*): IC_{50} ($\alpha_V\beta_3$ –)/IC_{50} ($\alpha_V\beta_3$ +). [c] Targeting index (TI): selectivity/selectivity observed with free paclitaxel.

These results can be rationalized taking into account that the CRISPR-Cas9 gene editing manipulation left untouched a variety of integrin receptors (*e.g.* $\alpha_V\beta_5$, $\alpha_V\beta_5$, $\alpha_5\beta_1$) able to interact with both **31** and **55**. However, due to the different structural properties of the RGD and *iso*DGR recognition sequences, ligands based on either the former or the latter motif interact with other integrins displaying different binding affinity, which could eventually explain the difference in biological activity of **31** and **55** against the U87/U87 β_3-KO cellular model. These preliminary results emphasize the central role of the biological system chosen to test and compare the synthesized compounds. The very different activity shown by *cyclo*[DKP3-RGD]-Val-Ala-PTX (**31**) first on CCRF-CEM (TABLE 4), then on U87 (TABLE 8) further prompted us to prepare a chemical tool as negative control in biological investigations (see PARAGRAPH I – 1.6 and PARAGRAPH I – 2.4).

2.3 CYCLIC *ISO*DGR PEPTIDES

2.3.1 SYNTHESIS OF *CYCLO*[G*ISO*DGRF] **84**

In the frame of *iso*DGR integrin ligands, I collaborated with Cristina Paissoni, a PhD student in Industrial Chemistry (R10582) working under the supervision of Dr. Giovanna Musco (Ospedale San Raffaele, Milano) and Prof. Laura Belvisi (Università degli Studi di Milano, Milano). Cristina worked on the development of computational methods to design new potent integrin ligands containing the *iso*DGR motif or related sequences. During my PhD, I synthesized the compound *cyclo*[G*iso*dGRf] (**84**, FIGURE 32), one of the most promising cyclic peptides resulting from theoretical calculations, to validate with experimental results the *in silico* method developed by Cristina. Compound **84** is a cyclic peptide readily accessible by solid-phase peptide synthesis using suitably protected amino acid building blocks (SCHEME 12). From a retrosynthetic point of view, macrocycle opening of **84** can be effected at each of the five amide bonds, but only the two choices depicted in SCHEME 12 will lead to primary, linear carboxylic acids, namely **A** and **B**. During the intramolecular cyclization, these intermediates (**A** and **B**) will not suffer from epimerization and should be more reactive in comparison with the other α-substituted amino acid residues present in the molecule (*i.e.* D-phenylalanine, arginine). Between the two retrosynthetic strategies, plan B is more appealing than plan A, as both the amine and the carboxylic acid moieties in **B** are primary. For this reason, we planned the synthesis of **84** as shown in SCHEME 13. The same color code used in the previous schemes is maintained, thus acid-labile protecting groups are in green (PG^1 = *t*Bu, PG^3 = Pbf, where Pbf = 2,2,4,6,7-pentamethyldihydrobenzofuran-5-sulfonyl), base-labile groups in cyan (PG^4 = PG^5 = PG^6 = Fmoc), and hydrogenation-labile groups in orange (PG^2 = Cbz). In the latter case, we preferred to use the

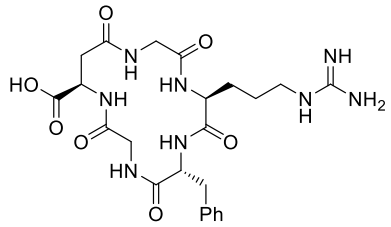

84

FIGURE 32. Retrosynthesis of cyclic peptide **84**.

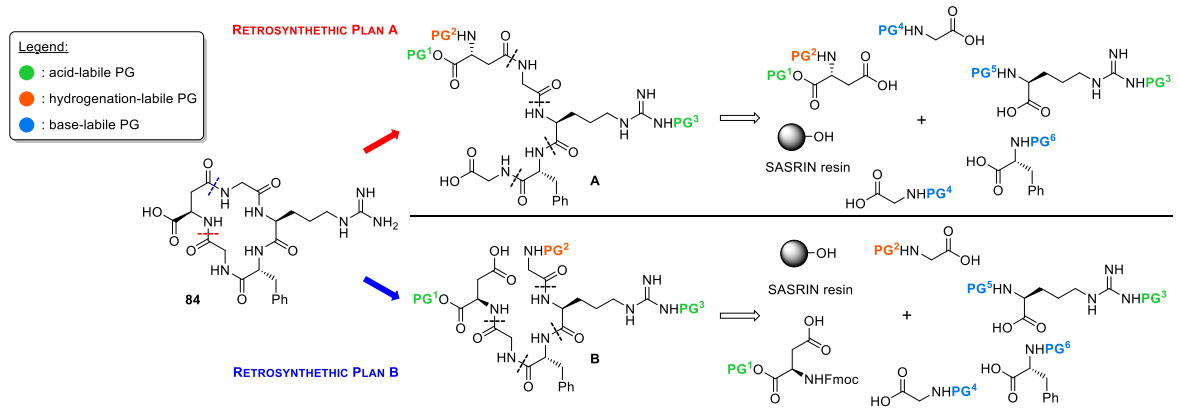

SCHEME 12. Retrosynthesis of cyclic peptide **84**.

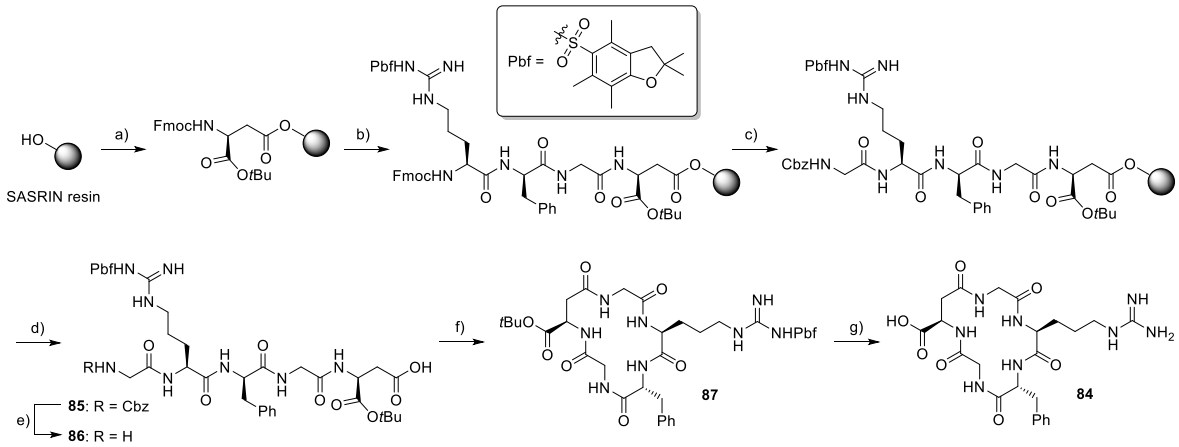

SCHEME 13. Synthesis of cyclic peptide **84**. Reagents and conditions: a) Fmoc-Asp(OH)-O*t*Bu, HATU, HOAt, *i*Pr$_2$NEt, DMF, M.W., 90%; b) 1. 25% piperidine in DMF; 2. Fmoc-AA-OH, HATU, HOAt, *i*Pr$_2$NEt, DMF, M.W.; c) 1. 25% piperidine in DMF; 2. Cbz-Gly-OH, HATU, HOAt, *i*Pr$_2$NEt, DMF, M.W.; d) 1% TFA in CH_2Cl_2, r.t., 3 min × 24 times, 73%; e) H_2, 10% Pd/C, THF/H_2O 2:1, overnight, r.t., quant.; f) HATU, HOAt, *i*Pr$_2$NEt, DMF/CH_2Cl_2 1:1 (1.4 mM), overnight, r.t., 39%; g) TFA/thioanisole/EDT/anisole 90:5:3:2, 2 h, r.t., 49%.

carboxybenzyl- instead of the Fmoc-carbamate because of the traceless byproducts deriving from the Cbz-deprotection reaction. Moreover, the presence of a protecting group at the *N*-terminus of the peptide allowed the purification of the linear carboxylic acid after the cleavage from the resin by FC on silica gel. On the other hand, a zwitterion peptide, bearing protected side chains, would have been very difficult to purify using either direct or reverse phase chromatography. The synthesis of **84** started with the coupling reaction between Fmoc-Asp(OH)-O*t*Bu and SASRIN resin (step a): the reaction proceeded without problems, especially thanks to the low steric hindrance around the β-carboxylic group involved. In any case, the reaction was performed two times to minimize the number of unreacted supported –OH groups. At the end of the second coupling, a few beads were subjected to Kaiser test: the test result was negative, thus the esterification of the resin was effective. We calculated the yield of the first step with the formula

$$y_{\%} = \frac{(m_{TOT} - m_{RESIN})}{(M.W._{AA} - M.W._{WATER})\, n_{RESIN}} \%\,,$$

where:

- $y_{\%}$ is the yield of the coupling reaction, expressed as percentage;
- m_{TOT} is the mass of the resin after the coupling reaction, expressed in mg;
- m_{RESIN} is the mass of the resin before the coupling reaction, expressed in mg;
- $M.W._{AA}$ is the molecular weight of the amino acid just attached to the resin;

- $M.W._{WATER}$ is the molecular weight of water, since, during the coupling reaction between the carboxylic acid and the SASRIN resin, extrusion of H_2O takes place (●–OH + HOOC-R → ●–OOC-R + H_2O);
- n_{RESIN} is the amount of resin used, expressed in mmol.

In this case, the $y_{\%}$ of step a was 90%: the amounts of reagents for the next steps were calculated consequently. The double coupling procedure was applied in order to limit the formation of truncated byproducts during the SPPS: in particular, it is better to carry out the coupling reaction steps involving amino acids with a bulky side chain (in this case D-phenylalanine) two times. At this stage, we continued the solid-phase peptide synthesis (step b): alternating Fmoc deprotection (step b1) and coupling reaction with the next building block (step b2), the tetrapeptide was built on the solid support. The last treatment with 25% piperidine in DMF (step c1) afforded the amine that attacked Cbz-protected glycine, previously activated in the presence of HATU, HOAt and *i*Pr_2NEt (step c2). A 1% TFA solution in dichloromethane resulted effective in removing the peptide from the beads (step d), without touching the acid-labile groups (*t*Bu ester and Pbf sulfonamide), that anyhow require harsher cleavage conditions. Step d was carried out until no peptide was spotted by eluting on TLC the liquid fractions from rinsing the resin: the crude compound **85** was obtained removing the solvent and purified by flash chromatography on silica gel. The linear amino acid **86** was obtained quantitatively by catalytic hydrogenation of Cbz-carbamate **85**, using 10% Pd/C as catalyst, under hydrogen atmosphere in 2:1 THF/H_2O (step e). Compound **86** was subjected to macrocyclization under high dilution conditions in 1:1 DMF/CH_2Cl_2 (step f): the reaction was stirred overnight at room temperature, then the mixture was concentrated and the crude compound **87** was purified by flash chromatography on silica gel. Deprotection in TFA with thioanisole, EDT and anisole scavengers gave the final compound **84** as trifluoroacetate salt, after reverse phase HPLC and freeze-drying from water (step g).

2.3.2 CONFORMATIONAL AND BIOLOGICAL INVESTIGATIONS ON *CYCLO*[G*ISO*DGRF] **84**

The cyclic pentapeptide **84** was studied in terms of conformation and biological activity by the research group of Dr. Giovanna Musco, where Cristina was carrying out her PhD. For this reason, these studies are not reported in this Thesis. By the way, NMR and *in vitro* investigations pointed out substantial differences between the predicted properties of the synthesized peptide and the experimental results actually shown by **84**. These findings allowed the optimization of the *in silico* model, leading to a reassessment of the variables involved in the force field calculations.

2.4 *CYCLO*[DKP-RAD] PEPTIDOMIMETICS

2.4.1 SYNTHESIS OF *CYCLO*[DKP-RAD] **88** AND *CYCLO*[DKP-RAD] **88-EPI**

The preparation of cyclic RAD-peptidomimetics bearing a DKP scaffold was achieved by following the procedure used in the synthesis of *cyclo*[DKP-RGD] compounds,[27] introducing an alanine residue instead of glycine. We decided to synthesize *cyclo*[DKP3-RAD] and *cyclo*[DKP3-RaD] peptidomimetics (**88** and **88-epi**, respectively, FIGURE 33), since the related *cyclo*[DKP3-RGD] **17** has been investigated extensively as integrin ligand and inhibitor (see PARAGRAPH I – 2.1.2). Since diastereoisomers **88** and **88-epi** may show different biological activities, we planned to test both isomers in *in vitro* binding assays.

We chose to synthesize first **88**, the isomer containing the alanine residue in the natural configuration. The synthesis of **88** is shown in SCHEME 14: compound **88-epi** can be obtained following a similar strategy, but using D-alanine instead. The coupling reaction between protected arginine **89** and alanine

benzyl ester (**90**, step a) and Boc-deprotection of the resulting dipeptide **91** in TFA/dichloromethane (step b) afforded amine **92**. Carboxylic acid **94** was prepared according to reported procedures starting from the known azide scaffold **44**, common intermediate in the preparation of both RGD and *iso*DGR ligands.[27] *In situ* reduction and protection (step c) on **44** gave allyl ester **93** that was cleaved in the presence of pyrrolidine, PPh_3 and $[Pd(PPh_3)_4]$ as catalyst (step d). **92** and **94** reacted forming **95** in good yields (step e). Treating Boc-carbamate **95** with TFA in CH_2Cl_2 resulted in full conversion into the corresponding amine **96** (step f) that was directly coupled with Cbz-Asp(O*t*Bu)-OH, using HATU and HOAt as condensing agents (step g). The linear protected compound **97** was submitted to catalytic hydrogenation with 10% Pd/C as catalyst to cleave both benzyl ester on alanine and carboxybenzyl carbamate on aspartic residues (step h): the linear deprotected amino acid **98** was isolated in quantitative yields. The macrocyclization on **98** (step i) turned out to be a crucial step of the synthesis. We performed the reaction under the well-established reaction conditions: the carboxylic acid (1.0 eq) was activated at 0 °C with HATU (4.0 eq), HOAt (4.0 eq) and *i*Pr_2NEt (6.0 eq) in high dilution (1.4 mM in DMF/CH_2Cl_2 1:1), then the reaction mixture was stirred overnight at room temperature. After solvent removal, the crude compound was purified by flash chromatography on silica gel and the expected desired compound was isolated as mixture of two inseparable isomers **99A** and **99B**. We suppose that

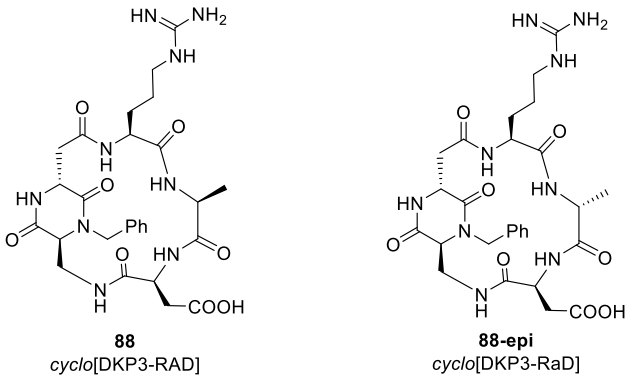

FIGURE 33. Structures of peptidomimetics *cyclo*[DKP3-RAD] **88** and *cyclo*[DKP3-RaD] **88-epi**.

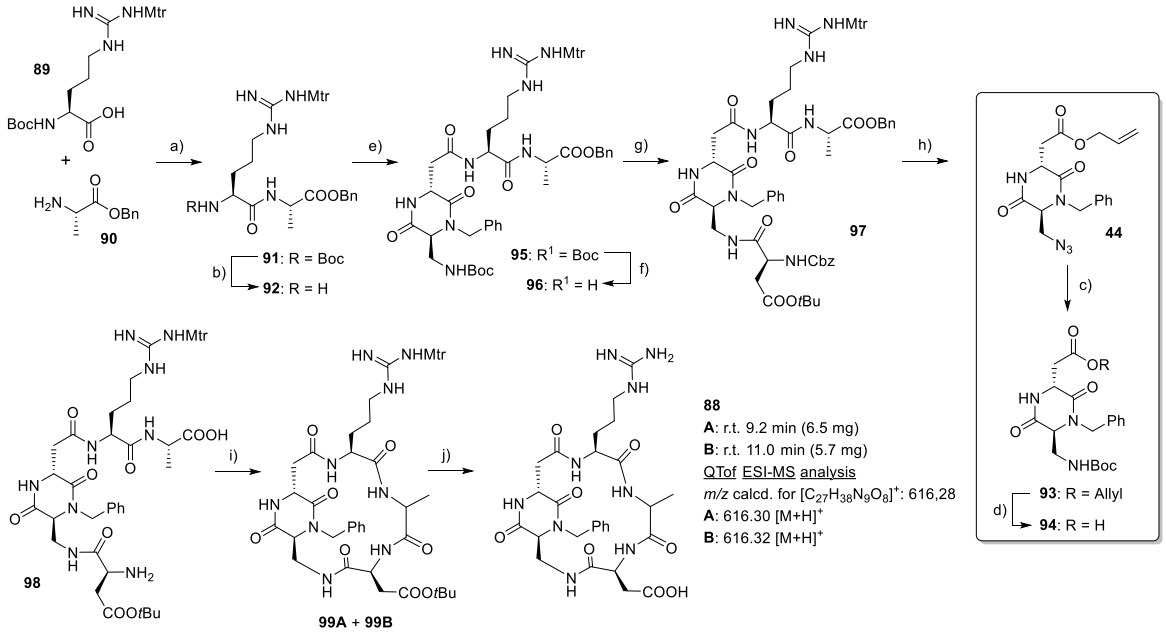

SCHEME 14. Synthesis of peptidomimetic **88**. Reagents and conditions. a) HATU, HOAt, *i*Pr_2NEt, DMF, 0 °C to r.t., overnight, 84%; b) TFA, CH_2Cl_2, r.t., 2 h; c) PMe_3 in toluene, Boc-ON, THF, -20 °C to r.t., 5 h, 78%; d) $[Pd(PPh_3)_4]$, pyrrolidine, PPh_3, CH_2Cl_2, 0 °C, 1 h, quant.; e) **94**, HATU, HOAt, *i*Pr_2NEt, DMF, 0 °C to r.t., overnight, 65%; f) TFA, CH_2Cl_2, r.t., 2 h; g) Cbz-Asp(O*t*Bu)-OH, HATU, HOAt, *i*Pr_2NEt, DMF, 0 °C to r.t., overnight, 83%; h) H_2, 10% Pd/C, THF/H_2O 1:1, overnight, r.t., quant.; i) HATU, HOAt, *i*Pr_2NEt, DMF/CH_2Cl_2 1:1 (1.4 mM), 0 °C to r.t., overnight, 82%; j) TFA/thioanisole/EDT/anisole 90:5:3:2, 2 h, r.t., 30%. The synthesis was performed according to ref. 27.

racemization at the alanine stereocenter occurred during the amide bond formation, following a reported mechanism (FIGURE 34). After activation of the carboxylic acid **A** by condensing agents, the intramolecular attack by the adjacent residue on the activated ester moiety in **B** leads to the formation of oxazolone derivative **C**. At this stage, the nucleophilic attack (in red, FIGURE 34) and the deprotonation at 4 position in **C** (in blue, FIGURE 34) are competitive, depending on the reaction conditions: the former pathway opens up the oxazolone ring and furnish peptide **F** (desired product, obtained *via* undesired mechanism); the latter forms oxazololate **D** that can undergo reprotonation on both the faces of the heterocycle, thus evolving into oxazolone **E** or coming back to **C**. If the nucleophile attacks **E**, peptide **G** is produced: this mechanism could explain why a mixture of (diastereo)isomers was obtained in step i.

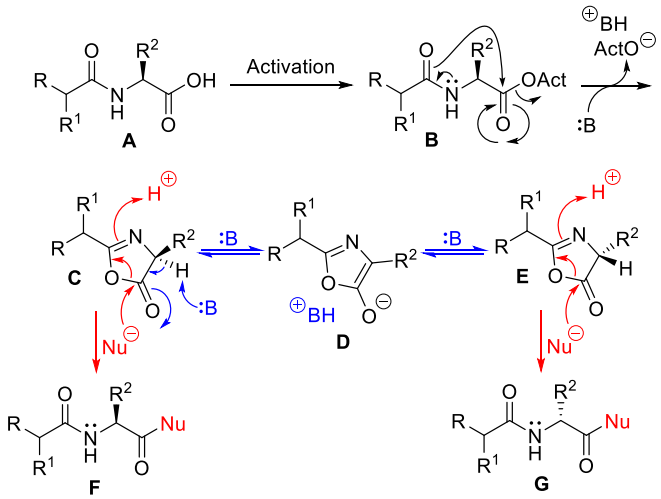

FIGURE 34. Racemization mechanism possibly active during amino acid coupling reaction.

The final deprotection on **99A** + **99B** (step j) afforded the crude compound, whose purification by reverse-phase HPLC allowed the separation of the two isomers, namely **88A** and **88B**, obtained in *ca.* 1:1 ratio after freeze-drying from water (FIGURE 34).

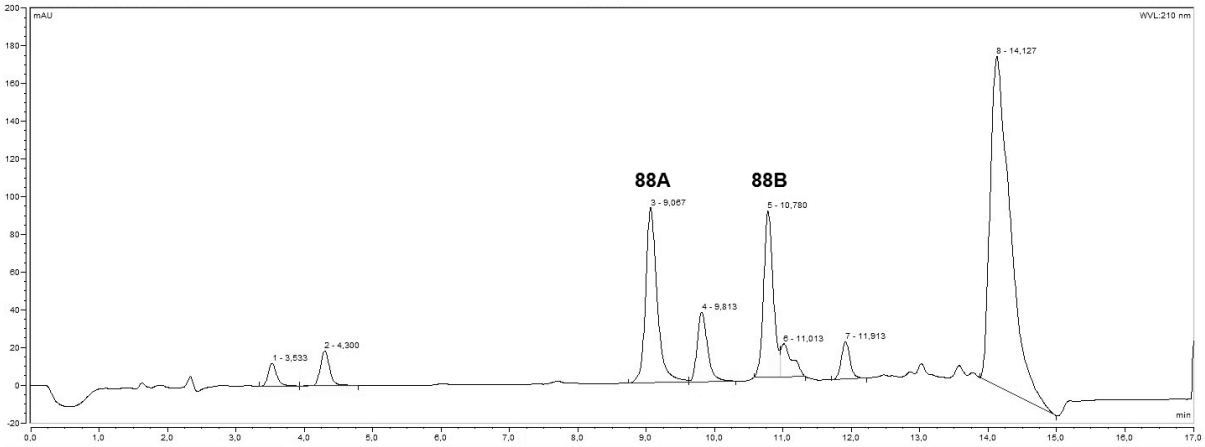

FIGURE 34. HPLC purification and separation of isomers **88A** and **88B**.

At the moment, we can adfirm that **88A** and **88B** are two isomers on the basis of MS analysis: further investigations are planned to elucidate the structure of each compound. In any case, if the hypothesis of alanine racemization will be confirmed, the synthetic strategy shown in SCHEME 14 will be useful to synthesize both *cyclo*[DKP3-RAD] **88** and *cyclo*[DKP3-RaD] **88-epi** starting from L-alanine.

2.4.2 BIOLOGICAL EVALUATION OF *CYCLO*[DKP-RAD] PEPTIDOMIMETICS **88A** AND **88B**

2.4.2.1 BINDING ASSAYS ON ISOLATED RECEPTOR

88A and **88B** were tested in *in vitro* binding assays on isolated $\alpha_V\beta_3$ receptor to assess their activity as integrin ligands (TABLE 8). Cilengitide (**4**) and *cyclo*[DKP3-RGD] (**17**) are reported as reference compounds. The experimental IC_{50} values shown by **88A** and **88B** (entries 3 and 4) demonstrate that the substitution of glycine with alanine affects the ability of the peptidomimetic to bind $\alpha_V\beta_3$ integrin: in particular, compound **88B** was found to be a very weak binder for the target integrin receptor, showing a 300-fold loss of potency when compared with the corresponding RGD ligand **17**. These results are promising and disclose the possibility to synthesize RAD-based fragments bearing a handle for conjugation to payloads, aiming at preparing RAD-drug conjugates as negative control in anti-proliferative assays. The low activity showed by peptidomimetics **88A** and **88B** is probably ascribable to the methyl group in alanine side chain, which may be responsible for critic steric clashes when the interaction with the integrin binding site takes place.

TABLE 9. Evaluation of the binding affinity of compounds **88A** and **88B** on isolated $\alpha_v\beta_3$ receptor.

Entry	Compound	Structure	IC_{50} (nM)[a]	
			$\alpha_V\beta_3$	$\alpha_V\beta_5$
1	**4**	Cilengitide	0.6 ± 0.1[b]	11.7 ± 1.5[b]
2	**17**	*cyclo*[DKP3-RGD]	4.5 ± 1.1	149 ± 25
3	**88A**	*cyclo*[DKP3-RAD] (r.t. 9.2 min)	360 ± 40	n.d.
4	**88B**	*cyclo*[DKP3-RAD] (r.t. 11.0 min)	1500 ± 500	n.d.

[a] IC_{50} values were calculated as the concentration of compound required for 50% inhibition of biotinylated vitronectin binding. Screening assays were performed by incubating the immobilized integrins $\alpha_V\beta_3$ and $\alpha_V\beta_5$ with increasing concentrations (10^{-12} – 10^{-5} M) of the RGD or RAD ligands in the presence of biotinylated vitronectin (1 mg/mL), and measuring the concentration of bound vitronectin in the presence of the competitive ligands. [b] Calculated as the concentration of compound required for 50% inhibition of biotinylated vitronectin binding, see ref. 20.

Moreover, the remarkable difference between RAD compounds may be addressed to different conformational preferences adopted by the tripeptide motif, as consequence of an inverted stereochemistry at the alanine α-carbon: as matter of fact, the ^{1}H-NMR spectra of **88A** and **88B** differ in both chemical shifts and multiplet systems, suggesting the presence of two different conformations (FIGURE 36 and FIGURE 37).

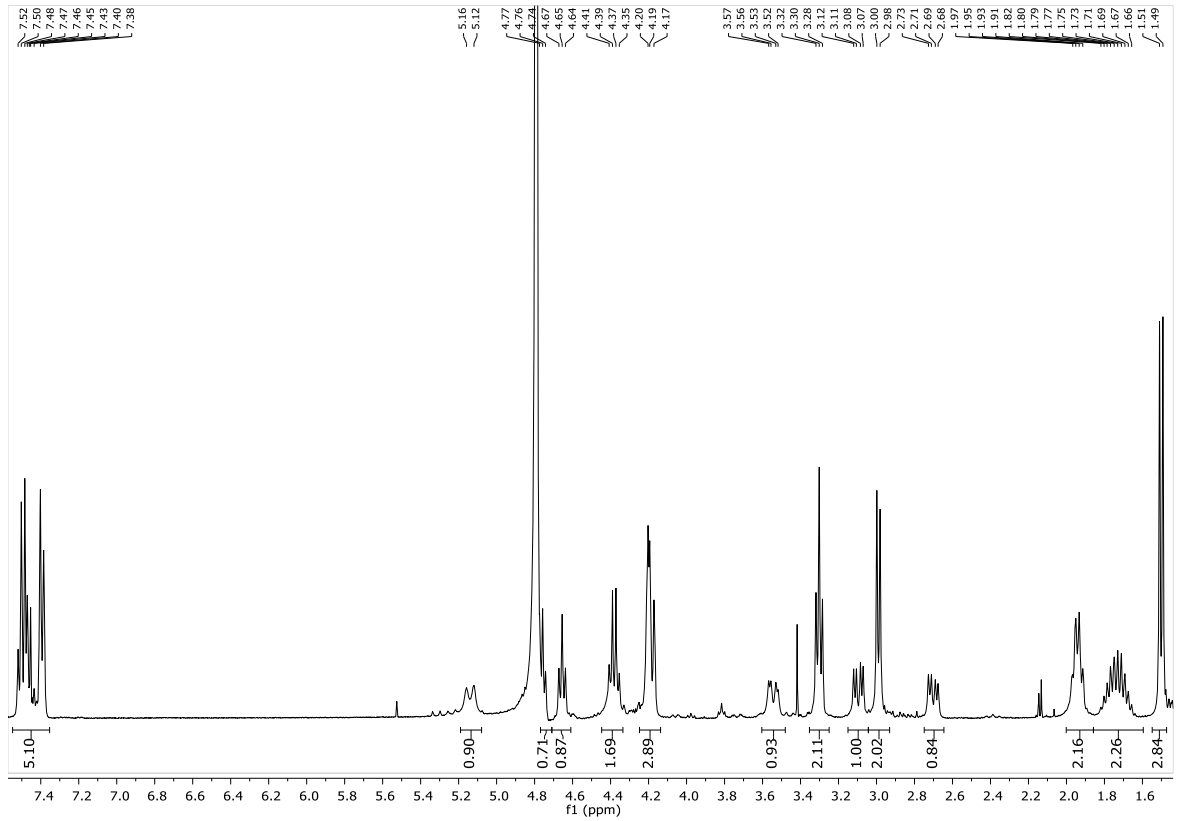

FIGURE 36. ^{1}H-NMR (400 MHz, D_2O) spectrum of compound **88A**.

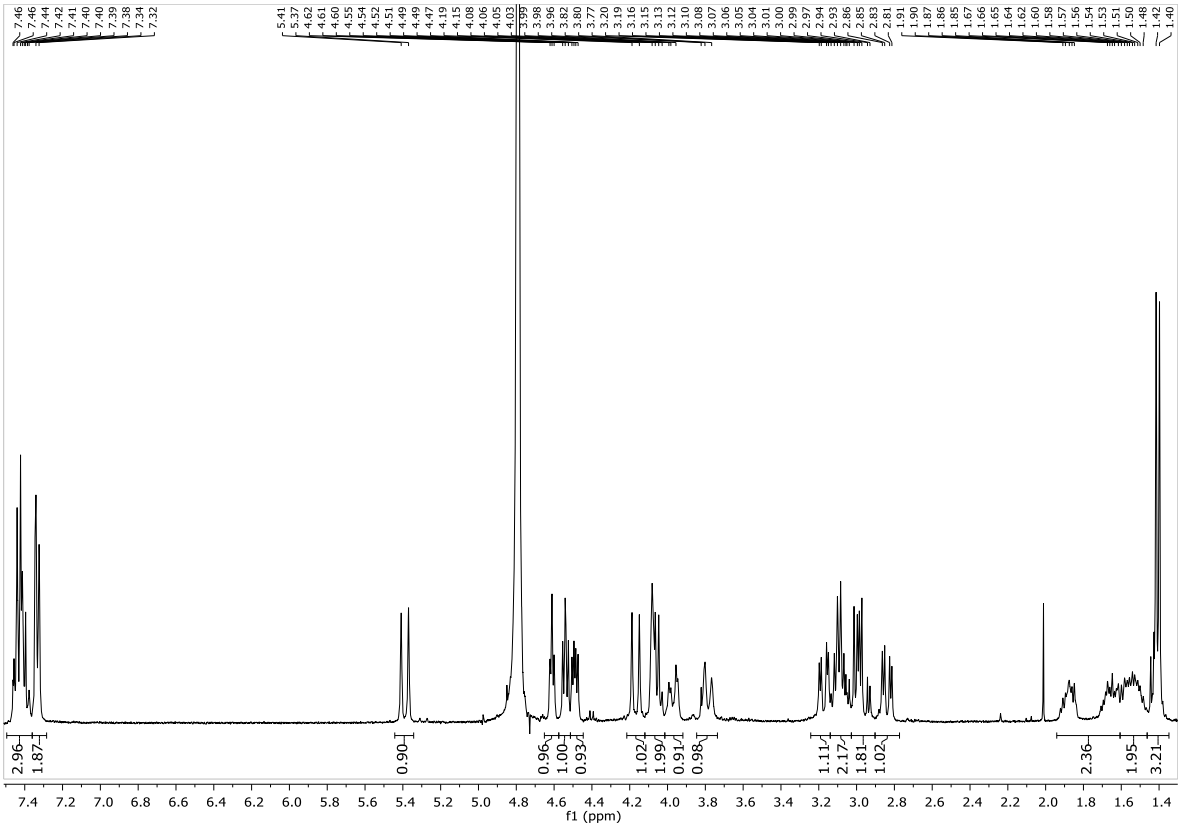

FIGURE 37. ^{1}H-NMR (400 MHz, D_2O) spectrum of compound **88B**.

3 CONCLUSIONS

In the first part of this Thesis, I described the synthesis of different classes of peptidomimetics targeting integrin receptors. Both simple ligands and drug conjugates were synthesized and tested to assess their biological activity.

First, I focused my attention on the synthesis of *cyclo*[DKP-*iso*DGR] ligands, expanding the library of peptidomimetics synthesized in our group with compounds *cyclo*[DKP5-*iso*DGR] (**39**) and *cyclo*[DKP7-*iso*DGR] (**40**). Ligands **39** and **40** showed only poor affinity for the isolated integrin receptors $\alpha_V\beta_3$ and $\alpha_V\beta_5$ *in vitro*: these observations suggested a major role of the DKP scaffold in the spatial arrangement of the *iso*DGR sequence, even more evident than the one observed in the correspoding *cyclo*[DKP-RGD] peptidomimetics. The previously reported *cyclo*[DKP3-*iso*DGR] (**26**) was confirmed as the best binder for integrin $\alpha_V\beta_3$ among the *iso*DGR ligands reported so far in the literature. For this reason, *cyclo*[DKP3-RGD] (**17**) and *cyclo*[DKP3-*iso*DGR] (**26**) were selected for further biological investigations in order to establish a comparison between the two different peptide sequences: both **17** and **26** exhibited a potent inhibitor effect on the phosphorylation of FAK and Akt, two proteins involved in integrin-mediated cellular processes. These experimental evidences qualified *cyclo*[DKP3-RGD] and *cyclo*[DKP3-*iso*DGR] as integrin antagonists: additional biological studies will be carried out to gather more information about the activity of these compounds in order to expand the RGD-*iso*DGR comparison.

Next, we developed a new synthetic strategy to prepare *cyclo*[DKP3-*iso*DGR]-CH_2NH_2 **56**, a derivative of *cyclo*[DKP3-*iso*DGR] (**26**) bearing a benzylic amine moiety as suitable handle for further conjugation to different payloads, such as cytotoxic and imaging agents. The synthesis of **56** and its linkage to paclitaxel *via* a cleavable linker were carried out entirely in solution-phase. The resulting *cyclo*[DKP3-*iso*DGR]-Val-Ala-PTX (**55**) showed a low nanomolar affinity towards purified $\alpha_V\beta_3$ integrin *in vitro*. Preliminary anti-proliferative assays assessed a remarkable targeting ability of **55** against cancer cells over-expressing integrin $\alpha_V\beta_3$. Lysosome extract digestion and stability tests on *cyclo*[DKP3-*iso*DGR]-Val-Ala-PTX are ongoing in order to evaluate the ability of the conjugate to release the paclitaxel fragment within the tumor environment. These data will be compared with those already reported for the related prodrug *cyclo*[DKP3-RGD]-Val-Ala-PTX (**31**): in this way the targeting ability of the two RGD- and *iso*DGR-based conjugates will be assessed. Future developments of this project will include the conjugation of *cyclo*[DKP3-*iso*DGR]-CH_2NH_2 (**56**) to other payloads using both different peptide- and non-peptide linker systems. As a matter of fact, we already synthesized a small library of *cyclo*[DKP3-RGD]-drug conjugates, with *cyclo*[DKP3-RGD]-Val-Ala-PTX (**31**) as representative example. Among the peptide sequences suitable for the drug release, the well-known dipeptide valine-citrulline (Val-Cit) is a specific substrate for cathepsin B,[50] a lysosomal protease: the inclusion of this fragment into an SMDC will avoid the premature cleavage of the peptide linker in the extracellular environment.

The design and synthesis of integrin ligands displaying the *iso*DGR motif was carried out also in collaboration with Cristina Paissoni, a PhD student working in the research group of Dr. Giovanna Musco (Ospedale San Raffaele, Milan). Based on computational studies carried out by Cristina, compound *cyclo*[G*iso*dGRf] (**84**) was identified as promising cyclic peptide and synthesized using SPPS protocols. A panel of conformational and biological studies are ongoing on **84** to validate the developed

in silico model: further optimization of the theoretical method will be required, since preliminary test results showed important inconsistencies between the predicted and the experimental properties of the cyclopeptide.

At last, I focused my efforts on the synthesis of *cyclo*[DKP3-RAD] (**88**) and *cyclo*[DKP3-RaD] (**88-epi**) peptidomimetics: during the macrocyclization step in the synthesis of compound **88**, epimerization at the α-carbon of alanine possibly occurred, leading to the formation of two diastereoisomers. Compounds **88A** and **88B** were separated after the final deprotection reaction by reverse-phase HPLC and tested *in vitro* to measure their ability to bind integrin $\alpha_V\beta_3$. As expected, the replacement of Gly with Ala (RGD → RAD) provoked a marked decrease in integrin affinity, with respect to the corresponding *cyclo*[DKP3-RGD] (**17**). The synthesis of RAD-containing peptidomimetics displaying a suitable functional group for the preparation of RAD-drug conjugates to be used as negative tools in anti-proliferative assays is currently in progress. On the other hand, additional analysis on **88A** and **88B** will be devoted to elucidate their structural and conformational properties.

PART II. TARGETING VEGFRS

The second part of my Thesis deals with the vascular endothelial growth factor receptors and their ligands.
A short presentation of this complex biological axis is given before showing some examples of molecules able to modulate VEGFRs activity by interacting either with the extracellular or with the intracellular domains of these proteins.
Then, the role of integrin-VEGFR cross-talk will be presented, with some experimental evidences demonstrating how the disruption of this direct co-operation can inhibit angiogenesis.
At last, I will describe the interaction of VEGF-C with its target receptors VEGFR-2 and VEGFR-3 and the reason why we considered this growth factor a privileged candidate for the preparation of a small library of VEGFR-selective peptides.

Part of the work described in this Chapter was published in the following article:

- Zanella, S.; Mingozzi, M.; Dal Corso, A.; Fanelli, R.; Arosio, D.; Cosentino, M.; Schembri, L.; Marino, F.; De Zotti, M.; Formaggio, F.; Pignataro, L.; Belvisi, L.; Piarulli, U.; Gennari, C. *ChemistryOpen* ***2015***, *4*, 633; cited in "Spotlights on our sister journals", *Chem. Eur. J.* **2015**, *21*, 18510.

1 VEGF RECEPTORS AND LIGANDS

1.1 BIOLOGY OF THE VEGF-VEGFR SYSTEM

Vascular endothelial growth factors (VEGFs) play a key role in the regulation of vasculogenesis and angiogenesis. Mammals present five different VEGFs, together with the correspondent splice and processed isoforms. These proteins are able to bind a common pattern of three receptor tyrosine kinases (RTKs), namely VEGF receptor-1, -2, and -3 (VEGFR-1, VEGFR-2, and VEGFR-3). Moreover, VEGFs can interact with some co-receptors, *i.e.* heparan sulfate proteoglycans (HSPGs) and neuropilins, and induce their biological activity.[51] The regulation mechanisms of these growth factors are very similar to those of well-known RTKs, *e.g.* the platelet-derived growth factor receptors (PDGFRs) and the epidermal growth-factor receptors (EGFRs). In general, VEGF ligands exert their biological activity by inducing receptor dimerization and activating the tyrosine kinase domain that transmit different signaling pathways related to cell migration, survival and proliferation.
On the other hand, VEGFR activity is unique in transducing such signals responsible for the formation of vascular tube network and for the regulation of vascular permeability. In particular, VEGFR-1 is able to affect both the migration of monocytes and macrophages, and the signaling efficacy of VEGFR-2. A soluble isoform of VEGFR-1 participates in the downregulation of VEGFR-2 activity by preventing its interaction with endogenous ligands. Most of the physiological and pathological events in vascular endothelial cells are regulated by VEGFR-2 activity, whereas VEGFR-3 fulfills an essential role in the growth and function of lymphatic endothelial cell. Due to their fundamental tasks, cancer therapy started targeting VEGF receptors using anti-VEGF antibodies and small molecules, aiming at neutralizing the growth factors or inhibiting the tyrosine-kinase activity, respectively (see PARAGRAPH II – 1.2 for further discussion). In mammals, the VEGF family consists of five dimeric glycoproteins, such as VEGF-A, VEGF-B, VEGF-C, VEGF-D, VEGF-E, and placenta growth factor (PLGF). Different growth factors exhibit selectivity for different VEGFRs: these proteins can acquire specificity toward a new target receptor upon proteolytic processing of the native VEGF (FIGURE 38).[51,52] From the structural point of view, VEGFs present intra- and inter-chain disulfide bonds involving eight, well-conserved cysteine amino acids. In particular, the crystallized VEGF-A revealed that the protein is composed by two monomers having an anti-parallel orientation giving rise to a dimer presenting the receptor binding site at each pole

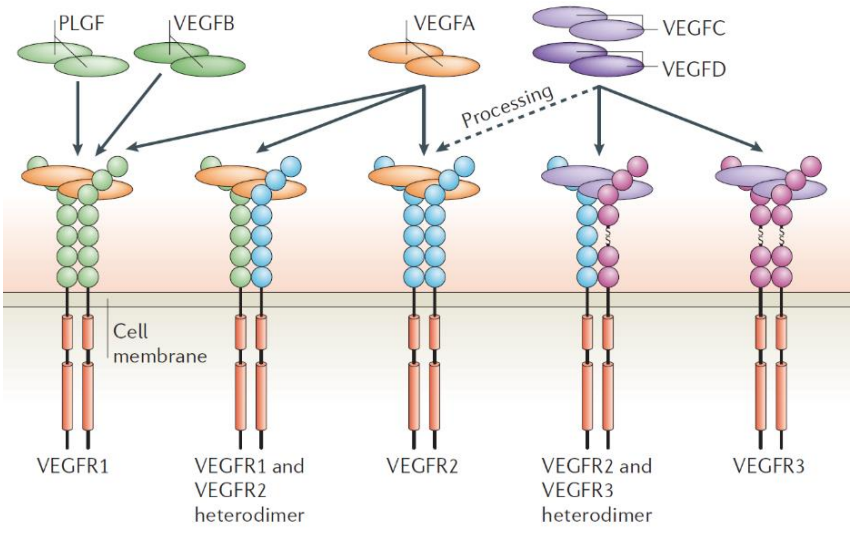

FIGURE 38. Selectivity of mammalian VEGFs towards homo- and heterodimeric VEGFRs. Adapted from ref. 51.

of the whole dimer (FIGURE 39).[53] Although homodimers are formed preferentially, also some heterodimeric complexes have been observed.

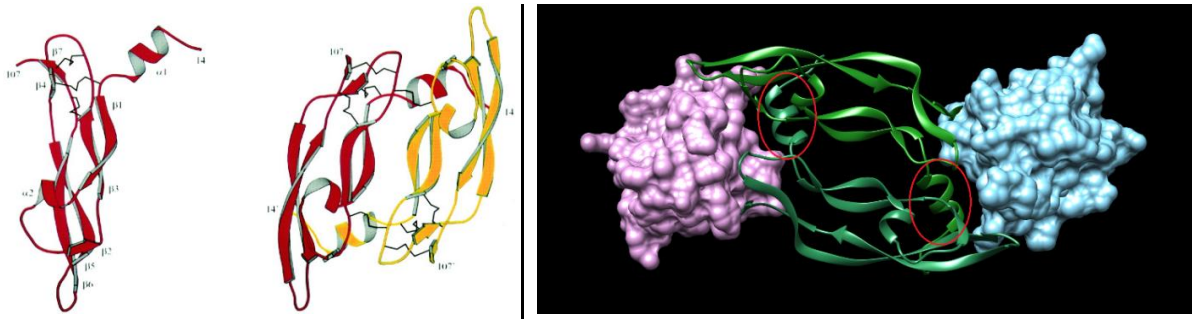

FIGURE 39. Receptor-binding domain of VEGF-A represented as monomer and homodimer (on the left) and VEGF-A interacting with VEGFR-1 as homodimer (on the right). Adapted from ref. 53a.

VEGFs can be present in different isoforms originated by alternative splicing of the native proteins: this differentiation mechanism, together with a parallel proteolytic processing, affects the interaction of the isoform with the target receptors, stimulating the wide pattern of biological functions exerted by the VEGF-VEGFR system. For example, upon the proteolysis of specific chains in the early proteins, VEGF-C and VEGF-D are allowed to bind both VEGFR-2 and VEGFR-3.

The VEGFRs belong to the receptor tyrosine kinases superfamily and share the subclass with PDGFRs and fibroblast growth factor receptors (FGFRs). Around 750 residues arranged into seven immunoglobulin-like folds compose the extracellular domain (ECD). In particular, the Ig domain-2 is responsible for ligand binding in VEGFR-1,[54] whereas the Ig domain-3 of VEGFR-2 determines the ligand specificity.[55] As well as VEGFs, VEGFRs can undergo splicing and/or proteolysis: for example, these transformations secrete processed VEGFR-1 and VEGFR-2, and a truncated variant of VEGFR-3.[56]

Neuropilins NRP-1 and NRP-2 were found to participate in VEGFR signaling: in particular, these co-receptors are able to bind only specific VEGF isoforms and then to present them to VEGF receptors in a certain way that increase the efficacy of VEGF signal transduction. Neuropilins are type I transmembrane proteins that lack kinase activity, but strengthen the signaling of VEGFRs and act as reserve of VEGF.

1.2 INTERFERING WITH THE VEGF-VEGFR SYSTEM IN ANTI-ANGIOGENIC THERAPY

Similarly to integrins, VEGFRs are over-expressed by hypoxic tumor cells: this peculiarity has been exploited in cancer treatment with the aim of impairing the VEGF-VEGFR interaction. Apart from bevacizumab, mentioned in PARAGRAPH I.2, other molecules able to interfere and disrupt this signaling system have been developed: as instance, clinical trials on a VEGFR-1/VEGFR-2 fusion protein, called VEGF-Trap, and on antibodies targeting VEGFs and VEGFRs are ongoing.[57]

Many efforts have been devoted to develop small molecules able to interfere with the activity of VEGF by targeting the intracellular tyrosine-kinase domain of VEGFRs:[58] sunitinib and sorafenib are two well-known examples. Sunitinib (Sutent™, **100**, FIGURE 40) was developed as broad RTK inhibitor[59] and approved by the FDA in 2006 for the treatment of renal cell carcinoma (RCC) and gastrointestinal stromal tumor (GIST).[60] Sorafenib (Nexavar™, **101**, FIGURE 40) was demonstrated to inhibit the activity of VEGFR-2, VEGFR-3 and PDGFRβ. First approved by US FDA in 2005 for the RCC-related therapy, in 2007 the use of sorafenib was extended to the treatment of hepatocellular carcinoma (HCC).[61]

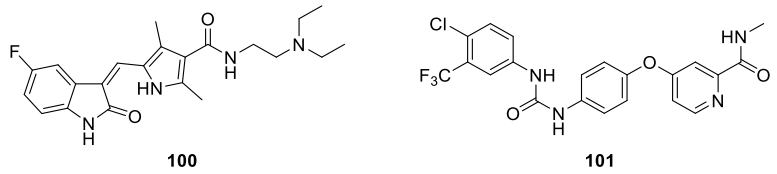

FIGURE 40. Structures of sunitinib (**100**) and sorafenib (**101**).

In addition, peptides and related derivatives have been proven efficient VEGF inhibitors: such compounds exert their biologically activity upon interaction with the extracellular portion of VEGFRs. Some examples of this class of molecules are shown in FIGURE 41, and they include peptoids (**102-103**)[62]; helical peptides (**104-105**)[63], designed starting from the Vammin hotspot; cyclopeptides (**106**)[64]; and foldamers (**107**)[65].

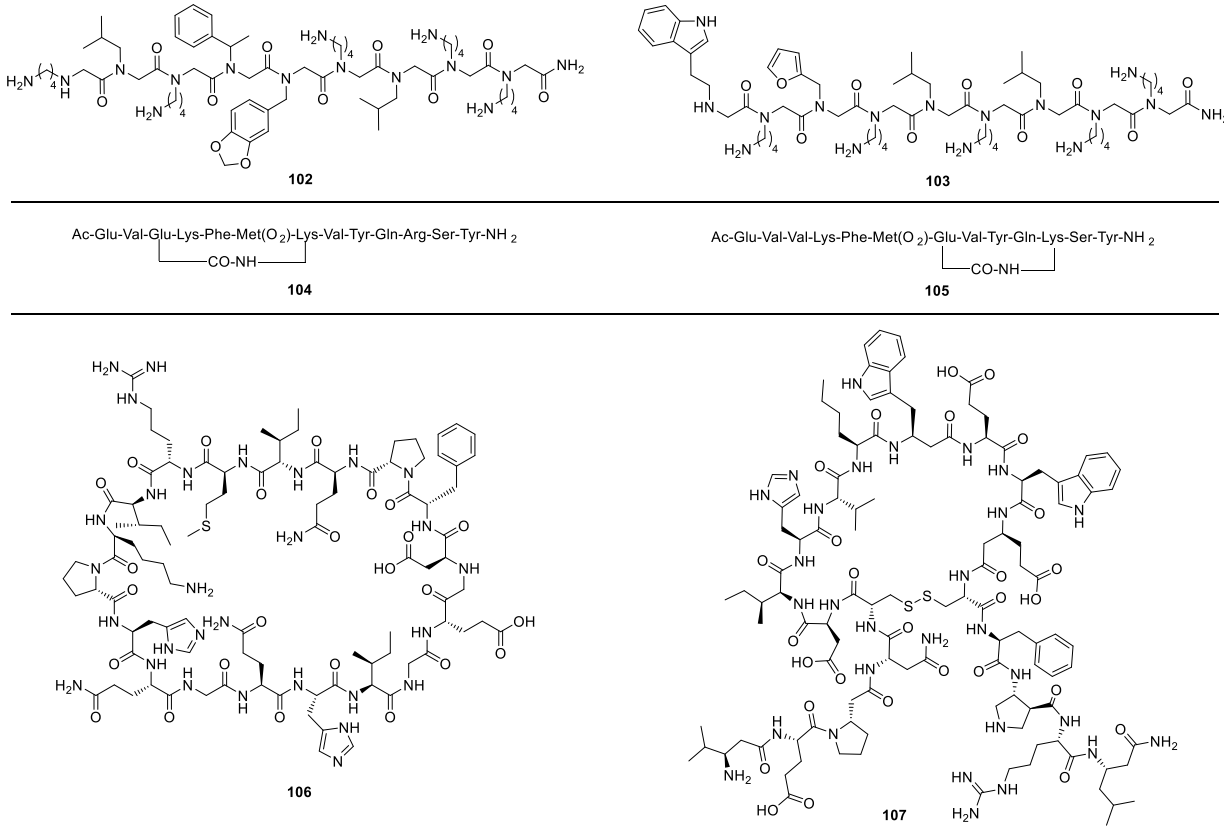

FIGURE 41. Peptides and related derivatives **102-107**.

In 2011, the research group of D'Andrea developed peptide **108** (FIGURE 42), which is characterized by a stable α-helical conformation in aqueous solution, a high affinity for VEGFRs and the ability to prevent the biological activity of VEGF on HUVECs.[66] Furthermore, *in vivo* studies on **108** showed its potent inhibition of capillary formation mediated by VEGF, thus restraining tumor growth. This angiogenesis inhibitor was designed starting from the pro-angiogenic agent **109** (FIGURE 42) that was developed by the same group in 2005 reproducing the helix region 17-25 involved in VEGF binding.[67] In this protein fragment, the authors decided to retain the three-dimensional disposition of amino acids interacting with the receptor and stabilized the helical folding by introducing capping sequences at both the peptide termini. Impressively, the modification of only two residues in **109** (Asn5→Met5 and Lys11→Ala11) completely modified the biological activity of the peptide compound: as a matter of fact, **109** is a potent angiogenesis agonist, whereas **108** was proved to inhibit morphogenesis efficiently.

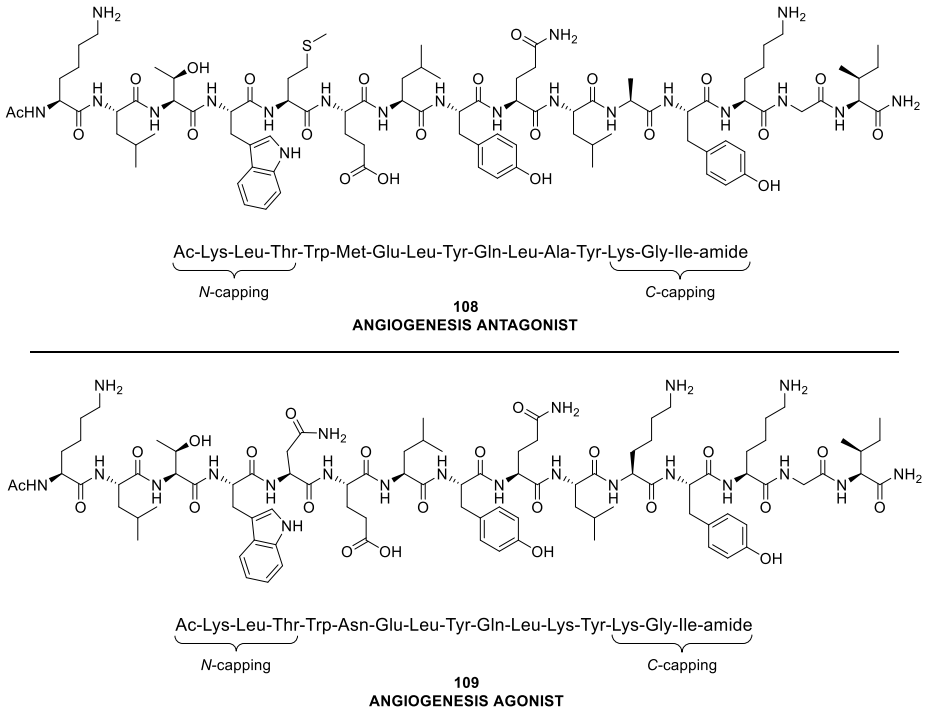

FIGURE 42. The helical peptides **108** and **109** developed by D'Andrea and co-workers.

In comparison with other examples shown above, **108** is a simple compound: indeed, this linear decapentapeptide can be easily synthesized by solid-phase peptide synthesis (SPPS). For this reason, we selected compound **108** as VEGFR-1 ligand and synthesized a dual action compound with the aim of targeting both integrin and VEGF receptors (see PARAGRAPH II – 1.2.1, **111**, FIGURE 46).

1.2.1 INTEGRIN-VEGFR CROSS-TALK

As a matter of fact, cooperation between integrins and VEGFRs was found to be crucial in pathological processes, such as tumor growth and development (FIGURE 43), as these receptors participate in the regulation of tumor angiogenesis by cross-talk mechanisms involving association and cluster formation, and affecting the activity of single receptor proteins.[68]

In 2000, Ruoslahti and colleagues reported a pioneer study in which the integrin $\alpha_V\beta_3$ portions interacting with VEGFR-2 and PDGFRβ were identified.[69] In particular, the ECD of the integrin β_3 subunit demonstrated to associate with both growth factor receptors, even without ligand-mediated phosphorylation and activation. These findings suggested the possibility of a direct, physical cooperation involving integrins and RTKs. In this field, Byzova and co-workers have extensively studied the cross-talk existing between integrin and VEGF receptors: since 2003, the authors collected a number of experimental evidences, encompassing receptor cluster formation and co-localization.[70] For instance, they demonstrated that VEGF stimulation was able to trigger the conformational change of integrin $\alpha_V\beta_3$ into the high affinity state and its subsequent co-localization with VEGFR-2 (FIGURE 44).[70b] Therefore, the population of activated integrin $\alpha_V\beta_3$ was found increased in highly-vascularized tumor masses, where hypoxic conditions lead to the up-regulation of growth factors and related receptors.

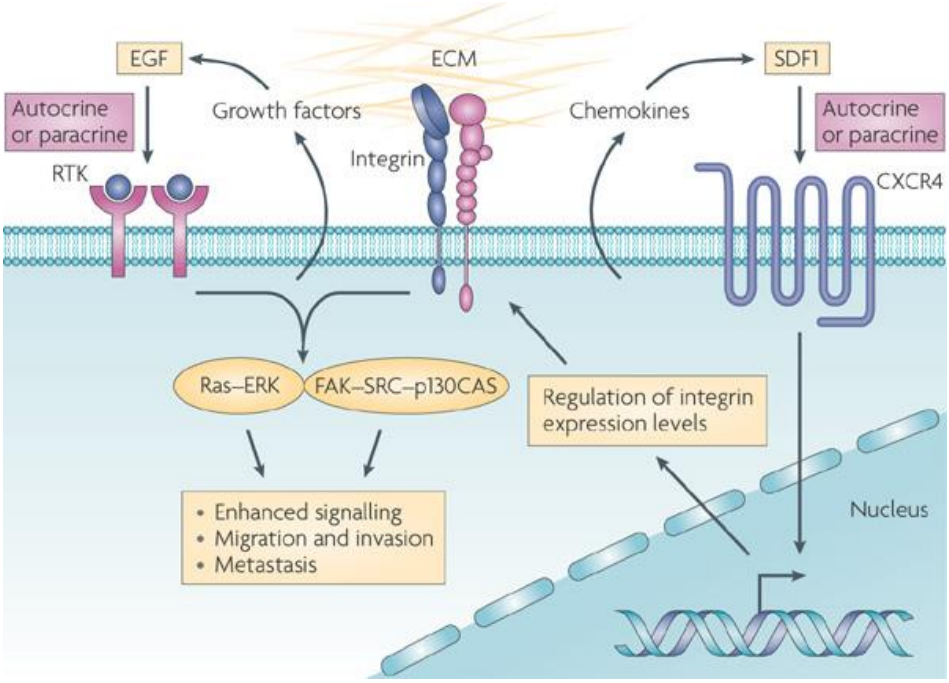

FIGURE 43. Integrin-VEGFR cooperation and signaling. Adapted from ref. 68.

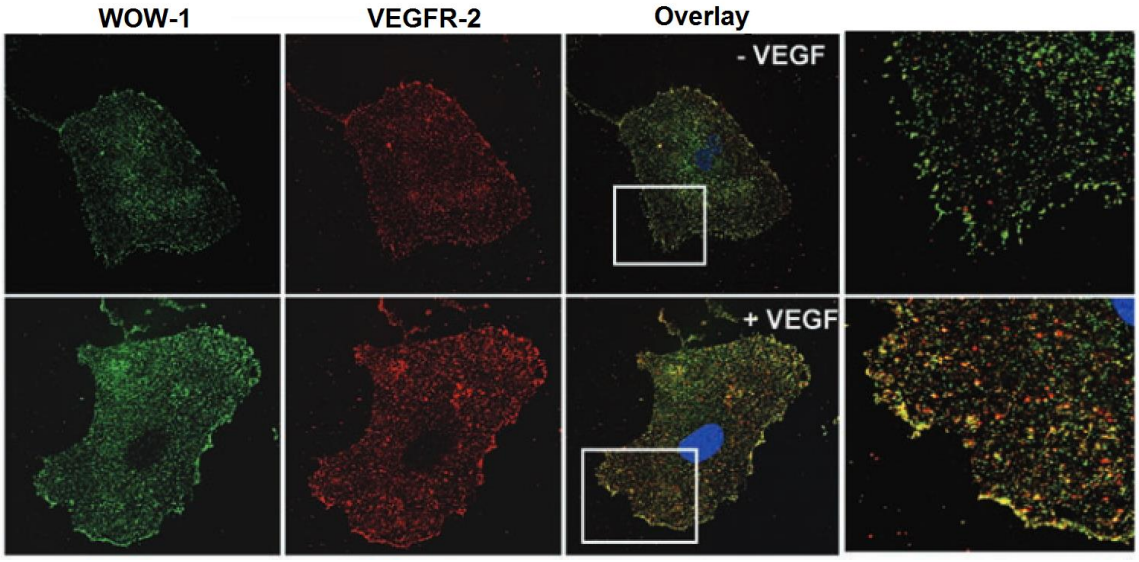

FIGURE 44. Co-localization of integrin $\alpha_V\beta_3$ and VEGFR-2 receptors. Adapted from ref. 70b.

In view of these experimental observations, the research group of Cochran designed and synthesized a dual action fusion protein, namely scVEGF (FIGURE 45, on the left), by equipping the natural VEGF (scVEGFwt) with an additional RGD recognition motif, maintaining the original biological activity of the growth factor.[71]

The benefit of displaying at the same time both the VEGFR and the integrin (RGD) binding motifs was demonstrated by inhibitory studies in which the interaction with these two receptors allowed to block the VEGFR-mediated cell proliferation. Moreover, *in vitro* test on HUVE cells qualified the dual specific variant scVEGF 7I as the most potent anti-angiogenic fusion protein among the three prepared (FIGURE 45, on the right). Indeed, scVEGF mut and scVEGF m27I, possessing only one binding epitope, showed incomplete inhibition of blood vessel formation. This strong inhibitory effect obtained when

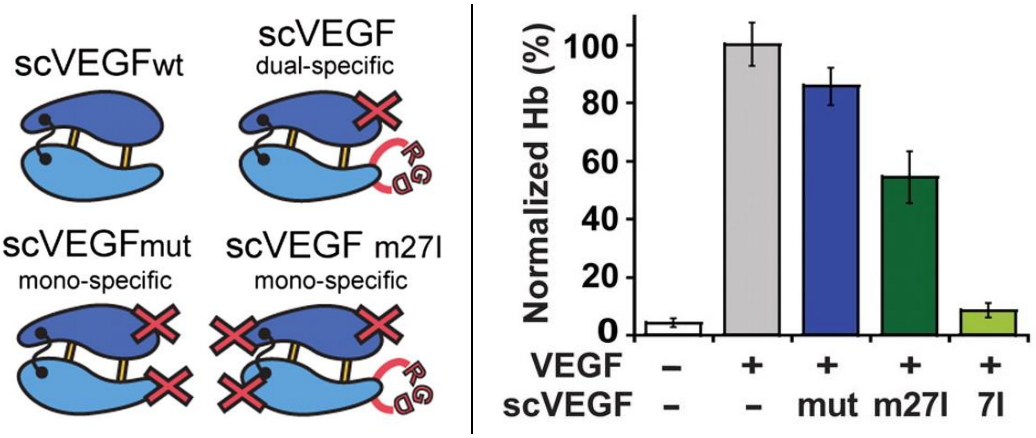

FIGURE 45. The engineered fusion protein scVEGF (on the left) and angiogenesis assay on the synthesized compounds. Adapted from ref. 71.

VEGFR-2 and integrin $\alpha_V\beta_3$ are simultaneously targeted is due to the disruption of the cross-talk interaction existing between these two receptor families. Intrigued by these results, in 2015 our research group reported the mixed solid-phase/solution-phase synthesis of a small dual action molecule targeting both integrin $\alpha_V\beta_3$ and VEGFR (**111**, FIGURE 46).[72] Our RGD-containing peptidomimetic **30** (see PARAGRAPH I – 1.5) and the peptide **110**, a derivative of **108** described by D'Andrea and colleagues, were chosen as integrin and VEGFR ligands, respectively, and linked covalently using an appropriate polyethylene glycol (PEG) spacer. We decided to protect the side chain of Lys13 in compound **110** since a free amino moiety could have interfered with the electrostatic interaction established by the RGD binding to integrin receptor.[73] On the other hand, the ε-NH_2 group of the *N*-terminal Lys1 was exploited to link the helical peptide and the peptidomimetic **30** by click chemistry.

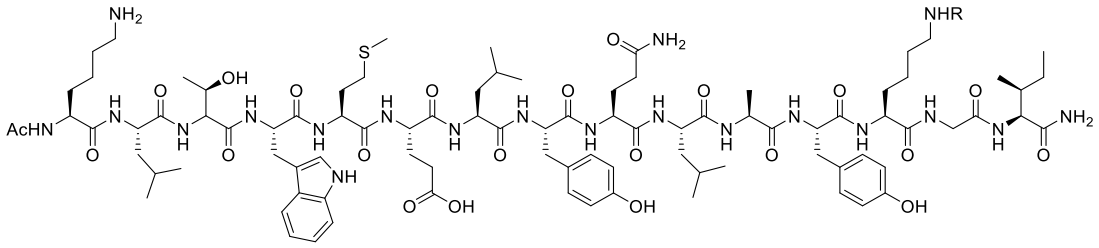

Ac-Lys-Leu-Thr-Trp-Met-Glu-Leu-Tyr-Gln-Leu-Ala-Tyr-Lys(R)-Gly-Ile-amide

108: R = H
110: R = Ac

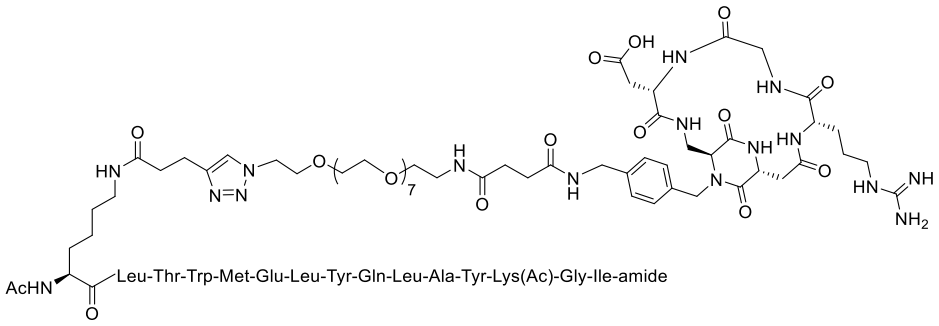

111

FIGURE 46. The helical peptide **108**, its derivative **110** and the dual action conjugate **111** developed in our group.

Circular dichroism (CD) studies on the final conjugate **111** showed that the VEGFR ligand almost retained its active conformation, considering that even minor structure modifications could affect the biological activity in a certain extent. The CD spectrum of **111** (FIGURE 47) demonstrated that, depending on the solvent, the VEGFR ligand presents a certain conformational flexibility: passing from water, to trifluoroethanol, to methanol, the secondary structure of the peptide adopted a more pronounced helical folding. Indeed, both the alcoholic solvents are known to induce specifically helicoidal conformation in peptides. Nevertheless, in aqueous medium, which is the most relevant considered that it resembles the natural cellular environment, the portion of **110** included in the conjugate still retains the native α-helix arrangement in a certain extent, thus its ability to interact with the target VEGF receptor. Compound **111** proved to interact *in vitro* with the isolated integrin $\alpha_V\beta_3$ and VEGFR-1 receptors and showed a potent inhibitory effect against VEGF-mediated angiogenesis on HUVE cells (FIGURE 48B). Control experiments were carried out in the presence of VEGF alone (FIGURE 48A) and of VEGF + **112** (Ac-Lys-Gln-Met-Tyr-Leu-Glu-Leu-Gly-Tyr-Ala-Thr-Ile-Lys-Trp-Leu-amide, FIGURE 48C), a negative control presenting the amino acid residues of peptide **108** in a scrambled order.

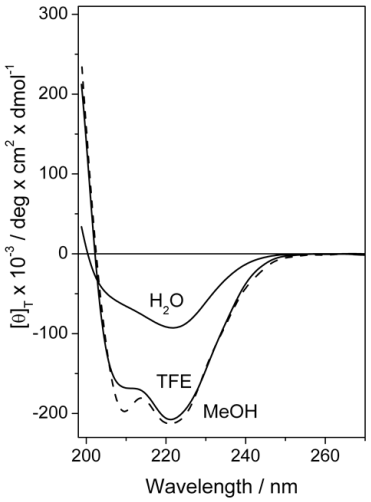

Figure 47. CD spectrum of dual action compound **111** in different solvents.

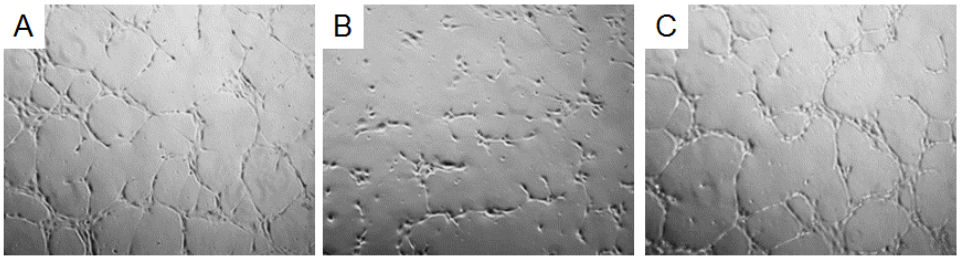

FIGURE 48. Phase contrast photomicrographs of HUVE cells on Matrigel plates, treated with: A) $VEGF_{165}$ (10 ng/mL); B) $VEGF_{165}$ (10 ng/mL) + **111** (1 μM); C) $VEGF_{165}$ (10 ng/mL) + **112** (1 μM). Images were elaborated by phase-contrast microscopy using a fluorescence microscope. Adapted from ref. 72.

1.2.2 VEGF-C DERIVED LIGANDS FOR VEGFR-2 AND VEGFR-3

Encouraged by the promising activity of the dual action conjugate **111**, we decided to further investigate the field of VEGFR ligands and, in particular, those able to selectively target VEGFR-2 and VEGFR-3 in order to prepare more potent and selective anti-angiogenic agents. With this aim, we focused our attention on VEGF-C, which demonstrated to be a multifaceted effector involved in progression of different cancer types by regulating tumor angiogenesis, upon interaction with both VEGFR-2 and VEGFR-3. In 2012, the binding affinity of vascular endothelial growth factor C towards the extracellular domain of VEGFR-2 was measured by calorimetry titration experiments and the experimental dissociation constant was K_d = 1210 nM.[74] Later, using a similar strategy, the K_d for the interaction VEGF-C -VEGFR-3 was determined (K_d = 5.6 nM).[75] The analysis on the crystal structure of VEGF-C bound to the high-affinity binding site of VEGFR-2 showed that the *N*-terminal α-helix (Ile122-Gln130 portion, in FIGURE 49) in the growth factor is responsible for the selectivity towards VEGFR-2 (FIGURE 50 on the left). In this nonapeptide sequence, one hydrophobic interaction (Ile122-Trp126) and two bridge salts (Asp123-Arg127 and Glu125-Lys128) stabilize the helical secondary structure of the backbone (FIGURE 50 on the right).[76]

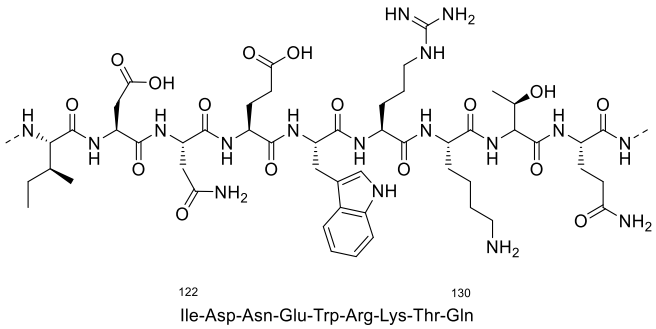

FIGURE 49. The α-helix Ile122-Gln130 deriving from the *N*-terminal natural sequence of VEGF-C (the numbers are referred to the natural amino acid chain).

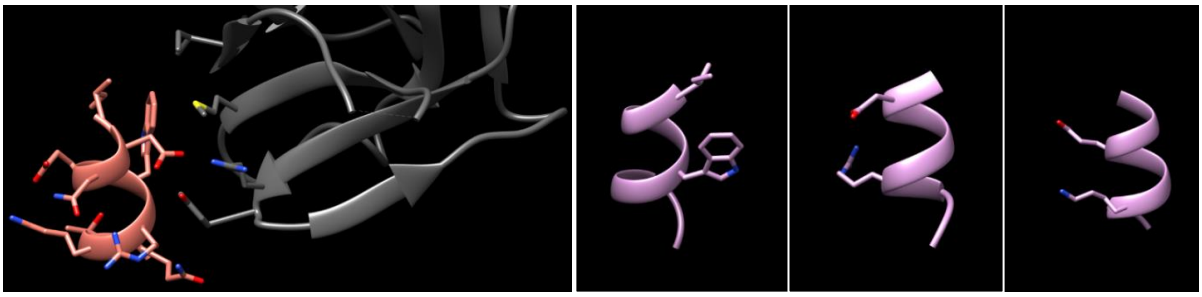

FIGURE 50. Fragment Ile122-Gln130 interacting with the high-affinity binding site of VEGFR-2 (on the left) and the three stabilizing interactions present along the peptide chain, Ile122-Trp126, Asp123-Arg127 and Glu125-Lys128 (on the right).

This helical fragment represents an attractive candidate for further structure optimization in order to obtain more potent and selective VEGFR-2 ligands to exploit in VEGFR-targeted anti-angiogenesis therapy. For this reason, in collaboration with Professor Lorenzo Stella (Università di Roma Tor Vergata, Rome), we designed and synthesized a small library of VEGF-C derived peptides starting from the natural portion Ile122-Gln130 (see PARAGRAPH II – 2.1 and II – 2.2).

2 SYNTHESIS OF VEGFR LIGANDS

2.1 STRATEGY

The portion Ile122-Gln130 is located at the *N*-terminal helix of VEGF-C: this fragment is not only responsible for the protein-protein interaction with the target receptors, but also for the intrinsic selectivity of the growth factor C towards VEGFR-2 and VEGFR-3, with respect to VEGFR-1. The biological activity of this small sequence, composed by nine amino acids, relies on the native helical folding, which displays relevant residue side chains in a proper orientation to engage the receptor hotspots during the interaction. The stability of this structural conformation arises from three fundamental intra-chain interactions: Ile122-Trp126, Asp123-Arg127 and Glu125-Lys128.
In collaboration with Professor Lorenzo Stella (Università di Roma Tor Vergata, Rome), we designed and synthesized VEGFR ligands deriving from the VEGF-C Ile122-Gln130 portion. We started preparing the nonapeptide **113**, a congener of the natural fragment in which both the *N*- and the *C*-terminal residues were capped (FIGURE 50). Since such short peptides seldom retain their biologically active secondary structure, we modified the native sequence by introducing both natural and non-natural amino acids. In a first approach, we synthesized peptide **114** (FIGURE 51) by replacing Ile122 and Gln130 with tryptophan residues, whose aromatic indole ring would have strengthened the pre-existing hydrophobic interactions with Trp126 and, at the same time, embedding an amine functionality able to participate in hydrogen bonds. Moreover, both Ile122 and Gln130 are involved in the interaction with hydrophobic regions of the receptor: for this reason, the substitution with two Trp residues would also improve the ligand-receptor binding.

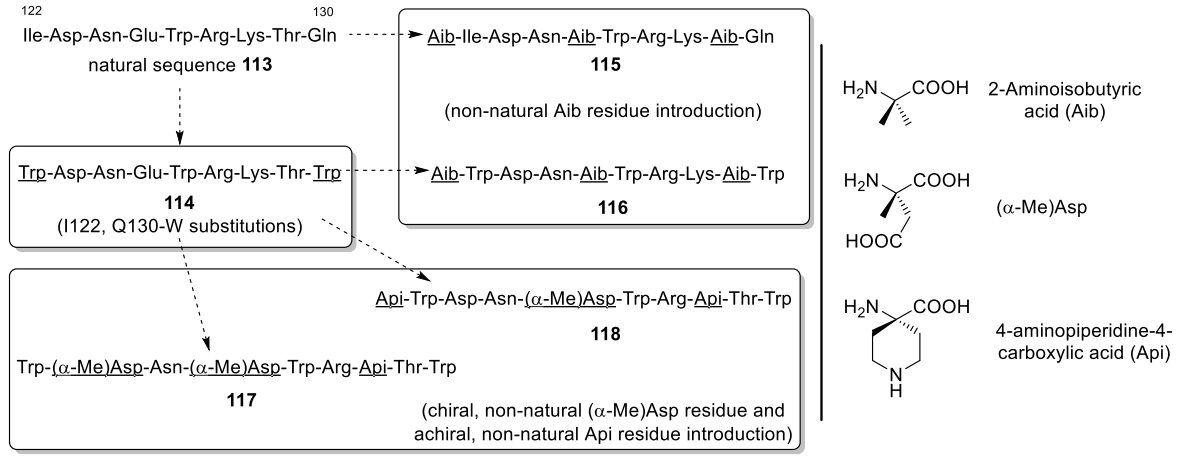

FIGURE 51 Overview of the natural portion **113** and the derived peptides **114**-**118**. The modifications are underlined.

On the other hand, we introduced non-natural residues bearing a quaternary stereocenter at the Cα, since α,α-disubstituted amino acids are known to induce helical folding. 2-Aminoisobutyric acid (Aib), α-methylaspartic acid [(α-Me)Asp] and 4-aminopiperidine-4-carboxylic acid (Api) were selected as achiral (Aib, Api) and chiral [(α-Me)Asp] amino acids to be introduced along **113** and **114** peptide sequences. We thus prepared compounds **115**-**118**, where the residues not involved in the interaction with the receptor were replaced or the (α-Me)Asp residue was employed to replace the cardinal residue Glu125 without impairing the ligand binding. Indeed, while the introduction of Aib residues allowed to

increase the backbone rigidity enhancing the helical folding, the quaternary residues (α-Me)Asp and Api had the additional advantage of displaying a carboxylate and an amine portions in the side chains, respectively. The α-NH_2 group of the *N*-terminal residue could be exploited as handle to conjugate these congeners to other molecular entities. Such direct manipulation of the backbone could affect the conformational structure of the peptide: for this reason, an Api residue was placed at position 1 in compound **118**, giving the possibility to exploit the secondary amine moiety in the side chain for further functionalization.

2.2 SYNTHESIS OF PEPTIDES **113-118**

A semi-automatic synthesizer was used to prepare sequences **113-118** *via* SPPS on Rink Amide MHBA resin with the Fmoc/*t*Bu strategy and assisting each coupling reaction with microwaves. A schematic representation of the SPPS is shown in SCHEME 15. First, the resin was swallen in DMF and treated with a 25% solution of piperidine in DMF to remove the Fmoc-protecting group, releasing the reactive amino moiety on the beads (step a). The Fmoc-amino acid to be attached to the solid support was activated with DIC and HOAt condensing agents in the presence of *i*Pr_2NEt in DMF: after stirring for 25 min at 0 °C, the mixture was added to the resin and a cycle of coupling, capping and deprotection was performed by the semi-synthesizer (step b). This procedure was repeated until the sequence was completed, then the *N*-terminal residue was acetylated and the beads were treated with TFA, using thioanisole, EDT and anisole as scavengers. Subsequent purification of the crude peptide with RP-HPLC and freeze-drying from glacial acetic acid gave the pure compound as a fluffy foam.

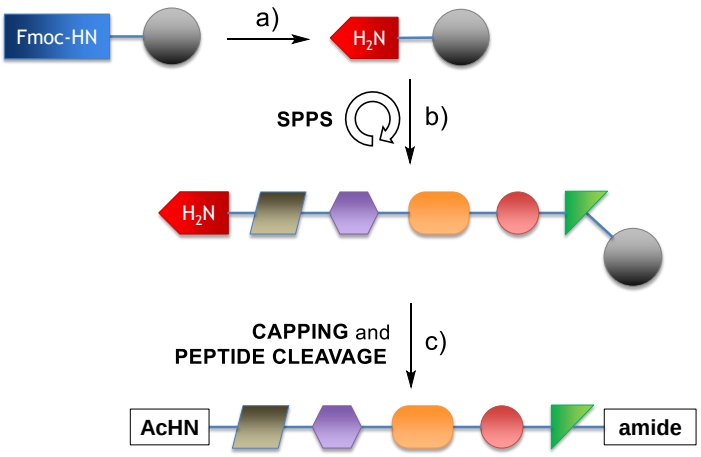

SCHEME 15. Synthesis of sequences **113-118**. Reagents and conditions: a) 25% piperidine in DMF; b) SPPS (repeat): 1. Fmoc-AA-OH (4.0 eq), DIC, HOAt, *i*Pr_2NEt, DMF, microwaves; 2. 25% Ac_2O in DMF; 3. 25% piperidine in DMF; c) Capping and peptide cleavage: 1. 25% Ac_2O in DMF; 2. TFA/thioanisole/EDT/anisole 90:5:3:2 v/v/v/v, r.t., 3 h, 7-30%.

α,α-Disubstituted residues are poorly reactive, even upon activation, because of the high steric congestion around the reactive ester moiety. For this reason, double coupling reactions were performed when a quaternary amino acid had to be attached to the resin: using this procedure, after the first coupling step, a second aliquot of the activated amino acid was added to the resin to perform another condensation reaction and to saturate free –NH_2 that did not react during the first coupling step.

2.3 STRUCTURAL INVESTIGATIONS ON PEPTIDES **113-118**

2.3.1 CIRCULAR DICHROISM (CD) EXPERIMENTS

In collaboration with Professor Fernando Formaggio and Dr. Marta De Zotti (Università degli Studi di Padova, Padua), VEGF-C derived peptides **113-118** were studied with NMR and CD spectroscopy to

evaluate their secondary structure. The CD spectrum arises from the sum of the contributes of each amide moiety present in the peptide. When a peptide folds into a helical conformation, the spatial distribution and orientation of its chromophores generate a CD spectrum, which usually consists of two major bands, corresponding to the π→π* and n→π* electronic transitions, located at about 208 and 220 nm (the wavelength values can be different due to the helix type, α-helix or 3_{10}-helix). Usually, in a CD spectrum the wavelength values are reported on the x-axis, while the molar ellipticity [θ] is on the y-axis. [θ] can be either positive or negative, depending on the rotatory direction of the helix: in the presence of a right-handed helical structure the ellipticity assumes negative values; instead, left-handed helices are characterized by positive [θ] values.

Compounds **113** and **114** exhibited a pronounced helical folding, mainly corresponding to a 3_{10}-helix, based on the corresponding CD spectra in FIGURE 52. This folding type is characterized by *i*-*i*+4 interactions along the peptide chain, and it is similar to the more compact α-helix that presents a *i*-*i*+5 hydrogen bonding pattern. In the CD spectra of **115** and **116** (FIGURE 52), the negative peaks at ≈200 nm were characterized by a lower intensity band with respect to the corresponding sequences **113** and **114**, in which the Aib residue was not present. On the other hand, the intensity of the transitions at ≈218 nm were not affected by the presence of aminoisobutyric acid. Moreover, the CD curve of **116** exhibited an additional negative peak at ≈238 nm that was not observed in the spectrum of the parental peptide **114**. Three tryptophan residues were included in the backbone of peptide **116** and their aromatic chromophores contributed to the absorbance in the near-UV region. In particular, this effect was enhanced by the higher structural rigidity resulting from quaternary Aib residues. This hypothesis was validated recording the near-UV CD spectra of **115** and **116** (FIGURE 53), which showed a positive transition at ≈270 nm that is absent in the near-UV spectrum of **113** and irrelevant in the spectrum of **114** (FIGURE 54). In the CD spectrum of peptide **116**, a further minimum was identified at ≈238 nm: this band could be due to stacking interactions between the indole portions of Trp side chains (Ac-U-W-D-N-U-W-R-K-U-W-amide, with U = Aib = 2-aminoisobutyric acid), or other effects provoked by peptide aggregation in the aqueous medium. In conclusion, the remarkable contribution of tryptophan amino acids in the CD spectra of **115** and **116** is strictly related to the higher backbone rigidity due to the presence of the Aib residues.

Sequences **117** and **118** exhibited a α-helical folding (FIGURE 52): these compounds showed a different conformational behavior with respect to that of **115** and **116**, probably due to the replacement of Aib with (α-Me)Asp and Api fragments, which imparted a lower, but still essential, rigidity to the backbone. As a matter of fact, the helical structure of **117** and **118** was slightly more flexible with respect to those of compounds **115** and **116**.

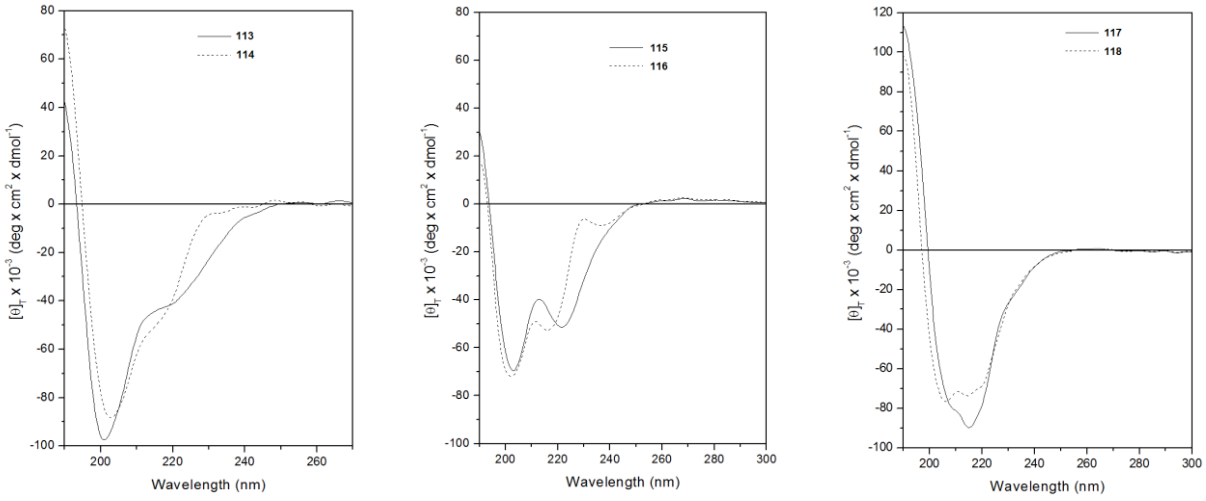

FIGURE 52. CD spectra of compounds **113-118** (*ca.* 10^{-4} M in H_2O).

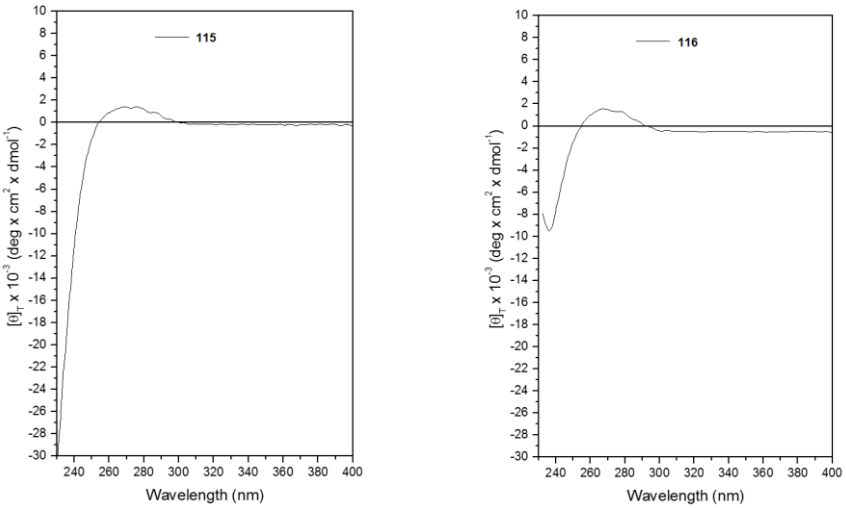

FIGURE 53. Near-UV CD spectra of compounds **115** and **116** (*ca.* 10^{-4} M in H_2O, pathlenght 1 cm).

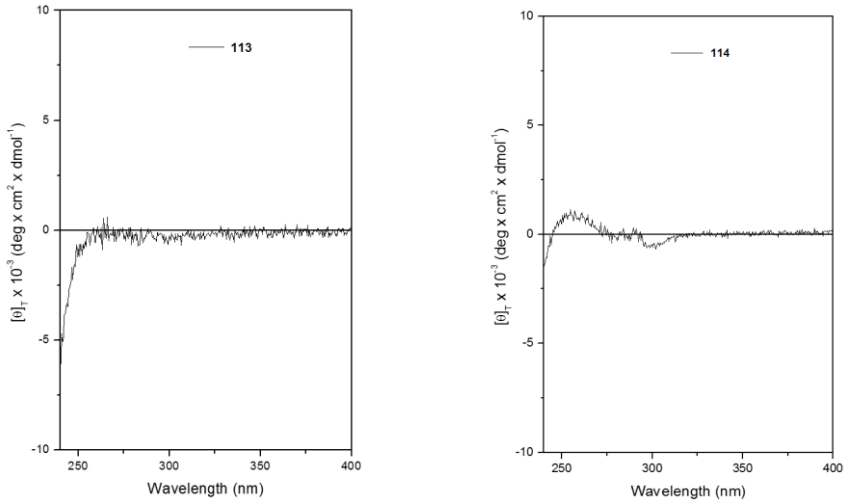

FIGURE 54. Near-UV CD spectra of compounds **113** and **114** (*ca.* 10^{-4} M in H_2O, pathlenght 1 cm).

2.3.2 BIDIMENSIONAL NMR EXPERIMENTS

Compound **115** was selected as example peptide and further investigated with 2D-NMR experiments. The ROESY (Rotating-frame nuclear Overhauser Effect Spectroscopy) spectrum of compound **115** is shown in FIGURE 55. The presence of the $NH_i \rightarrow NH_{i+1}$ cross-peaks confirmed that **115** adopts a helical conformation in solution. Moreover, the fingerprint region of the spectrum provided an additional evidence of the helical secondary structure of **115**: as a matter of fact, the presence of $\alpha H_i \rightarrow NH_{i+n}$ cross-peaks allowed the identification of the helical structure type (FIGURE 56).

Indeed, $\alpha H_i \rightarrow NH_{i+3}$ cross-peaks are common features of both α-helices and 3_{10}-helices, but $\alpha H_i \rightarrow NH_{i+2}$ cross-peaks are typical of 3_{10}-helices, while $\alpha H_i \rightarrow NH_{i+4}$ cross-peaks are present only in α-helical structures. In the first part of the peptide chain, the interaction $\alpha H_3 \rightarrow NH_5$ denoted that the *N*-terminal fragment adopts a 3_{10}-helical conformation, while the $\alpha H_6 \rightarrow NH_9$ cross-peak demonstrated only that the *C*-terminal part of the peptide is characterized by a helical folding, although neither the 3_{10}-helix typical cross-peaks nor those of the α-helix were observed. In conclusion, ROESY experiments on **115** confirmed the helical secondary structure adopted by the peptide. The helix type was prevalently a 3_{10}-helical structure for the *N*-terminal region. The *C*-terminal region presented a similar folding, but a certain conformational flexibility was observed and it was not possible to assign a defined helical subtype to this peptide portion.

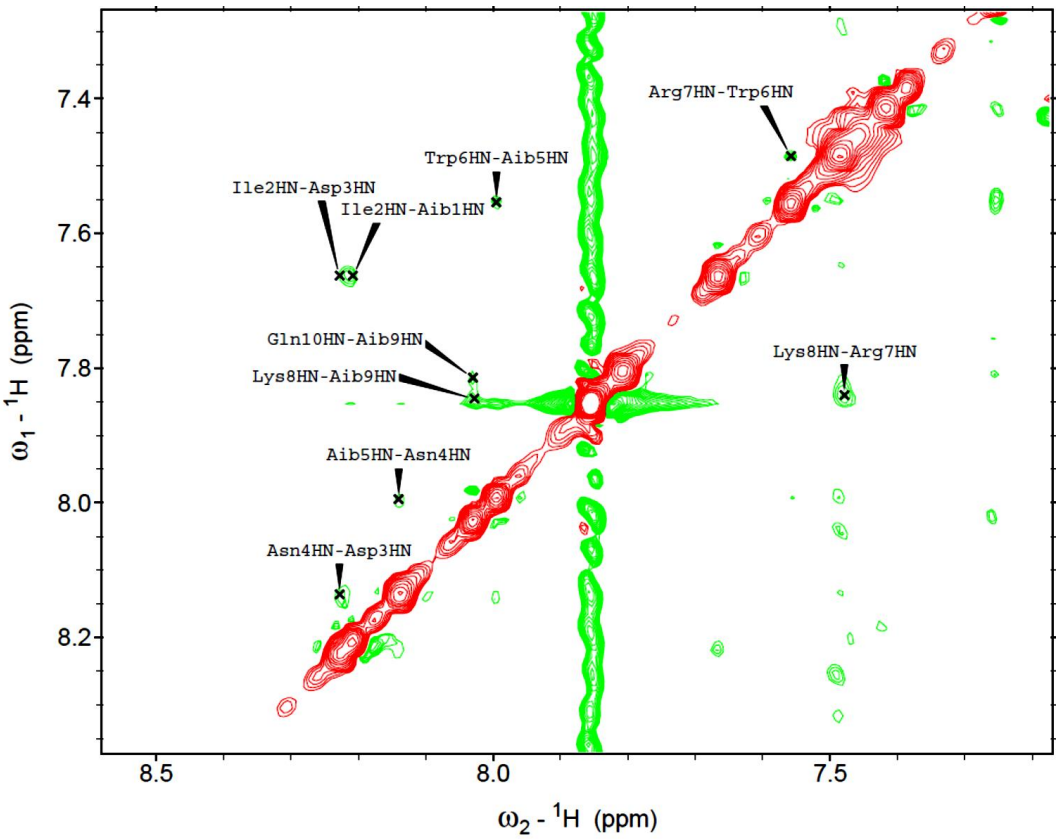

FIGURE 55. Portion of the ROESY spectrum of **115** [298 K, 600 MHz] in H_2O/D_2O 9:1 (pH ≈4).

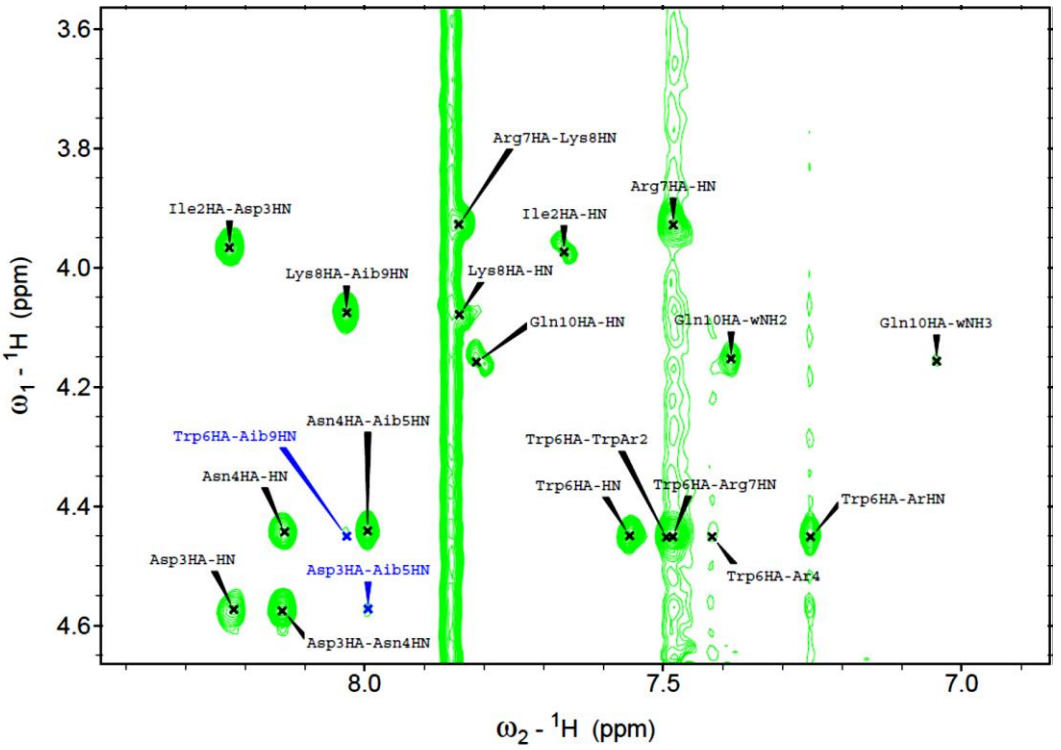

FIGURE 56. Fingerprint region of the ROESY spectrum of **115** [298 K, 600 MHz] in H_2O/D_2O 9:1 (pH ≈4).

2.4 BIOLOGICAL INVESTIGATIONS ON PEPTIDES **114-118**

2.4.1 BINDING ASSAYS ON ISOLATED VEGFR-1

In collaboration with Dr. Daniela Arosio (CNR-ISTM, Milan), the VEGF-C derived peptides **114-118** were investigated with *in vitro* binding assays to evaluate the affinity of the synthesized peptides towards the isolated VEGFR-1 receptor (TABLE 10).

TABLE 10. Inhibition of biotinylated $VEGF_{165}$ binding to isolated VEGFR-1.

Compound	Sequence	% Inhibition[a]	IC_{50} (μM)[b]
114	Ac-Trp-Asp-Asn-Glu-Trp-Arg-Lys-Thr-Trp-amide	29.2 ± 6.9	n.d.
115	Ac-Aib-Ile-Asp-Asn-Aib-Trp-Arg-Lys-Aib-Gln-amide	86.3 ± 1.2	125
116	Ac-Aib-Trp-Asp-Asn-Aib-Trp-Arg-Lys-Aib-Trp-amide	35.1 ± 12.7	n.d.
117	Ac-Trp-(α-Me)Asp-Asn-(α-Me)Asp-Trp-Arg-Api-Thr-Trp-amide	81.8 ± 0.7	52
118	Ac-Api-Trp-Asp-Asn-(α-Me)Asp-Trp-Arg-Api-Thr-Trp-amide	82.6 ± 2.5	69

[a] % of inhibition of biotinylated $VEGF_{165}$ binding to VEGFR-1 at 500 μM. [b] IC_{50} values were extrapolated by GraphPad Prism.

Peptides **115**, **117** and **118** showed a remarkable inhibition of biotinylated $VEGF_{165}$ binding to isolated VEGFR-1 and the corresponding IC_{50} values were calculated by extrapolation. For this reason, these data have to be considered as range of concentrations, but in any case they are still indicative of the *in vitro* biological activity of the tested compounds. The introduction of quaternary amino acids resulted in a beneficial effect in terms of affinity towards VEGFR-1 receptor, except for peptide **116**, which derives from **115** by replacement of Ile2 and Gln10 with Trp. This modification enhanced both the helical content of the peptide backbone (as demonstrated by the CD analysis) and the hydrophobicity of the compound with a possible negative effect on its solubility. As mentioned above, the CD spectrum in the near-UV of peptide **116** exhibited an additional minimum at 238 nm that possibly arose from aggregation phenomena (FIGURE 52 and FIGURE 53). This fact could also have affected the affinity of peptide **116**. On the contrary, compounds **117** and **118** represented a good compromise between the conformational rigidity of the backbone and the biological activity of the peptide. The introduction of α,α-disubstituted amino acids like (α-Me)Asp and Api had two main advantages: decreasing the conformational flexibility and retaining the important functional groups (such as a carboxylate and a secondary amine functionalities) in the side chains. Indeed, with respect to Aib residues, the FGs in α-methylaspartate and 4-aminopiperidine-4-carboxylate could play a fundamental role both in the interaction with the receptor and in the peptide solvation, thus explaining the promising results obtained with *in vitro* affinity assays on VEGFR-1.

The next step will be the evaluation of the affinity of all the synthesized peptides towards isolated VEGFR-2: indeed, since these sequences derive from the VEGF-C *N*-terminal helix, they should bind preferentially VEGFR-2 and VEGFR-3 with respect to VEGFR-1. We decided to perform in any case *in vitro* assays on isolated VEGFR-1 since the experimental protocol was already assessed and exploited to evaluate the affinity of the dual action compound **111** (FIGURE 46): the results obtained on VEGFR-1 (TABLE 10), can be used to set a preliminary comparison among the tested peptides. For this reason, the two promising sequences **117** and **118** were subjected to additional biological investigations.

2.4.2 MORPHOGENESIS ASSAYS

In collaboration with Dr. Marino (Università degli Studi dell'Insubria, Varese), peptides **117** and **118** were further studied *in vitro* on HUVE cells. FIGURE 57 shows the macroscopic effects resulting from the administration of either **117** or **118** to HUVECs, in the presence of $VEGF_{165}$ as angiogenesis agonist:

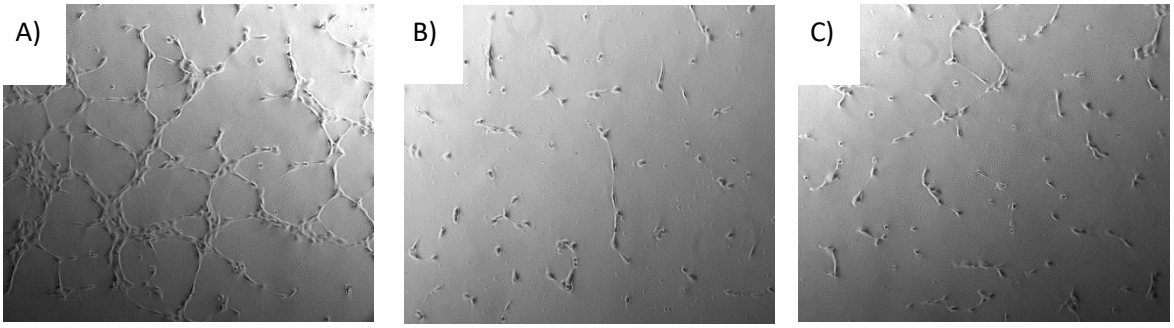

FIGURE 57. Representative phase contrast photomicrographs of HUVE cells plated on Matrigel in the presence of: A) $VEGF_{165}$ (10 ng/mL); B) $VEGF_{165}$ (10 ng/mL) + **117** (1 μM); C) $VEGF_{165}$ (10 ng/mL) + **118** (1 μM).

in comparison with the control experiment (FIGURE 57A), **117** and **118** (FIGURE 57B and FIGURE 57C, respectively) prevented the formation of capillary network efficiently. Interestingly, peptides **117** and **118** exhibited a remarkable anti-angiogenic activity in the concentration range 10^{-9} – 10^{-6} M (FIGURE 58): in particular, compound **117** was found more effective than **118** in reducing both loops and branches formation. This pronounced biological activity against VEGF-mediated morphogenesis could be ascribed to the interference of the tested compounds with the VEGF-VEGFR axis. The *in vitro* binding studies presented in PARAGRAPH II – 2.4.1 demonstrated the ability of these compounds to interact with VEGFR-1. The biological activity of such compounds could be the result of a complex mechanism of signalling involving different effectors and related receptors. In this case, $VEGF_{165}$ was used as only stimulator of angiogensis, thus the inhibition of morphogenesis suggests that compounds **117** and **118** can interfere with the interaction of $VEGF_{165}$ with its biological targets (*i.e.* VEGFR-1 and VEGFR-2).

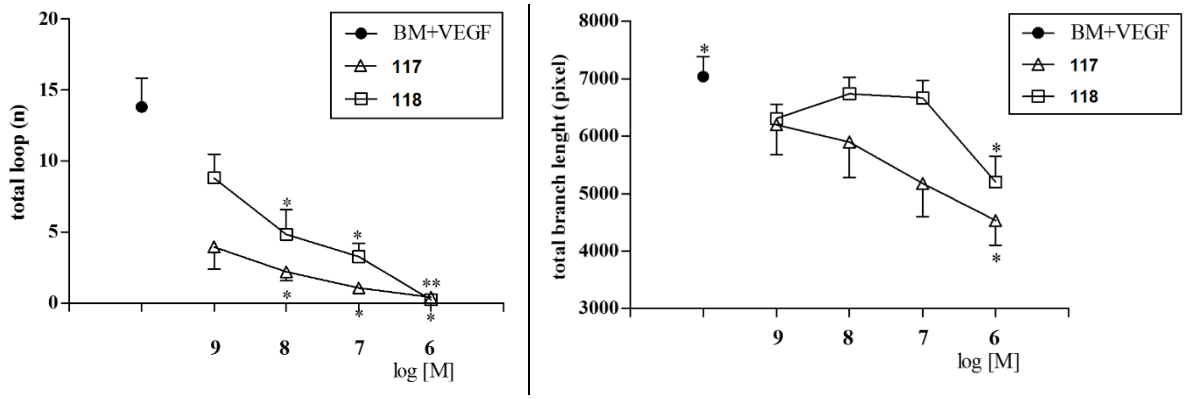

FIGURE 58. Inhibition of VEGF-mediated angiogenesis on HUVE cells upon treatment with compound **117** or **118**.

Based on these experimental results, the evaluation of the affinity towards VEGFR-2 receptor becomes more and more important: screening all the synthesized peptides will allow to identify the most promising ones, which will be further optimized by computational studies.

3 CONCLUSIONS

With the aim of synthesizing potent VEGFR ligands, we selected the *N*-terminal helix of VEGF-C, the natural ligand of VEGFR-2 and VEGFR-3, and designed a small library of peptides (**113-118**) by introducing systematic modifications along the native sequence. In particular, both natural and non-natural amino acids were included in the new peptides, in order to stabilize the helical folding that is essential for the biological activity of such compounds. For this reason, tryptophan residues, as well as 2-aminoisobutyrric acid (Aib), α-methylaspartic acid [(α-Me)Asp] and 4-aminopiperidine-4-carboxylic acid (Api) were placed at specific backbone positions. The synthesis of sequences **113-118** was carried out with a semi-automatic synthesizer using SPPS protocols: the procedure was straightforward and the cleavage from the resin afforded the desired peptides upon HPLC purification and freeze-drying.

Structural investigation on the synthesized compounds were conducted by NMR and CD spectroscopy. The CD spectra of **113-118** presented the typical features of a helical folding, with certain variations in the position and intensity of UV transitions due to the presence of specific amino acids along the chain. Moreover, compound **115** was selected as example and it was studied using bidimensional NMR experiments (ROESY): the fingerprint region presented the diagnostic cross-peaks of a 3_{10}-helical conformation.

Peptides **114-118** were tested *in vitro* to determine their ability to bind isolated VEGFR-1 receptor: compounds **117-118** turned out to be the most promising ones, with IC_{50} values in the range of 50-70 μM. Further investigations on compounds **117-118** demonstrated their potent biological activity as inhibitors of $VEGF_{165}$-mediated angiogenesis in HUVE cells: in particular, both the tested compounds were active in the $10^{-9} – 10^{-6}$ M range.

The affinity of compounds **114-118** towards VEGFR-2 is currently ongoing and, together with the biological data already in our hands, will allow the identification of the best peptide sequences that will be optimized by computational studies, aimed at designing a non-peptide VEGFR-2 binder. The latter compound will be also exploited in the preparation of dual-action ligands able to interact with both integrin and VEGF receptors and thus impair the tumor angiogenesis.

EXPERIMENTAL PART

GENERAL REMARKS AND PROCEDURES

MATERIALS AND METHODS

All manipulations requiring anhydrous conditions were carried out in flame-dried glassware, with magnetic stirring and under a nitrogen atmosphere. All commercially available reagents were used as received. Anhydrous solvents were purchased from commercial sources and withdrawn from the container by syringe, under a slight positive pressure of nitrogen. The reactions were monitored by analytical TLC using silica gel 60 F_{254} pre-coated glass plates (0.25 mm thickness). Visualization was accomplished by irradiation with a UV lamp and/or staining with a potassium permanganate alkaline solution, ninhydrin or ceric ammonium molibdate solution. Flash column chromatography was performed according to the method of Still and co-workers[77] using Chromagel 60 ACC (40-63 μm) silica gel. Proton NMR spectra were recorded on a spectrometer operating at 400.16 MHz. Proton chemical shifts are reported in ppm (δ) with the solvent reference relative to TMS employed as the internal standard. The following abbreviations are used to describe spin multiplicity s = singlet, d = doublet, t = triplet, q = quartet, m = multiplet, bs = broad signal, dd = doublet of doublet, ddd = doublet of doublet of doublet, ddt = doublet of doublet of triplet. Carbon NMR spectra were recorded on a spectrometer operating at 100.63 MHz, with complete proton decoupling. Carbon chemical shifts are reported in ppm (δ) relative to TMS with the respective solvent resonance as the internal standard. In the case of 2D-NMR experiments for conformational studies, all NMR spectra were acquired on a Bruker Avance DMX-600 instrument, using the TOPSPIN 1.3 software package. A CLEAN-TOCSY spectrum (spin-lock pulse, 70 ms)[78] was acquired by collecting 200 recordings of 40 scans each, whilst, for the NOESY spectrum, 400 recordings, each one consisting of 64 scans, were acquired. The NOESY experiment (mixing time, 150 ms) was exploited for the sequential assignment. ESI-MS spectra were recorded on the ion trap mass spectrometer Finnigan LCQ Advantage. The MALDI-TOF-MS spectra were recorded on the instrument Bruker Microflex™ LT, supporting the sample on the 2,5-dihydroxybenzoic acid (DHB), α-cyano-4-hydroxycinnamic acid (HCCA) and sinapinic acid (SIN) matrices. The peptide calibration standard (300-3000 Da range), which consisted of Angiotensin II, Angiotensin I, Substance P, Bombesin; ACTH clip 1-17, ACTH clip 18-39, Somatostatin 28, was purchased from Bruker Daltonics® and used to calibrate the MALDI-TOF-MS instrument. The sample was mixed in equal volumes with the matrix solution: a small amount (1 μL) of this mixture was spotted on the target surface. The target matrix was dried at room temperature and then analyzed.

EP.1 RP-HPLC PURIFICATION

The HPLC purifications were performed using a Dionex Ultimate 3000 instrument equipped with a Dionex RS Variable Wavelength Detector (column: Atlantis® Prep T3 OBD™ 5 μm 19 × 100 mm). The crude reaction mixture was dissolved in H_2O or, if the compound was insoluble in water, adding first DMF, then diluting slowly with H_2O until reaching a 1:1 mixture DMF/H_2O (ultrasonic sonicator was used to assist the dissolution). The solution so obtained was filtered (polypropylene, 0.45 μm, 13 mm ø, PK/100) and injected in the HPLC, affording purified products.

EP.2 RP-HPLC ANALYSIS

Purity analyses were carried on a Dionex Ultimate 3000 instrument equipped with a Dionex RS Variable Wavelenght detector (column: Atlantis® Prep T3 OBD™ 5 μm 19 x 100 mm). 1 mg of analyte was dissolved in 1 mL of H_2O and was injected using the same gradient used in the purification step. The analysis of the integrals and the relative percentage of purity was performed with the software Cromeleon 6.80 SR11 Build 3161.

EP.3 FREEZE-DRYING

The product was dissolved in water or glacial acetic acid and frozen with dry ice: the freeze-drying was carried out at least for 48 h at -50 °C using the instrument 5Pascal Lio5P DGT.

EP.4 CIRCULAR DICHROISM SPECTROSCOPY

The circular dichroism measures were registered on the CD instrument Jasco J-715 with Hellma 0.1 cm quartz cell in milliQ H_2O as solvent. The spectra were elaborated with Origin and the Jasco instrument associated software. The values are reported as total molar ellipticity $[\theta]_T$ (deg × cm^2 × $dmol^{-1}$).

EP.5 SOLID PHASE RECEPTOR BINDING ASSAYS

INTEGRIN RECEPTOR

Purified $\alpha_v\beta_3$ receptor (Chemicon International, Inc., Temecula, CA) were diluted to 0.5 μg/mL in coating buffer containing 20 mmol/L Tris-HCl (pH 7.4), 150 mmol/L NaCl, 1 mmol/L $MnCl_2$, 2 mmol/L $CaCl_2$ and 1 mmol/L $MgCl_2$. An aliquot of diluted receptors (100 μL/well) was added to 96-well microtiter plates (NUNC MW 96F MEDISORP STRAIGHT) and incubated overnight at 4 °C. The plates were then incubated with blocking solution (coating buffer plus 1% bovine serum albumin) for additional 2 hours at room temperature to block nonspecific binding followed by 3-hour incubation at room temperature with various concentrations (10^{-12} – 10^{-5} M) of test compounds in the presence of 1 μg/mL vitronectin biotinylated using EZ-Link Sulfo-NHS-Biotynilation kit (Pierce, Rockford, IL). After washing, the plates were incubated for 1 hour at room temperature with streptavidin-biotinylated peroxidase complex (Amersham Biosciences, Uppsala, Sweden) followed by 30 minutes incubation with 100 μL Substrate Reagent Solution (R&D Systems, Minneapolis, MN) before stopping the reaction by addition of 50 μL of 1 N H_2SO_4. Absorbance at 415 nm was read in a Synergy™ HT Multi-Detection Microplate Reader (BioTek Instruments, Inc.). Each data point is the result of the average of duplicate wells and was analysed by nonlinear regression analysis with Prism GraphPad program.

VEGF RECEPTOR

The surface of white high-binding 96-well microplates (Corning Life Sciences, Netherlands) was coated with 100 μL of phosphate-buffered saline solution (PBS, pH 7.4) containing 200 ng/mL of VEGFR-1 ECD/Fc chimera (R& D Systems, Minneapolis, MN, USA) and incubated overnight at 4 °C. After three washes with 150 μL of PBS 0.1%, (v/v) Tween 20 (buffer A), the plate was blocked by 160 μL of PBS with 3% (w/v) of BSA and incubated at r.t. for 2 h. The plate was washed three times with buffer A. Then, 100 μL of a solution of $btVEGF_{165}$ at 131 pM (5 ng/mL) and the tested compounds at various concentrations diluted in PBS containing 5% DMSO were added to each well. After 3 h at 37 °C, the plate was washed three times with buffer A and 100 μL of streptavidin–horseradish peroxidase diluted at 1:1000 in PBS containing 0.1% (v/v) Tween 20 and 0.3% (w/v) BSA were added per well. After 1 h of incubation at r.t., the plate was washed five times with 150 μL of buffer A and 100 μL of SuperSignal West Pico Chemiluminescent Substrate (Pierce, Rockford, IL, USA) were added. The remaining bt-$VEGF_{165}$ was detected by chemiluminescence, which was quantified with a Synergy™ HT Multi-

Detection Microplate Reader (BioTek Instruments, Inc.). The percentages of $btVEGF_{165}$ displacement were calculated by the following formula: percentage of displacement = $100\times[1-(S-NS) / (MS-NS)]$, where *S* is the signal measured, *NS* is the nonspecific binding signal and *MS* is the maximum binding signal observed with $btVEGF_{165}$ without tested compounds.

EP.6 EVALUATION OF INTEGRIN EXPRESSION BY FLOW CYTOMETRY

Cells were collected, washed with PBS and counted. For each sample, 5×105 cells were resuspended in 100 µL of 1% BSA-PBS containing (or not in the case of the negative control) the anti-$\alpha_V\beta_3$ antibody (clone LM609-Millipore MAB 1976) at 1:50 dilution. After incubation for 30 min at 4 °C, samples were washed with PBS and incubated with the secondary antibody (CF488A-goat anti-mouse IgG, Biotium 20011) diluted 1:300 for 30 min at 4 °C. After washing, samples were acquired by a Facscalibur (Becton Dickinson) cytometer and analyzed by CellQuest software.

EP.7 CELL PROLIFERATION ASSAY

Cells were seeded in 96-well plates with the appropriate complete medium (RPMI 1640 medium with 2 mM L-glutamine, 10% fetal calf serum, 10 mM 2-[4-(2-hydroxyethyl)-1-piperazinyl]ethanesulfonic acid, and 1 mM sodium pyruvate). 48 h after seeding, the medium was replaced with medium containing serial dilutions of the test compounds. The cells were incubated for 144 h at 37 °C. Cell viability was assessed with the CellTiter-Glo luciferase-based ATP detection assay (Promega) by following manufacturer's instructions. Growth inhibitory activity was evaluated at the end of incubation by using GraphPad Prism software. Experimental data were normalized versus untreated control samples and interpolated by nonlinear regression analysis with GraphPad Prism software to generate dose-response curves. IC_{50} values were calculated by using sigmoidal interpolation curve fitting.

EP.8 CELL CULTURES

HUVE cells were cultured in a medium supplemented with FBS (2%), L-glutamine (10 mM), heparin sulfate (0.75 U/mL), VEGF (15 ng/mL), EGF (5 ng/mL), FGF2 (5 ng/mL), IGF-I (15 ng/mL) and ascorbic acid (50 µg/mL) at 37 °C, in a moist atmosphere of 5% CO_2. HUVECs were used for the experiment between passage 2 to 10.

EP.9 *IN VITRO* MORPHOGENESIS ASSAYS ON HUVEC

To assess anti-angiogenic activity, HUVECs (2.5×10^4 cells) were seeded in a 24-well plate coated with 100 µL/well of Matrigel previously polymerized for 1 h at 37 °C. Cells were then incubated for 5 h at 37 °C in a moist atmosphere of 5% CO_2 without or with tested compounds under either resting (cell cultured in EndoGRO medium alone, without FBS and all the growth factors) or stimulated conditions (addition of VEGF, 10 ng/mL). Network formation was evaluated by phase-contrast microscopy using a fluorescence microscope (Axiovert 40CFL, Carl Zeiss S.p.A. Milan, Italy). Network formation was finally quantified in terms of total length of the branches. For the purpose of the analysis, open ramifications were considered as branches. The total branch length (pixels) was quantified using the ImageJ image analysis software (http://rsbweb.nih.gov/ij/).

EP.10 STATISTICAL ANALYSIS

Data are shown as means ± standard deviation (SD) unless otherwise indicated. Statistical significance of the differences was assessed by two-tailed Student's *t* test for paired data. Calculations were

performed using a commercial software (GraphPad Prism version 5.00 for Windows, GrapPad Software, San Diego California USA, www.graphpad.com).

EP.11 GENERAL PROCEDURES FOR SOLID-PHASE SYNTHESIS

GP1. GENERAL PROCEDURE 1 FOR KAISER TEST

A few drops of solution A (80% phenol solution in ethanol), solution B (6% ninhydrin solution in ethanol) and solution C (98:2 pyridine/KCN aq. 0.1 mM) were added to a small sample of the resin and then shaken at 100 °C for 1 min. If the solution maintained its yellow color, quantitative coupling was achieved. On the contrary, in case of a slight blue color, the coupling step was not fully completed and it was then repeated.

GP2. GENERAL PROCEDURE 2 FOR SOLID-PHASE PEPTIDE SYNTHESIS (SPPS)

The SPPS was accomplished using the semi-automatic synthesizer Biotage® Initiator™ assisted by microwaves. Fmoc/*t*Bu strategy and Rink Amide MHBA Resin (100-200 mesh; loading: 0.5 mmol/g) were used for the synthesis of compounds **113-118**. Fmoc/*t*Bu strategy and SASRIN™ Resin (200-400 mesh, loading: 1.02 mmol/g) were used for the synthesis of compounds **39**, **40** and **84**.
Each coupling step consisted in:

1) activation of the Fmoc-protected amino acid;
2) addition of the activated amino acid to the resin at the synthesizer to start the coupling;
3) steps of capping, deprotection and washing.

SOLUTIONS AND SOLVENTS

To perform the automated SPPS, two solutions and two solvents were prepared: 25% Ac_2O in DMF (v/v), 25% piperidine in DMF (v/v), methanol and DMF. While MeOH was used only as washing solvent, DMF was necessary either for washings and as solvent for the reactions of coupling, capping and deprotection.

RESIN PREPARATION

The resin was weighted in a 10 mL Teflon vial (Biotage®) and processed with the swelling task and the swelling-Fmoc deprotection task, required when using Rink Amide MHBA Resin. At the end of these operations the resin was ready for the SPPS.

ACTIVATION OF FMOC-AA-OH AMINO ACIDS

Procedure A: To a solution of the desired Fmoc-AA-OH (4.0 eq with respect to the resin) in DMF (3.5 mL, dry solvent) DIC (4.0 eq), HOAt (4.0 eq) and *i*Pr_2NEt (8.0 eq) were added at 0 °C, under stirring and inert atmosphere. After 25 min, the reaction mixture was added to the resin in the reaction vessel of the synthesizer.
Procedure B: To a solution of the desired Fmoc-AA-OH (3.0 eq with respect to the resin) in DMF (3.5 mL, dry solvent) HATU (3.0 eq), HOAt (3.0 eq) and *i*Pr_2NEt (6.0 eq) were added at 0 °C, under stirring and inert atmosphere. After 25 min, the reaction mixture was added to the resin in the reaction vessel of the synthesizer.

RESIN STORAGE

SASRIN™ Resin: The resin was washed several times with dichloromethane and dried under high vacuum. The dry beads were stored at -20 °C. The next SPPS cycle restarted with a swelling-deprotection step, before continuing the peptide synthesis.

Rink Amide MHBA Resin: The on-beads peptides were stored at -20 °C in a small volume of DMF (2-3 mL), with the terminal amino group of the peptide left Fmoc-protected. The next SPPS cycle restarted with a swelling-deprotection step before continuing the peptide synthesis.

BIOTAGE® INITIATOR PROGRAMS

The programs "Tasks" used in the SPPS instrument are reported below. Each task can be modified in every parameter and it was performed under mechanical stirring at 1000 rpm.

Swelling

DMF (3.0 mL) was added to the resin: the swelling was accomplished at r.t. in 30 min. At the end of the swelling step, the liquid phase was drained.

Swelling-Fmoc deprotection

DMF (3.5 mL) was added to the resin and the swelling step was performed at r.t. for 15 min. Two deprotection steps were carried out adding 25% piperidine in DMF (3.0 mL for each step): the reaction was performed at r.t. under inert atmosphere for 5 min and 15 min for the first and the second deprotection step, respectively. The resin was washed eight times with DMF (3 mL × 30 s for every wash). At the end of each step, the liquid phase was drained.

Coupling (Double coupling)-capping-Fmoc deprotection

The activated Fmoc-AA-OH residue was added to the resin in the reaction vessel of the synthesizer and the coupling reaction assisted by microwaves was carried out at 70 °C under inert atmosphere for 12 min. When a double coupling was required, another aliquot of the activated Fmoc-AA-OH residue was added to the resin and a second coupling reaction was performed. The beads were washed six times with DMF (2.5 mL × 20 s for every wash). The capping solution (3 mL) was added to the resin: the capping step was performed at r.t. under inert atmosphere for 15 min. The beads were washed six times with DMF (2.5 mL × 20 s for every wash). Two deprotection steps were carried out adding the deprotection solution (3.0 mL for each step) to the beads: the reaction was performed at r.t. under inert atmosphere for 5 min and 7 min for the first and the second deprotection step, respectively. The beads were washed twice with DMF, MeOH, DMF, MeOH and DMF (3.0 mL × 20 s for every wash; 3.0 mL × 20 s for the last washes in MeOH and DMF). At the end of each step, the liquid phase was drained.

Coupling (Double coupling)-capping

The activated Fmoc-AA-OH residue was added to the resin in the reaction vessel of the synthesizer, and the coupling reaction assisted by microwaves was carried out at 70 °C under inert atmosphere for 12 min. When a double coupling was required, another aliquot of the activated Fmoc-AA-OH was added to the resin and a second coupling reaction was performed. The beads were washed six times with DMF (2.5 mL × 20 s for every wash). The capping solution (3 mL) was added to the resin: the capping step was performed at r.t. under inert atmosphere for 15 min. The beads were washed six times with DMF (2.5 mL × 20 s for every wash). The beads were washed twice with DMF, MeOH, DMF, MeOH (3.0 mL × 20 s for every wash). Eventually, the beads were washed eight times with DMF (3.0 mL × 30 s). At the end of each step, the liquid phase was drained.

Capping

The solution 25% Ac_2O in DMF (3 mL) was added to the resin: the capping step was performed at r.t. under inert atmosphere for 15 min. The beads were washed six times with DMF (2.5 mL × 20 s for every wash). The beads were washed twice with DMF, MeOH, DMF (3.0 mL × 20 s for every wash).

Eventually, the beads were washed twice with MeOH (3.0 mL × 30 s) and eight times with DMF (3.0 mL × 30 s). At the end of each step, the liquid phase was drained.

GP3. GENERAL PROCEDURE 3 FOR AZIDE REDUCTION ON RESIN

Azidopeptidyl resin (1.0 eq) was suspended in a 4:1 mixture of dioxane/water. Trimethylphosphine (1 M solution in toluene, 6.0 eq) was added and the reaction vessel was shaken for 40 min. The resin was then washed with dioxane (three times) and the conversion was checked by Kaiser test (GP3).

GP4. GENERAL PROCEDURE 4 FOR PEPTIDE CLEAVAGE

All the cleavage reactions from the resin were performed manually, under inert atmosphere and vortex mixing.

Rink Amide MHBA Resin: The protected on-beads peptide was swollen first with DMF (3.5 mL), then with dichloromethane (3.5 mL). Under stirring and nitrogen atmosphere, the beads were treated three times with the cleavage cocktail (3.0 mL per 0.1 mmol of resin) 90:5:3:2 TFA / thioanisole / EDT / anisole (v/v/v/v). After 1 h, the liquid phase was filtered off under nitrogen flow and collected in a round bottom flask: the beads were washed with neat TFA (1.0 mL) that was collected. The combined filtered fractions were concentrated and poured in cold diethyl ether, provoking precipitation of the product. Diethyl ether was removed with a syringe, affording the crude product, which was purified with RP-HPLC and freeze-dried.

SASRIN™ Resin: The resin was thoroughly washed with dichloromethane (ten times) and then treated with 1% TFA in dichloromethane (2 mL) for 2-5 min. The mixture was filtered off with a N_2 pressure into a vial containing 0.2 mL of 12% of pyridine in MeOH. The presence of the peptide was monitored by TLC (CH_2Cl_2/MeOH 9:1): after 5-8 cycles the peptide was completely cleaved from the resin. The fractions were collected and concentrated at reduced pressure. The mixture was then diluted with AcOEt and washed with 1 M $KHSO_4$ (four times). The organic layer was dried over Na_2SO_4 and concentrated affording a white solid. The crude compounds were purified by flash chromatography on silica gel (gradient: CH_2Cl_2/MeOH 95:5 to 8:2) to give the desired products.

EP.12 GENERAL PROCEDURES FOR SOLUTION-PHASE SYNTHESIS

GP5. GENERAL PROCEDURE 5 FOR BOC DEPROTECTION REACTIONS

To a solution of the *N*-Boc-protected amino acid or peptide in CH_2Cl_2 (0.13 M) was added half volume of TFA and the reaction was stirred at r.t. for 2 h. The solvent was evaporated, toluene (two times) was added followed by evaporation, and then ether was added and evaporated to afford the corresponding TFA salt.

GP6. GENERAL PROCEDURE 6 FOR CBZ-CARBAMATE AND BENZYL ESTER HYDROGENOLYTIC CLEAVAGE

Protected compound (1.0 eq) was dissolved in a mixture of THF/H_2O (1:1) and Pd/C 10% (0.1 eq) was added. The reaction mixture was subjected to three vacuum/hydrogen cycles and then left stirring overnight at room temperature under 1 bar of hydrogen. The mixture was filtered through Celite, and the cake was washed thoroughly with THF/H_2O (1:1) or MeOH. The filtrate was concentrated and dried.

GP7. GENERAL PROCEDURE 7 FOR MACROLACTAMIZATION REACTIONS

Procedure A: HATU (4.0 eq), HOAt (4.0 eq) and *i*Pr_2NEt (6.0 eq) were added successively to a solution of deprotected linear compound (1.0 eq) in DMF (1.4 mM), under a nitrogen atmosphere at 0°C. After stirring the reaction mixture at 0 °C for 1 h, it was allowed to reach room temperature and stirred overnight. DMF was then removed under reduced pressure.

Procedure B: HATU (4.0 eq), HOAt (4.0 eq) and *i*Pr_2NEt (6.0 eq) were added successively to a solution of deprotected linear compound (1.0 eq) in DMF/CH_2Cl_2 1:1 (1.4 mM), under a nitrogen atmosphere at

0 °C. After stirring the reaction mixture at 0 °C for 1 h, it was allowed to reach room temperature and stirred overnight. DMF was then removed under reduced pressure.

GP8. GENERAL PROCEDURE 8 FOR MTR AND O*T*BU ESTER REMOVAL

Procedure A: Protected macrolactam was treated for 2 h with TFA (0.01 M), in the presence of ion scavengers: thioanisole (5%), ethanedithiol (3%), anisole (2%). After TFA removal under reduced pressure, the residue was dissolved in a 1:1 mixture of diisopropyl ether/water. Phases were separated and the aqueous layer was washed several times with diisopropyl ether. The aqueous phase was concentrated under reduced pressure to give the crude product, which was purified by HPLC.

Procedure B: Protected macrolactam was treated for 2 h with TFA (0.01 M), in the presence of ion scavengers. For 10 mL of TFA, thioanisole (1.5 mL), ethanedithiol (0.75 mL) and phenol (150 mg) were required. The mixture was cooled to 0 °C and flushed with N_2. Trimethylsilylbromide (2 mL) was then added, the flask was open and the mixture warmed up to room temperature and stirred for 2 h. After TFA removal under reduced pressure, the residue was dissolved in a 1:1 mixture of diisopropyl ether/water. Phases were separated and the aqueous layer was washed several times with diisopropyl ether. The aqueous phase was concentrated under reduced pressure to give the crude product, which was purified by HPLC.

SYNTHESIS OF SCAFFOLDS N_3-DKP5-COOH **41** AND N_3-DKP5-COOH **42**

N_3-DKP5-COOAllyl **53**, N_3-DKP7-COOAllyl **54**, N_3-DKP2-COOAllyl **43**, N_3-DKP3-COOAllyl **44**, *cyclo*[DKP2-*iso*DGR] **25** and *cyclo*[DKP3-*iso*DGR] **26** were synthesized according to literature procedure and their analytical data were in agreement with those already published.[27]

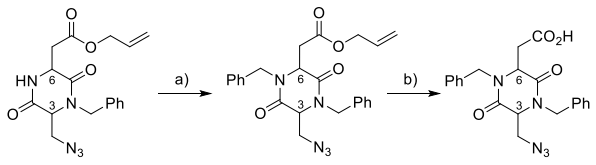

43: 3*R*, 6*S*
44: 3*S*, 6*R*
53: 3*R*, 6*S*
54: 3*S*, 6*R*
41: 3*R*, 6*S*
42: 3*S*, 6*R*

Reagents and conditions: a) KHMDS, BnBr, THF/DMF, -70 to -40 °C, 5 h, 66%; b) [$Pd(PPh_3)_4$], *N*-methylaniline, CH_2Cl_2, 0 °C, 1 h, 70%.

N_3-DKP5-COOAll **53** and N_3-DKP7-COOAll **54**

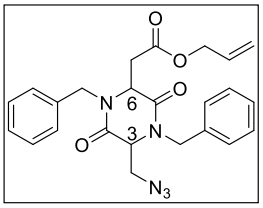

Chemical Formula: $C_{24}H_{25}N_5O_4$
Molecular Weight: 447.50

The reaction was performed in a flame-dried flask under nitrogen atmosphere. KHMDS (111 mg, 0.55 mmol, 1.1 eq) was dissolved in dry toluene to give a 0.5 M solution. The solution was cooled to -70 °C and **43** or **44** (180 mg, 0.5 mmol, 1.0 eq), previously dissolved in dry THF (9.9 mL), was added dropwise. The mixture was stirred under these conditions for 30 minutes, then benzyl bromide (0.30 µL, 2.5 mmol, 5.0 eq) and DMF (4.2 mL) were sequentially added under these conditions. The reaction was allowed to reach -40 °C and it was stirred under these conditions for 5 h. After this time, a saturated solution of NH_4Cl was added and the mixture was extracted three times with AcOEt (3 × 40 mL). Organic layers were combined, washed with brine and dried over Na_2SO_4 anhydrous. Volatiles were removed under reduced pressure then the crude was purified by flash chromatography on silica gel eluting Hexane/AcOEt (from 7:3 to 6:4). The product was recovered as a transparent oil (134 mg, 66%).

R_f = 0.4 (Hexane/AcOEt 6:4); ^{1}H-NMR (400 MHz, $CDCl_3$,) δ 7.40 – 7.23 (m, 10H, overlapped with solvent signal), 5.82 (ddt, *J* = 16.4, 10.8, 5.9 Hz, 1H), 5.36 (dd, *J* = 15.4, 6.3 Hz, 2H), 5.31 – 5.21 (m, 2H), 4.50 (ddd, *J* = 45.8, 13.0, 5.9 Hz, 2H), 4.27 – 4.20 (m, 1H), 4.17 – 4.16 (m, 1H), 4.16 (d, *J* = 15.3 Hz, 1H), 4.10 (d, *J* = 14.8 Hz, 2H), 3.74 (dd, *J* = 12.8, 3.1 Hz, 1H), 3.31 (dd, *J* = 17.6, 2.7 Hz, 1H), 2.93 (dd, *J* = 17.6, 5.0 Hz, 1H). ^{13}C-NMR (101 MHz, $CDCl_3$) δ 169.5, 166.1, 164.9, 135.3, 131.8, 128.8, 128.8, 128.6, 128.1, 128.0, 127.9, 127.8, 127.8, 127.3, 126.6, 118.4, 103.7, 65.6, 58.4, 55.0, 51.4, 47.1, 47.0, 34.8. MS (ESI) *m/z* calcd. for $[C_{24}H_{24}N_5O_4Na]^+$: 470.2; found: 470.4 $[M+Na]^+$.

N_3-DKP5-COOH **41** and N_3-DKP7-COOH **42**

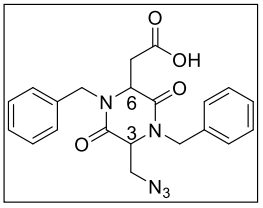

Chemical Formula: $C_{21}H_{21}N_5O_4$
Molecular Weight: 407.43

N_3-DKP5-COOAll (**53**) or N_3-DKP7-COOAll (**54**) (120 mg, 0.27 mmol, 1.0 eq) was dissolved in CH_2Cl_2 (2.7 mL) under a nitrogen atmosphere, and the mixture was cooled to 0 °C. [$Pd(PPh_3)_4$] (94 mg, 0.08 mmol, 0.3 eq) and freshly distilled *N*-methylaniline (35 µL, 0.32 mmol, 1.2 eq) were added

successively. The mixture was then allowed to reach room temperature. After 1 h of stirring, the mixture was diluted with AcOEt (40 mL) and extracted with aqueous $NaHCO_3$ (4 × 20 mL). The combined aqueous phases were acidified to pH 2 by adding $KHSO_4$ (1 M solution) and then extracted with CH_2Cl_2 (4 × 20 mL). The resulting organic phase was dried over Na_2SO_4 and the solvent was evaporated to afford the desired product as a slightly yellow solid (77 mg, 70%) which was used without further purification.

R_f = 0.20 (Hexane/AcOEt 1:1); ^{1}H-NMR (400 MHz, $CDCl_3$) δ 7.40 – 7.27 (m, 10H, overlapped with solvent signal), 5.46 (dd, J = 40.1, 15.4 Hz, 2H), 4.25 (s, 1H), 4.11 – 4.06 (m, 2H), 4.04 (s, 1H), 4.00 (s, 1H), 3.76 (dd, J = 12.7, 2.9 Hz, 1H), 3.36 (dd, J = 17.7, 2.2 Hz, 1H), 2.96 (dd, J = 17.7, 5.0 Hz, 1H). ^{13}C-NMR (101 MHz, $CDCl_3$) δ 173.8, 166.1, 165.3, 134.8, 134.4, 129.1, 129.0, 128.2, 128.1, 127.9, 127.8, 58.2, 54.3, 51.4, 47.1, 46.9, 34.2. MS (ESI) *m/z* calcd. for $[C_{21}H_{20}N_5O_4Na]^+$: 430.15; found: 430.10 $[M+Na]^+$.

SYNTHESIS OF *CYCLO*[DKP5-*ISO*DGR] **39** AND *CYCLO*[DKP7-*ISO*DGR] **40**

The synthesis of *cyclo*[DKP5-*iso*DGR] (**39**) and *cyclo*[DKP7-*iso*DGR] (**40**) was accomplished as described in EP.11 GENERAL PROCEDURES FOR SOLID-PHASE SYNTHESIS, using SASRIN™: the exact amounts of reagents used in the solid-phase peptide synthesis are reported in TABLE 11 for *cyclo*[DKP5-*iso*DGR] (**39**) and in TABLE 12 for *cyclo*[DKP7-*iso*DGR] (**40**).

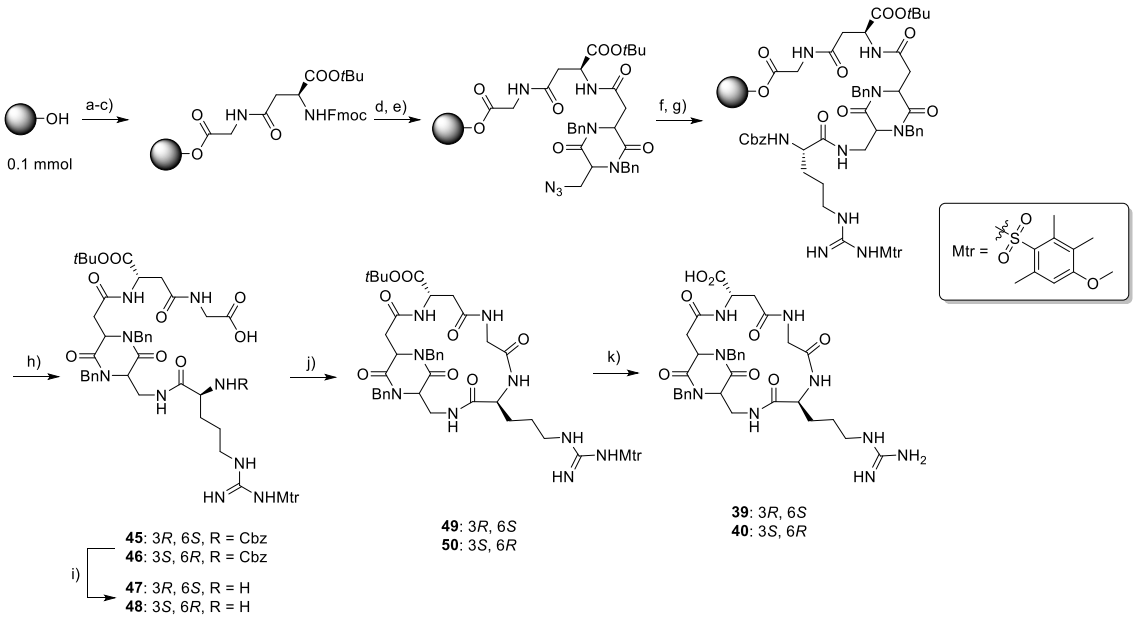

Reagents and conditions: a) Fmoc-Gly-OH, DIC, DMAP (cat.), DMF; b) 2% piperidine and 2% DBU in DMF; c) Fmoc-Asp(OH)-O*t*Bu, DIC, HOAt, DMF; d) 2% piperidine and 2% DBU in DMF; e) **41-42**, DIC, HOAt, DMF; f) PMe_3, dioxane/water 4:1, 20 min × 3 times; g) Cbz-Arg(Mtr)-OH, DIC, HOAt, DMF; h) 1% TFA in CH_2Cl_2, r.t., 5 min × 10 times, 71-81%; i) H_2, 10% Pd/C, THF/H_2O 1:1, 98%-quant.; j) HATU, HOAt, *i*Pr_2NEt, DMF (1.4 mM), 32%; k) TFA/thioanisole/EDT/anisole 90:5:3:2, 25-37%.

TABLE 11. Amounts of reagents used in the SPPS of compound **39**.

REAGENTS	eq or concentration	mmol	amounts
SASRIN™ Resin	1.0 eq	0.2	200 mg
Fmoc-Gly-OH*	4.0 eq	0.8	238 mg
DIC	4.0 eq	0.8	124 µL
DMAP	0.1 eq	0.02	2.4 mg
DMF	0.27 M	/	3 mL
Fmoc-L-Asp(OH)-O*t*Bu*	3.0 eq	0.6	247 mg
DIC	3.0 eq	0.6	93 µL
HOAT	3.0 eq	0.6	82 mg
DMF	0.20 M	/	3 mL
N_3-DKP5-COOH **45**	2.3 eq	0.46	185 mg
DIC	2.3 eq	0.46	71 µL
HOAT	2.3 eq	0.46	63 mg
DMF	0.15 M	/	3 mL
Cbz-L-Arg(Mtr)-OH · CHA*	2.5 eq	0.5	310 mg
DIC	2.5 eq	0.5	77 µL
HOAT	2.5 eq	0.5	68 mg
DMF	0.17 M	/	3 mL

* a double coupling step was performed.

TABLE 12. Amounts of reagents used in the SPPS of compound **40**.

REAGENTS	eq or concentration	mmol	amounts
SASRIN™ resin	1.0 eq	0.1	100 mg
Fmoc-Gly-OH*	4.0 eq	0.4	119 mg
DIC	4.0 eq	0.4	62 µL
DMAP	0.1 eq	0.01	1.2 mg
DMF	0.27 M	/	1.5 mL
Fmoc-L-Asp(OH)-O*t*Bu*	3.0 eq	0.3	124 mg
DIC	3.0 eq	0.3	47 µL
HOAT	3.0 eq	0.3	41 mg
DMF/DCM	0.20 M	/	1.5 mL
N_3-(3*S*,6*R*)-DKP-COOH **9**	2.3 eq	0.23	93 mg
DIC	2.3 eq	0.23	36 µL
HOAT	2.3 eq	0.23	32 mg
DMF/DCM	0.15 M	/	1.5 mL
Cbz-L-Arg(Mtr)-OH · CHA*	2.5 eq	0.25	155 mg
DIC	2.5 eq	0.25	39 µL
HOAT	2.5 eq	0.25	34 mg
DMF	0.17 M	/	1.5 mL

* a double coupling step was performed.

Cbz-Arg(Mtr)-DKP5-*iso*Asp(O*t*Bu)-Gly-OH (**45**)
Cbz-Arg(Mtr)-DKP7-*iso*Asp(O*t*Bu)-Gly-OH (**46**)

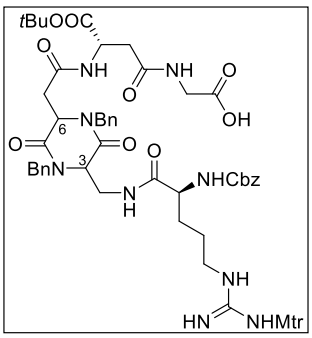

Chemical Formula: $C_{55}H_{69}N_9O_{14}S$
Molecular Weight: 1112.27

The linear carboxylic acids **41** and **42** were obtained by cleaving the corresponding supported compounds from the resin according to GP4. The desired products were obtained as white foams (**45**: 157 mg, 71%; **46**: 90 mg, 81%).

Compound **45**:
R_f = 0.15 (CH_2Cl_2/MeOH 9:1); ^{1}H-NMR (400 MHz, CD_3OD) δ 7.43 – 7.20 (m, 15H), 6.63 (s, 1H), 5.39 (d, J = 15.4 Hz, 1H), 5.14 – 4.99 (m, 3H), 4.57 (t, J = 6.2 Hz, 1H), 4.38 (s, 1H), 4.32 (dd, J =15.5, 6.9 Hz, 2H), 4.09 (s, 1H), 4.03 (s, 1H), 3.80 (s, 5H), 3.74 (s, 2H), 3.19 – 3.04 (m, 3H), 2.90 (dd, J = 16.9, 4.5 Hz, 1H), 2.72 – 2.64 (m, 5H), 2.59 (s, 3H), 2.10 (s, 3H), 1.68 (s, 1H), 1.58 – 1.38 (m, 12H). ^{13}C-NMR (101 MHz, CD_3OD) δ 178.2, 175.4, 172.1, 171.5, 171.1, 168.7, 167.8, 159.9,158.4, 158.2, 139.5, 138.1, 137.9, 137.1, 136.8, 134.8, 130.0, 130.0, 129.5, 129.4, 129.0, 128.9,125.7, 112.8, 83.2, 67.9, 59.8, 56.8, 56.3, 56.0, 51.6, 44.5, 40.5, 38.6, 36.4, 30.1, 28.3, 24.4, 18.9, 12.1. MS (ESI) *m/z* calcd. for $[C_{55}H_{70}N_9O_{14}S]^+$: 1112.5; found: 1112.5 $[M+H]^+$.

Compound **46**:
R_f = 0.15 (CH_2Cl_2/MeOH 9:1); ^{1}H NMR (400 MHz, CD_3OD) δ 7.43 – 7.20 (m, 15H), 6.63 (s, 1H), 5.39 (d, J = 15.4 Hz, 1H), 5.14 – 4.98 (m, 3H), 4.57 (t, J = 6.2 Hz, 1H), 4.38 (bs, 1H), 4.32 (dd, J = 15.4, 6.9

Hz, 2H), 4.09 (bs, 1H), 4.03 (bs, 1H), 3.80 (bs, 5H), 3.74 (s, 2H), 3.21 – 3.08 (m, 3H), 2.90 (dd, *J* = 16.9, 4.5 Hz, 1H), 2.72 – 2.64 (m, 5H), 2.59 (s, 3H), 2.10 (s, 3H), 1.75 – 1.63 (m, 1H), 1.63 – 1.39 (m, 13H). ^{13}C NMR (101 MHz, CD_3OD) δ 172.3, 171.4, 171.0, 168.5, 167.8, 159.9, 159.4, 158.2, 139.5, 137.9, 137.6, 136.7, 130.0, 129.9, 129.6, 129.2, 128.9, 125.7, 112.8, 83.2, 67.78, 59.7, 57.2, 56.0, 54.0, 51.1, 50.5, 47.9, 42.5, 40.4, 38.4, 37.0, 30.5, 28.2, 24.3, 18.8. MS (ESI) *m/z* calcd. for $[C_{55}H_{70}N_9O_{14}S]^+$: 1156.4; found: 1156.6 $[M+2Na-H]^+$.

H-Arg(Mtr)-DKP5-*iso*Asp(O*t*Bu)-Gly-OH (**47**)
H-Arg(Mtr)-DKP7-*iso*Asp(O*t*Bu)-Gly-OH (**48**)

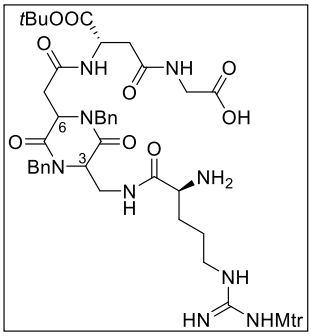

Chemical Formula: $C_{47}H_{63}N_9O_{12}S$
Molecular Weight: 978.13

Compound **45** or **46** (**45**: 145 mg, 0.14 mmol, 1.0 eq; **46**: 90 mg, 0.08 mmol, 1.0 eq) was treated with 10% Pd/C (**45**: 14 mg, 0.014 mmol, 0.1 eq; **46**: 8 mg, 0.008 mmol, 0.1 eq) under the conditions described in GP6. The desired products were obtained as white solids (**47**: 134 mg, 98%; **48**: 80 mg, quantitative yield) and they were used without further purification.

Compound **47**:
^{1}H-NMR (400 MHz, CD_3OD) δ 7.44 – 7.15 (m, 10H), 6.64 (s, 1H), 5.45 (d, *J* = 15.4 Hz, 1H), 4.58 (t, *J* = 4.9 Hz, 1H), 4.43 (d, *J* = 15.4 Hz, 1H), 4.34 (bs, 1H), 4.24 (d, *J* = 15.7 Hz, 1H), 4.11 (bs, 1H), 3.90 (s, 3H), 3.79 (s, 3H), 3.71 (dd, *J* = 14.2, 5.9 Hz, 1H), 3.24 – 3.10 (m, 2H), 3.06 (d, *J* = 15.2 Hz, 1H), 2.92 (dd, *J* = 16.8, 4.9 Hz, 1H), 2.72 (d, *J* = 6.0 Hz, 2H), 2.66 (s, 3H), 2.59 (s, 3H), 2.10 (s,3H), 1.88-1.75 (m, *J* = 14.3, 7.1 Hz, 2H), 1.61-1.49 (m, 2H), 1.43 (s, 9H), 1.46 – 1.35 (m, 2H). ^{13}C-NMR (101 MHz, CD_3OD) δ 172.4, 171.3, 171.0, 170.8, 168.7, 167.8, 163.0, 162.7, 159.9, 158.1, 139.4, 137.9, 137.3, 136.6, 134.5, 129.9, 129.8, 129.4, 129.1, 128.8, 128.1, 126.1, 125.7, 112.8, 83.2, 59.2, 57.7, 56.9, 56.0, 53.9, 51.3, 50.4, 49.8, 48.0, 41.9, 40.7, 38.3, 36.4, 35.8, 30.8, 30.7,30.5, 29.6, 28.2, 24.3, 18.8, 12.1. MS (ESI) *m/z* calcd. for $[C_{47}H_{64}N_9O_{12}S]^+$: 978.4; found: 978.7 $[M+H]^+$.

Compound **48**:
MS (ESI) *m/z* calcd. for $[C_{47}H_{63}N_9O_{12}SNa]^+$: 1000.4; found: 1000.5 $[M+Na]^+$.

Cyclo[DKP5-*iso*Asp(O*t*Bu)-Gly-Arg(Mtr)] (**49**)
Cyclo[DKP7-*iso*Asp(O*t*Bu)-Gly-Arg(Mtr)] (**50**)

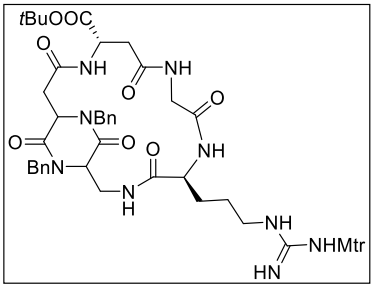

Chemical Formula: $C_{47}H_{61}N_9O_{11}S$
Molecular Weight: 960.12

Compound **47** (127 mg, 0.13 mmol, 1.0 eq) was cyclized in the presence of HATU (198 g, 0.52mmol, 4.0 eq), HOAt (71 mg, 0.52 mmol, 4.0 eq) and *i*Pr_2NEt (136 µL, 0.78 mmol, 6.0 eq) under the conditions

described in GP7 (Procedure A). The crude product was purified by RP-HPLC (gradient: 90% H_2O + 0.1% TFA / 10% CH_3CN + 0.1% TFA to 100% CH_3CN + 0.1% TFA in 10 min; t_R (product) = 4.6 min) to afford the desired product **49** as a white foam (39 mg, 32%).

Compound **49**:
^{1}H-NMR (400 MHz, CD_3OD) δ 7.44 – 7.15 (m, 10H), 6.68 (s, 1H), 5.37 (d, J = 15.1 Hz, 1H), 5.26 (d, J = 16.0 Hz, 1H), 5.15 (d, J = 8.0 Hz, 1H), 4.73-4.62 (m, J = 5.4 Hz, 1H), 4.40 (d, J = 16.1 Hz,1H), 4.29 – 4.07 (m, 4H), 3.99 (s, 1H), 3.83 (s, 3H), 3.68 (d, J = 16.5 Hz, 1H), 3.47 (d, J = 13.5 Hz,1H), 3.37 (s, 1H), 3.28 – 3.15 (m, 2H), 2.86 (dd, J = 14.6, 3.3 Hz, 1H), 2.77 (d, J = 6.6 Hz, 2H), 2.70 (s, 3H), 2.64 (s, 3H), 2.34 – 2.23 (m, 1H), 2.15 (s, 3H), 1.80 – 1.55 (m, J = 18.4, 14.0, 5.9 Hz, 3H), 1.49 (s, 9H). ^{13}C-NMR (101 MHz, CD_3OD) δ 175.4, 172.2, 171.7, 171.2, 171.1, 167.8, 167.1, 160.0, 157.9, 139.5, 138.8, 136.8, 130.1, 129.8, 129.5, 129.2, 128.9, 128.4, 128.1 , 125.8, 112.9, 83.4, 60.0, 59.4, 56.0, 55.0, 51.8, 51.3, 49.9, 47.7, 42.8, 40.5, 38.8, 29.0, 28.2, 24.3, 18.8, 12.1. MS(ESI) *m/z* calcd. for $[C_{47}H_{62}N_9O_{11}S]^+$: 960.4 $[M+H]^+$; found: 960.6.

Compound **48** (40 mg, 0.04 mmol, 1.0 eq) was cyclized in the presence of HATU (60 mg, 0.16 mmol, 4.0 eq), HOAt (22 mg, 0.16 mmol, 4.0 eq) and *i*Pr_2NEt (62 µL, 0.24 mmol, 6.0 eq) under the conditions described in GP7 (Procedure A). The residue was purified by flash chromatography on silica gel (CH_2Cl_2/MeOH 97:3 to 9:1, solid load) affording the crude product **50** as a pale yellow foam.

Compound **50**:
R_f = 0.16 (CH_2Cl_2/MeOH 9:1). MS (ESI) *m/z* calcd. for $[C_{47}H_{62}N_9O_{11}S]^+$: 960.4; found: 960.6 $[M+H]^+$.

Cyclo[DKP5-*iso*DGR] (**39**)
Cyclo[DKP7-*iso*DGR] (**40**)

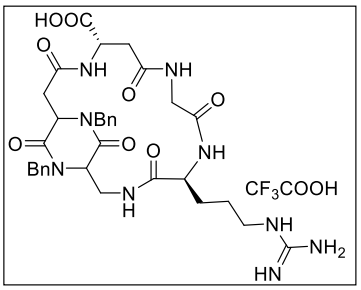

Chemical Formula: $C_{35}H_{42}F_3N_9O_{10}$
Molecular Weight: 805.77

Compound **49** (39 mg, 0.04 mmol, 1.0 eq) or **50** (15 mg, 0.015 mmol, 1.0 eq) was deprotected under the conditions described in GP8 (Procedure A). The crude product was purified by RP-HPLC (compound **39** = gradient: 90% H_2O + 0.1% TFA / 10% CH_3CN + 0.1% TFA to 100% CH_3CN + 0.1% TFA in 10 min; flow: 15 mL/min, t_R (product) = 5.7 min; compound **40** = gradient: 100% H_2O + 0.1% TFA to 50% H_2O + 0.1% TFA / 50% CH_3CN + 0.1% TFA in 11 min; t_R (product) = 9.6 min). The pure fractions were concentrated and freeze-dried from water, affording **39** or **40** as a white solid (**39**: 12.5 mg, 37%; **40**: 3.0 mg, 25%).

Compound **39**:
^{1}H-NMR (400 MHz, D_2O) δ 7.54 – 7.31 (m, 10H), 5.26 (d, J = 15.3 Hz, 1H), 5.09 – 5.00 (m, 2H), 4.79(d , 1H), 4.67 (d, J = 16.4 Hz, 1H), 4.33 – 4.30 (m, 1H), 4.29 – 4.17 (m, 3H), 4.11 (dd, J = 14.7, 3.6Hz, 1H), 3.91 (d, J = 16.8 Hz, 1H), 3.68 (dd, J = 14.6, 1.6 Hz, 1H), 3.25 (t, J = 6.8 Hz, 2H), 3.02 (dd, J = 14.8, 3.9 Hz, 1H), 2.90 (d, J = 5.9 Hz, 2H), 2.45 (dd, J = 14.8, 11.2 Hz, 1H), 1.88 – 1.55 (m, 4H).^{13}C-NMR (101 MHz, D_2O) δ 175.3, 174.2, 172.1, 171.5, 170.5, 156.8, 135.8, 135.1, 129.2,128.9, 128.3 128.1, 127.7, 126.8, 66.6, 59.1, 57.7, 54.2, 50.1, 49.7, 47.2, 41.6, 40.7, 40.4, 39.8, 37.3, 27.5, 24.4.

Compound **40**:

^{1}H-NMR (400 MHz, CD_3OD) δ 7.48 – 7.15 (m, 10H), 5.20 (d, J = 15.4 Hz, 1H), 4.68 – 4.56 (m, 2H), 4.50 (dd, J = 9.4, 2.4 Hz, 1H), 4.43 – 4.37 (m, 1H), 4.27 (d, J = 5.4 Hz, 1H), 4.19 (d, J = 15.4 Hz,1H), 4.07 (d, J = 8.8 Hz, 1H), 4.03 (d, J = 5.4 Hz, 1H), 3.75 – 3.65 (m, 2H), 3.13 (dd, J = 11.7, 6.5Hz, 2H), 2.96 (dd, J = 15.3, 8.6 Hz, 1H), 2.83 (dd, J = 14.5, 2.4 Hz, 1H), 2.67 (dd, J = 15.3, 3.8 Hz,1H), 2.55 (dd, J = 14.5, 9.5 Hz, 1H), 1.94-1.83 (m, 1H), 1.62-1.48 (m, 3H), 1.32-1.20 (m, 2H); ^{13}C-NMR (101 MHz, CD_3OD, HSQC projection) δ 135.2, 129.2, 129.0, 128.3, 127.7, 126.7, 59.7, 56.3, 53.2, 52.2, 47.8, 40.5, 39.4, 36.5, 26.9, 24.4.

SYNTHESIS OF *CYCLO*[DKP3-*ISO*DGR]-CH_2NH_2 PEPTIDOMIMETIC **56**

N_3-DKP3(CH_2NHMtr)-COOAllyl **57** was synthesized according to literature procedure and its analytical data were in agreement with those already published.[40]

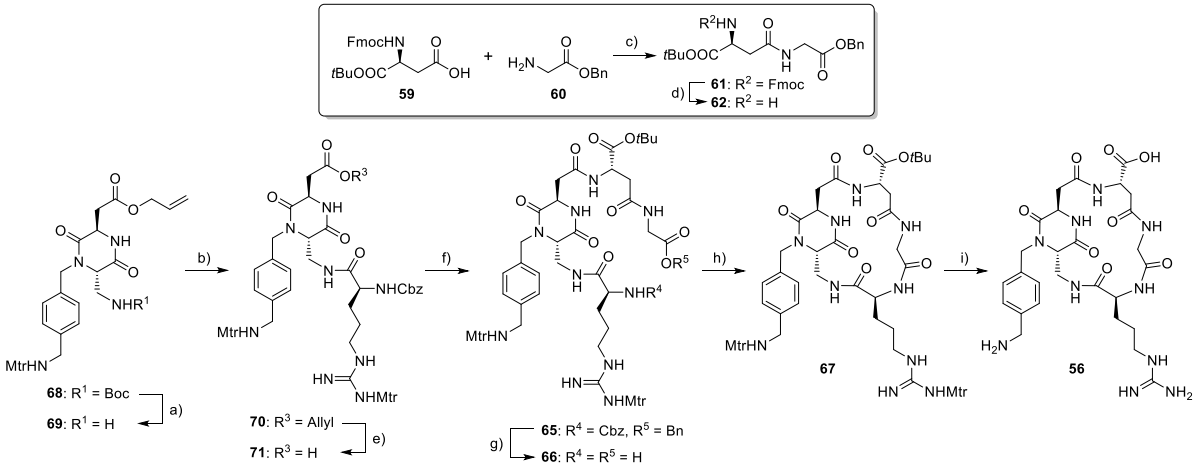

Reagents and conditions: a) TFA, CH_2Cl_2, r.t., 2 h; b) Cbz-Arg(Mtr)-OH, HATU, HOAt, *i*Pr_2NEt, DMF, 0 °C to r.t., overnight, 94% over 2 steps; c) HATU, HOAt, *i*Pr_2NEt, DMF, 0 °C to r.t., overnight, 86%; d) piperidine, DMF, 2 h, r.t., 67%; e) [$Pd(PPh_3)_4$], *N*-Methylaniline, CH_2Cl_2, 0 °C, 1 h, 88%; f) **62**, HATU, HOAt, *i*Pr_2NEt, DMF, 0 °C to r.t., overnight, 95%; g) H_2, 10% Pd/C, THF/H_2O 1:1, overnight, r.t., 95%; h) HATU, HOAt, *i*Pr_2NEt, DMF/CH_2Cl_2 1:1 (1.4 mM), 0 °C to r.t., overnight, 79%; i) TFA/TMSBr/thioanisole/EDT/phenol 70:14:10:5:1, 2 h, r.t., 47%.

FmocHN-*iso*Asp(O*t*Bu)-Gly-OBn (**61**)

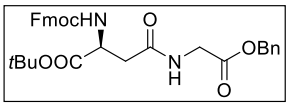

Chemical Formula: $C_{32}H_{34}N_2O_7$
Molecular Weight: 558.63

To a solution of Fmoc-L-Asp(OH)-O*t*Bu (1.15 g, 2.80 mmol, 1.2 eq) in DMF (28 mL), at 0 °C and under nitrogen atmosphere, HATU (1.06 g, 2.80 mmol, 1.2 eq), HOAt (380 mg, 2.80 mmol, 1.2 eq) and *i*Pr_2NEt (810 µL, 4.66 mmol, 2.0 eq) were added: the reaction mixture was stirred at 0 °C for 30 min. A solution of H_2N-Gly-OBn·TFA (650 mg, 2.3 mmol, 1.0 eq) in DMF (30 mL) and *i*Pr_2NEt (1.22 mL, 2.33 mmol, 3.0 eq) was added dropwise to the previous solution: the reaction mixture was stirred at 0 °C for 1 h and at room temperature overnight. The mixture was diluted with AcOEt (500 mL) and washed with $KHSO_4$ 1 M (3 × 100 mL), saturated aqueous $NaHCO_3$ (3 × 100 mL) and brine (1 × 100 mL). The organic phase was dried over Na_2SO_4 and volatiles were removed under reduced pressure. The residue was purified by flash chromatography on silica gel (CH_2Cl_2 100% to CH_2Cl_2/MeOH 9:1, solid load) affording the desired product **61** as a white foam (1.3 g, quantitative).

R_f = 0.8 (CH_2Cl_2/MeOH 9:1); ^{1}H-NMR (400 MHz, $CDCl_3$) δ 7.76 (d, J = 7.5 Hz, 2H), 7.61 (d, J = 7.4 Hz, 2H), 7.44 – 7.27 (m, 9H), 6.20 (s, 1H), 6.02 (d, J = 8.1 Hz, 1H), 5.16 (s, 2H), 4.50 (dt, J = 8.1, 4.2 Hz, 1H), 4.36 (m, 2H), 4.22 (t, J = 7.1 Hz, 1H), 4.07 (d, J = 5.1 Hz, 2H), 2.96 (dd, J = 15.8, 4.3 Hz, 1H), 2.79 (dd, J = 15.8, 4.3 Hz, 1H), 1.47 (s, 9H). ^{13}C-NMR (101 MHz, $CDCl_3$) δ 170.1, 170.0, 169.7, 156.3, 144.1, 141.4, 135.2, 128.81 128.8, 128.6, 127.8, 127.2, 125.4, 120.1, 82.7, 67.5, 67.3, 51.4, 47.3, 41.5, 38.1, 28.0. MS (ESI) *m/z* calcd. for $[C_{32}H_{34}N_2NaO_7]^+$: 581.6; found: 581.4 $[M+Na]^+$.

H-*iso*Asp(O*t*Bu)-Gly-OBn (**62**)

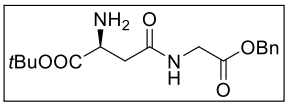

Chemical Formula: $C_{17}H_{24}N_2O_5$
Molecular Weight: 336.39

To a solution of **61** (1.3 g, 2.33 mmol, 1.0 eq) in DMF (47 mL), at 0 °C under nitrogen atmosphere, piperidine (1.15 mL, 11.16 mmol, 5.0 eq) was added and the reaction mixture was stirred at 0 °C for 10 min and at room temperature for 3 h. The mixture was diluted with AcOEt (400 mL) and washed with H_2O (4 × 100 mL). The organic phase was dried over Na_2SO_4 and volatiles were removed under reduced pressure. The residue was purified using a Grace Reveleris system (column: Reveleris Silica 40 g; liquid load; flow rate: 33 mL/min; gradient: CH_2Cl_2/MeOH 98:2 to 8:2 in 35 min) affording the desired product **62** as a white foam (613 mg, 78%).

R_f = 0.35 (CH_2Cl_2/MeOH 95:5); ^{1}H-NMR (400 MHz, $CDCl_3$) δ 7.92 (bs, 1H), 7.38 – 7.27 (m, 5H), 5.13 (s, 2H), 4.04 (qd, *J* = 18.2, 5.4 Hz, 2H), 3.67 (dd, *J* = 9.1, 3.2 Hz, 1H), 2.66 (dd, *J* = 15.5, 3.2 Hz, 1H), 2.44 (dd, *J* = 15.5, 9.1 Hz, 1H), 2.12 (bs, 2H), 1.42 (s, 9H). MS (ESI) *m/z* calcd. for $[C_{17}H_{24}N_2NaO_5]^+$: 359.4; found: 359.1 $[M+Na]^+$.

BocHN-DKP3(CH_2NHMtr)-COOAllyl (**68**)

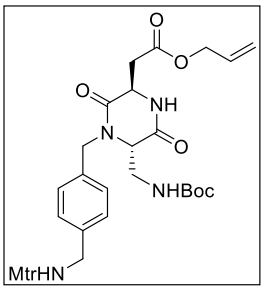

Chemical Formula: $C_{33}H_{44}N_4O_9S$
Molecular Weight: 672.79

To a solution of azide **57** (1.00 g, 1.67 mmol, 1.0 eq) in THF (28 mL), at -20 °C and under nitrogen atmosphere, PMe_3 (4.2 mL of 1 M solution in THF, 4.18 mmol, 2.5 eq) and 2-(*t*-butoxycarbonyloxyimino)-2-phenylacetonitrile (Boc-ON, 1.03 g, 4.18 mmol, 2.5 eq) were added: the reaction was stirred at room temperature for 5 h.The mixture was diluted with CH_2Cl_2 (270 mL) and washed with H_2O (4 × 100 mL) and brine (1 × 100 mL). The organic phase was dried over Na_2SO_4 and volatiles were removed under reduced pressure. The residue was purified by flash chromatography on silica gel (100% CH_2Cl_2 to CH_2Cl_2/MeOH 9:1) affording the desired product **68** as a white foam (790 mg, 70%).

R_f = 0.23 (Hexane/AcOEt 3:7); ^{1}H-NMR (400 MHz, $CDCl_3$) δ 7.22 – 7.11 (m, 4H), 6.80 (s, 1H), 6.59 (s, 1H), 5.90 (ddt, *J* = 16.3, 10.5, 5.8 Hz, 1H), 5.41 (d, *J* = 15.2 Hz, 1H), 5.37 – 5.30 (m, 1H), 5.29 – 5.24 (m, 1H), 5.02 – 4.93 (m, 1H), 4.63 (d, *J* = 5.8 Hz, 2H), 4.44 (dd, *J* = 9.3, 3.2 Hz, 1H), 4.04 (s, 2H), 3.86 (s, 3H), 3.77 – 3.66 (m, 2H), 3.50 (d, *J* = 12.7 Hz, 1H), 3.29 (dd, *J* = 17.6, 3.2 Hz, 1H), 2.76 (dd, *J* = 17.6, 9.3 Hz, 1H), 2.68 (s, 3H), 2.56 (s, 3H), 2.14 (s, 3H), 1.43 (s, 9H). MS (ESI) *m/z* calcd for $[C_{33}H_{45}N_4O_9S]^+$: 673.3; found: 673.3 $[M+H]^+$.

Cbz-Arg(Mtr)-DKP3(CH_2NHMtr)-COOAllyl (**70**)

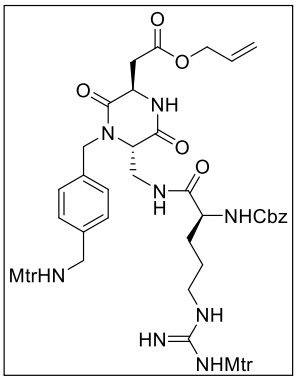

Chemical Formula: $C_{52}H_{66}N_8O_{13}S_2$
Molecular Weight: 1075.26

Cbz-Arg(Mtr)-OH (850 mg, 1.63 mmol, 1.2 eq) was dissolved in DMF (12 mL) under nitrogen atmosphere. HATU (621 mg, 1.63 mmol, 1.2 eq), HOAt (222 mg, 1.63 mmol, 1.2 eq) and *i*Pr_2NEt (711 µL, 4.08 mmol, 3.0 eq) were added at 0 °C: the mixture was stirred at 0 °C for 30 minutes. BocHN-DKP3(CH_2NHMtr)-COOAllyl (**68**) was deprotected according to GP5. The corresponding trifluoroacetate **69** (931 mg, 1.36 mmol, 1.0 eq) was dissolved in DMF (15 mL) and *i*Pr_2NEt (237 µL, 1.36 mmol, 1.0 eq) was added: this mixture was added to the previous solution of Cbz-Arg(Mtr)-OH in DMF and the reaction mixture was stirred at 0 °C for 1 h, then at room temperature overnight. The mixture was diluted with AcOEt (270 mL) and washed with $KHSO_4$ 1 M (3 × 90 mL), saturated aqueous $NaHCO_3$ (3 × 90 mL) and brine (1 × 100 mL). The organic phase was dried over Na_2SO_4 and the volatiles were removed under reduced pressure. The residue was purified using a Grace Reveleris system (column: Reveleris Silica 12 g; dry load; flow rate: 27 mL/min; gradient: CH_2Cl_2/MeOH 98:2 to 9:1 in 35 min) affording the desired product **70** as a white foam (1.28 g, 90%).

R_f = 0.5 (CH_2Cl_2/MeOH 9:1); ^{1}H-NMR (400 MHz, CD_3OD) δ 7.37 – 7.25 (m, 5H), 7.13 (dd, J = 33.7, 8.1 Hz, 4H), 6.67 (s, 1H), 6.63 (s, 1H), 5.96 – 5.84 (m, 1H), 5.34 – 5.27 (m, 2H), 5.22 – 5.17 (m, 1H), 5.07 (dd, J = 12.5 Hz, 2H), 4.64 – 4.50 (m, 3H), 4.13 – 4.07 (m, 1H), 4.05 – 3.98 (m, 3H), 3.90 – 3.82 (m, 4H), 3.81 (s, 3H), 3.78 – 3.74 (m, 1H), 3.60 (dd, J = 12.0 Hz, 1H), 3.21 (bs, 1H), 3.15 – 3.10 (m, 1H), 3.06 (dd, J = 17.5, 4.5 Hz, 1H), 2.88 (dd, J = 17.5, 4.5 Hz, 1H), 2.66 (s, 3H), 2.60 (s, 6H), 2.48 (s, 3H), 2.10 (s, 3H), 2.07 (s, 3H), 1.83 – 1.64 (m, 1H), 1.79 – 1.66 (m, 1H), 1.62 – 1.47 (m, 3H). ^{13}C-NMR (101 MHz, CD_3OD) δ 171.3, 168.8, 168.2, 160.7, 159.9, 158.2, 139.9, 139.5, 138.6, 137.9, 136.0, 134.8, 133.5, 131.0, 129.5, 129.4, 129.2, 129.1, 128.9, 126.1, 125.7, 118.6, 113.2, 112.8, 67.8, 66.5, 60.4, 56.2, 56.0, 52.0, 47.8, 46.9, 40.1, 37.0, 30.2, 24.4, 24.3, 18.8, 18.2, 12.1. MS (ESI) *m/z* calcd. for $[C_{52}H_{66}N_8NaO_{13}S_2]^+$: 1097.4; found: 1097.4 $[M+Na]^+$.

Cbz-Arg(Mtr)-DKP3(CH_2NHMtr)-COOH (**71**)

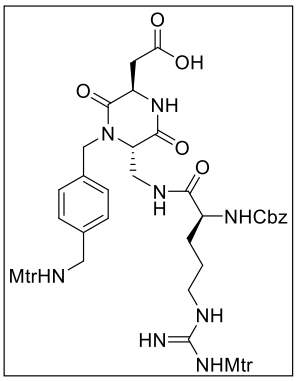

Chemical Formula: $C_{49}H_{62}N_8O_{13}S_2$
Molecular Weight: 1035.20

To a solution of **70** (1.26 g, 1.17 mmol, 1.0 eq) under nitrogen atmosphere at 0 °C, [$Pd(PPh_3)_4$] (392 mg, 0.35 mmol, 0.3 eq) and *N*-methylaniline (106 µL, 0.98 mmol, 1.2 eq) were added. The reaction mixture

was stirred 5 min at 0 °C and 2 h at room temperature. The mixture was diluted with CH_2Cl_2 (150 mL) and washed with $KHSO_4$ 1 M (4 × 50 mL). The organic phase was dried over Na_2SO_4 and volatiles were removed under reduced pressure. The residue was purified using a Grace Reveleris system (column: Reveleris HP Silica 40 g; liquid load; flow rate: 33 mL/min; gradient: CH_2Cl_2/MeOH 98:2 to 8:2 in 1 h) affording the desired product **71** as a pale yellow foam (1 g, 82%).

R_f = 0.2 (CH_2Cl_2/MeOH 95:5). ^{1}H-NMR (400 MHz, CD_3OD) δ 7.37 – 7.24 (m, 8H), 7.20 – 7.06 (m, 4H), 6.67 (s, 1H), 6.63 (s, 1H), 5.32 (d, J = 15.3 Hz, 1H), 5.14 – 5.00 (m, 2H), 4.83 (s, 6H), 4.51 – 4.45 (m, 1H), 4.13 – 4.07 (m, 1H), 4.06 – 3.98 (m, 3H), 3.91 – 3.82 (m, 4H), 3.81 (s, 3H), 3.78 – 3.73 (m, 1H), 3.58 (dd, J = 13.5 Hz, 1H), 3.26 – 3.07 (m, 2H), 2.96 (dd, J = 17.5, 4.7 Hz, 1H), 2.85 (dd, J = 17.5, 4.7 Hz, 1H), 2.66 (s, 3H), 2.60 (s, 6H), 2.48 (s, 3H), 2.10 (s, 3H), 2.07 (s, 3H), 1.78 – 1.67 (m, 1H), 1.62 – 1.44 (m, 3H). MS (ESI) *m/z* calcd. for $[C_{49}H_{61}N_8Na_2O_{13}S_2]^+$: 1080.2; found: 1080.3 $[M+Na]^+$.

Cbz-Arg(Mtr)-DKP3(CH_2NHMtr)-*iso*Asp(O*t*Bu)-Gly-OBn (**65**)

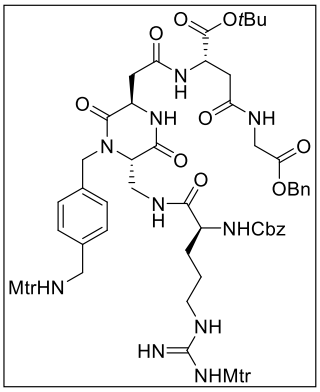

Chemical Formula: $C_{66}H_{84}N_{10}O_{17}S_2$
Molecular Weight: 1353.57

To a solution of **71** (1.00 g, 0.97 mmol, 1.0 eq) in DMF (10 mL) under nitrogen atmosphere at 0 °C, HATU (443 mg, 1.16 mmol, 1.2 eq), HOAt (158 mg, 1.16 mmol, 1.2 eq) and *i*Pr_2NEt (507 µL, 2.91 mmol, 3.0 eq) were added: the reaction mixture was stirred at 0 °C for 30 min. **62** (392 mg, 1.16 mmol, 1.2 eq) was dissolved in DMF (9.5 mL) and added to the previous solution: the reaction mixture was stirred at 0 °C for 1 h, then at room temperature overnight. The mixture was diluted with CH_2Cl_2 (50 mL) and washed with $KHSO_4$ 1 M (4 × 80 mL), saturated aqueous $NaHCO_3$ (4 × 80 mL) and brine (1 × 100 mL). The organic phase was dried over Na_2SO_4 and volatiles were removed under reduced pressure. The residue was purified using a Grace Reveleris system (column: Reveleris Silica 40 g; dry load; flow rate: 30 mL/min; gradient: 100% CH_2Cl_2 to CH_2Cl_2/MeOH 8:2 in 45 min) affording the desired product **65** as a white foam (715 mg, 54%).

R_f = 0.4 (CH_2Cl_2/MeOH 9:1); ^{1}H-NMR (400 MHz, Acetone-d_6) δ 7.79 (s, 1H), 7.67 (t, J = 5.7 Hz, 1H), 7.62 (d, J = 8.3 Hz, 1H), 7.48 (s, 1H), 7.40 – 7.27 (m, 10H), 7.24 – 7.14 (m, 4H), 6.76 (s, 1H), 6.70 – 6.68 (m, 1H), 6.66 (s, 1H), 6.57 (s, 1H), 6.53 – 6.45 (m, 1H), 5.29 (d, J = 15.1 Hz, 1H), 5.14 (s, 2H), 5.12 – 5.01 (m, 2H), 4.73 (dt, J = 8.3, 5.5 Hz, 1H), 4.67 – 4.61 (m, 1H), 4.29 – 4.21 (m, 1H), 4.12 – 4.00 (m, 4H), 3.95 (dd, J = 18.5, 5.7 Hz, 2H), 3.88 (s, 3H), 3.82 (s, 3H), 3.81 – 3.77 (m, 1H), 3.55 – 3.47 (m, 1H), 3.36 – 3.25 (m, 1H), 3.20 – 3.08 (m, 1H), 3.05 (dd, J = 15.4, 5.3 Hz, 1H), 2.80 – 2.75 (m, 2H), 2.73 (d, J = 5.3 Hz, 1H), 2.68 (s, 3H), 2.64 (s, 3H), 2.62 (s, 3H), 2.55 (s, 3H), 2.12 – 2.08 (m, 6H), 1.89 – 1.77 (m, 1H), 1.68 – 1.53 (m, 3H), 1.44 (s, 9H). ^{13}C-NMR (101 MHz, Acetone-d_6) δ 174.1, 171.1, 171.0, 170.7, 167.6, 160.2, 159.1, 157.8, 139.7, 139.5, 139.3, 138.4, 138.3, 137.3, 137.2, 136.5, 136.1, 131.4, 129.5, 129.4, 129.2, 129.2, 129.0, 128.8, 125.7, 125.0, 113.2, 112.7, 82.4, 67.4, 67.2, 60.3, 56.3, 56.1, 55.6, 52.5, 51.2, 47.6, 47.0, 42.0, 40.4, 40.0, 39.5, 38.3, 30.7, 28.3, 26.6, 24.6, 24.5, 18.9, 18.3, 12.3, 12.3. MS (ESI) *m/z* calcd. for $[C_{66}H_{84}N_{10}NaO_{17}S_2]^+$: 1375.5; found: 1375.4 $[M+Na]^+$.

H-Arg(Mtr)-DKP3(CH_2NHMtr)-*iso*Asp(O*t*Bu)-Gly-OH (**66**)

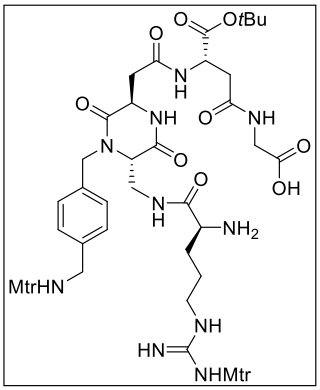

Chemical Formula: $C_{51}H_{72}N_{10}O_{15}S_2$
Molecular Weight: 1129.31

To a solution of **65** (410 mg, 0.30 mmol, 1.0 eq) in THF/H_2O 1:1 (30 mL), Pd/C 10% (32 mg, 0.03 mmol, 0.1 eq) was added: the hydrogenolythic cleavage was carried out as described in GP6. The desired compound **66** was obtained as a white solid (328 mg, 96%) and used without further purification.

MS (ESI) *m/z* calcd. for $[C_{51}H_{72}N_{10}Na_2O_{15}S_2]^{2+}$: 1174.44; found: 1174.62 $[M+2Na]^{2+}$.

Cyclo[DKP3-*iso*Asp(O*t*Bu)-Gly-Arg(Mtr)]-CH_2NHMtr (**67**)

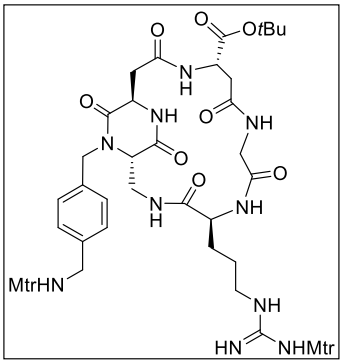

Chemical Formula: $C_{51}H_{70}N_{10}O_{14}S_2$
Molecular Weight: 1111.30

The macrolactamization reaction was carried out on **66** (328 mg, 0.29 mmol, 1.0 eq) according to GP7 (Procedure B). The mixture was concentrated affording an orange oil, which was diluted with AcOEt (350 mL) and washed with $KHSO_4$ 1 M (4 × 90 mL). The organic phase was dried over Na_2SO_4 and volatiles were removed under reduced pressure. The residue was purified using a Grace Reveleris system (column: Reveleris HP Silica 12 g; dry load; flow rate: 24 mL/min; gradient: 100% CH_2Cl_2 to CH_2Cl_2/MeOH 7:3 in 25 min) affording the desired product **67** as a white solid (255 mg, 79%).

R_f = 0.4 (CH_2Cl_2/MeOH 9:1); ^{1}H-NMR (400 MHz, DMSO-d_6) δ 8.60 (d, J = 9.0 Hz, 1H), 8.30 (t, J = 6.1 Hz, 1H), 8.16 (d, J = 7.3 Hz, 1H), 7.87 (t, J = 6.3 Hz, 1H), 7.64 (dd, J = 7.1, 3.8 Hz, 1H), 7.51 (s, 1H), 7.17 – 7.07 (m, 4H), 6.75 (s, 1H), 6.68 (s, 1H), 6.39 (s, 1H), 5.20 (d, J = 15.2 Hz, 1H), 4.80 – 4.69 (m, 1H), 4.35 (dd, J = 11.8, 2.3 Hz, 1H), 4.17 (dd, J = 16.9, 7.3 Hz, 1H), 4.10 – 3.99 (m, 1H), 3.92 (d, J = 6.2 Hz, 2H), 3.89 – 3.80 (m, 4H), 3.79 (s, 3H), 3.65 – 3.56 (m, 2H), 3.54 – 3.43 (m, 3H), 3.10 – 2.97 (m, 3H), 2.62 – 2.51 (m, 11H), 2.43 (s, 3H), 2.16 – 2.07 (m, 1H), 2.06 (s, 3H), 2.04 (s, 3H), 1.65 – 1.54 (m, 1H), 1.49 – 1.29 (m, 12H). ^{13}C-NMR (101 MHz, DMSO-d_6) δ 172.8, 170.7, 169.9, 168.9, 168.7, 166.1, 165.8, 158.5, 157.5, 156.2, 138.2, 137.8, 137.6, 137.2, 135.6, 135.2, 130.0, 127.9, 127.6, 124.0, 123.6, 112.2, 111.7, 81.4, 58.8, 55.7, 55.5, 53.0, 50.0, 49.6, 45.5, 45.1, 41.3, 38.4, 37.8, 36.4, 28.8, 27.6, 25.5, 23.9, 23.7, 18.1, 17.7, 11.8, 11.8. MS (ESI) *m/z* calcd. for $[C_{51}H_{70}N_{10}NaO_{14}S_2]^+$: 1133.44 ; found: 1133.40 $[M+Na]^+$.

Cyclo[DKP3-*iso*DGR)]-CH_2NH_2 (**56**)

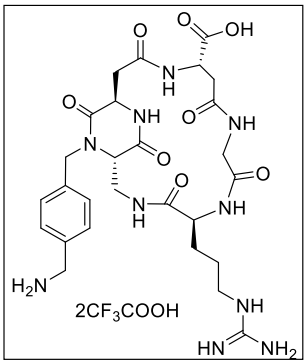

Chemical Formula: $C_{31}H_{40}F_6N_{10}O_{12}$
Molecular Weight: 858.71

67 (220 mg, 0.20 mmol) was deprotected according to GP 8 (Procedure B). The crude compound was purified by RP-HPLC (gradient: 100% H_2O + 0.1% TFA for 2 min, then from 100% H_2O + 0.1% TFA to 77% H_2O + 0.1% TFA / 23% CH_3CN + 0.1% TFA in 9 min, t_R (product) = 9.9 min). The purified product was freeze-dried from water to give **56** (as trifluoroacetate salt) as a white solid (80 mg, 47%).

^{1}H-NMR (400 MHz, D_2O) δ 7.47 – 7.34 (m, 4H), 5.26 (d, J = 15.7 Hz, 1H), 4.87 (dd, J = 11.8, 3.9 Hz, 1H), 4.47 – 4.41 (m, 1H), 4.28 (d, J = 17.3 Hz, 1H), 4.25 – 4.19 (m, 2H), 4.18 (s, 2H), 4.16 – 4.13 (m, 1H), 4.02 (dd, J = 15.0, 4.7 Hz, 1H), 3.80 (d, J = 17.3 Hz, 1H), 3.68 (dd, J = 15.0, 1.5 Hz, 1H), 3.21 (t, J = 6.8 Hz, 2H), 3.15 (dd, J = 13.7, 3.0 Hz, 1H), 3.02 (dd, J = 15.1, 3.9 Hz, 1H), 2.69 (dd, J = 15.1, 11.8 Hz, 1H), 2.37 (dd, J = 13.7, 11.9 Hz, 1H), 1.90 – 1.81 (m, 1H), 1.79 – 1.57 (m, 2H). ^{13}C-NMR (101 MHz, D_2O) δ 176.0, 175.8, 172.8, 172.0, 171.4, 168.0, 167.2, 156.9, 136.2, 132.4, 129.5, 129.5, 128.3, 128.2, 59.7, 54.2, 51.3, 50.5, 47.5, 42.8, 41.6, 40.5, 39.3, 38.3, 38.2, 28.1, 24.6. MS (ESI) *m/z* calcd. for $[C_{27}H_{39}N_{10}O_8]^+$: 631.29; found: 631.21 $[M+H]^+$.

SYNTHESIS OF *CYCLO*[DKP3-*ISO*DGR]-VAL-ALA-PTX CONJUGATE **55**

Dipeptide linker **72** was synthesized according to literature procedure and its analytical data were in agreement with those already published.[25a]

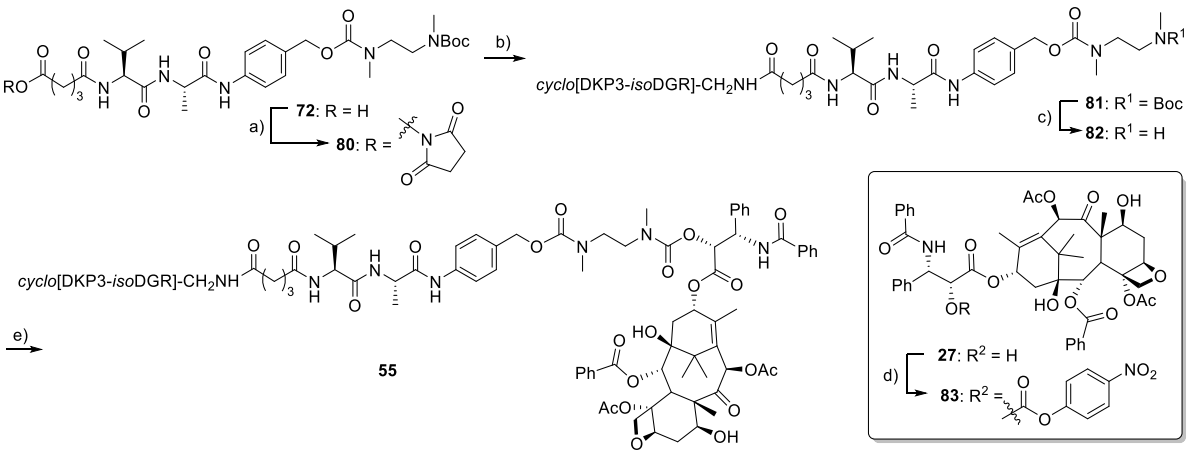

Reagents and conditions: a) NHS, EDC·HCl, DMF, 0 °C to r.t., overnight; b) **56**, PBS/CH_3CN, pH 7.5, 0 °C to r.t., overnight; c) TFA, CH_2Cl_2, r.t., 1 h, 55% over three steps; d) 4-nitrophenylchloroformate, pyridine, CH_2Cl_2, -50 °C to -20 °C, 4 h, 84% based on recovered starting material; e) **83**, *i*Pr_2NEt, DMF, 0 °C to r.t., overnight, 52%.

N-Hydroxysuccinimidyl ester of **72** (**80**)

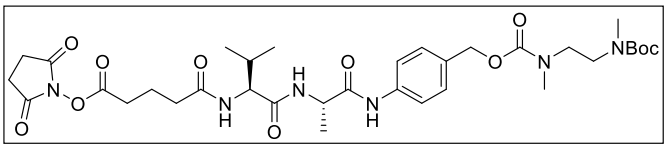

Chemical Formula: $C_{34}H_{50}N_6O_{11}$
Molecular Weight: 718.81

NHS (9.6 mg, 0.084 mmol, 1.3 eq) and EDC·HCl (16 mg, 0.084 mmol, 1.3 eq) were added under nitrogen atmosphere at 0 °C to a solution of **72** (40 mg, 0.064 mmol, 1.0 eq) in DMF (2 mL): the mixture was stirred at 0 °C for 5 min, then at room temperature overnight. The mixture was diluted with AcOEt (100 mL) and washed with H_2O (3 × 20 mL). The organic phase was dried over Na_2SO_4 and concentrated under reduced pressure affording the desired product **80** as white solid (46 mg). The product was used without further purification.

R_f = 0.5 (CH_2Cl_2/MeOH 9:1 + 0.1% CH_3COOH).

Cyclo[DKP-*iso*DGR]-Val-Ala-PAB-OC(O)N(Me)-CH_2CH_2-N(Me)Boc (**81**)

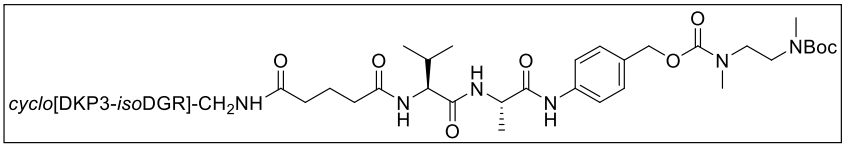

Chemical Formula: $C_{59}H_{84}F_3N_{15}O_{18}$
Molecular Weight: 1348.40

A solution of **56** (28 mg, 0.032 mmol, 1.0 eq) in phosphate buffer (1.5 mL, pH 7.5) was added to a solution of **80** (46 mg, 0.064 mmol, 2.0 eq) in CH_3CN (1.5 mL) under nitrogen atmosphere at 0 °C, adjusting the pH at 7.3-7.6 with aqueous NaOH (0.2 M) during the first 5 h. The resulting solution was stirred at room temperature overnight. The reaction mixture was concentrated and the residue was centrifuged with MeOH/Et_2O affording the desired product **73** as a white solid (40 mg), which was used without further purification.

MS (ESI) *m/z* calcd. for $[C_{57}H_{84}N_{15}O_{16}]^+$: 1234.62; found: 1234.64 $[M+H]^+$.

Cyclo[DKP-*iso*DGR]-Val-Ala-PAB-OC(O)N(Me)-CH_2CH_2-NHMe (**82**)

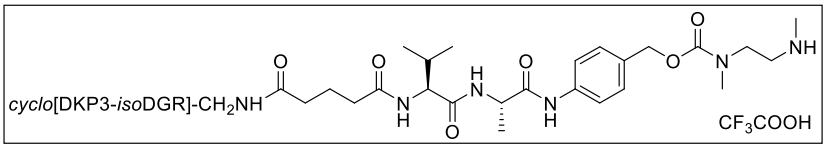

Chemical Formula: $C_{56}H_{77}F_6N_{15}O_{18}$
Molecular Weight: 1362.31

81 (40 mg, 0.032 mmol) was deprotected according to GP5. The crude residue was purified by RP-HPLC (gradient: 100% H_2O + 0.1% TFA for 2 min, then from 90% H_2O + 0.1% TFA / 10% CH_3CN + 0.1% TFA to 50% H_2O + 0.1% TFA / 50% CH_3CN + 0.1% TFA in 12 min, t_R (product) = 9.0 min). The purified product was freeze-dried from glacial acetic acid to give **82** (as trifluoroacetate salt) as a white solid (24 mg, 55% over three steps).

^{1}H-NMR (400 MHz, DMSO-d_6) δ 9.92 (s, 1H), 8.34 – 8.28 (m, 1H), 8.26 (t, J = 5.6 Hz, 1H), 8.21 – 8.15 (m, 1H), 8.17 – 8.11 (m, 1H), 7.93 (s, 1H), 7.83 (d, J = 8.3 Hz, 1H), 7.66 (d, J = 9.1 Hz, 1H), 7.59 (d, J = 8.4 Hz, 2H), 7.54 (d, J = 8.5 Hz, 1H), 7.49 – 7.44 (m, 1H), 7.31 (d, J = 8.4 Hz, 2H), 7.25 – 7.17 (m, 4H), 5.23 (d, J = 15.3 Hz, 1H), 5.00 (s, 2H), 4.62 – 4.54 (m, 1H), 4.44 – 4.34 (m, 2H), 4.26 – 4.20 (m, 2H), 4.20 – 4.10 (m, 3H), 3.90 (d, J = 15.3 Hz, 1H), 3.68 – 3.53 (m, 4H, overlapped with solvent signal), 3.52 – 3.45 (m, 2H, overlapped with solvent signal), 3.06 (d, J = 11.3 Hz, 4H, overlapped with solvent signal), 2.86 (s, 2H), 2.57 (d, J = 17.9 Hz, 2H), 2.23 – 2.16 (m, 2H), 2.16 – 2.09 (m, 1H), 2.03 – 1.95 (m, 1H), 1.90 (s, 6H), 1.80 – 1.70 (m, 2H), 1.69 – 1.62 (m, 1H), 1.56 – 1.39 (m, 3H), 1.30 (d, J = 7.0 Hz, 3H), 1.26 – 1.21 (m, 2H), 0.86 (m, 6H).^{13}C-NMR (101 MHz, DMSO-d_6) δ 172.5, 172.5, 172.2, 171.9, 171.7, 171.1, 169.1, 166.1, 166.0, 163.6, 156.8, 151.2, 138.9, 138.6, 134.9, 133.6, 131.4, 128.4, 127.7, 127.5, 126.8, 119.0, 118.9, 109.5, 74.8, 66.3, 62.6, 59.0, 57.7, 56.1, 52.7, 52.1, 49.0, 49.0, 45.6, 41.7, 41.6, 41.4, 37.8, 36.3, 34.7, 32.8, 30.2, 28.9, 28.4, 25.1, 21.6, 21.0, 19.1, 18.1, 17.8, 14.1. MS (ESI) *m/z* calcd. for $[C_{52}H_{76}N_{15}O_{14}]^+$: 1134.57; found: 1134.77 $[M+H]^+$.

2'-(4-Nitrophenoxycarbonyl)paclitaxel (**83**)

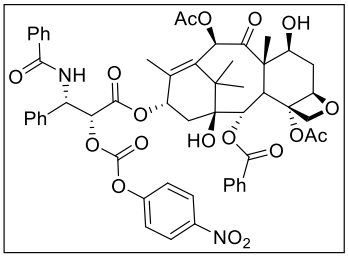

Chemical Formula: $C_{54}H_{54}N_2O_{18}$
Molecular Weight: 1019.02

Paclitaxel (**27**, 500 mg, 0.586 mmol, 1.0 eq) was dissolved in dry CH_2Cl_2 (6 mL) under nitrogen atmosphere. Pyridine (142 µL, 1.76 mmol, 3.0 eq) was added dropwise and the mixture was cooled to -50 °C. A solution of 4-nitrophenylchloroformate (177 mg, 0.878 mmol, 1.5 eq) in dry CH_2Cl_2 (2.5 mL) was added under nitrogen atmosphere: the mixture was stirred at -20 °C for 4 h. The mixture was diluted with AcOEt (200 mL) and washed with $KHSO_4$ 1 M (2 × 30 mL) and brine (1 × 30 mL). The organic phase was dried over Na_2SO_4 and concentrated under reduced pressure. The crude residue was purified using a Grace Reveleris system (column: Reveleris Silica 12 g; dry load; flow rate: 36 mL/min; gradient: 100% Hexane to 100% AcOEt in 19 min) affording the desired product **83** as a white solid (300 mg, 84% based on recovered starting material).

R_f = 0.3 (Hexane/AcOEt 4:6).

Cyclo[DKP3-*iso*DGR]-Val-Ala-PTX (**55**)

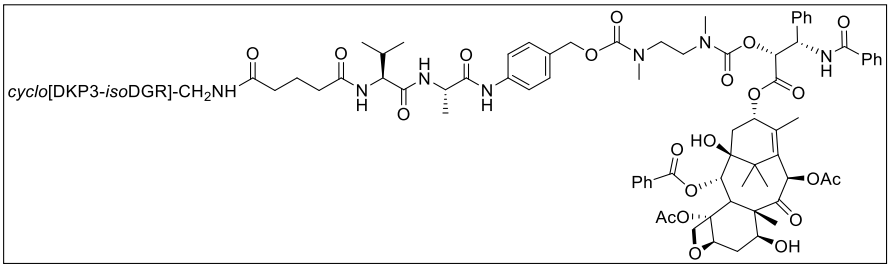

Chemical Formula: $C_{102}H_{125}F_3N_{16}O_{31}$
Molecular Weight: 2128.20

82 (12 mg, 0.009 mmol, 1.0 eq) was dissolved in dry DMF (100 µL) under nitrogen atmosphere and cooled to 0 °C. A solution of **83** (27 mg, 0.026 mmol, 3.0 eq) in dry DMF (900 µL) and *i*Pr$_2$NEt (8 µL, 0.045 mmol, 5.0 eq). were subsequently added to the previous solution: the mixture was stirred at room temperature overnight. The solvent was removed under vacuum; the crude residue was centrifuged (H_2O/CH_3CN) and purified by RP-HPLC (gradient: 90% H_2O + 0.1% TFA / 10% CH_3CN + 0.1% TFA for 2 min, then from 90% H_2O + 0.1% TFA / 10% CH_3CN + 0.1% TFA to 32% H_2O + 0.1% TFA / 68% CH_3CN + 0.1% TFA in 13 min, t_R (product) = 13.2 min). The purified product was freeze-dried from H_2O affording the desired product **55** (as trifluoroacetate salt) as a white solid (10 mg, 52%).

^{1}H-NMR (400 MHz, DMSO-d$_6$) δ 9.91 (s, 1H), 9.18 (d, J = 8.6 Hz, 1H), 8.57 (d, J = 9.1 Hz, 1H), 8.30 – 8.23 (m, 2H), 8.18 – 8.11 (m, 2H), 8.02 – 7.96 (m, 2H), 7.87 – 7.79 (m, 4H), 7.76 – 7.70 (m, 1H), 7.70 – 7.40 (m, 12H), 7.29 – 7.16 (m, 6H), 6.30 (s, 1H), 5.84 (s, 1H), 5.70 – 5.54 (m, 1H), 5.42 (d, J = 6.8 Hz, 1H), 5.22 (d, J = 15.0 Hz, 1H), 4.99 – 4.74 (m, 4H), 4.64 – 4.54 (m, 1H), 4.44 – 4.38 (m, 1H), 4.37 – 4.31 (m, 1H), 4.26 – 4.07 (m, 6H), 4.06 – 3.98 (m, 2H), 3.90 (d, J = 15.0 Hz, 1H), 3.74 – 3.64 (m, 1H), 3.63 – 3.46 (m, 5H), 3.13 – 2.99 (m, 3H), 2.91 – 2.66 (m, 4H), 2.63 – 2.53 (m, 2H), 2.36 – 2.03 (m, 10H), 2.02 – 1.92 (m, 1H), 1.82 (s, 3H), 1.79 – 1.70 (m, 2H), 1.69 – 1.59 (m, 2H), 1.52 (s, 6H), 1.30 (d, J = 7.0 Hz, 3H), 1.24 (s, 4H), 1.06 – 0.98 (m, 6H), 0.91 – 0.80 (m, 6H). ^{13}C-NMR (101 MHz, DMSO-d$_6$) δ 201.6, 172.5, 172.1, 171.7, 170.9, 170.6, 169.5, 168.9, 168.6, 166.0, 165.2, 158.3, 156.6, 138.9, 134.8, 129.9, 129.5, 128.6, 128.2, 127.7, 127.5, 127.3, 119.0, 109.4, 83.6, 74.7, 70.5, 69.3, 66.0, 58.9, 57.5, 52.8, 50.4, 48.8, 46.3, 41.7, 41.3, 38.9, 34.8, 34.4, 30.3, 28.9, 28.5, 28.5, 28.2, 26.3, 22.4, 21.6, 21.4, 19.1, 18.1, 17.9, 13.8, 9.7. MS (MALDI-TOF) *m/z* calcd. for $[C_{100}H_{124}N_{16}O_{29}]^+$: 2015.2; found: 2016.1 $[M+H]^+$ (HCCA matrix).

SYNTHESIS OF *CYCLO*[G*ISO*DGRF] **84**

The synthesis of *cyclo*[G*iso*dGRf] (**84**) was accomplished as described in EP.11 GENERAL PROCEDURES FOR SOLID-PHASE SYNTHESIS on SASRIN™ Resin (400 mg, 0.404 mmol).

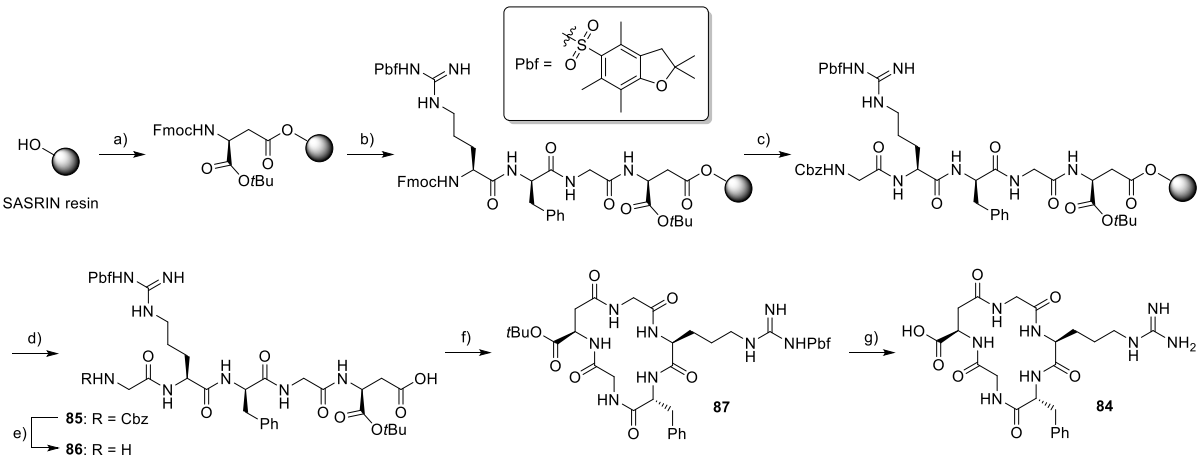

Reagents and Conditions: a) Fmoc-Asp(OH)-O*t*Bu, HATU, HOAt, *i*Pr$_2$NEt, DMF, M.W., 90%; b) 1. 25% piperidine in DMF; 2. Fmoc-AA-OH, HATU, HOAt, *i*Pr$_2$NEt, DMF, M.W.; c) 1. 25% piperidine in DMF; 2. Cbz-Gly-OH, HATU, HOAt, *i*Pr$_2$NEt, DMF, M.W.; d) 1% TFA in CH_2Cl_2, r.t., 3 min × 24 times, 73%; e) H_2, 10% Pd/C, THF/H_2O 2:1, overnight, r.t., quant.; f) HATU, HOAt, *i*Pr$_2$NEt, DMF/CH_2Cl_2 1:1 (1.4 mM), overnight, r.t., 39%; g) TFA/thioanisole/EDT/anisole 90:5:3:2, 2 h, r.t., 49%.

Loading of Fmoc-Asp(OH)-O*t*Bu on SASRIN™ Resin

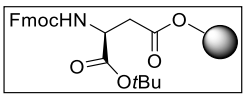

The loading of Fmoc-L-Asp(OH)-O*t*Bu (500 mg, 1.22 mmol) on SASRIN™ Resin was carried out according to EP.11 GENERAL PROCEDURES FOR SOLID-PHASE SYNTHESIS, swelling the beads with DMF. The amino acid was activated as described in GP2 (Procedure B) and added to the resin: a double coupling performed, then the solid support was washed thoroughly with dichloromethane and methanol. After drying under vacuum, the beads were weighted and the yield of the loading calculated.

$$y_{\%} = \frac{(m_{TOT} - m_{RESIN})}{(M.W._{AA} - M.W._{WATER})\, n_{RESIN}}\% = \frac{(544 - 400)\, mg}{(411.46 - 18.02)\, mg/mmol \times 0.404\, mmol}\% = 90\%$$

The amounts of reagents for the next steps were calculated consequently and are reported in TABLE 13.

TABLE 13. Amounts of amino acids used in the SPPS of compound **84**.

Fmoc-AA-OH	Molecular Weight (g/mol)	Amount (mg)
Fmoc-Gly-OH	297.31	324
		324
Fmoc-D-Phe-OH	387.43	423
		423
Fmoc-Arg(Pbf)-OH	648.78	707
		707
Cbz-Gly-OH	209.2	229
		229

Double coupling reactions were performed for all the amino acid residues.

Cbz-Gly-Arg(Mtr)-D-Phe-Gly-Asp(OH)-O*t*Bu (**85**)

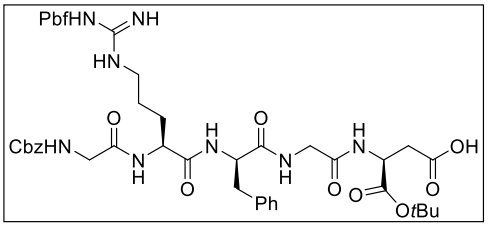

Chemical Formula: $C_{48}H_{64}N_8O_{13}S$
Molecular Weight: 993.14

The peptide cleavage from the resin was performed according to GP4. The desired product **85** was obtained as white foam (293 mg, 73%).

R_f = 0.50 (CH_2Cl_2/MeOH 9:1, CH_3COOH drops); ^{1}H-NMR (400 MHz, CD_3OD) δ 7.42 – 7.09 (m, 10H), 5.09 (s, 2H), 4.73 – 4.61 (m, 2H), 4.34 – 4.25 (m, 1H), 3.96 – 3.75 (m, 4H), 3.31 (bs, 2H, overlapped with solvent signal), 3.03 – 2.89 (m, 4H), 2.70 (bs, 2H), 2.60 (s, 3H), 2.54 (s, 3H), 2.08 (s, 3H), 1.61 – 1.47 (m, 2H), 1.43 (s, 6H), 1.42 (s, 9H), 1.20 (s, 2H). ^{13}C-NMR (101 MHz, CD_3OD) δ 174.3, 174.3, 172.5, 172.5, 171.6, 171.4, 171.4, 159.9, 158.2, 158.2, 139.5, 139.5, 138.7, 138.7, 133.6, 133.6, 130.4, 130.4, 130.2, 130.2, 129.6, 129.6, 129.5, 129.5, 129.4, 129.4, 129.1, 129.1, 128.9, 128.9, 127.8, 127.8, 126.1, 126.1, 118.5, 87.7, 87.7, 83.3, 83.3, 68.0, 68.0, 56.5, 54.5, 51.4, 44.9, 44.0, 44.0, 43.8, 43.8, 38.0, 38.0, 29.4, 28.7, 28.7, 28.2, 28.2, 26.3, 19.7, 19.7, 18.5, 12.5, 12.5. MS (ESI) *m/z* calcd. for $[C_{48}H_{64}N_8NaO_{13}S]^+$: 1015.4; found: 1015.4 $[M+Na]^+$.

H-Gly-Arg(Mtr)-D-Phe-Gly-Asp(OH)-O*t*Bu (**86**)

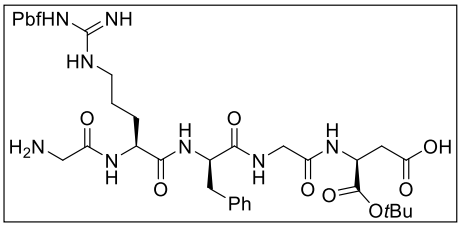

Chemical Formula: $C_{40}H_{58}N_8O_{11}S$
Molecular Weight: 859.01

The Cbz-removal from compound **85** was carried out according to GP6. The desired product **86** was obtained as white foam (260 mg, quantitative).

MS (ESI) *m/z* calcd. for $[C_{40}H_{58}N_8NaO_{11}S]^+$: 881.38; found: 881.49 $[M+Na]^+$.

Cyclo[Gly-Asp(O*t*Bu)-Gly-Arg(Mtr)-D-Phe] (**87**)

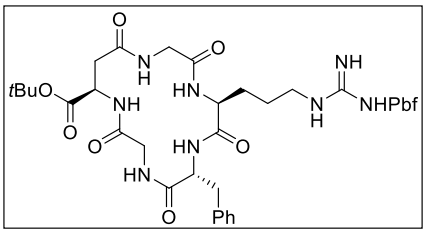

Chemical Formula: $C_{40}H_{56}N_8O_{10}S$
Molecular Weight: 840.99

The macrolactamization reaction on **86** was performed according to GP7 (Procedure B). The crude compound was dissolved with AcOEt (300 mL) and washed with $KHSO_4$ 1 M (4 × 100 mL) and brine (2 × 50 mL). The organic layer was dried over Na_2SO_4 and volatiles were removed under reduced pressure. The residue was purified by flash chromatography on silica gel (CH_2Cl_2 100% to CH_2Cl_2/MeOH 9:1, solid load) affording the desired product **87** as a white foam (95 mg, 39%).

R_f = 0.50 (CH_2Cl_2/MeOH 9:1); ^{1}H-NMR (600 MHz, CD_3OD) δ 7.27 – 7.17 (m, 4H), 7.17 – 7.09 (m, 1H), 4.71 (dd, J = 5.9, 4.7 Hz, 1H), 4.64 (dd, J = 11.3, 4.4 Hz, 1H), 4.10 (d, J = 16.6 Hz, 1H), 4.01 (t, J = 6.3 Hz, 1H), 3.85 (d, J = 15.8 Hz, 1H), 3.76 (d, J = 16.6 Hz, 1H), 3.61 (d, J = 15.8 Hz, 1H), 3.38 (dd, J = 14.1, 4.4 Hz, 1H), 3.03 – 2.97 (m, 4H), 2.84 – 2.76 (m, 3H), 2.72 (dd, J = 14.7, 4.7 Hz, 1H), 2.59 (s,

4H), 2.53 (s, 4H), 2.09 (s, 3H), 1.48 (s, 8H), 1.44 (d, *J* = 3.1 Hz, 9H), 1.20 – 1.12 (m, 3H), 0.99 – 0.88 (m, 2H). ^{13}C-NMR (151 MHz, CD_3OD) δ 173.8, 172.9, 172.3, 171.1, 170.9, 159.9, 139.4, 138.9, 134.4, 133.5, 130.1, 129.6, 127.8, 126.1, 118.5, 87.7, 83.5, 56.6, 55.7, 51.4, 44.1, 44.0, 43.5, 38.1, 37.7, 28.7, 28.2, 26.3, 26.3, 26.3, 19.6, 18.4, 12.5. [Due to technical problems, compound **87** was characterized using a spectrometer operating at 600 MHz]. MS (ESI) *m/z* calcd. for $[C_{40}H_{56}N_8NaO_{10}S]^+$: 863.37; found: 863.38 $[M+Na]^+$.

Cyclo[G*iso*dGRf] (**84**)

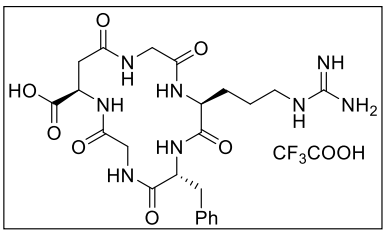

Chemical Formula: $C_{25}H_{33}F_3N_8O_9$
Molecular Weight: 646.58

The final deprotection on compound **87** was carried out as described in GP8 (Procedure A). The residue was purified by RP-HPLC (gradient: from 90% H_2O + 0.1% TFA / 10% CH_3CN + 0.1% TFA to 60% H_2O + 0.1% TFA / 40% CH_3CN + 0.1% TFA in 8 min, t_R (product) = 4.4 min). The purified product was freeze-dried from water to give **84** (as trifluoroacetate salt) as a white solid (35 mg, 49%).

^{1}H-NMR (400 MHz, CD_3OD) δ 7.12 – 6.97 (m, 5H), 4.62 (dd, *J* = 6.4, 4.5 Hz, 1H), 4.44 (dd, *J* = 10.7, 4.8 Hz, 1H), 3.83 (t, *J* = 7.5 Hz, 1H), 3.77 (d, *J* = 16.5 Hz, 1H), 3.69 – 3.60 (m, 2H), 3.45 (d, *J* = 15.8 Hz, 1H), 3.16 (dd, *J* = 14.0, 4.8 Hz, 1H), 2.88 – 2.76 (m, 2H), 2.71 – 2.54 (m, 3H), 1.47 – 1.29 (m, 2H), 1.20 – 1.05 (m, 1H), 0.90 – 0.77 (m, 1H). [Compound **84** was fully characterized by Cristina Paissoni (R10582)]. MS (ESI) *m/z* calcd. for $[C_{23}H_{33}N_8O_7]^+$: 533.25; found: 533.24 $[M+H]^+$.

SYNTHESIS OF *CYCLO*[DKP3-RAD] **88A** AND **88B**

N_3-DKP3-COOAllyl **44**, BocHN-DKP3-COOAllyl **93** and BocHN-DKP3-COOH **94** were synthesized according to literature procedure and their analytical data were in agreement with those already published.[27]

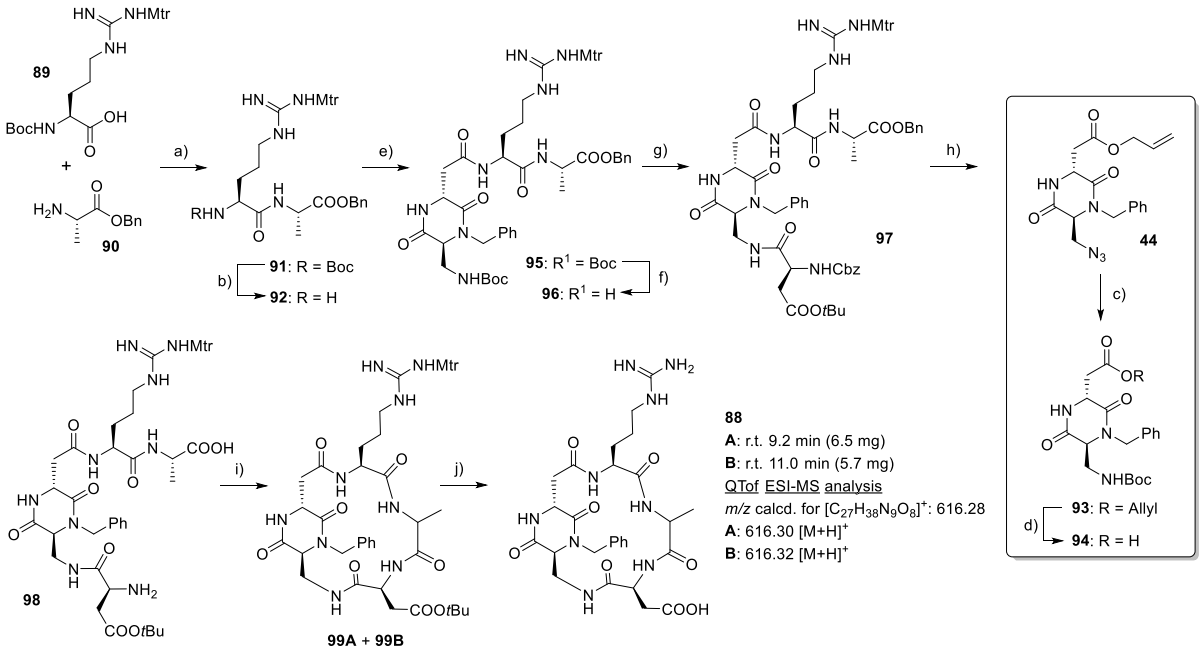

Reagents and conditions. a) HATU, HOAt, *i*Pr$_2$NEt, DMF, 0 °C to r.t., overnight, 84%; b) TFA, CH_2Cl_2, r.t., 2 h; c) PMe_3 in toluene, Boc-ON, THF, -20 °C to r.t., 5 h, 78%; d) [$Pd(PPh_3)_4$], pyrrolidine, PPh_3, CH_2Cl_2, 0 °C, 1 h, quant.; e) **94**, HATU, HOAt, *i*Pr$_2$NEt, DMF, 0 °C to r.t., overnight, 65%; f) TFA, CH_2Cl_2, r.t., 2 h; g) Cbz-L-Asp(O*t*Bu)-OH, HATU, HOAt, *i*Pr$_2$NEt, DMF, 0 °C to r.t., overnight, 83%; h) H_2, 10% Pd/C, THF/H_2O 1:1, overnight, r.t., quant.; i) HATU, HOAt, *i*Pr$_2$NEt, DMF/CH_2Cl_2 1:1 (1.4 mM), 0 °C to r.t., overnight, 82%; j) TFA/thioanisole/EDT/anisole 90:5:3:2, 2 h, rt, 30%. The synthesis was performed according to ref. 27.

BocHN-Arg(Mtr)-Ala-OBn (**91**)

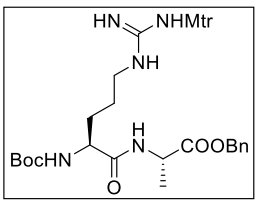

Chemical Formula: $C_{31}H_{45}N_5O_8S$
Molecular Weight: 647.79

To a solution of BocHN-Arg(Mtr)-OH **89** (290 mg, 0.60 mmol, 1.0 eq) in DMF (9.0 mL), at 0 °C and under nitrogen atmosphere, HATU (250 mg, 0.66 mmol, 1.1 eq), HOAt (90 mg, 0.66 mmol, 1.1 eq) and *i*Pr$_2$NEt (315 µL, 1.8 mmol, 3.0 eq) were added: the reaction was stirred at 0 °C for 30 min. A solution of L-Ala-OBn·HCl (140 mg, 0.66 mmol, 1.1 eq) in DMF (3.0 mL) and *i*Pr$_2$NEt (209 µL, 1.2 mmol, 2.0 eq) was added dropwise to the previous solution: the reaction mixture was stirred at 0 °C for 1 h and at room temperature overnight. The mixture was diluted with AcOEt (50 mL) and washed with $KHSO_4$ 1 M (4 × 50 mL), saturated aqueous $NaHCO_3$ (4 × 50 mL) and brine (2 × 50 mL). The organic phase was dried over Na_2SO_4 and volatiles were removed under reduced pressure. The residue was purified by flash chromatography on silica gel (Hexane/AcOEt 3:7, solid load) affording the desired product **91** as a white foam (332 mg, 84%).

R_f = 0.13 (Hexane/AcOEt 3:7); ^{1}H-NMR (400 MHz, $CDCl_3$) δ 7.41 (d, J = 6.9 Hz, 1H), 7.37 – 7.26 (m, 5H), 6.52 (s, 1H), 6.31 (bs, 2H), 5.52 (d, J = 7.5 Hz, 1H), 5.12 (d, J = 12.4 Hz, 2H), 4.61 – 4.46 (m, 1H), 4.27 (bs, 1H), 3.81 (s, 3H), 3.19 (bs, 2H), 2.68 (s, 3H), 2.61 (s, 3H), 2.12 (s, 4H), 1.88 – 1.76 (m, 1H),

1.67 – 1.52 (m, 3H), 1.40 (s, 12H). ^{13}C-NMR (101 MHz, $CDCl_3$) δ 173.0, 172.4, 158.7, 156.4, 156.1, 138.8, 136.9, 135.5, 128.7, 128.5, 128.2, 125.0, 111.9, 80.1, 67.3, 55.6, 53.4, 48.5, 40.7, 30.6, 28.5, 25.2, 24.3, 18.5, 17.4, 12.1. MS (ESI) *m/z* calcd. for $[C_{31}H_{45}N_5NaO_8S]^+$: 670.29; found: 670.09 $[M+Na]^+$.

BocHN-DKP3-Arg(Mtr)-Ala-OBn (**95**)

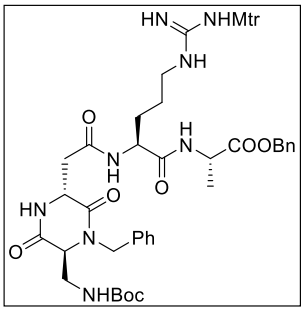

Chemical Formula: $C_{45}H_{60}N_8O_{11}S$
Molecular Weight: 921.08

To a solution of BocHN-DKP3-COOH **94** (160 mg, 0.41 mmol, 1.0 eq), prepared as described in ref. 27, in DMF (4.1 mL), under nitrogen atmosphere and at 0 ºC, HATU (186 mg, 0.49 mmol, 1.2 eq), HOAt (67 mg, 0.49 mmol, 1.2 eq) and *i*Pr$_2$NEt (271 µL, 1.64 mmol, 4.0 eq.) were added successively. After 30 min, a solution of the TFA salt **92** (324 mg, 0.49 mmol, 1.2 eq), obtained treating **91** according to GP5, in DMF (4.1 mL) was added and the reaction mixture was stirred at 0 ºC for 1 h and at r.t. overnight. The mixture was afterwards diluted with AcOEt (50 mL) and washed with $KHSO_4$ 1 M (3 × 90 mL), saturated aqueous $NaHCO_3$ (3 × 90 mL) and brine (2 × 90 mL). The organic phase was dried over Na_2SO_4 and volatiles were removed under reduced pressure. The residue was purified by flash chromatography on silica gel (from CH_2Cl_2/MeOH 96:4 to CH_2Cl_2/MeOH 9:1, solid load) affording the desired product **95** as a white foam (246 mg, 65%).

R_f = 0.29 (CH_2Cl_2/MeOH 95:5); ^{1}H-NMR (400 MHz, CD_2Cl_2) δ 7.92 (bs, 1H), 7.79 – 7.41 (m, 2H), 7.37 – 7.15 (m, 10H), 6.54 (s, 1H), 6.25 (bs, 2H), 5.65 (bs, 1H), 5.43 – 5.34 (m, 1H), 5.09 (q, *J* = 12.3 Hz, 2H), 4.60 (bs, 1H), 4.54 – 4.34 (m, 2H), 4.08 (d, *J* = 15.0 Hz, 1H), 3.92 – 3.68 (m, 3H), 3.70 – 3.36 (m, 2H), 3.24 – 2.78 (m, 4H), 2.64 (s, 3H), 2.57 (s, 3H), 2.09 (s, 3H), 1.78 (bs, 1H), 1.60 (bs, 1H), 1.56 – 1.45 (m, 2H), 1.36 (s, 12H). ^{13}C-NMR (101 MHz, CD_2Cl_2) δ 173.0, 172.4, 170.5, 168.1, 166.8, 158.9, 157.0, 156.5, 138.9, 136.9, 136.2, 136.0, 133.9, 129.2, 128.9, 128.7, 128.4, 125.2, 112.1, 80.2, 67.4, 60.3, 55.8, 53.0, 51.8, 48.9, 47.7, 41.2, 40.9, 38.3, 30.3, 28.5, 25.4, 24.3, 18.6, 17.4, 12.1. MS (ESI) *m/z* calcd. for $[C_{45}H_{60}N_8NaO_{11}S]^+$: 943.40; found: 943.61 $[M+Na]^+$.

CbzHN-Asp(O*t*Bu)-DKP3-Arg(Mtr)-Ala-OBn (**97**)

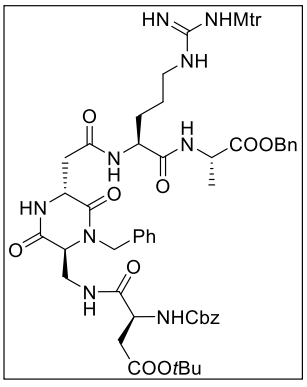

Chemical Formula: $C_{56}H_{71}N_9O_{14}S$
Molecular Weight: 1126.29

To a solution of Cbz-L-Asp(O*t*Bu)-OH (136 mg, 0.42 mmol, 1.5 eq.) in DMF (2.6 mL), under nitrogen atmosphere and at 0 ºC, HATU (160 mg, 0.42 mmol, 1.5 eq), HOAt (57 mg, 0.42 mmol, 1.5 eq) and *i*Pr$_2$NEt (195 µL, 1.12 mmol, 4.0 eq.) were added successively. Compound **95** (255 mg, 0.28 mmol, 1.0 eq) was deprotected according to GP5 and the corresponding trifluoroacetate salt **96** was dissolved in

DMF (3.0 mL) and added to the previous solution after 30 min. The reaction mixture was stirred at 0 ºC for 1 h and at r.t. overnight. The mixture was afterwards diluted with AcOEt (45 mL) and washed with $KHSO_4$ 1 M (3 × 40 mL), saturated aqueous $NaHCO_3$ (3 × 40 mL) and brine (1 × 40 mL). The organic phase was dried over Na_2SO_4 and volatiles were removed under reduced pressure. The residue was purified by flash chromatography on silica gel (CH_2Cl_2/MeOH 95:5, solid load) affording the desired product **97** as a white foam (263 mg, 83%).

R_f = 0.27 (CH_2Cl_2/MeOH 95:5); ^{1}H-NMR (400 MHz, CD_2Cl_2) δ 7.72 (bs, 1H), 7.59 (bs, 2H), 7.39 – 7.16 (m, 15H), 6.53 (s, 1H), 6.25 (bs, 2H), 6.17 (d, *J* = 7.5 Hz, 1H), 5.23 (d, *J* = 15.2 Hz, 1H), 5.16 – 5.01 (m, 3H), 4.88 (d, *J* = 12.0 Hz, 1H), 4.63 – 4.51 (m, 2H), 4.50 – 4.39 (m, 3H), 4.15 (d, *J* = 15.2 Hz, 1H), 3.86 – 3.81 (m, 2H), 3.79 (s, 3H), 3.63 – 3.51 (m, 1H), 3.17 – 3.04 (m, 2H), 2.99 (d, *J* = 14.0 Hz, 1H), 2.81 (d, *J* = 14.0 Hz, 1H), 2.77 – 2.68 (m, 1H), 2.64 (s, 3H), 2.57 (s, 3H), 2.09 (s, 3H), 1.86 – 1.74 (m, 1H), 1.67 – 1.56 (m, 1H), 1.51 (s, 2H), 1.34 (s, 12H). ^{13}C-NMR (101 MHz, CD_2Cl_2) δ 173.1, 172.3, 172.1, 170.9, 170.7, 168.0, 166.8, 158.8, 156.9, 156.8, 138.8, 136.9, 136.6, 136.3, 136.0, 134.0, 129.2, 128.9, 128.7, 128.5, 128.4, 128.2, 125.1, 112.1, 82.0, 67.6, 67.4, 59.9, 55.8, 53.0, 52.1, 51.7, 48.9, 47.9, 40.9, 40.0, 38.5, 37.5, 30.3, 30.1, 28.1, 25.3, 24.3, 18.6, 17.4, 12.1. MS (ESI) *m/z* calcd. for $[C_{56}H_{71}N_9NaO_{14}S]^+$: 1148.47; found: 1148.58 $[M+Na]^+$.

CbzHN-Asp(O*t*Bu)-DKP3-Arg(Mtr)-Ala-OBn (**98**)

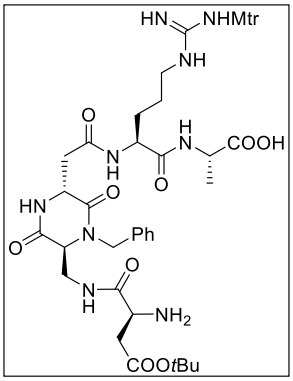

Chemical Formula: $C_{41}H_{59}N_9O_{12}S$
Molecular Weight: 902.03

Cbz-carbamate and benzyl ester protecting groups were removed by hydrogenolysis of compound **97** as described in GP6. The desired product was obtained as white foam (185 mg, quantitative).

MS (ESI) *m/z* calcd. for $[C_{41}H_{59}N_9NaO_{12}S]^+$: 924.39; found: 924.61 $[M+Na]^+$.

Cyclo[DKP3-Arg(Mtr)-Ala-Asp(O*t*Bu)] (**99A** + **99B**)

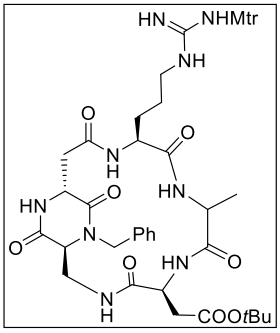

Chemical Formula: $C_{41}H_{57}N_9O_{11}S$
Molecular Weight: 884.02

The macrolactamization reaction on **98** was performed according to GP7 (Procedure A). The crude compound was dissolved with AcOEt (150 mL) and washed with $KHSO_4$ 1 M (3 × 100 mL). The organic layer was dried over Na_2SO_4 and volatiles were removed under reduced pressure. The residue was purified by flash chromatography on silica gel (from CH_2Cl_2/MeOH 96:4 to CH_2Cl_2/MeOH 92:8, solid

load) affording the desired product as mixture of two inseparable isomers **99A** and **99B** as a white foam (150 mg, 81%).

R_f = 0.60, 0.52 (CH_2Cl_2/MeOH 9:1); ^{1}H-NMR (400 MHz, CD_3OD) δ 7.39 – 7.21 (m, $5H_A$ + $5H_B$), 6.66 (s, $1H_A$), 6.65 (s, $1H_B$), 5.51 (d, J = 17.8 Hz, $1H_A$), 5.29 – 5.12 (m, $1H_B$), 4.74 (d, J = 6.4 Hz, $1H_B$), 4.60 (bs, $2H_A$), 4.58 – 4.49 (m, $1H_B$), 4.45 – 4.34 (m, $1H_A$), 4.20 – 4.03 (m, $1H_A$ + $3H_B$), 4.03 – 3.89 (m, $2H_A$ + $1H_B$), 3.89 – 3.79 (m, $4H_A$ + $4H_B$), 3.64 (bs, $1H_A$), 3.61 – 3.50 (m, $1H_B$), 3.41 (dd, J = 14.0, 5.0 Hz, $1H_B$), 3.28 – 3.12 (m, $1H_A$ + $2H_B$), 3.12 – 3.03 (m, $2H_A$), 3.02 – 2.70 (m, $3H_A$+ $2H_B$), 2.68 (s, $3H_A$), 2.67 (s, $3H_B$), 2.61 (s, $3H_A$), 2.60 (s, $3H_B$), 2.52 – 2.38 (m, $1H_B$), 2.36 – 2.20 (m, $1H_B$), 2.13 (s, $3H_A$), 2.10 (s, $3H_B$), 1.95 – 1.75 (m, $1H_A$ + $2H_B$), 1.75 – 1.52 (m, $3H_A$ + $2H_B$), 1.52 – 1.36 (m, $12H_A$ + $12H_B$). ^{13}C-NMR (101 MHz, CD_3OD) δ 175.0, 174.1, 173.5, 172.3, 171.5, 170.7, 169.4, 168.6, 159.9, 158.1, 139.5, 137.9, 137.3, 136.6, 134.9, 130.7, 130.0, 129.9, 129.4, 129.1, 128.9, 125.7, 113.2, 112.8, 82.7, 82.5, 60.5, 60.2, 56.0, 53.2, 53.0, 47.8, 41.4, 40.5, 40.2, 39.6, 38.6, 37.1, 36.7, 30.7, 28.4, 28.3, 27.8, 24.4, 18.8, 18.2, 16.8, 12.2. MS (ESI) *m/z* calcd. for $[C_{41}H_{57}N_9NaO_{11}S]^+$: 906.38; found: 906.56 $[M+Na]^+$.

Cyclo[DKP3-RAD] Peptidomimetics **88A** and **88B**

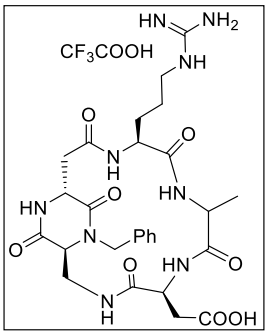

Chemical Formula: $C_{29}H_{38}F_3N_9O_{10}$
Molecular Weight: 729.67

The final deprotection on the mixture **99A** + **99B** was carried out as described in GP8 (Procedure A). The residue was purified by RP-HPLC (gradient: from 90% H_2O + 0.1% TFA / 10% CH_3CN + 0.1% TFA to 72% H_2O + 0.1% TFA / 28% CH_3CN + 0.1% TFA in 12 min, t_R (product **88A**) = 9.2 min, t_R (product **88B**) = 11.0 min). The purified products were freeze-dried from water to give **88A** (6.5 mg) and **88B** (5.7 mg) trifluoroacetate salts as a white solids (30%).

Compound **88A**: ^{1}H-NMR (400 MHz, D_2O) δ 7.56 – 7.35 (m, 5H), 5.14 (d, J = 15.7 Hz, 1H), 4.80 – 4.72 (m, 1H, overlapped with solvent signal), 4.65 (t, J = 6.8 Hz, 1H), 4.38 (q, J = 7.1 Hz, 2H), 4.25 – 4.14 (m, 3H), 3.54 (dd, J = 14.9, 4.8 Hz, 1H), 3.30 (t, J = 6.8 Hz, 2H), 3.10 (dd, J = 14.2, 5.7 Hz, 1H), 2.99 (d, J = 6.9 Hz, 2H), 2.70 (dd, J = 14.2, 6.0 Hz, 1H), 1.94 (dd, J = 14.9, 6.9 Hz, 2H), 1.85 – 1.63 (m, 2H), 1.50 (d, J = 7.2 Hz, 3H). ^{13}C-NMR (101 MHz, D_2O) δ 174.4, 173.6, 173.2, 172.8, 169.3, 168.0, 156.8, 135.3, 129.1, 128.2, 127.6, 60.3, 55.7, 52.3, 51.0, 49.9, 48.1, 40.5, 39.5, 38.2, 34.7, 26.6, 24.6, 16.0. MS (ESI) *m/z* calcd. for $[C_{27}H_{38}N_9O_8]^+$: 616.28; found: 616.30 $[M+H]^+$.

Compound **88B**: ^{1}H-NMR (400 MHz, D_2O) δ 7.51 – 7.30 (m, 5H), 5.39 (d, J = 15.6 Hz, 1H), 4.61 (t, J = 4.2 Hz, 1H), 4.54 (t, J = 6.1 Hz, 1H), 4.49 (dd, J = 8.5, 4.5 Hz, 1H), 4.17 (d, J = 15.6 Hz, 1H), 4.12 – 4.02 (m, 2H), 4.02 – 3.74 (m, 2H), 3.17 (dd, J = 15.3, 4.2 Hz, 1H), 3.09 (dt, J = 11.2, 5.5 Hz, 2H), 3.04 – 2.90 (m, 2H), 2.84 (dd, J = 15.3, 4.9 Hz, 1H), 1.93 – 1.60 (m, 2H), 1.62 – 1.46 (m, 2H), 1.41 (d, J = 7.2 Hz, 3H). ^{13}C-NMR (101 MHz, D_2O) δ 175.0, 174.4, 173.9, 173.1, 170.7, 168.0, 167.4, 156.6, 135.0, 129.2, 129.0, 128.1, 127.5, 59.3, 52.4, 51.6, 51.1, 50.8, 47.3, 40.7, 39.6, 37.6, 34.5, 29.9, 24.5, 15.9. MS (ESI) *m/z* calcd. for $[C_{27}H_{38}N_9O_8]^+$: 616.28; found: 616.32 $[M+H]^+$.

SYNTHESIS OF VEGF-C DERIVED PEPTIDES **113-118**

The synthesis of VEGF-C derived peptide sequences (**113-118**, FIGURE 56) was accomplished as described in EP.11 GENERAL PROCEDURES FOR SOLID-PHASE SYNTHESIS on Rink Amide MHBA Resin (200 mg, 0.100 mmol).

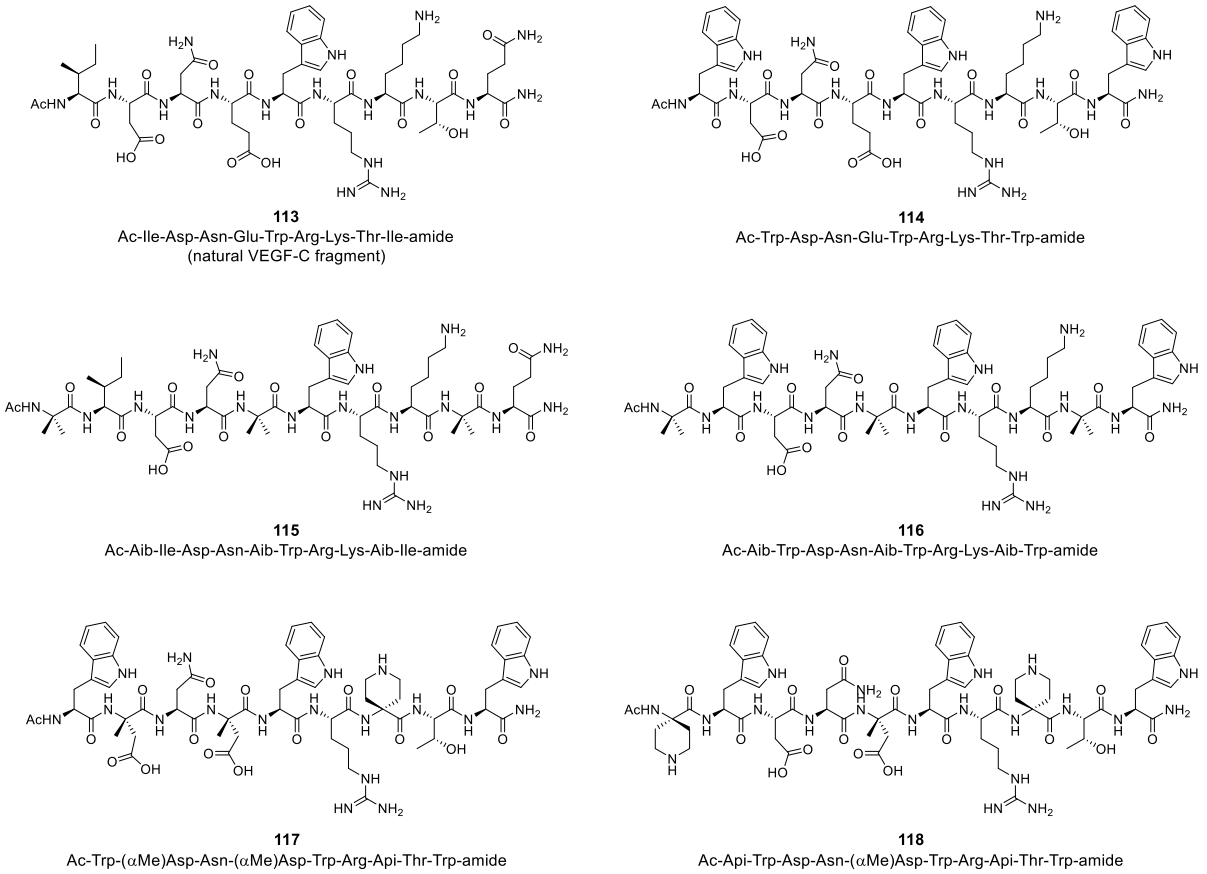

FIGURE 56. VEGF-C derived peptides 113-118.

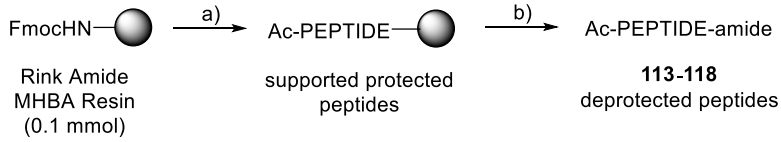

Reagents and conditions: a) SPPS: 1. 25% piperidine in DMF; 2. Fmoc-AA-OH (4.0 eq), DIC, HOAt, *i*Pr$_2$NEt, DMF; 3. 25% Ac$_2$O in DMF; b) TFA/thioanisole/EDT/anisole 90:5:3:2 v/v/v/v, r.t., 3 h, 7-30%.

The exact amounts of the amino acids used for each peptide sequence are reported in the corresponding TABLE.

Natural VEGF-C fragment Ac-Ile-Asp-Asn-Glu-Trp-Arg-Lys-Thr-Ile-amide (**113**)

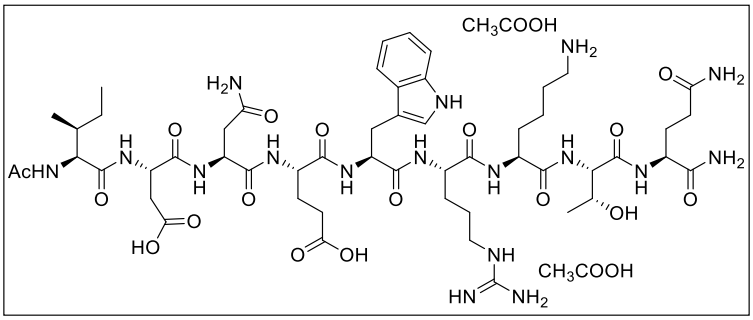

Chemical Formula: $C_{57}H_{91}N_{17}O_{21}$
Molecular Weight: 1350.45

TABLE 14. Amounts of amino acids used in the SPPS of compound **113**.

Fmoc-AA-OH	Molecular Weight (g/mol)	Amount (mg)
Fmoc-Gln(Trt)-OH	610.70	244
Fmoc-Thr(*t*Bu)-OH	397.46	159
Fmoc-Lys(Boc)-OH	468.54	187
Fmoc-Arg(Pbf)-OH	648.78	260
Fmoc-Trp(Boc)-OH	526.58	211
Fmoc-Glu(O*t*Bu)-OH	425.47	170
Fmoc-Asn(Trt)-OH	596.69	239
Fmoc-Asp(O*t*Bu)-OH	411.46	165
Fmoc-Ile-OH	353.41	141

The supported peptide (0.100 mmol) was deprotected as described in GP4 and purified by RP-HPLC (gradient: 80% H_2O + 0.1% CH_3COOH / 20% CH_3CN + 0.1% CH_3COOH for 5 min, then from 80% H_2O + 0.1% CH_3COOH / 20% CH_3CN + 0.1% CH_3COOH to 37% H_2O + 0.1% CH_3COOH / 63% CH_3CN+ 0.1% CH_3COOH in 10 min; t_R (product) = 7.9 min).

The desired peptide **113** was freeze-dried from glacial acetic acid, obtaining the corresponding salt as white solid (6 mg, 12%).

MS (MALDI-TOF) *m/z* calcd. for $[C_{53}H_{84}N_{17}O_{17}]^+$: 1231.6; found:1231.2 $[M+H]^+$ (SIN matrix).

Peptide Ac-Trp-Asp-Asn-Glu-Trp-Arg-Lys-Thr-Trp-amide (**114**)

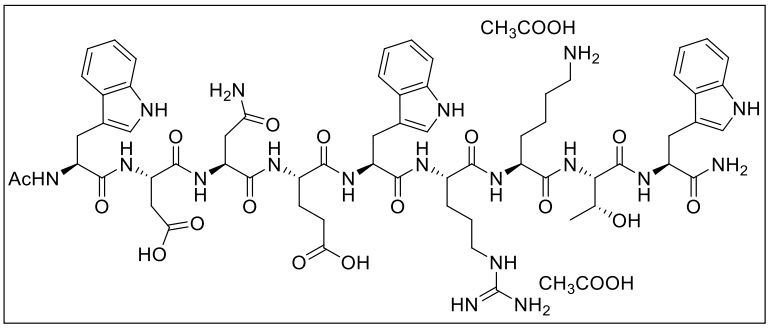

Chemical Formula: $C_{68}H_{92}N_{18}O_{20}$
Molecular Weight: 1481.59

TABLE 15. Amounts of amino acids used in the SPPS of compound **114**.

Fmoc-AA-OH	Molecular Weight (g/mol)	Amount (mg)
Fmoc-Trp(Boc)-OH	526.58	211
Fmoc-Thr(*t*Bu)-OH	397.46	159
Fmoc-Lys(Boc)-OH	468.54	187
Fmoc-Arg(Pbf)-OH	648.78	260
Fmoc-Trp(Boc)-OH	526.58	211
Fmoc-Glu(O*t*Bu)-OH	425.47	170
Fmoc-Asn(Trt)-OH	596.69	239
Fmoc-Asp(O*t*Bu)-OH	411.46	165
Fmoc-Trp(Boc)-OH	526.58	211

The supported peptide (0.100 mmol) was deprotected as described in GP4 and purified by RP-HPLC (gradient: 80% H_2O + 0.1% CH_3COOH / 20% CH_3CN + 0.1% CH_3COOH for 5 min, then from 80% H_2O + 0.1% CH_3COOH / 20% CH_3CN + 0.1% CH_3COOH to 37% H_2O + 0.1% CH_3COOH / 63% CH_3CN+ 0.1% CH_3COOH in 10 min; t_R (product) = 11.2 min).

The desired peptide **114** was freeze-dried from glacial acetic acid, obtaining the corresponding salt as white solid (22 mg, 16%).

MS (MALDI-TOF) *m/z* calcd. for $[C_{64}H_{85}N_{18}O_{16}]^+$: 1361.6; found: 1361.6 $[M+H]^+$ (HCCA matrix).

Peptide Ac-Aib-Ile-Asp-Asn-Aib-Trp-Arg-Lys-Aib-Ile-amide (**115**)

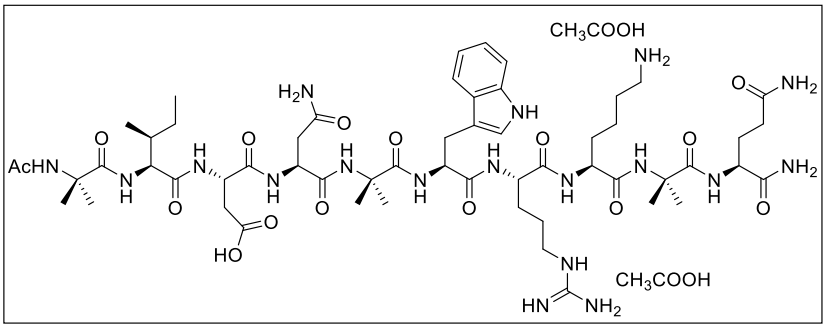

Chemical Formula: $C_{60}H_{98}N_{18}O_{19}$
Molecular Weight: 1375.55

TABLE 16. Amounts of amino acids used in the SPPS of compound **115**.

Fmoc-AA-OH	Molecular Weight (g/mol)	Amount (mg)
Fmoc-Gln(Trt)-OH	610.70	244
Fmoc-2-Aminoisobutyric acid-OH*	325.36	130
		130
Fmoc-Lys(Boc)-OH	468.54	187
Fmoc-Arg(Pbf)-OH	648.78	260
Fmoc-Trp(Boc)-OH	526.58	211
Fmoc-2-Aminoisobutyric acid-OH*	325.36	130
		130
Fmoc-Asn(Trt)-OH	596.69	239
Fmoc-Asp(O*t*Bu)-OH	411.46	165
Fmoc-Ile-OH	353.41	141
Fmoc-2-Aminoisobutyric acid-OH*	325.36	130
		130

*A double coupling was performed.

The supported peptide (0.100 mmol) was deprotected as described in GP4 and purified by RP-HPLC (gradient: 80% H_2O + 0.1% CH_3COOH / 20% CH_3CN + 0.1% CH_3COOH for 5 min, then from 80% H_2O + 0.1% CH_3COOH / 20% CH_3CN + 0.1% CH_3COOH to 37% H_2O + 0.1% CH_3COOH / 63% CH_3CN+ 0.1% CH_3COOH in 10 min; t_R (product) = 10.6 min).

The desired peptide **115** was freeze-dried from glacial acetic acid, obtaining the corresponding salt as white solid (25 mg, 20%).

MS (MALDI-TOF) *m/z* calcd. for $[C_{56}H_{91}N_{18}O_{15}]^+$: 1256.5; found: 1256.4 $[M+H]^+$ (SIN matrix).

Peptide Ac-Aib-Trp-Asp-Asn-Aib-Trp-Arg-Lys-Aib-Trp-amide (**116**)

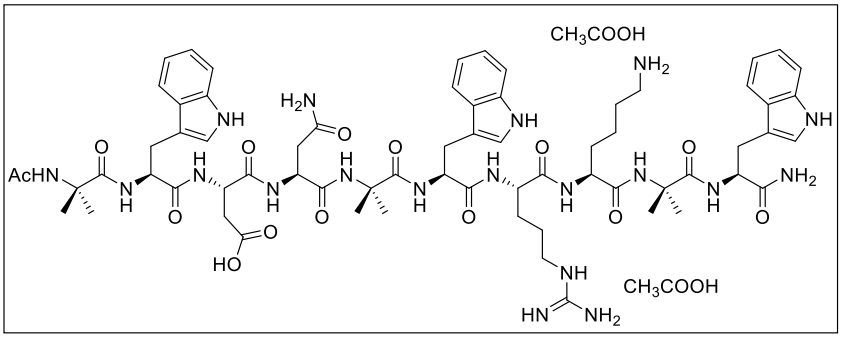

Chemical Formula: $C_{71}H_{99}N_{19}O_{18}$
Molecular Weight: 1506.69

TABLE 17. Amounts of amino acids used in the SPPS of compound **116**.

Fmoc-AA-OH	Molecular Weight (g/mol)	Amount (mg)
Fmoc-Trp(Boc)-OH	526.58	211
Fmoc-2-Aminoisobutyric acid-OH*	325.36	130
		130
Fmoc-Lys(Boc)-OH	468.54	187
Fmoc-Arg(Pbf)-OH	648.78	260
Fmoc-Trp(Boc)-OH	526.58	211
Fmoc-2-Aminoisobutyric acid-OH*	325.36	130
		130
Fmoc-Asn(Trt)-OH	596.69	239
Fmoc-Asp(O*t*Bu)-OH	411.46	165
Fmoc-Trp(Boc)-OH	526.58	211
Fmoc-2-Aminoisobutyric acid-OH*	325.36	130
		130

*A double coupling was performed.

The supported peptide (0.100 mmol) was deprotected as described in GP4 and purified by RP-HPLC (gradient: 80% H_2O + 0.1% CH_3COOH / 20% CH_3CN + 0.1% CH_3COOH for 5 min, then from 80% H_2O + 0.1% CH_3COOH / 20% CH_3CN + 0.1% CH_3COOH to 37% H_2O + 0.1% TFA / 63% CH_3CN+ 0.1% CH_3COOH in 10 min; t_R (product) = 12.6 min).

The desired peptide **116** was freeze-dried from glacial acetic acid, obtaining the corresponding acetate salt as white solid (41 mg, 30%).

MS (MALDI-TOF) *m/z* calcd. for $[C_{67}H_{92}N_{19}O_{14}]^+$: 1387.6; found: 1387.3 $[M+H]^+$ (SIN matrix).

Peptide Ac-Trp-(αMe)Asp-Asn-(αMe)Asp-Trp-Arg-Api-Thr-Trp-amide (**117**)

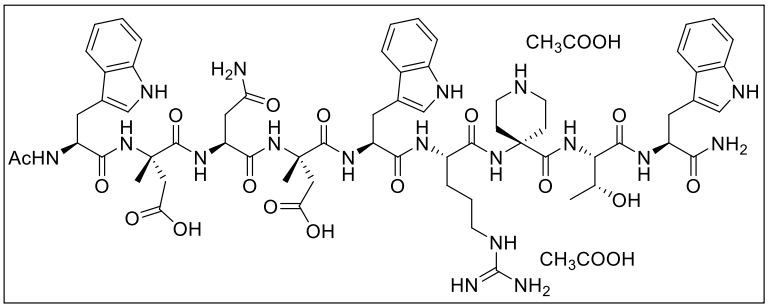

Chemical Formula: $C_{69}H_{92}N_{18}O_{20}$
Molecular Weight: 1493.60

TABLE 18. Amounts of amino acids used in the SPPS of compound **117**.

Fmoc-AA-OH	M.W. (g/mol)	Amount (mg)
Fmoc-Trp(Boc)-OH	526.58	211
Fmoc-Thr(*t*Bu)-OH	397.46	159
Fmoc-Api(Boc)-OH*	466.53	187
		187
Fmoc-Arg(Pbf)-OH*	648.78	260
		260
Fmoc-Trp(Boc)-OH	526.58	211
Fmoc-(αMe)Asp(O*t*Bu)-OH*	425.47	170
		170
Fmoc-Asn(Trt)-OH*	596.69	239
		239
Fmoc-(αMe)Asp(O*t*Bu)-OH*	425.47	170
		170
Fmoc-Trp(Boc)-OH*	526.58	211
		211

*A double coupling was performed.

The supported peptide (0.100 mmol) was deprotected as described in GP4 and purified by RP-HPLC (gradient: 80% H_2O + 0.1% CH_3COOH / 20% CH_3CN + 0.1% CH_3COOH for 5 min, then from 80% H_2O + 0.1% CH_3COOH / 20% CH_3CN + 0.1% CH_3COOH to 37% H_2O + 0.1% CH_3COOH / 63% CH_3CN+ 0.1% CH_3COOH in 10 min; t_R (product) = 13.1 min).

The desired peptide **117** was freeze-dried from glacial acetic acid, obtaining the corresponding salt as white solid (18 mg, 13%).

MS (MALDI-TOF) *m/z* calcd. for $[C_{65}H_{85}N_{18}O_{16}]^+$: 1373.6; found: 1373.8 $[M+H]^+$ (HCCA matrix).

Peptide Ac-Api-Trp-Asp-Asn-(αMe)Asp-Trp-Arg-Api-Thr-Trp-amide (**118**)

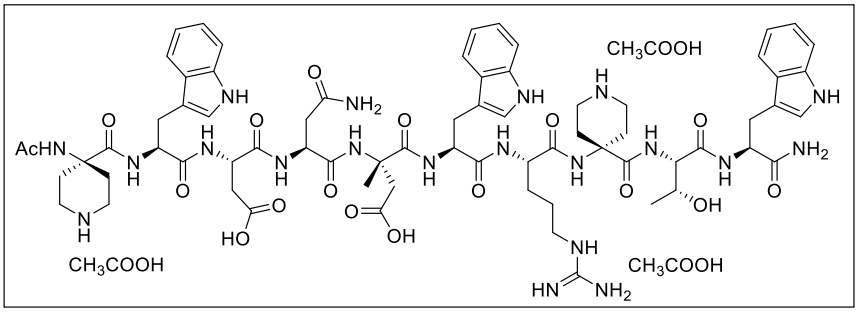

Chemical Formula: $C_{76}H_{104}N_{20}O_{23}$
Molecular Weight: 1665.79

TABLE 19. Amounts of amino acids used in the SPPS of compound **118**.

Fmoc-AA-OH	M.W. (g/mol)	Amount (mg)
Fmoc-Trp(Boc)-OH	526.58	211
Fmoc-Thr(*t*Bu)-OH	397.46	159
Fmoc-Api(Boc)-OH*	466.53	187
		187
Fmoc-Arg(Pbf)-OH	648.78	260
Fmoc-Trp(Boc)-OH	526.58	211
Fmoc-(αMe)Asp(O*t*Bu)-OH*	425.47	170
		170
Fmoc-Asn(Trt)-OH	596.69	239
Fmoc-Asp(O*t*Bu)-OH	411.46	165
Fmoc-Trp(Boc)-OH	526.58	211
Fmoc-Api(Boc)-OH*	466.53	187
		187

*A double coupling was performed.

The supported peptide (0.100 mmol) was deprotected as described in GP4 and purified by RP-HPLC (gradient: 80% H_2O + 0.1% CH_3COOH / 20% CH_3CN + 0.1% CH_3COOH for 5 min, then from 80% H_2O + 0.1% CH_3COOH / 20% CH_3CN + 0.1% CH_3COOH to 37% H_2O + 0.1% CH_3COOH / 63% CH_3CN+ 0.1% CH_3COOH in 10 min; t_R (product)= 11.7 min).

The desired peptide **118** was freeze-dried from glacial acetic acid, obtaining the corresponding acetate salt as white solid (11 mg, 7%).

MS (MALDI-TOF) *m/z* calcd. for $[C_{70}H_{93}N_{20}O_{17}]^+$: 1485.7; found: 1485.7 $[M+H]^+$ (HCCA matrix).

HPLC TRACES OF THE FINAL PRODUCTS

Cyclo[DKP5-*iso*DGR] (**39**)

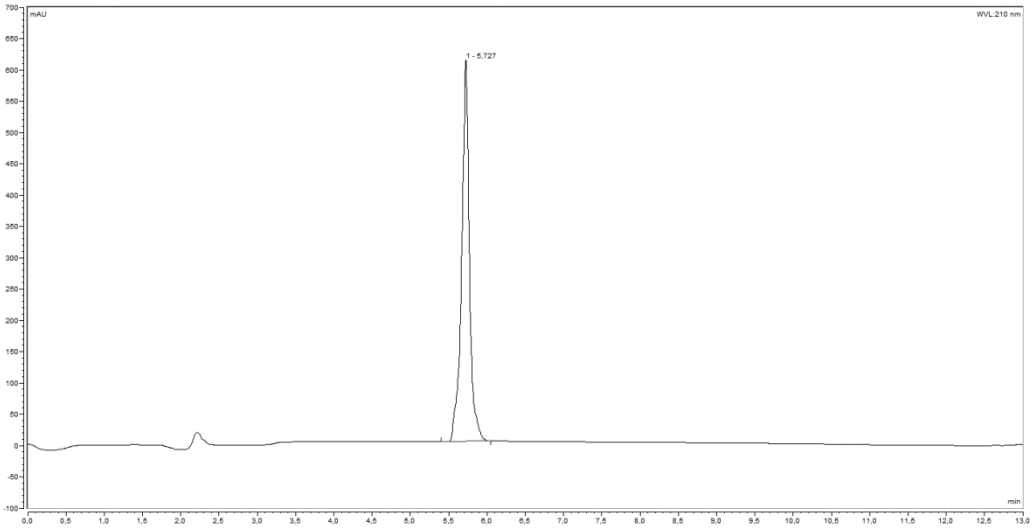

Purity: >99%

Cyclo[DKP7-*iso*DGR] (**40**)

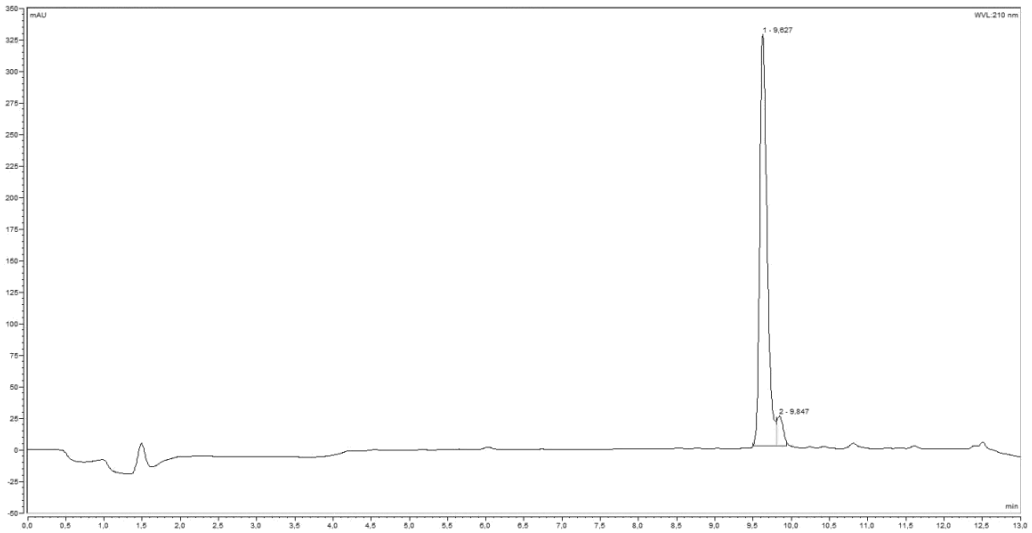

Purity: 94%

Cyclo[DKP3-*iso*DGR)]-CH_2NH_2 (**56**)

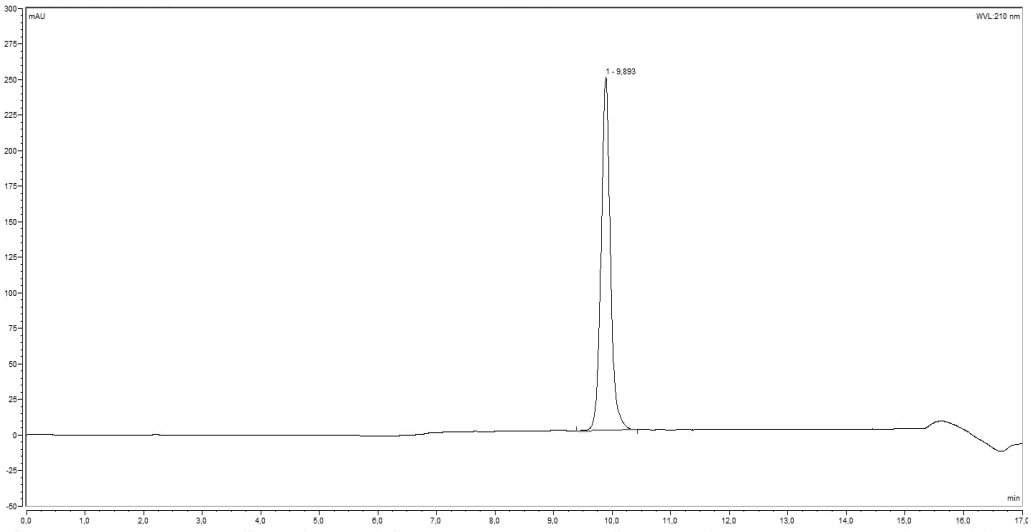

Purity: >99%

Cyclo[DKP3-*iso*DGR]-Val-Ala-PTX (**55**)

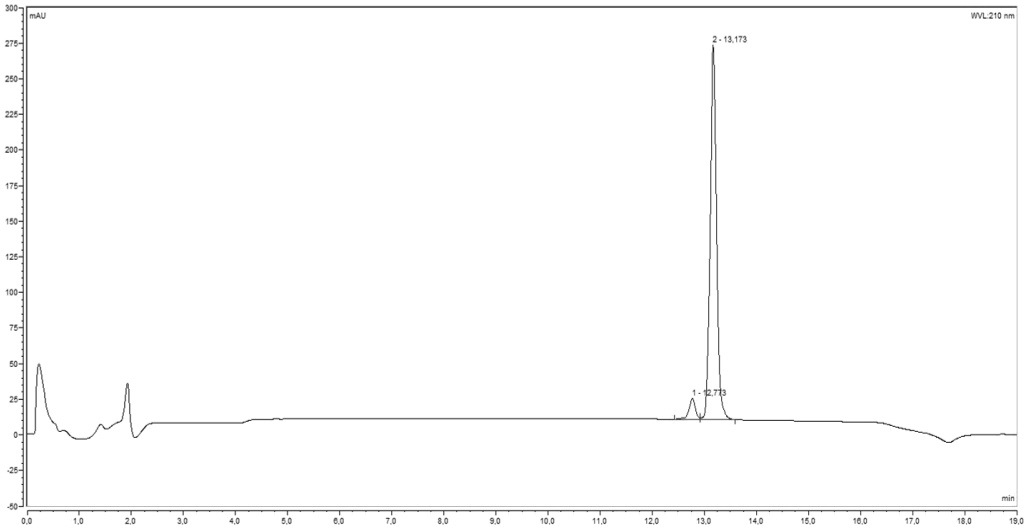

Purity: 95%

Cyclo[G*iso*dGRf] (**84**)

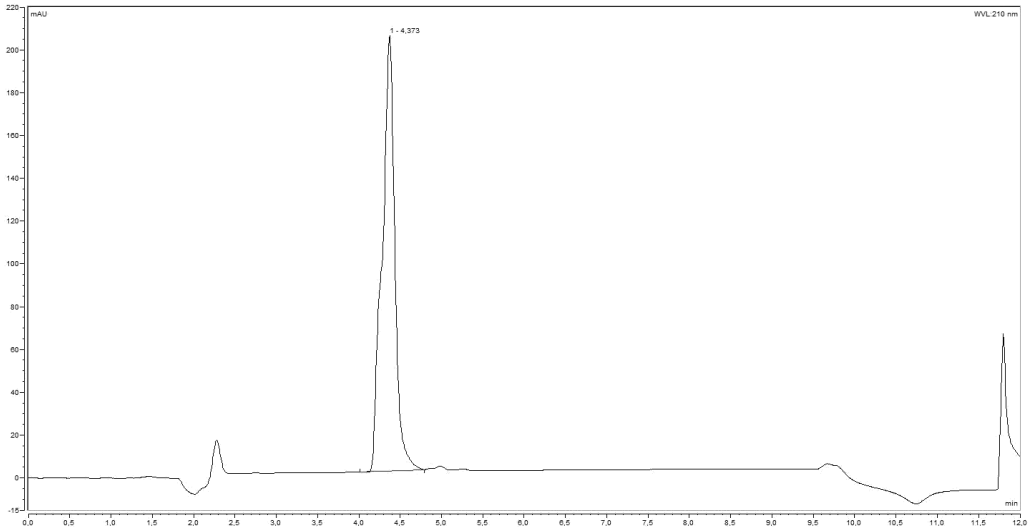

Purity: >99%

Cyclo[DKP3-RAD] isomer A (**88A**)

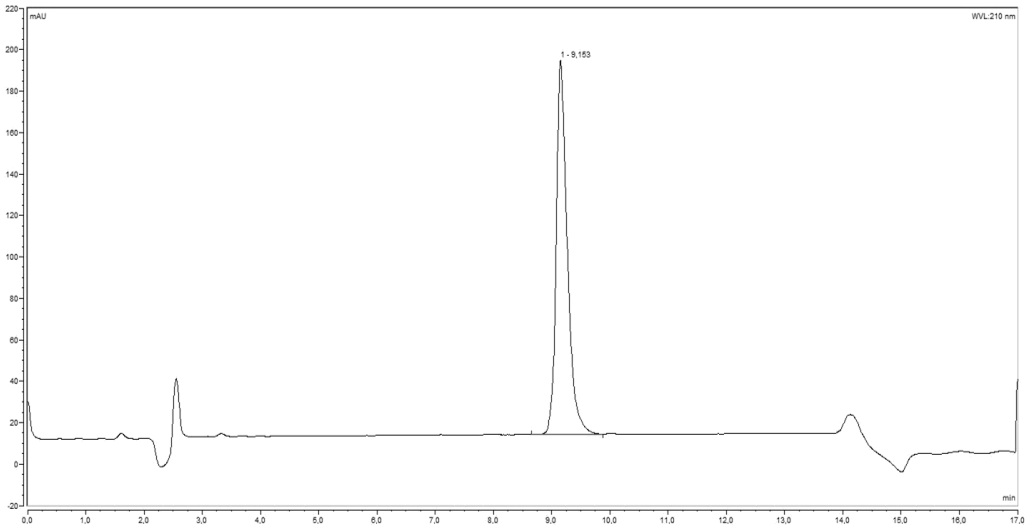

Purity: >99%

Cyclo[DKP3-RAD] isomer B (**88B**)

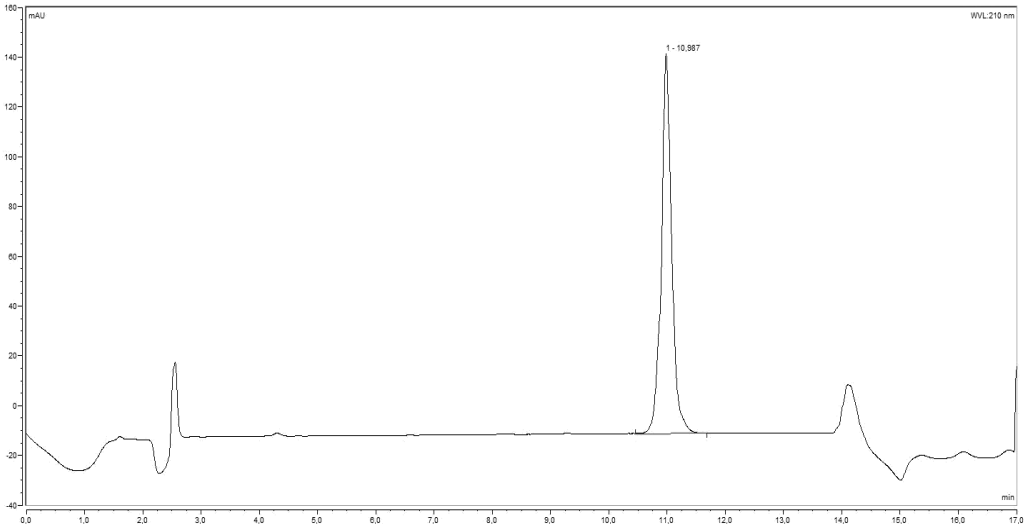

Purity: >99%

Ac-Ile-Asp-Asn-Glu-Trp-Arg-Lys-Thr-Ile-amide (**113**)

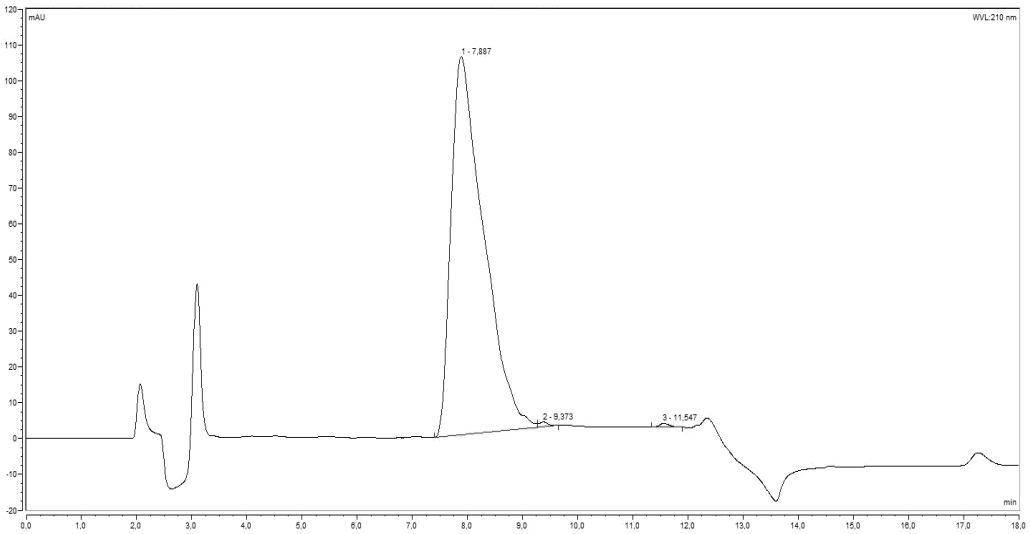

Purity: >99%

Ac-Trp-Asp-Asn-Glu-Trp-Arg-Lys-Thr-Trp-amide (**114**)

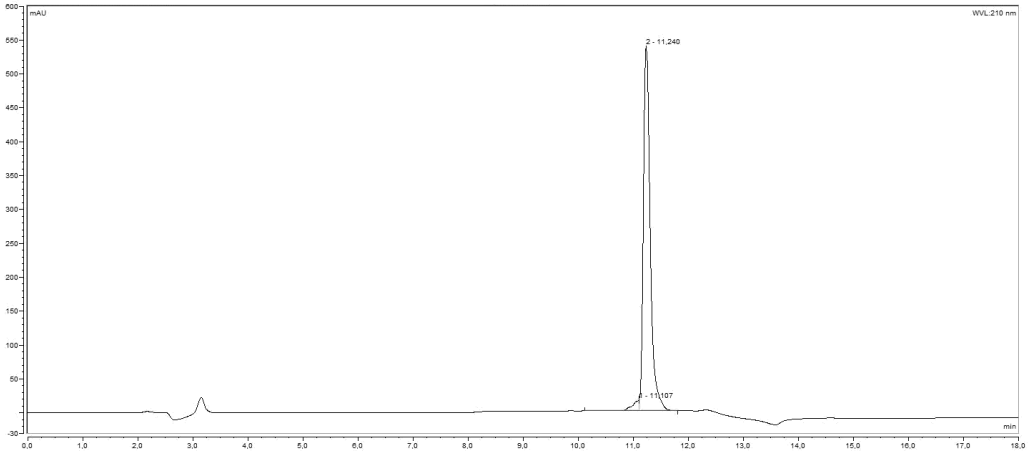

Purity: 97%

Ac-Aib-Ile-Asp-Asn-Aib-Trp-Arg-Lys-Aib-Ile-amide (**115**)

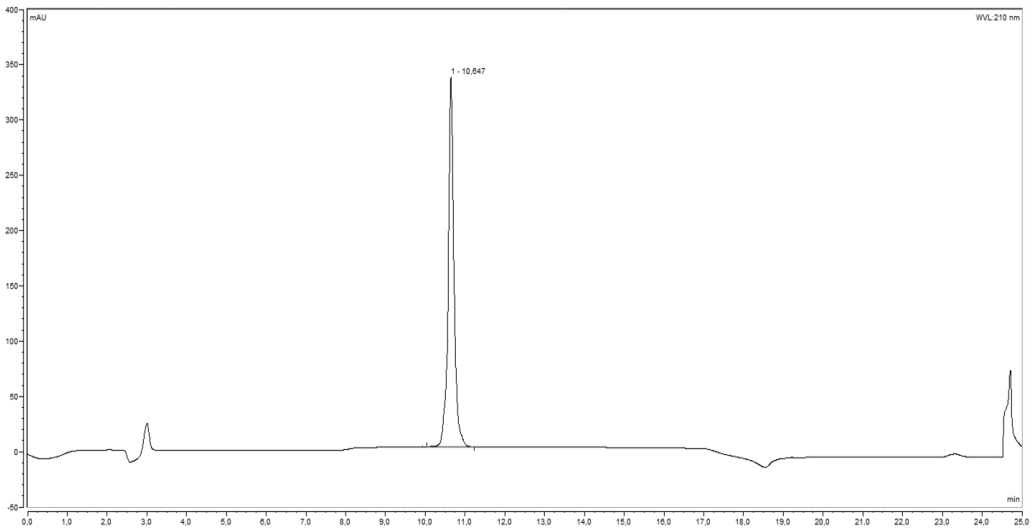

Purity: >99%

Ac-Aib-Trp-Asp-Asn-Aib-Trp-Arg-Lys-Aib-Trp-amide (**116**)

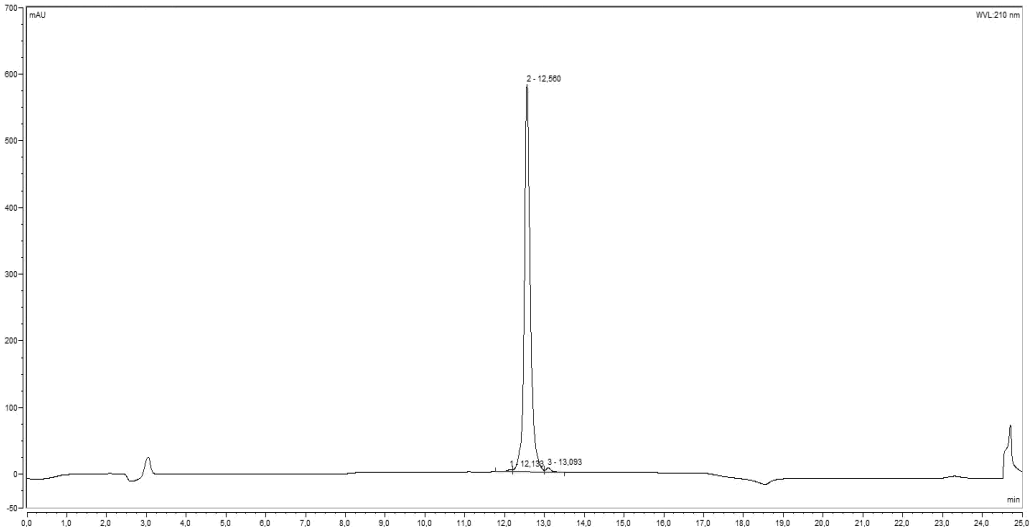

Purity: 99%

Ac-Trp-(αMe)Asp-Asn-(αMe)Asp-Trp-Arg-Api-Thr-Trp-amide (**117**)

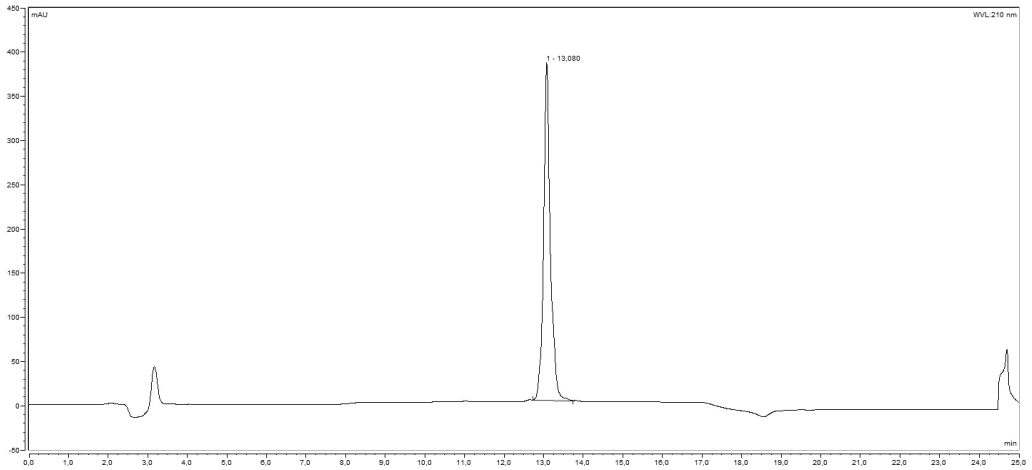

Purity: >99%

Ac-Api-Trp-Asp-Asn-(αMe)Asp-Trp-Arg-Api-Thr-Trp-amide (**118**)

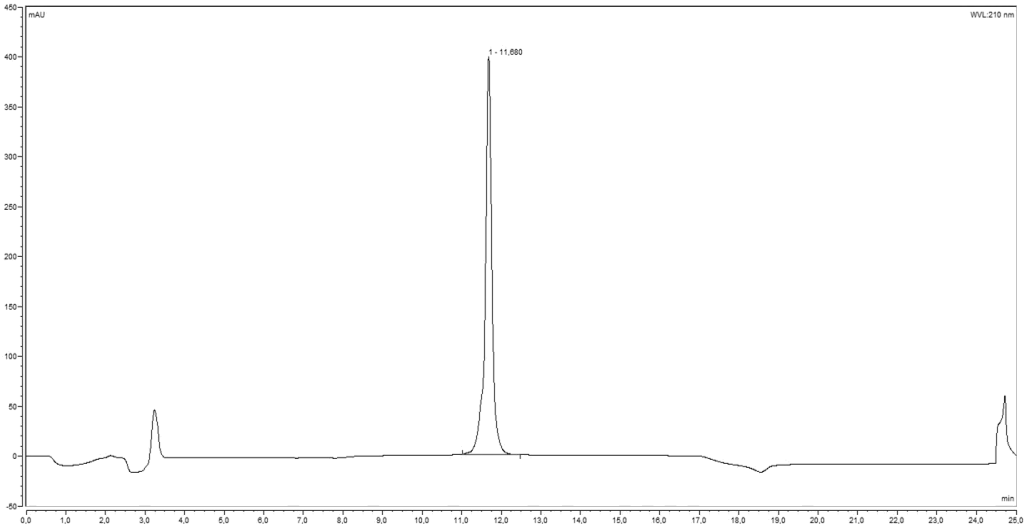

Purity: >99%

APPENDIX OF NMR SPECTRA

SYNTHESIS OF SCAFFOLDS N_3-DKP5-COOH **41** AND N_3-DKP5-COOH **42**

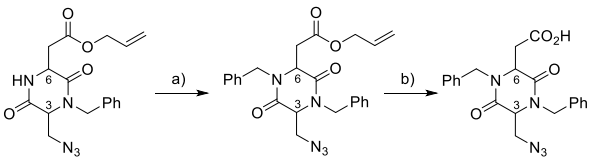

Reagents and conditions: a) KHMDS, BnBr, THF/DMF, -70 to -40 °C, 5 h, 66%; b) [$Pd(PPh_3)_4$], *N*-methylaniline, CH_2Cl_2, 0 °C, 1 h, 70%.

SYNTHESIS OF *CYCLO*[DKP5-*ISO*DGR] **39** AND *CYCLO*[DKP7-*ISO*DGR] **40**

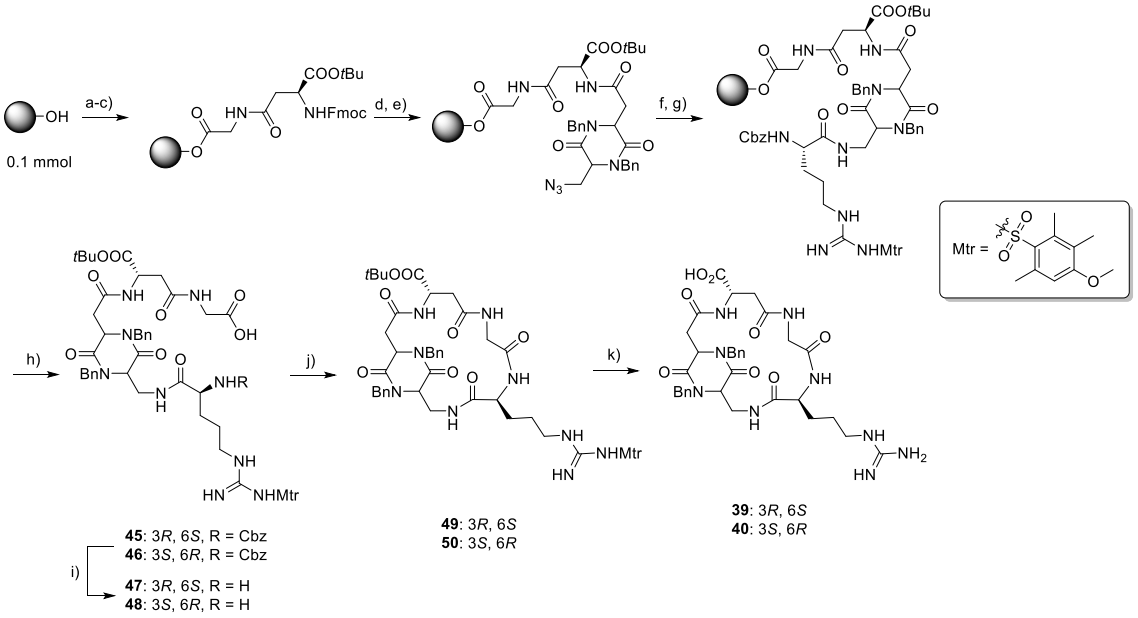

Reagents and conditions: a) Fmoc-Gly-OH, DIC, DMAP (cat.), DMF; b) 2% piperidine and 2% DBU in DMF; c) Fmoc-Asp(OH)-O*t*Bu, DIC, HOAt, DMF; d) 2% piperidine and 2% DBU in DMF; e) **41**-**42**, DIC, HOAt, DMF; f) PMe_3, dioxane/water 4:1, 20 min × 3 times; g) Cbz-Arg(Mtr)-OH, DIC, HOAt, DMF; h) 1% TFA in CH_2Cl_2, r.t., 5 min × 10 times, 71-81%; i) H_2, 10% Pd/C, THF/H_2O 1:1, 98%-quant.; j) HATU, HOAt, *i*Pr_2NEt, DMF (1.4 mM), 32%; k) TFA/thioanisole/EDT/anisole 90:5:3:2, 25-37%.

Compound **53** and compound **54**

^{1}H-NMR (400 MHz, $CDCl_3$)

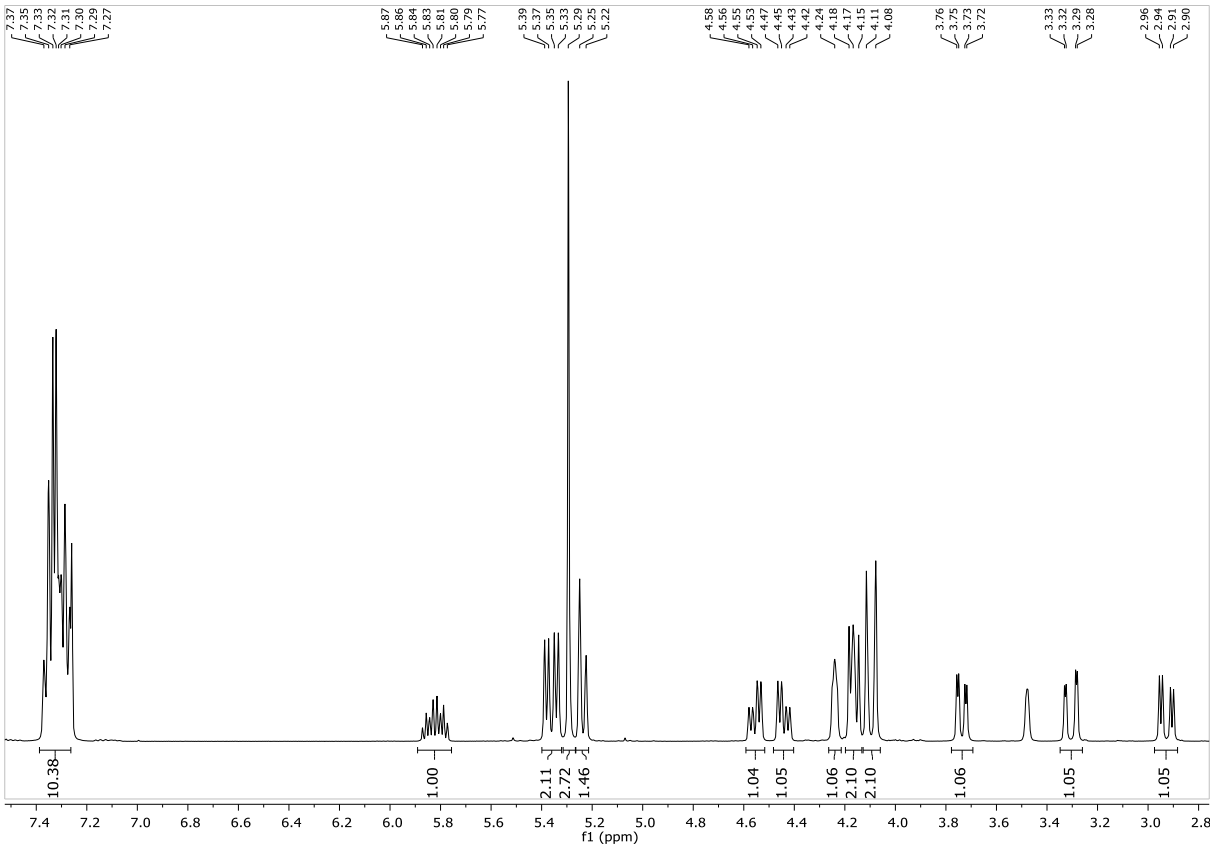

^{13}C-NMR (101 MHz, $CDCl_3$)

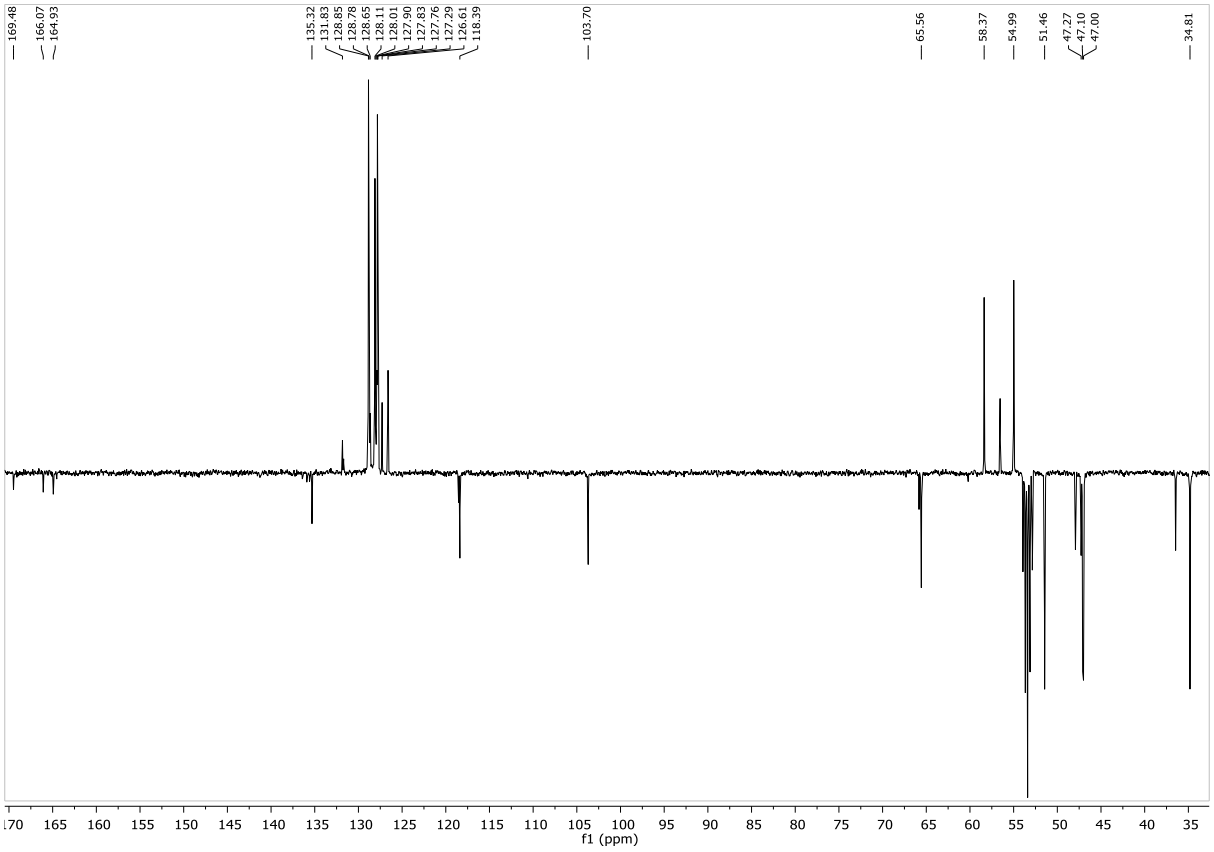

Compound **41** and compound **42**

^{1}H-NMR (400 MHz, $CDCl_3$)

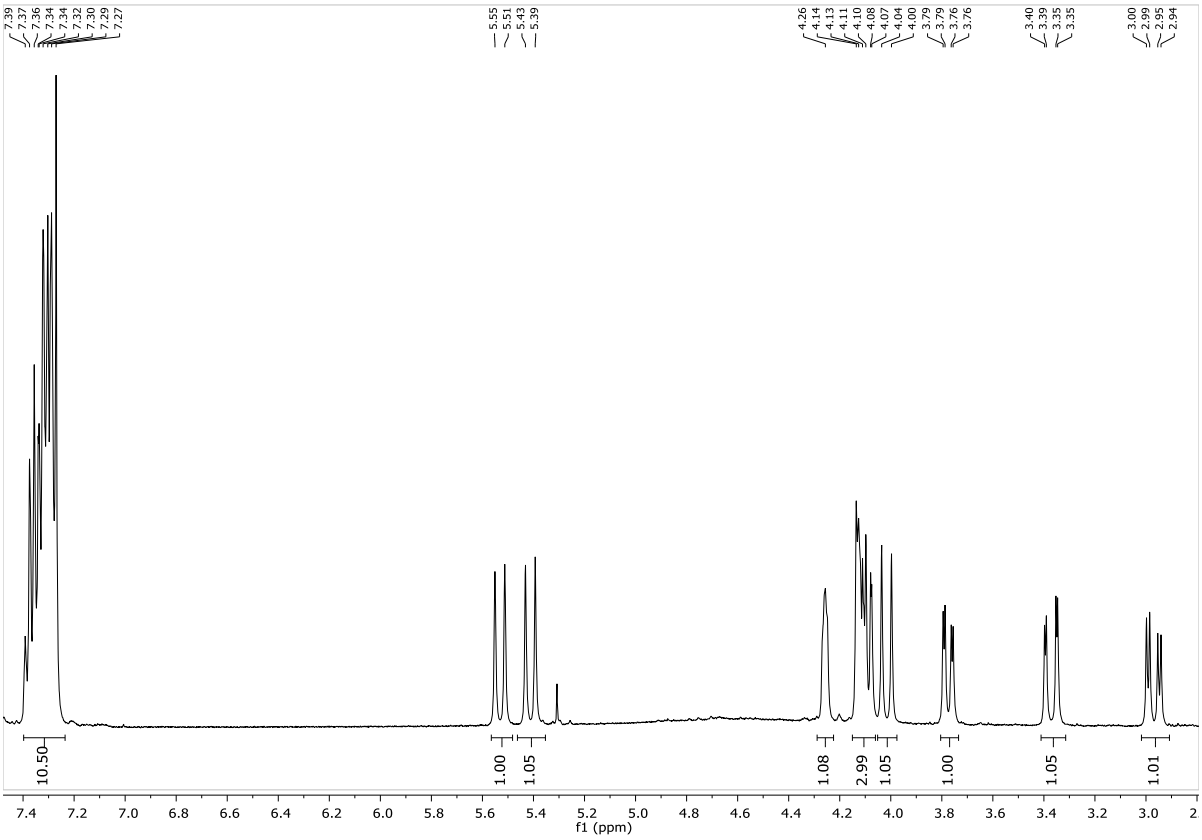

^{13}C-NMR (101 MHz, $CDCl_3$)

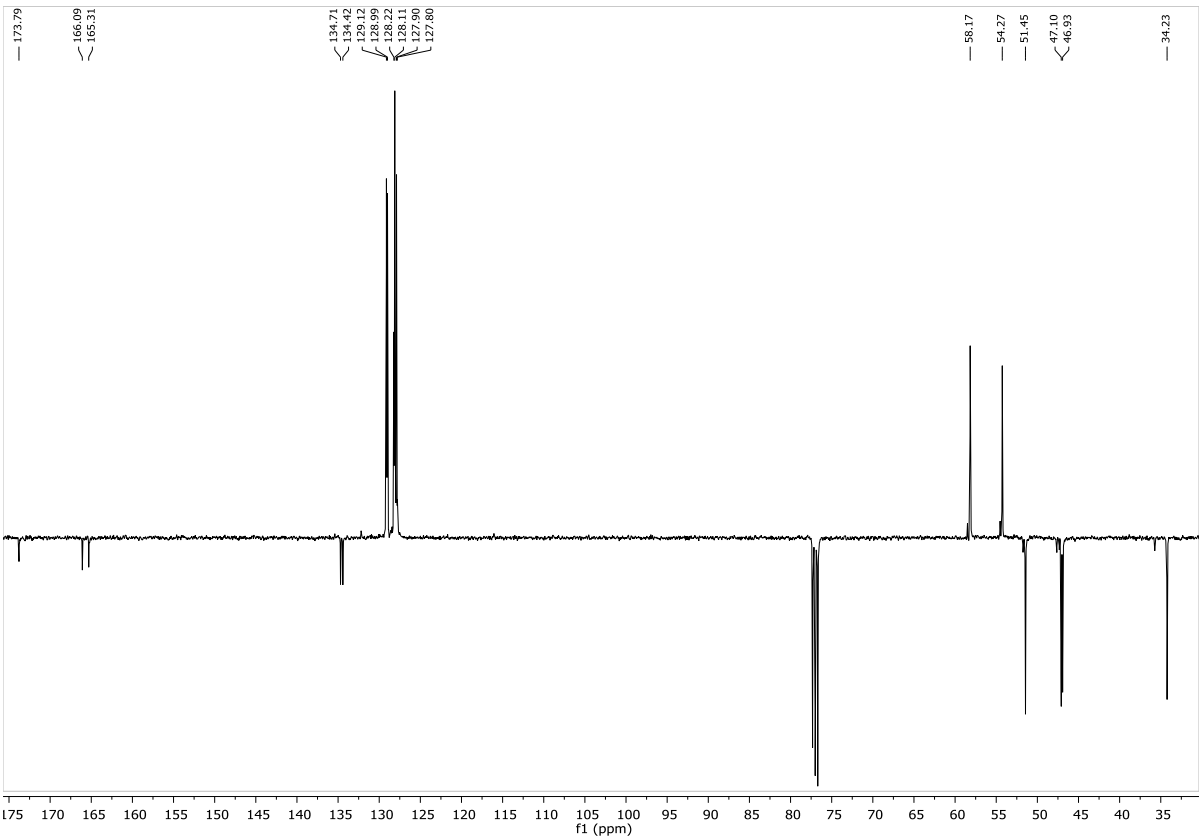

Compound **45**

^{1}H-NMR (400 MHz, CD_3OD)

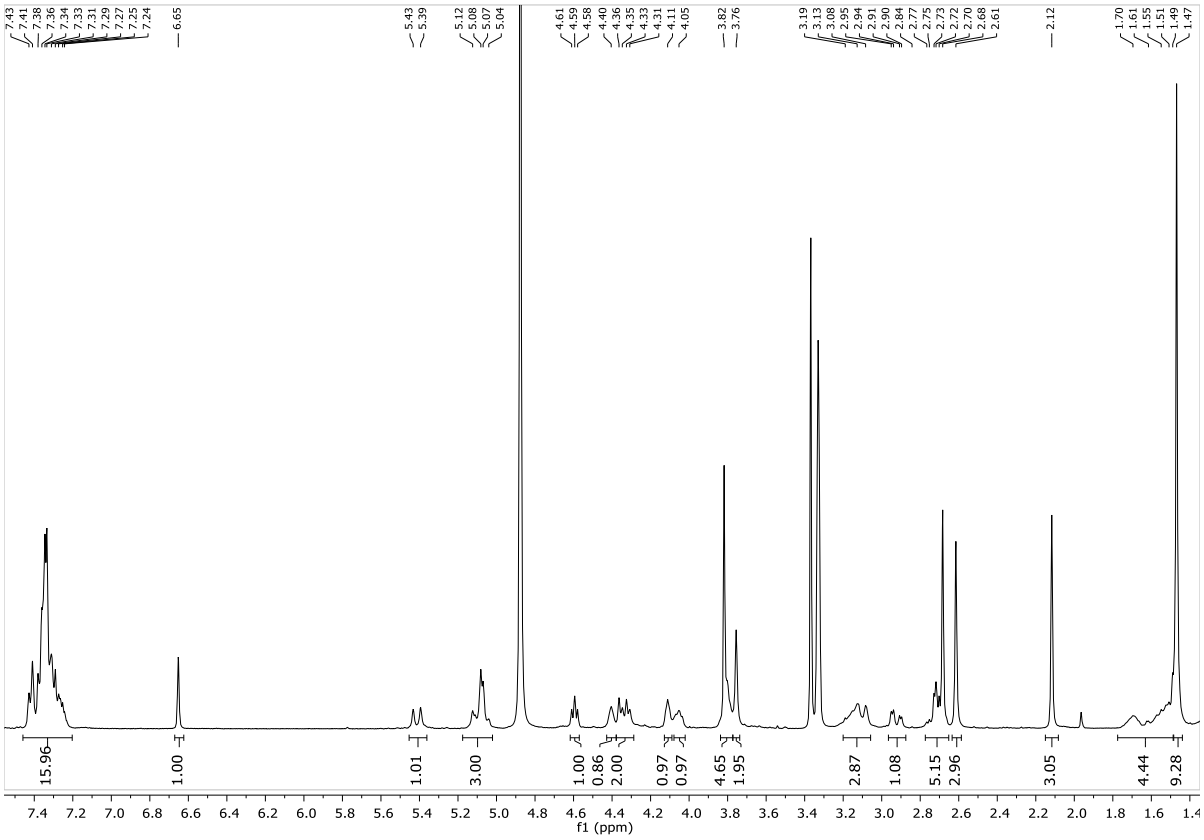

^{13}C-NMR (101 MHz, CD_3OD)

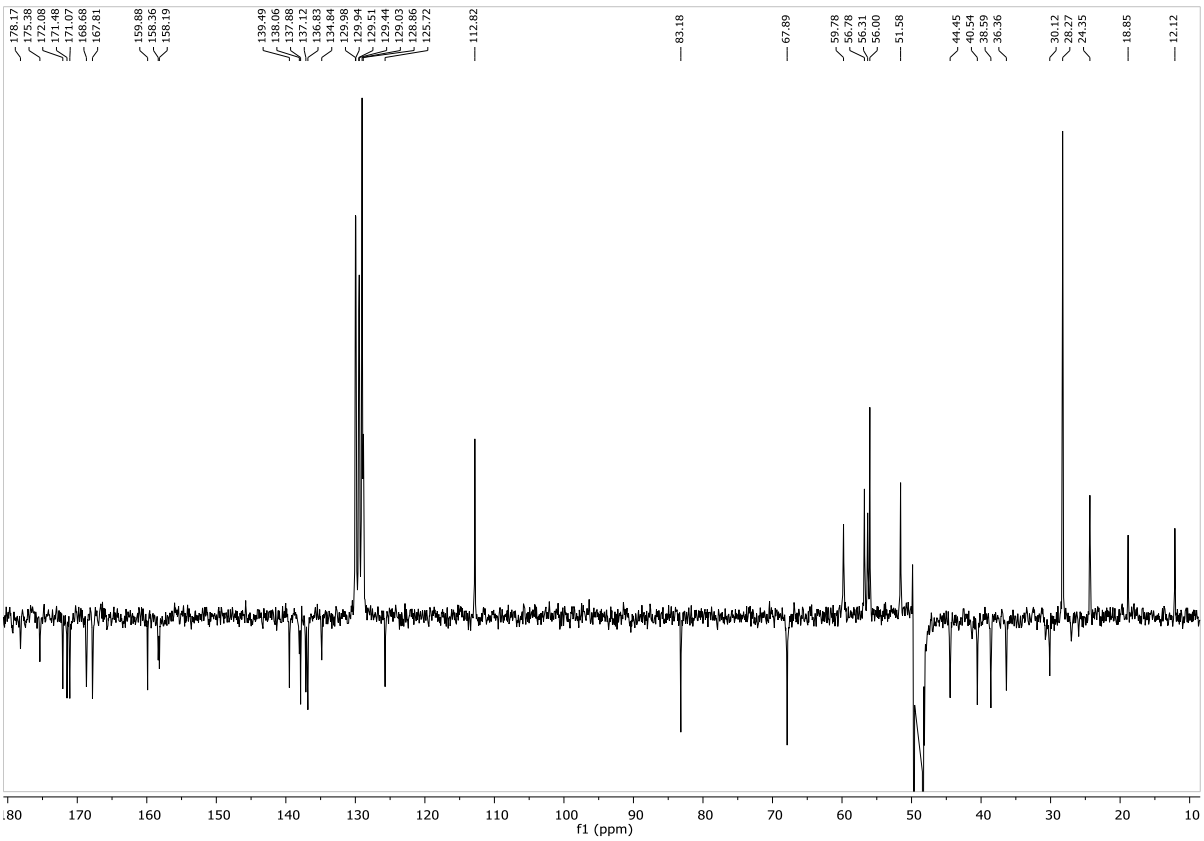

Compound **46**

^{1}H-NMR (400 MHz, CD_3OD)

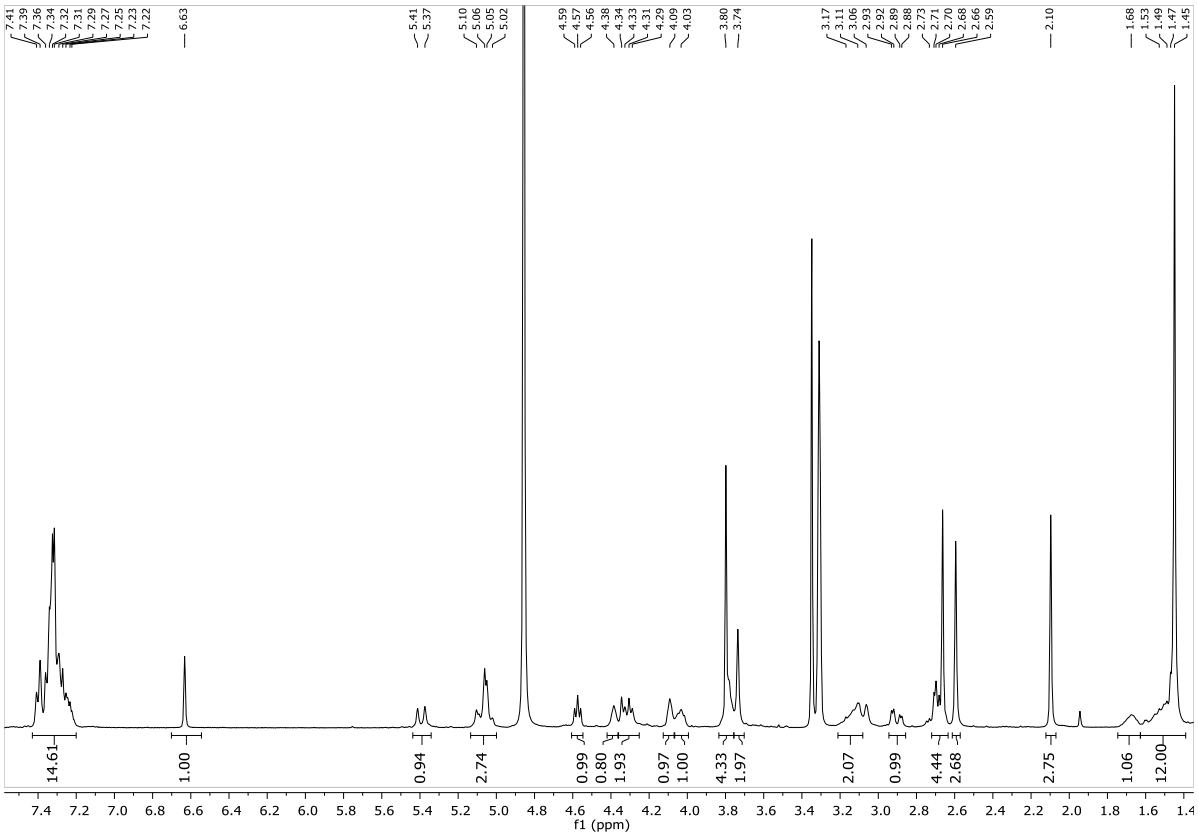

^{13}C-NMR (101 MHz, CD_3OD)

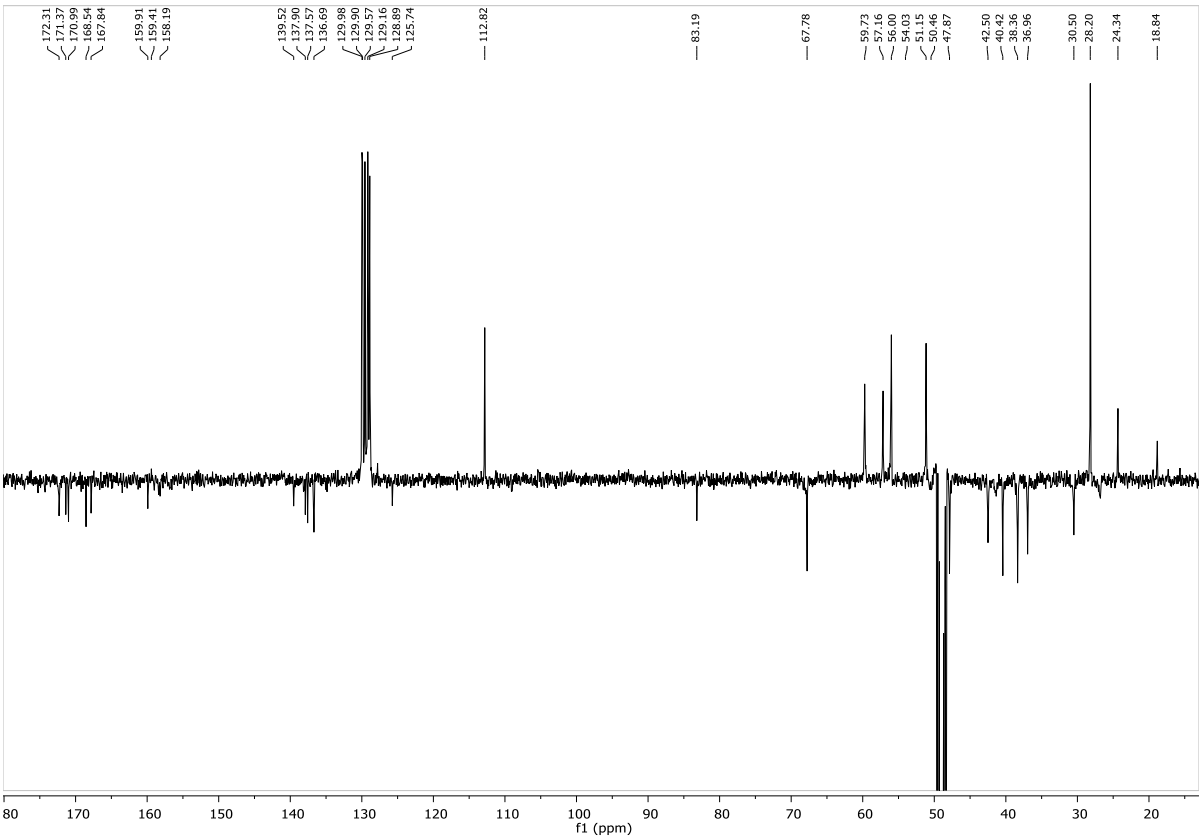

Compound **47**

^{1}H-NMR (400 MHz, CD_3OD)

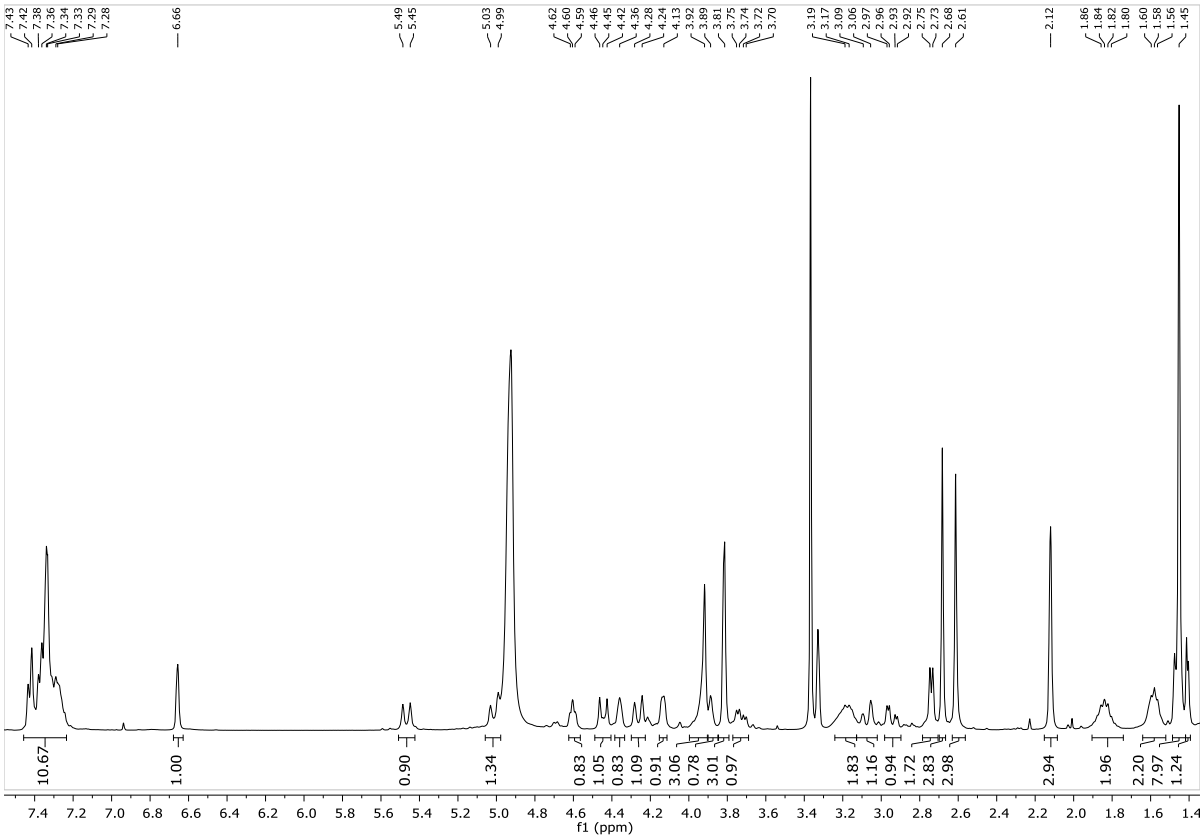

^{13}C-NMR (101 MHz, CD_3OD)

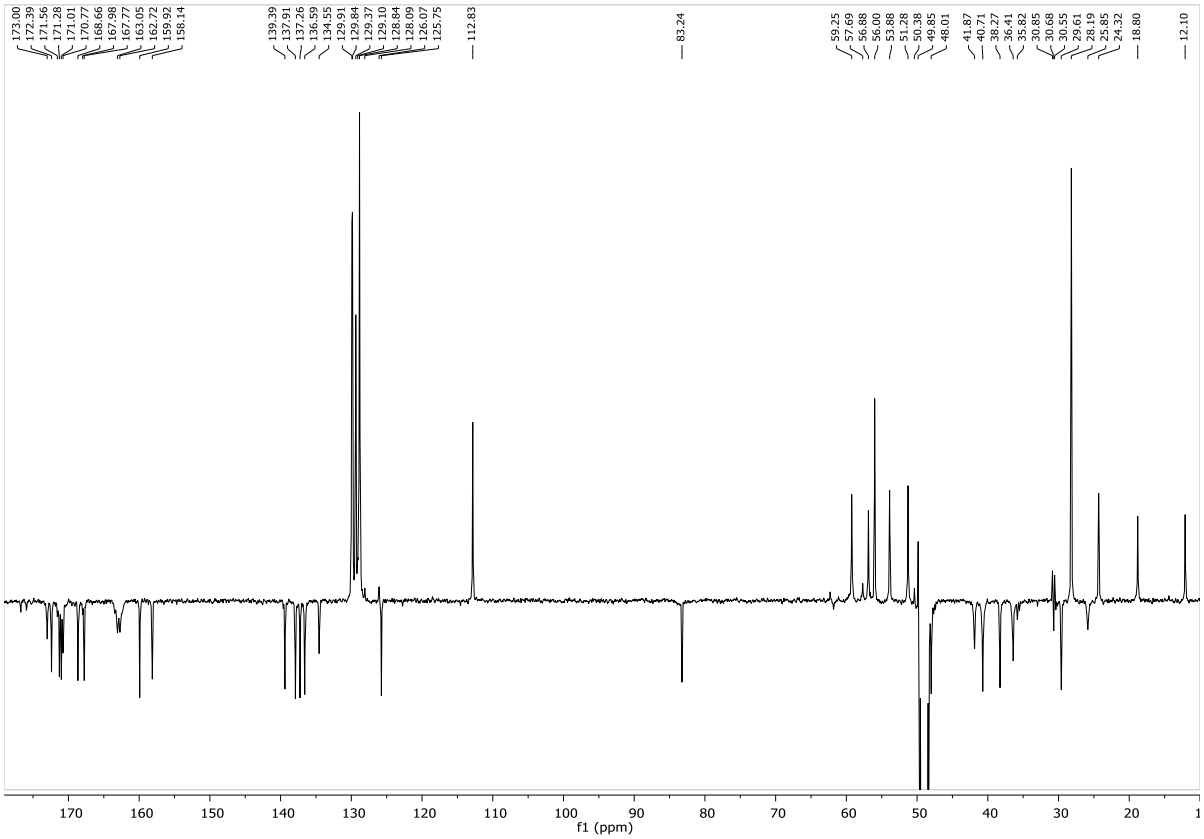

Compound **49**

^{1}H-NMR (400 MHz, CD_3OD)

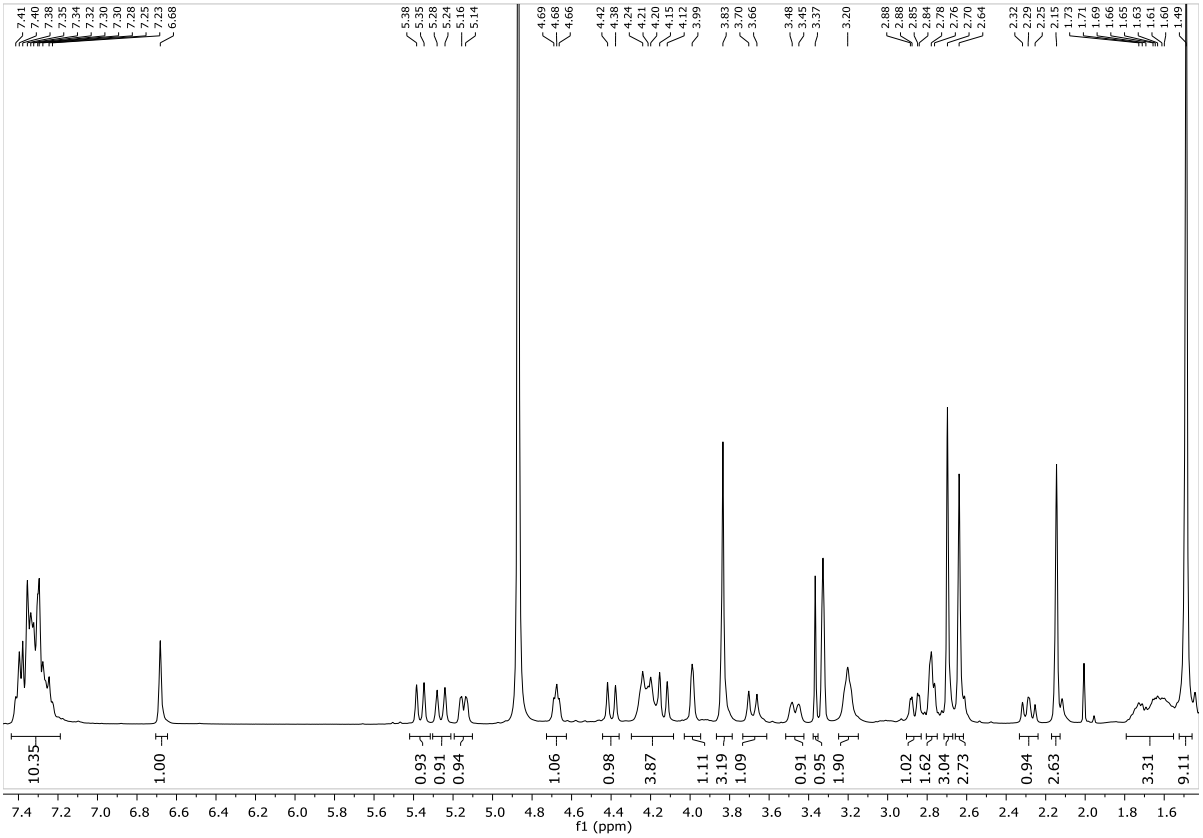

^{13}C-NMR (101 MHz, CD_3OD)

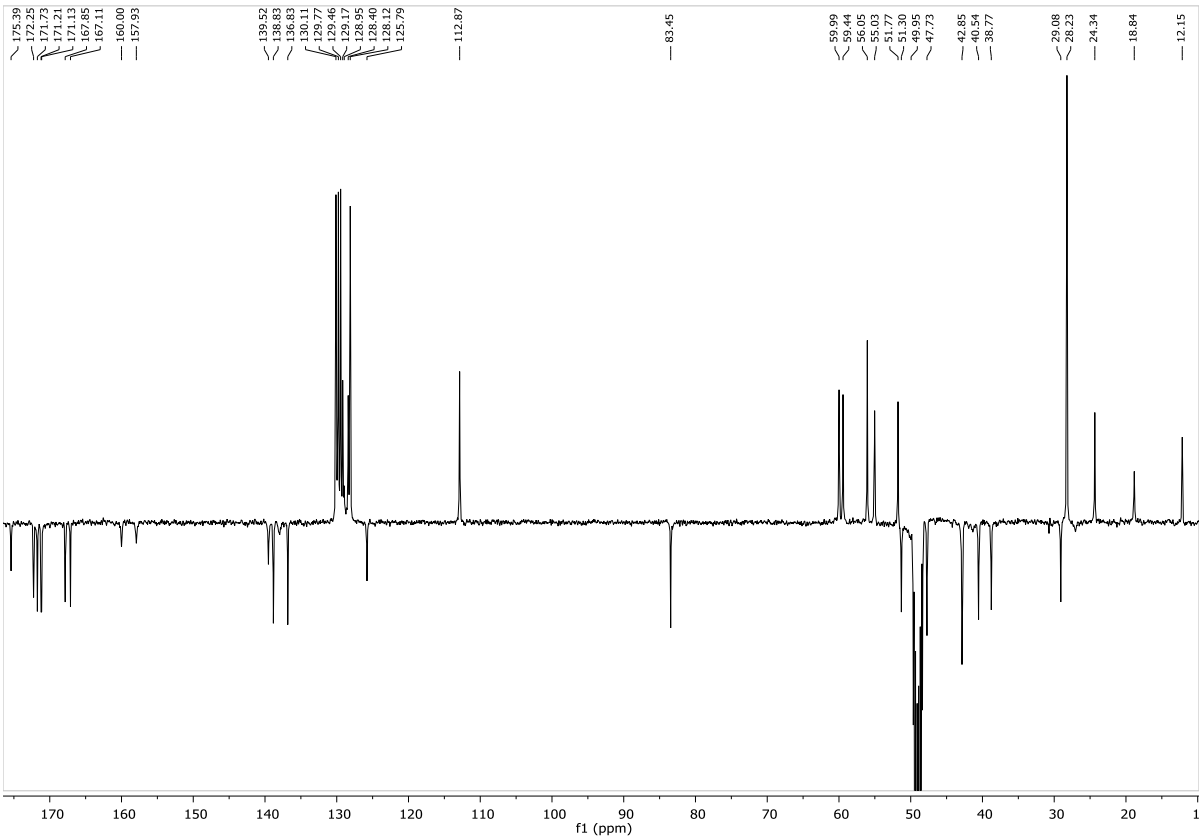

Compound **39**

^{1}H-NMR (400 MHz, D_2O)

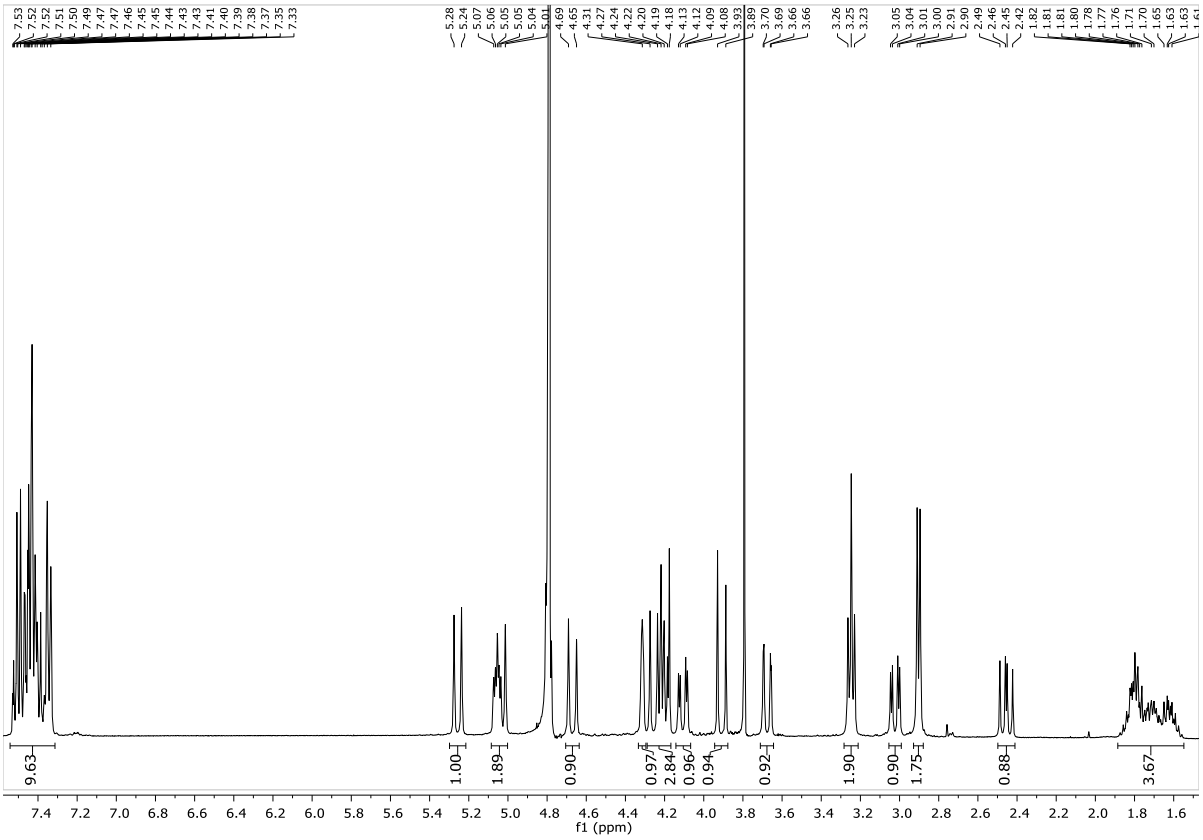

^{13}C-NMR (101 MHz, D_2O)

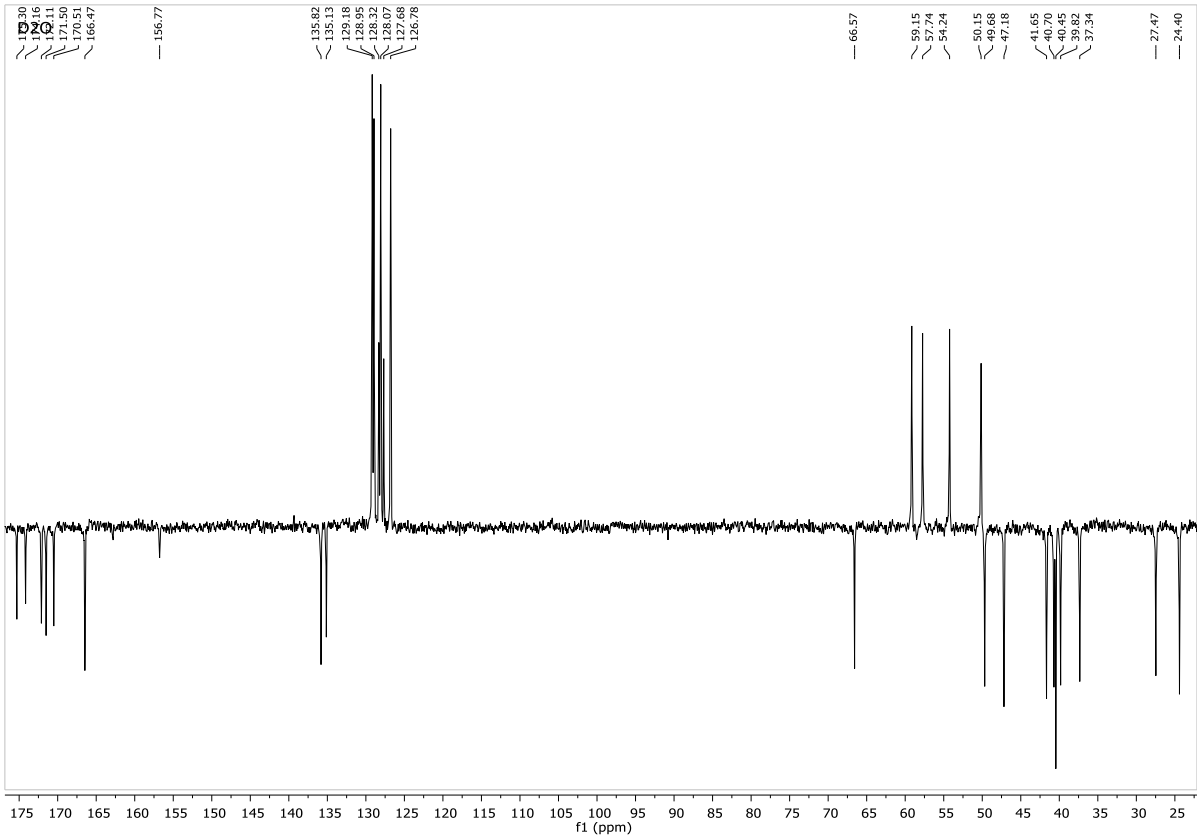

Compound **40**

^{1}H-NMR (400 MHz, D_2O)

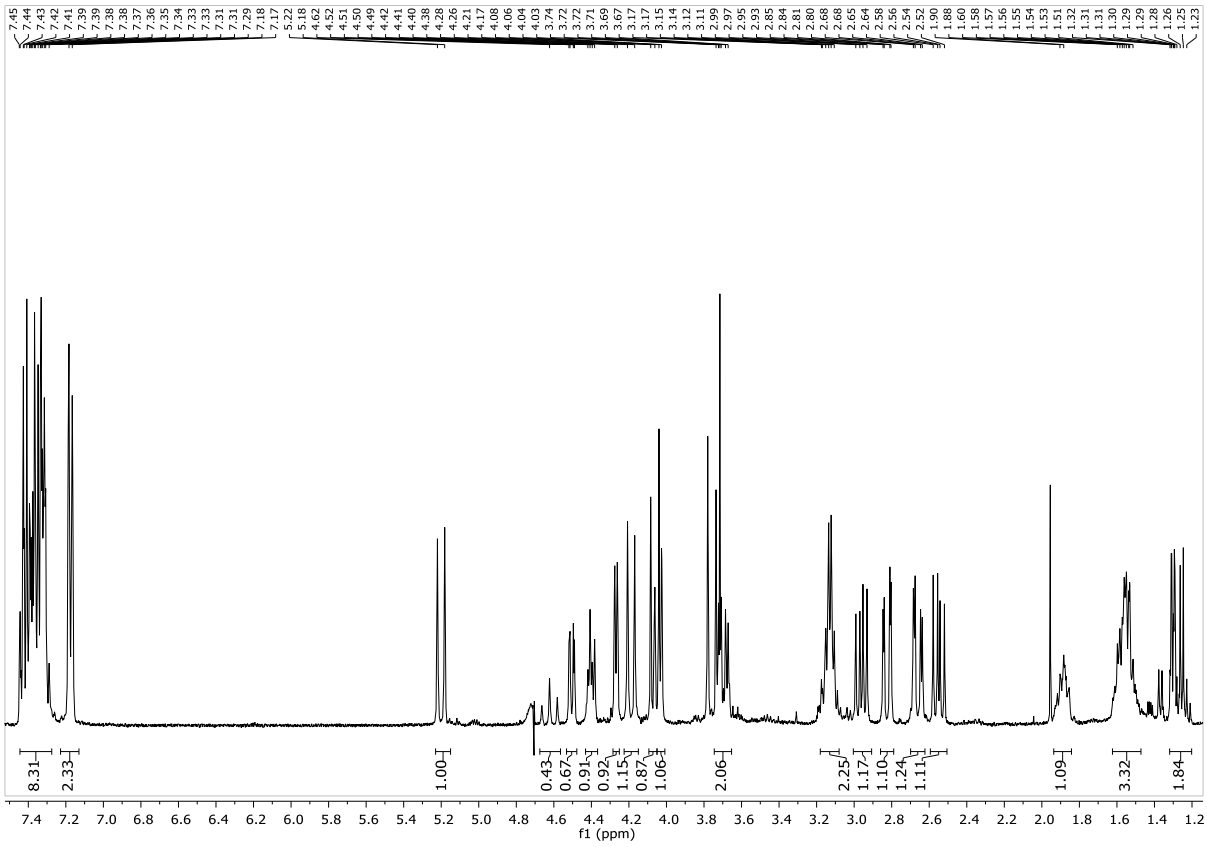

^{13}C-NMR (101 MHz, D_2O)

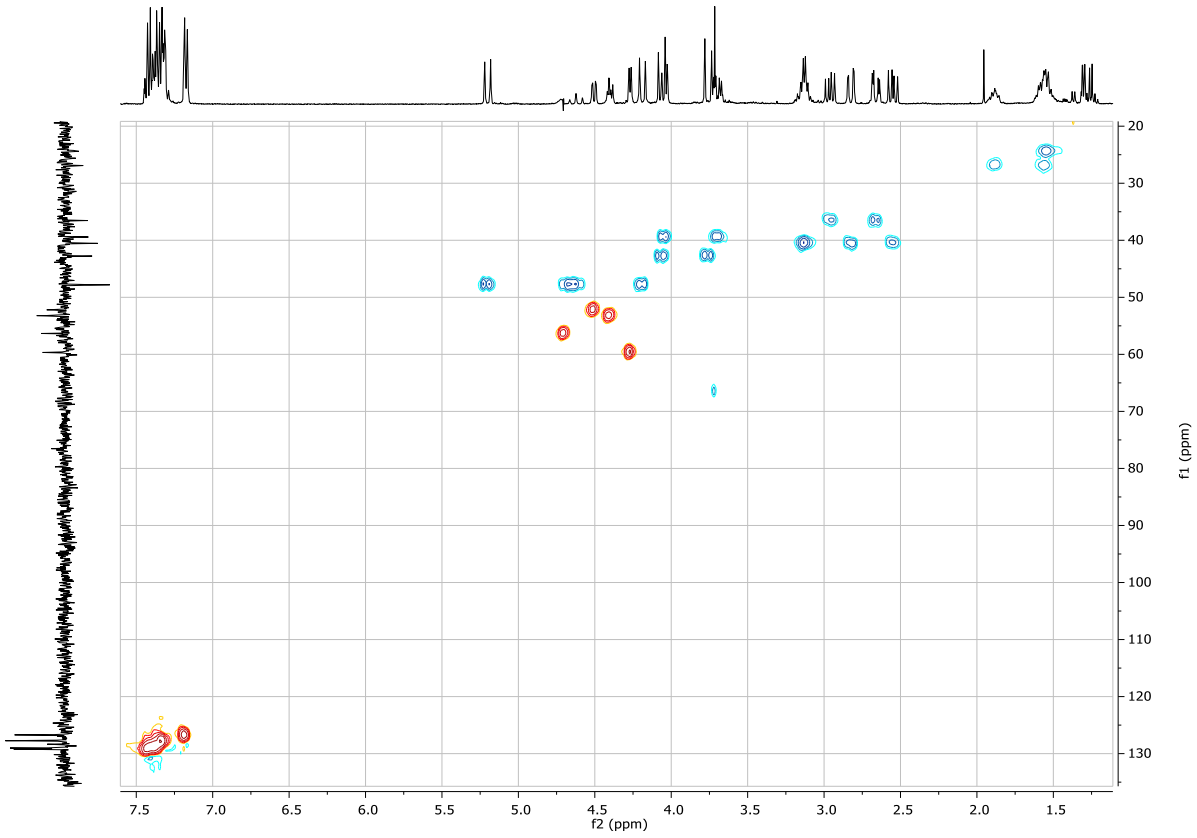

SYNTHESIS OF *CYCLO*[DKP3-*ISO*DGR]-CH_2NH_2 PEPTIDOMIMETIC **56**

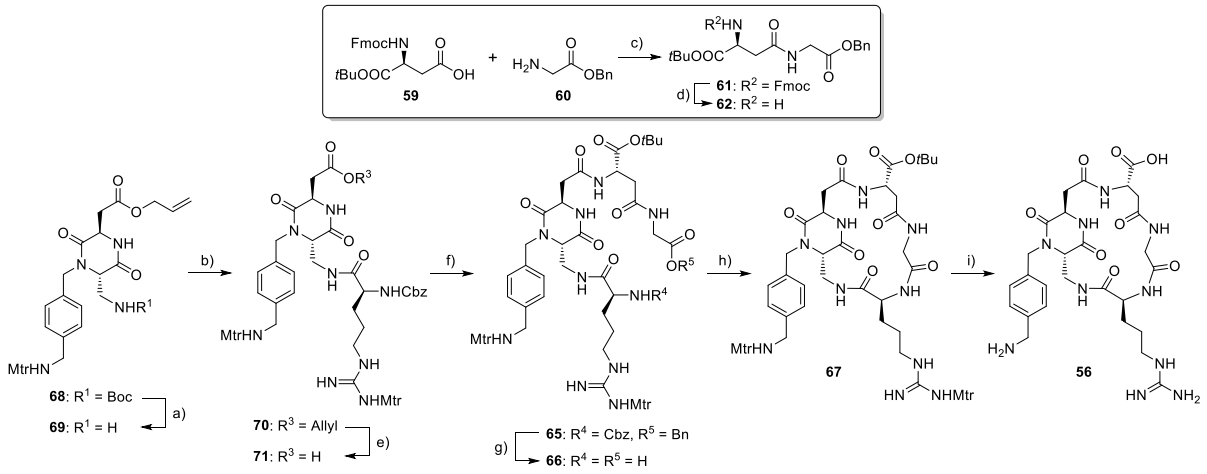

Reagents and conditions: a) TFA, CH_2Cl_2, r.t., 2 h; b) Cbz-Arg(Mtr)-OH, HATU, HOAt, *i*Pr_2NEt, DMF, 0 °C to r.t., overnight, 94% over 2 steps; c) HATU, HOAt, *i*Pr_2NEt, DMF, 0 °C to r.t., overnight, 86%; d) piperidine, DMF, 2 h, r.t., 67%; e) [$Pd(PPh_3)_4$], *N*-Methylaniline, CH_2Cl_2, 0 °C, 1 h, 88%; f) **62**, HATU, HOAt, *i*Pr_2NEt, DMF, 0 °C to r.t., overnight, 95%; g) H_2, 10% Pd/C, THF/H_2O 1:1, overnight, r.t., 95%; h) HATU, HOAt, *i*Pr_2NEt, DMF/CH_2Cl_2 1:1 (1.4 mM), 0 °C to r.t., overnight, 79%; i) TFA/TMSBr/thioanisole/EDT/phenol 70:14:10:5:1, 2 h, r.t., 47%.

SYNTHESIS OF *CYCLO*[DKP3-*ISO*DGR]-VAL-ALA-PTX CONJUGATE **55**

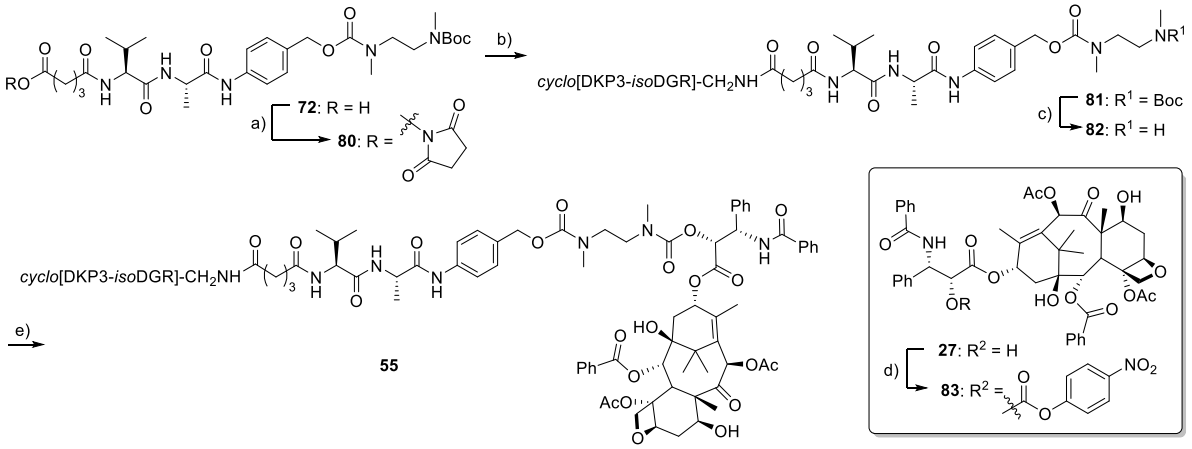

Reagents and conditions: a) NHS, EDC·HCl, DMF, 0 °C to r.t., overnight; b) **56** PBS/CH_3CN, pH 7.5, 0 °C to r.t., overnight; c) TFA, CH_2Cl_2, r.t., 1 h, 55% over three steps; d) 4-nitrophenylchloroformate, pyridine, CH_2Cl_2, -50 °C to -20 °C, 4 h, 84% based on recovered starting material; e) **83**, *i*Pr_2NEt, DMF, 0 °C to r.t., overnight, 52%.

Compound **61**

^{1}H-NMR (400 MHz, $CDCl_3$)

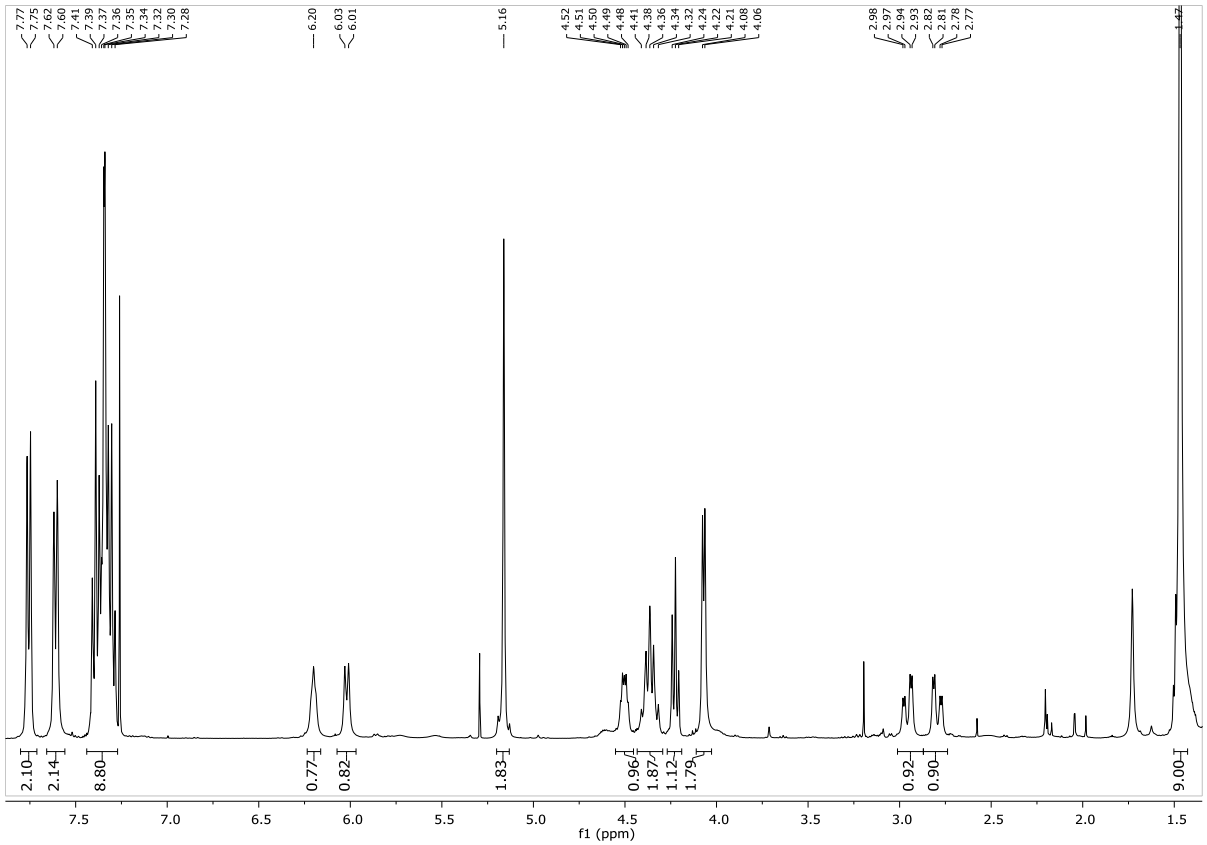

^{13}C-NMR (101 MHz, $CDCl_3$)

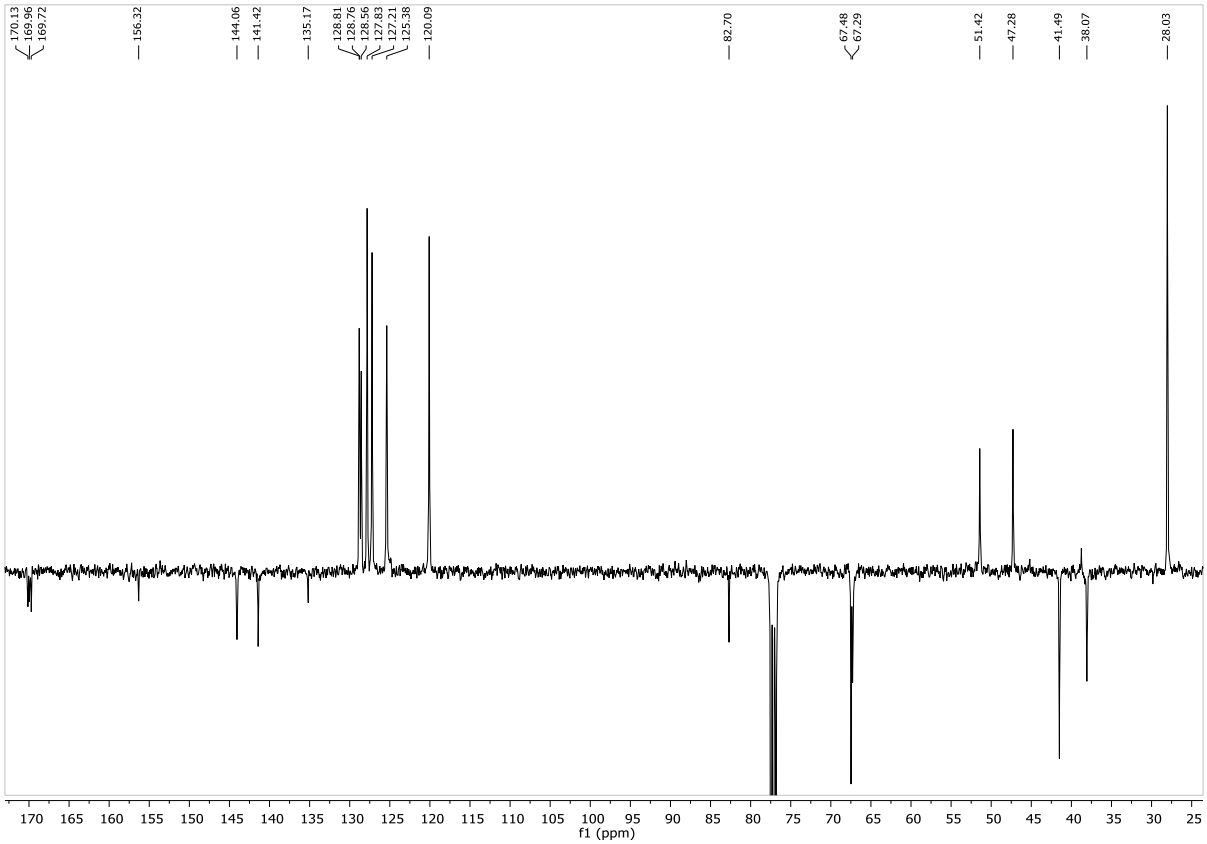

Compound **62**

^{1}H-NMR (400 MHz, $CDCl_3$)

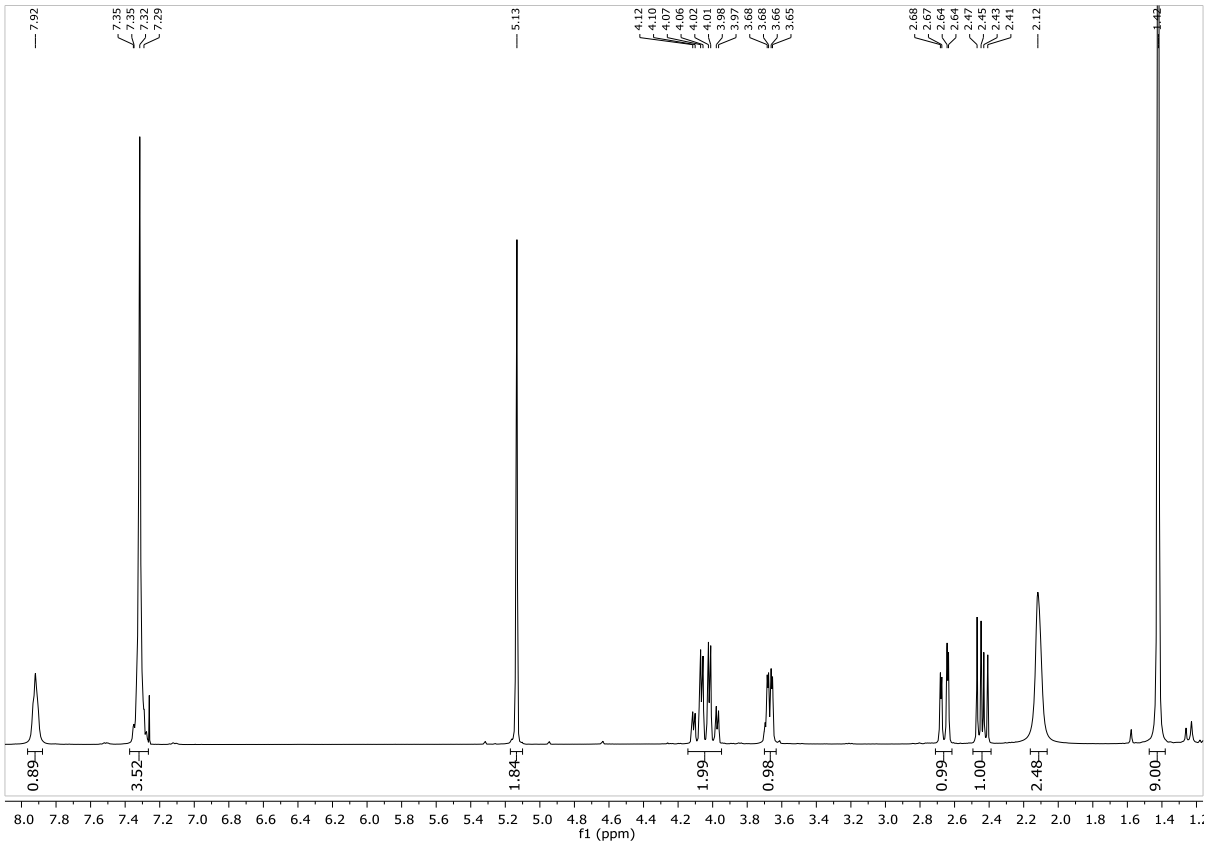

Compound **68**

^{1}H-NMR (400 MHz, $CDCl_3$)

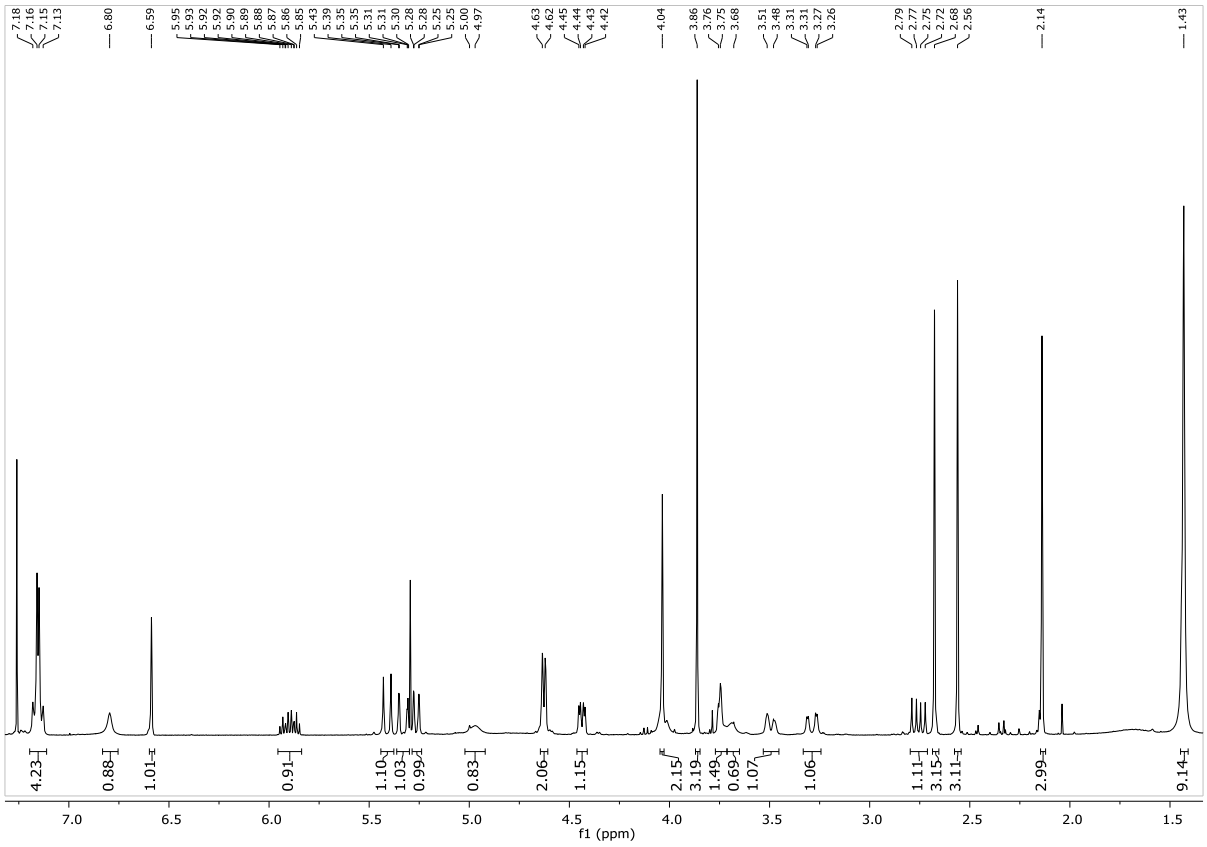

Compound **70**

^{1}H-NMR (400 MHz, CD_3OD)

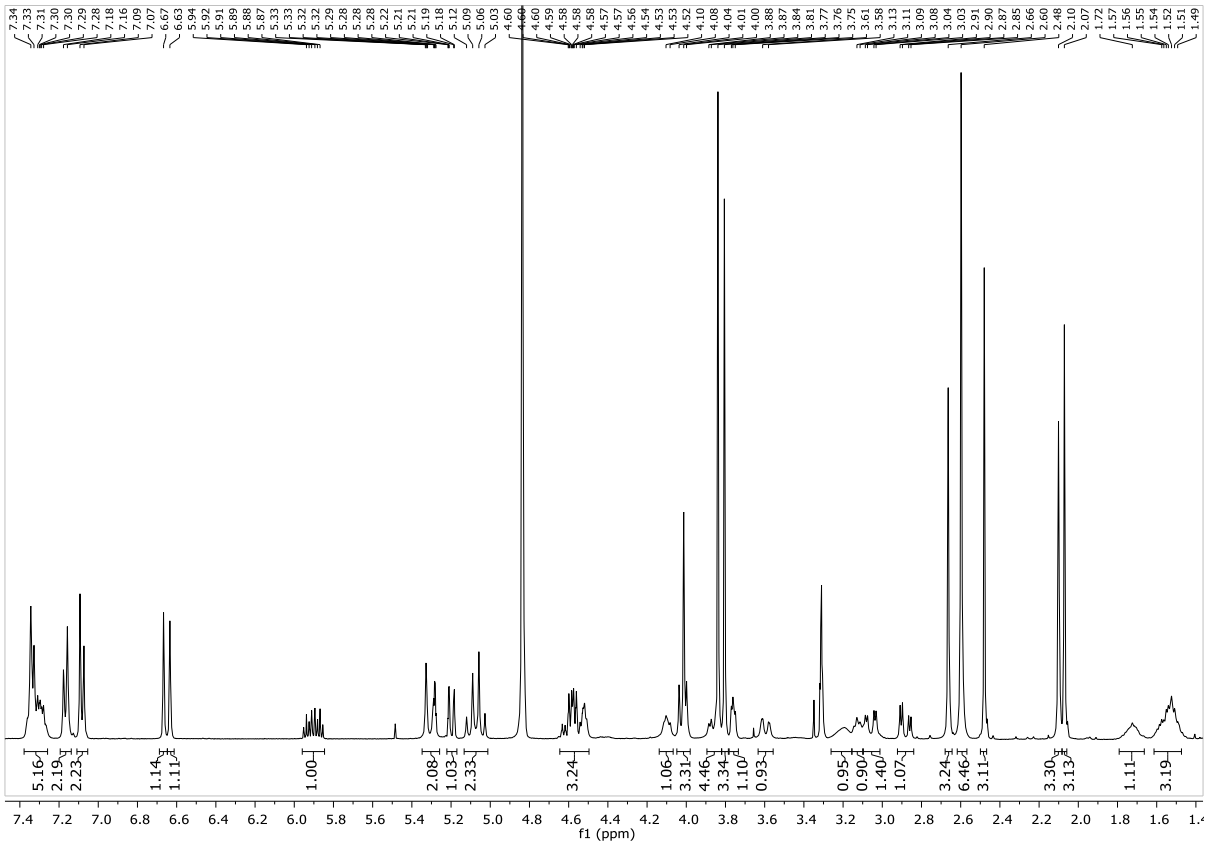

^{13}C-NMR (101 MHz, CD_3OD)

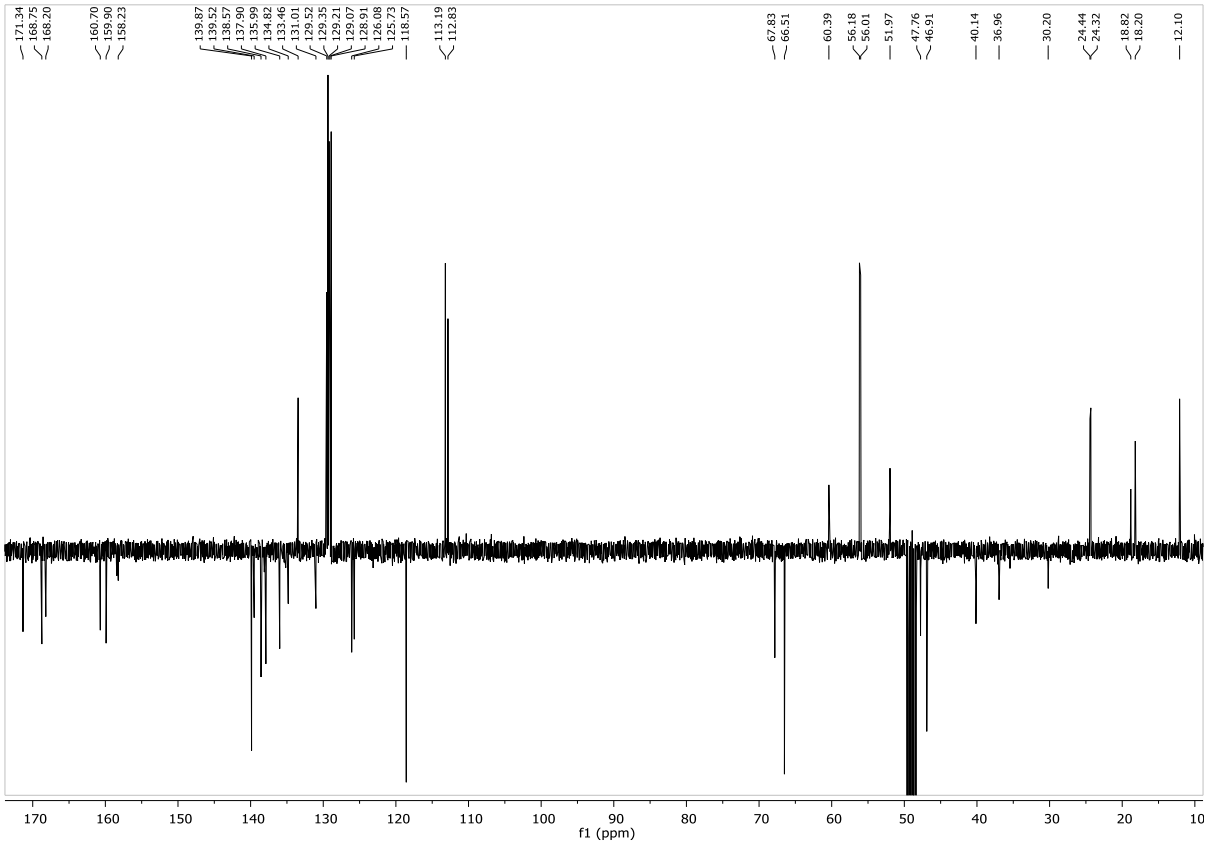

Compound **71**

^{1}H-NMR (400 MHz, CD_3OD)

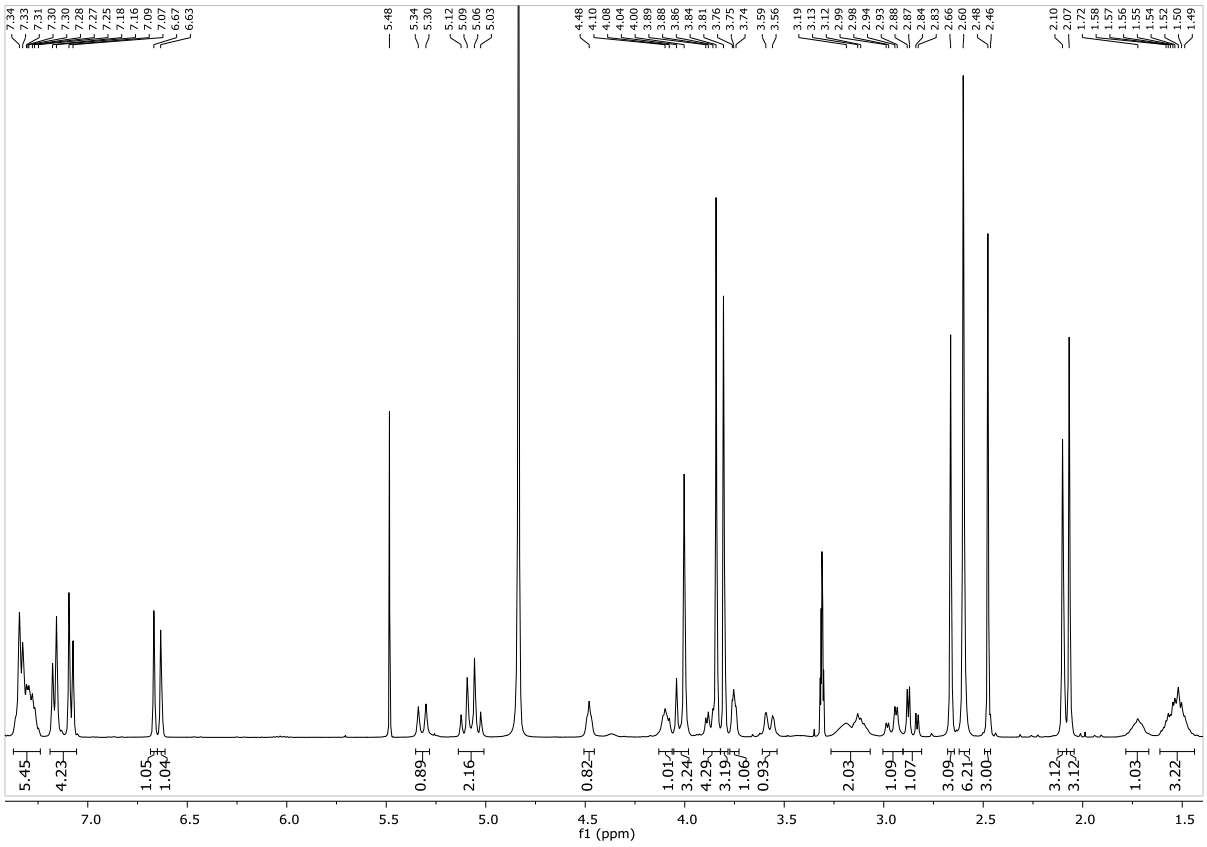

Compound **65**

^{1}H-NMR (400 MHz, Acetone-d_6)

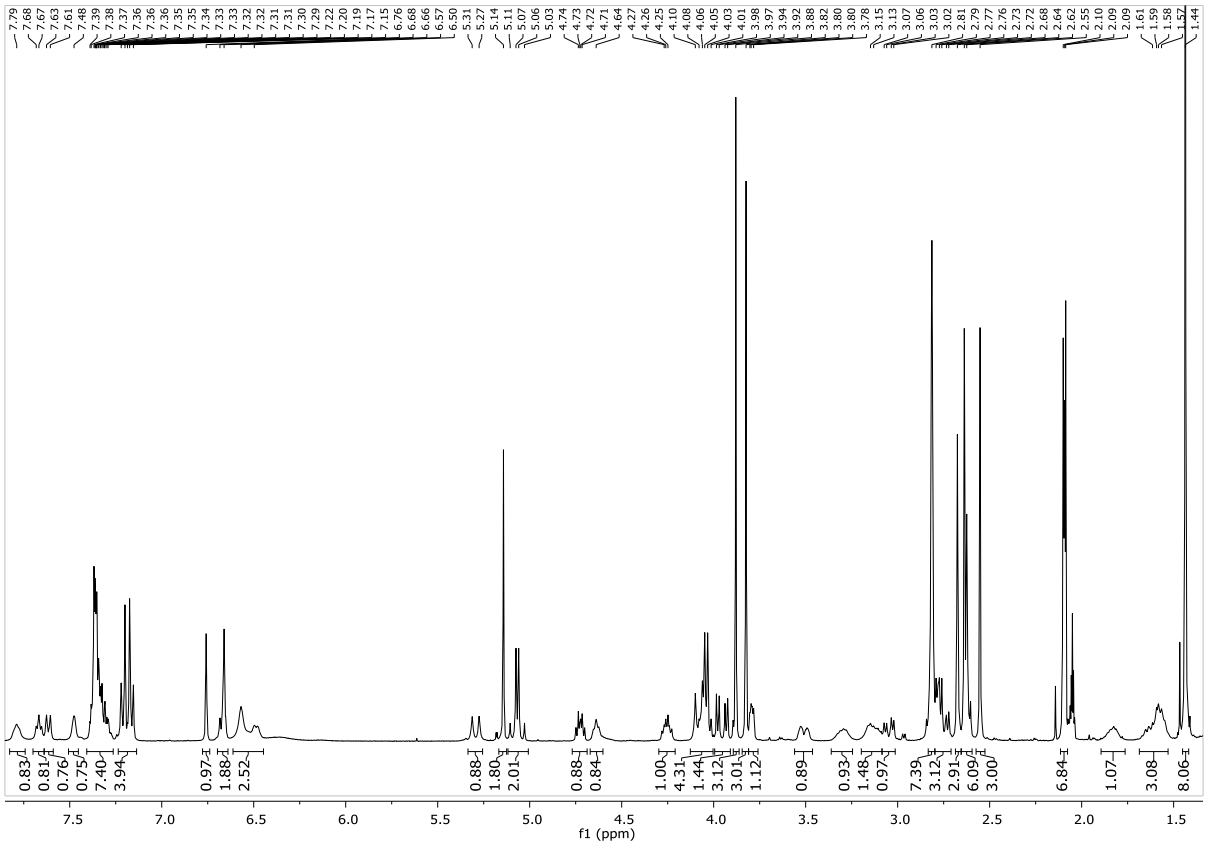

^{13}C-NMR (101 MHz, Acetone-d_6)

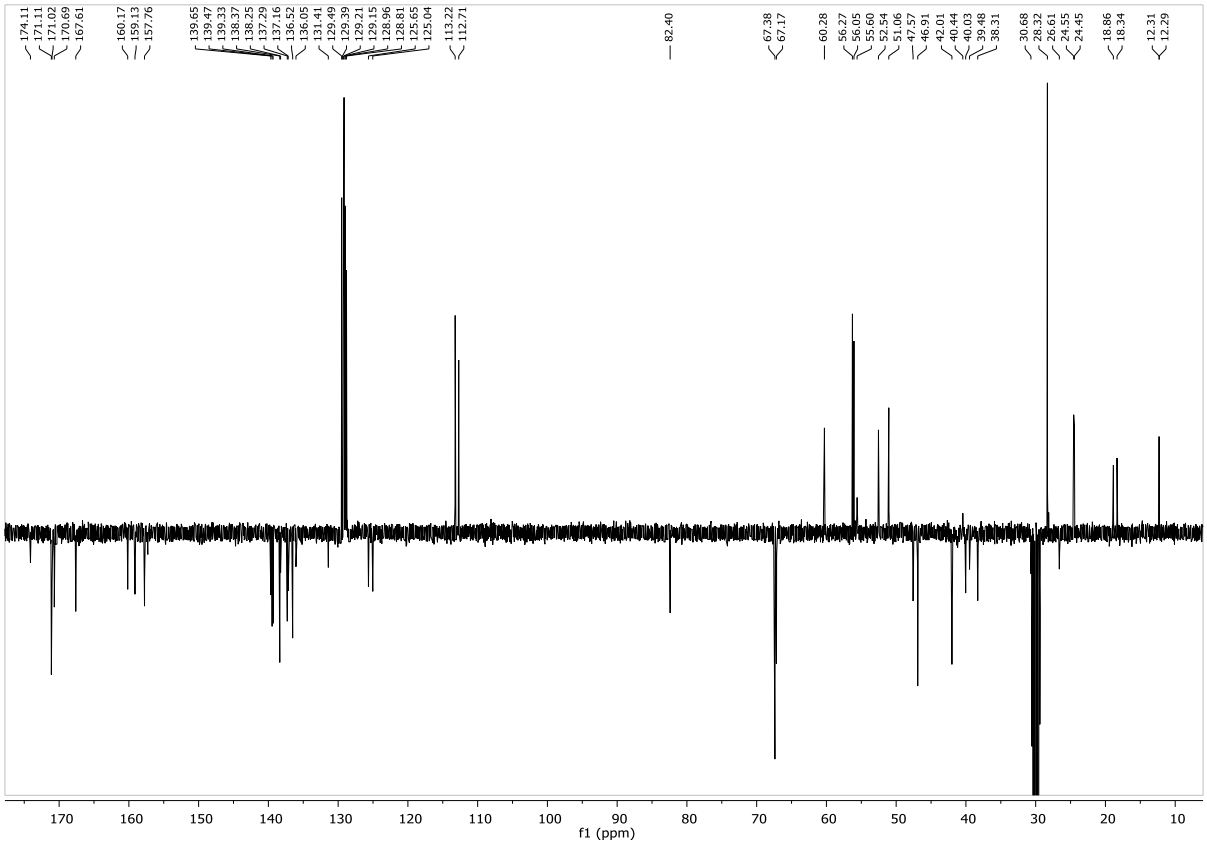

Compound **67**

^{1}H-NMR (400 MHz, DMSO-d_6)

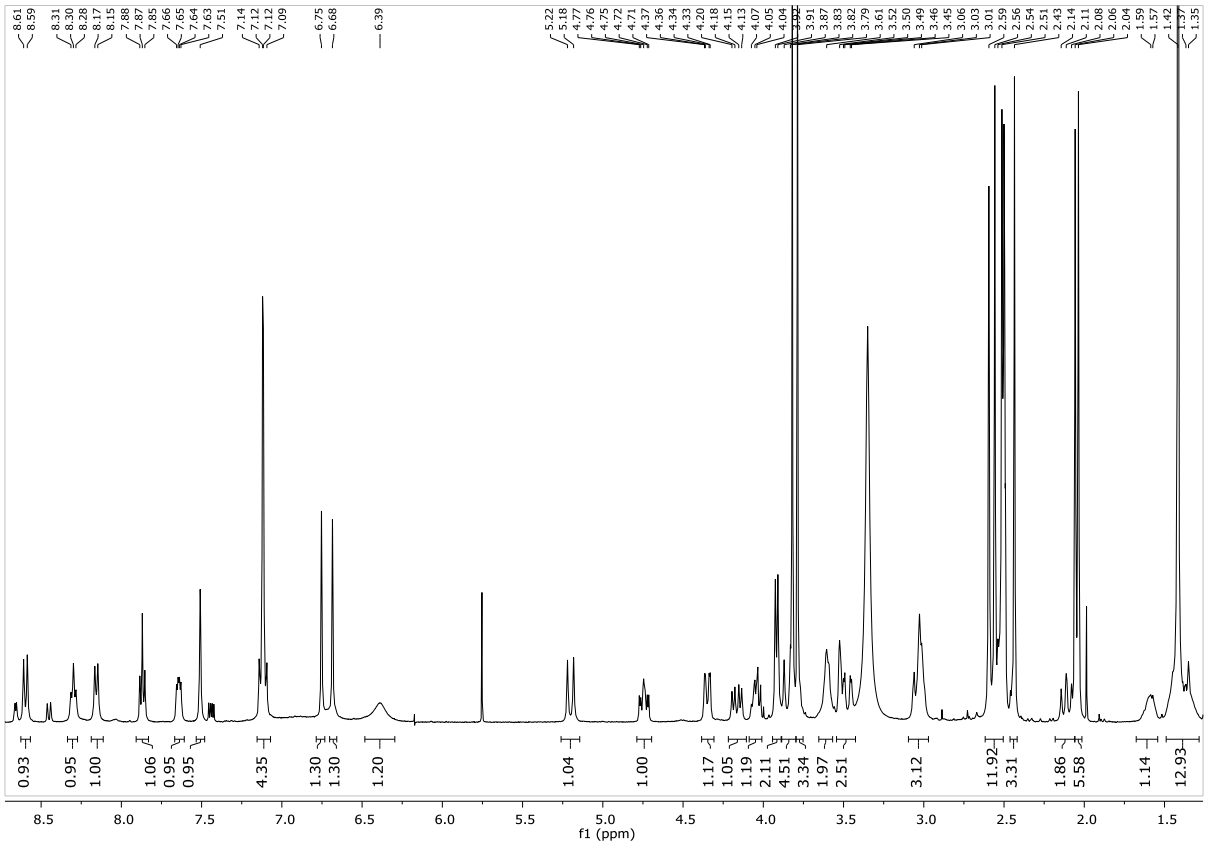

^{13}C-NMR (101 MHz, DMSO-d_6)

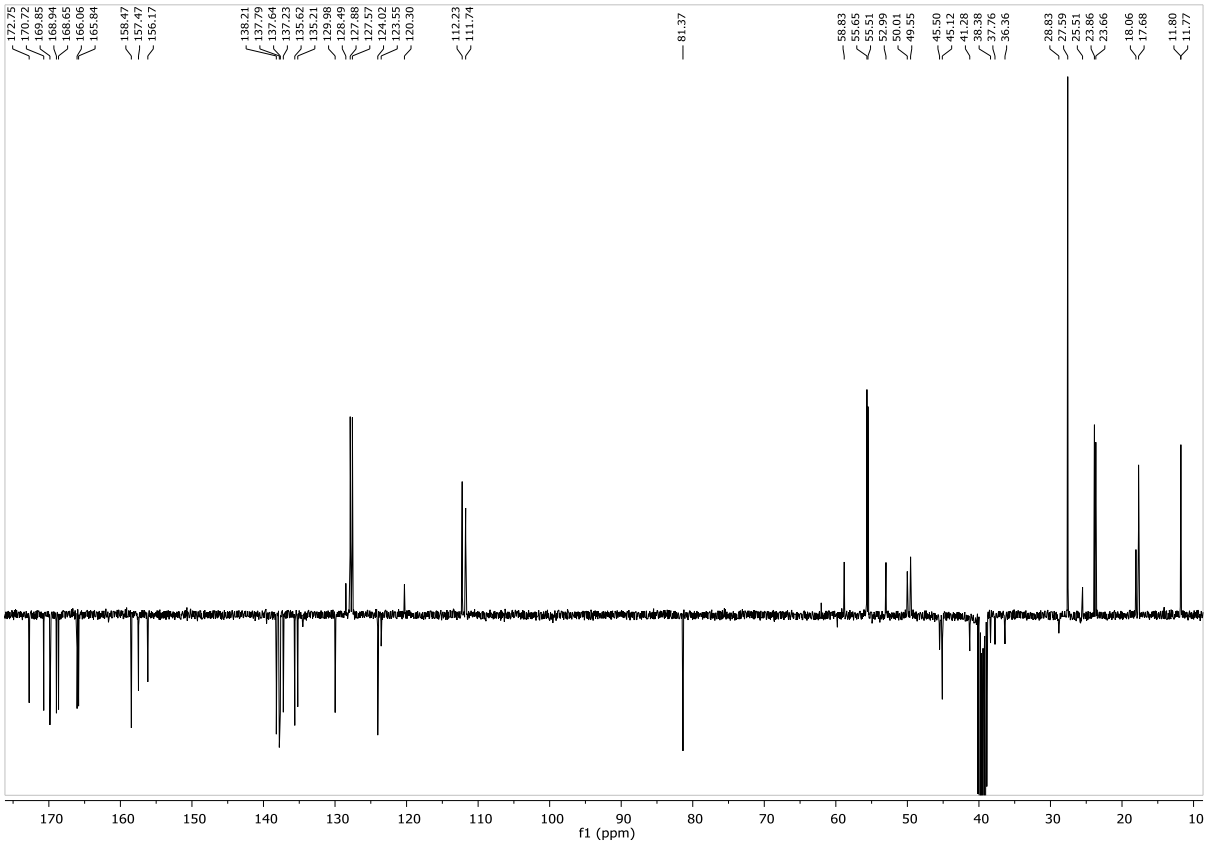

Compound **56**

^{1}H-NMR (400 MHz, D_2O)

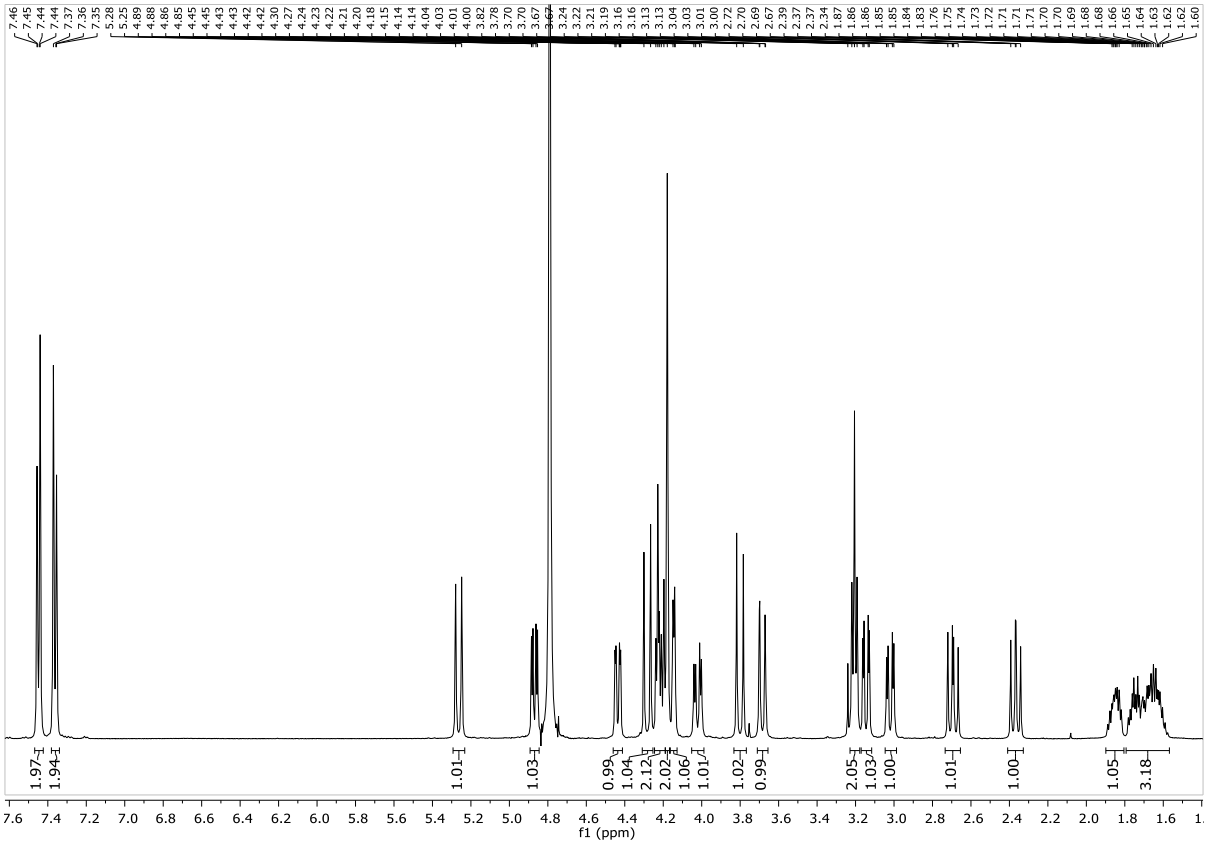

^{13}C-NMR (101 MHz, D_2O)

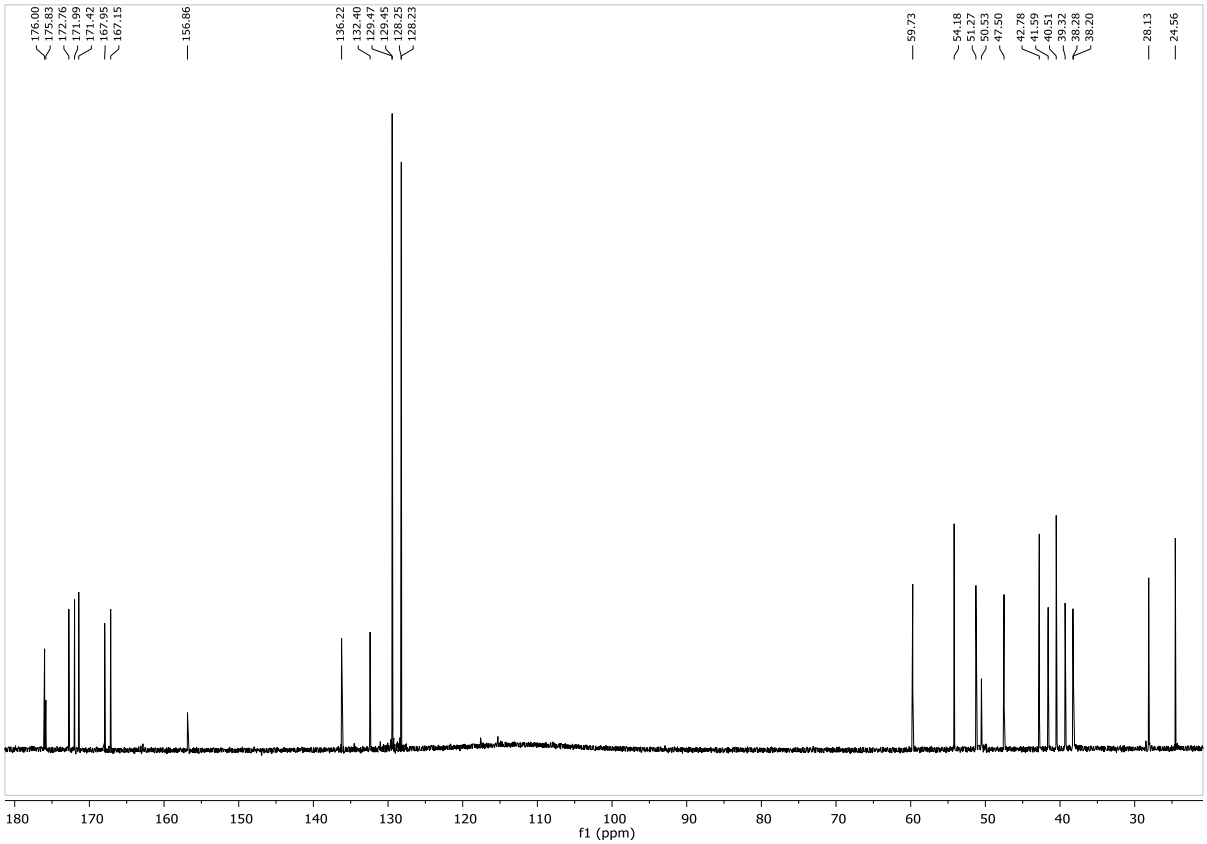

Compound **82**

^{1}H-NMR (400 MHz, DMSO-d_6)

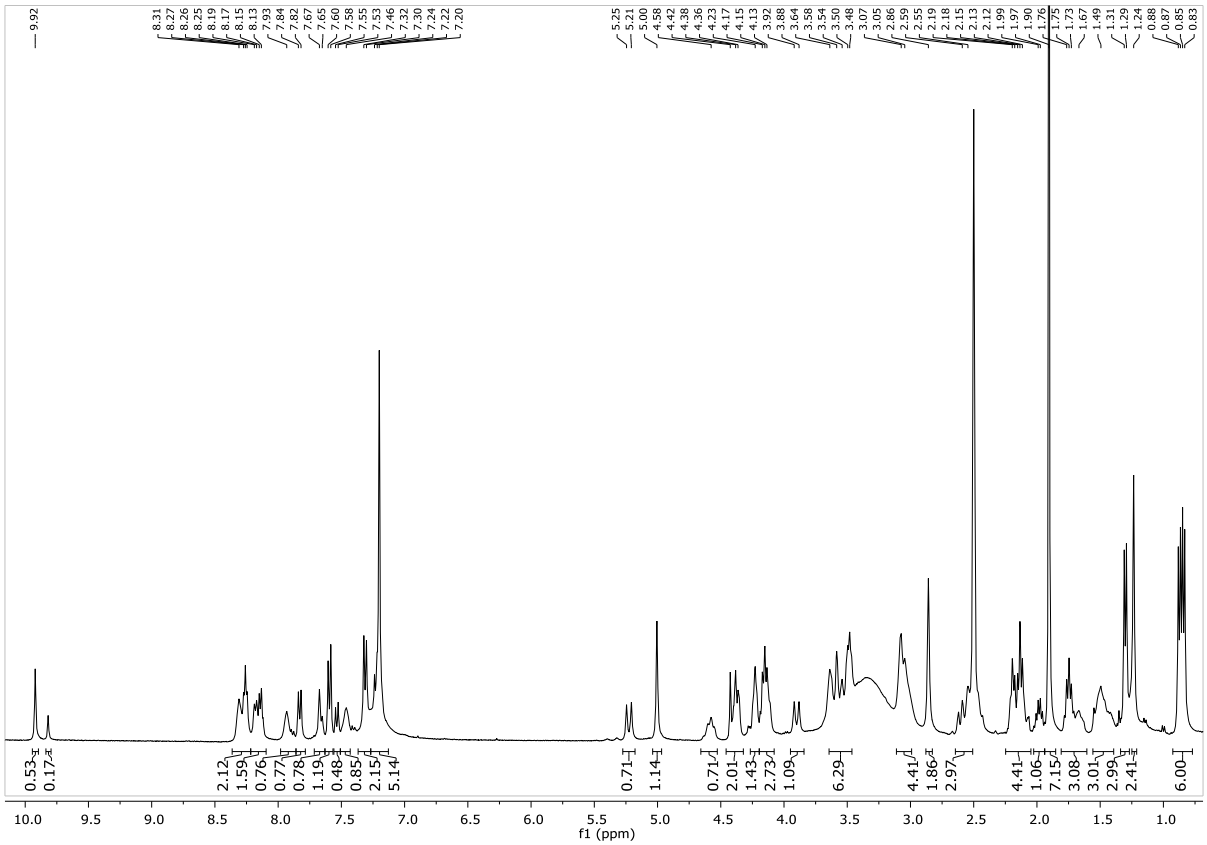

^{13}C-NMR (101 MHz, DMSO-d_6)

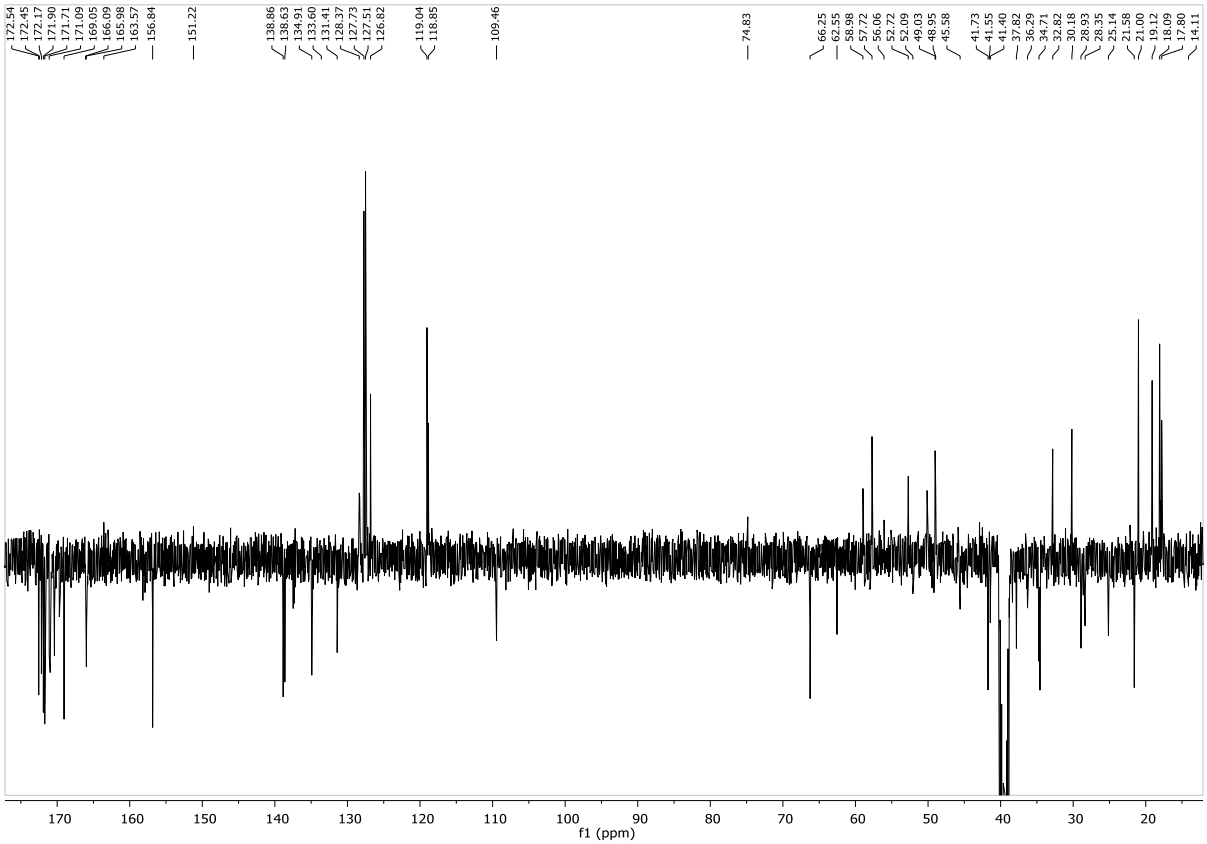

Compound **55**

^{1}H-NMR (400 MHz, DMSO-d_6)

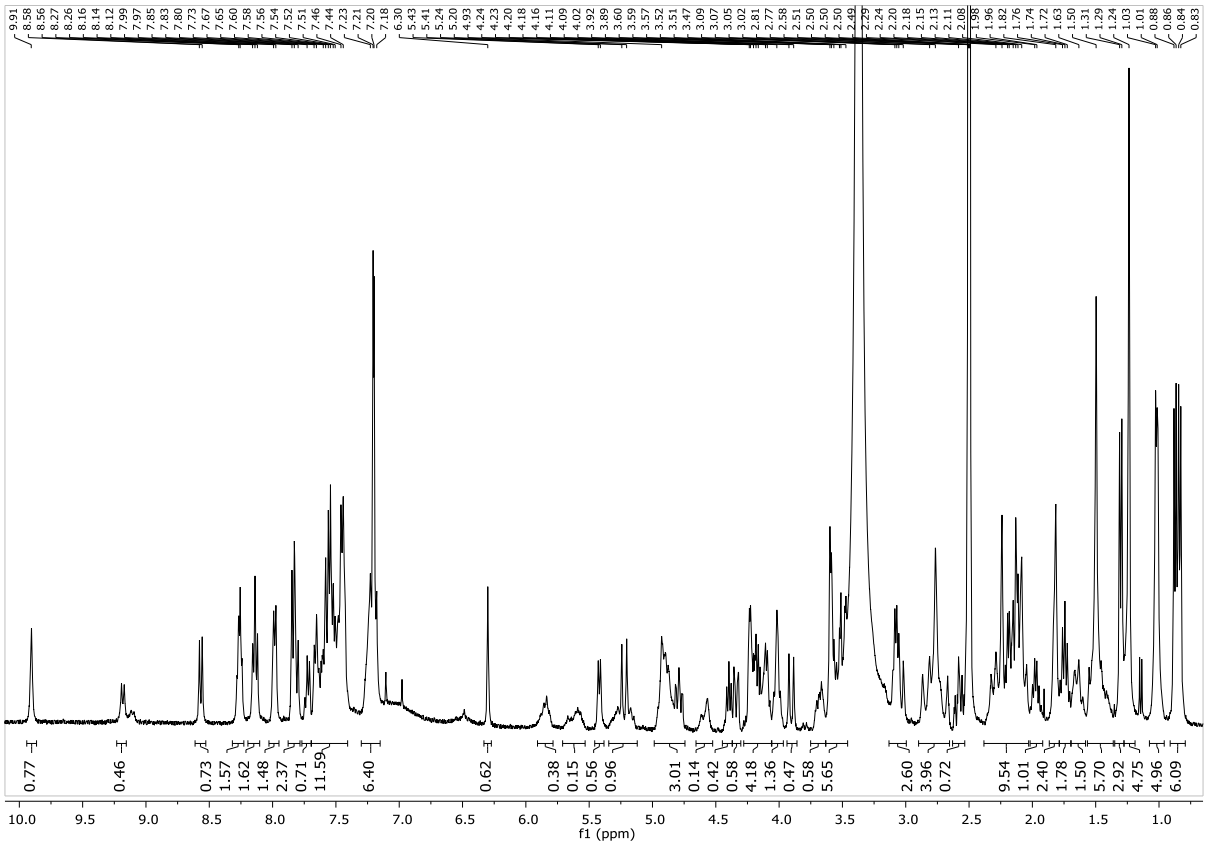

^{13}C-NMR (101 MHz, DMSO-d_6)

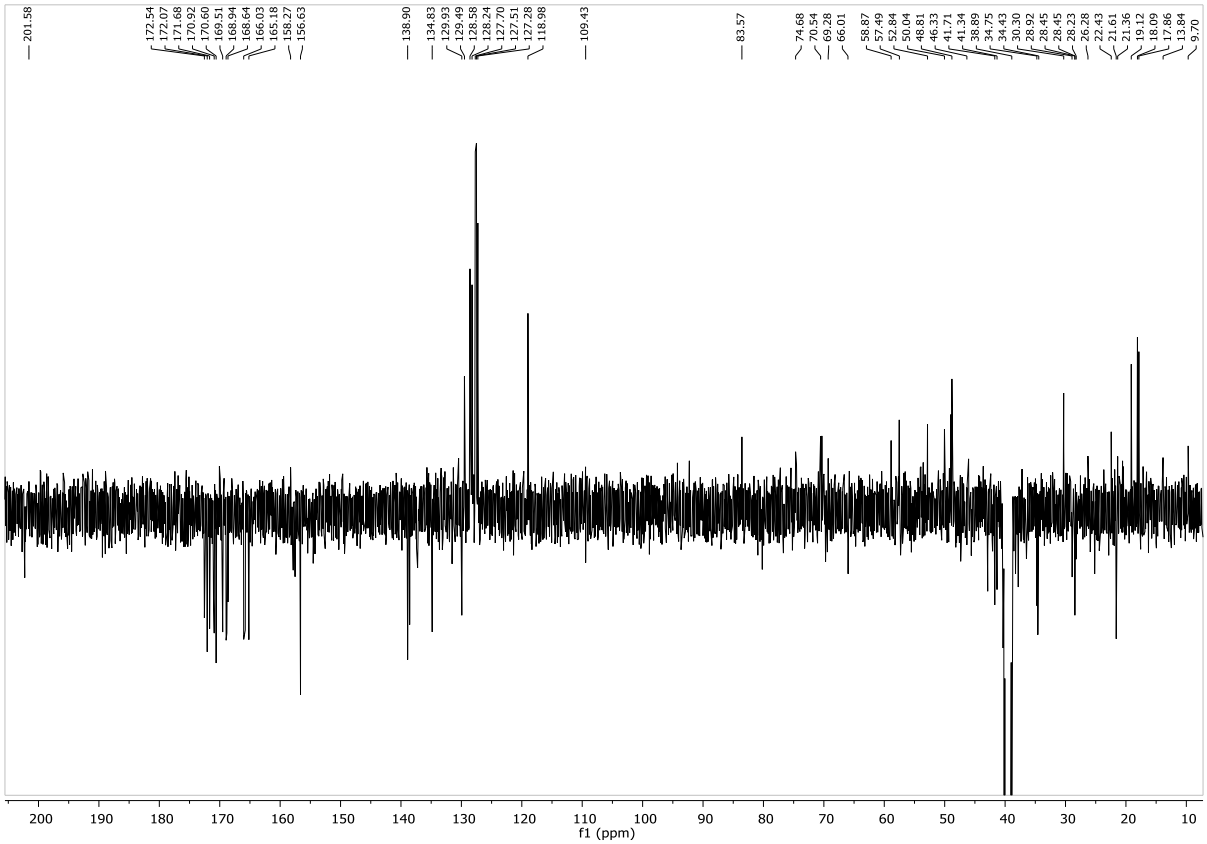

SYNTHESIS OF *CYCLO*[G*ISO*DGRF] **84**

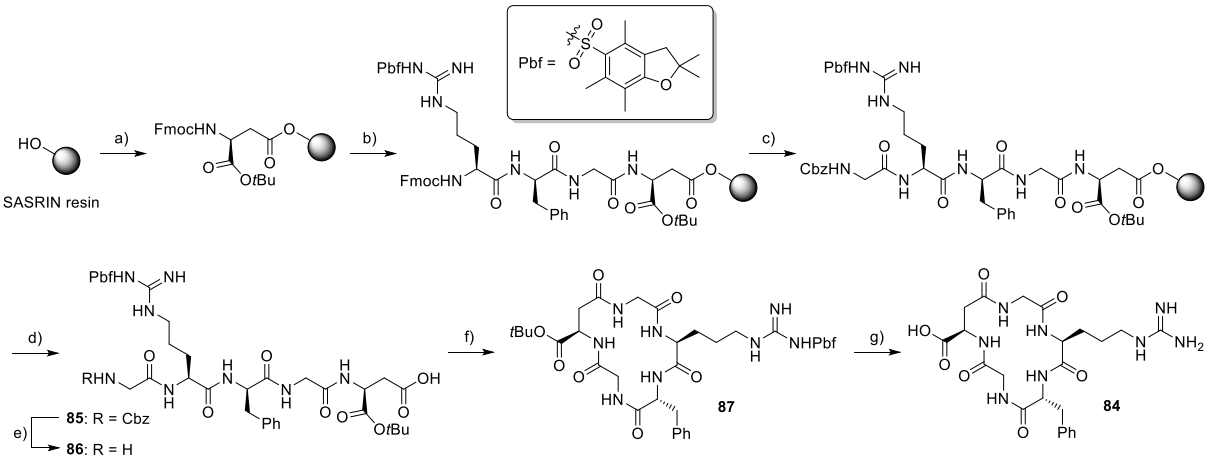

Reagents and Conditions: a) Fmoc-Asp(OH)-O*t*Bu, HATU, HOAt, *i*Pr$_2$NEt, DMF, M.W., 90%; b) 1. 25% piperidine in DMF; 2. Fmoc-AA-OH, HATU, HOAt, *i*Pr$_2$NEt, DMF, M.W.; c) 1. 25% piperidine in DMF; 2. Cbz-Gly-OH, HATU, HOAt, *i*Pr$_2$NEt, DMF, M.W.; d) 1% TFA in CH_2Cl_2, r.t., 3 min x 24 times, 73%; e) H_2, 10% Pd/C, THF/H_2O 2:1, overnight, r.t., quant.; f) HATU, HOAt, *i*Pr$_2$NEt, DMF/CH_2Cl_2 1:1 (1.4 mM), overnight, r.t., 39%; g) TFA/thioanisole/EDT/anisole 90:5:3:2, 2 h, r.t., 49%.

Compound **85**

^{1}H-NMR (400 MHz, CD_3OD)

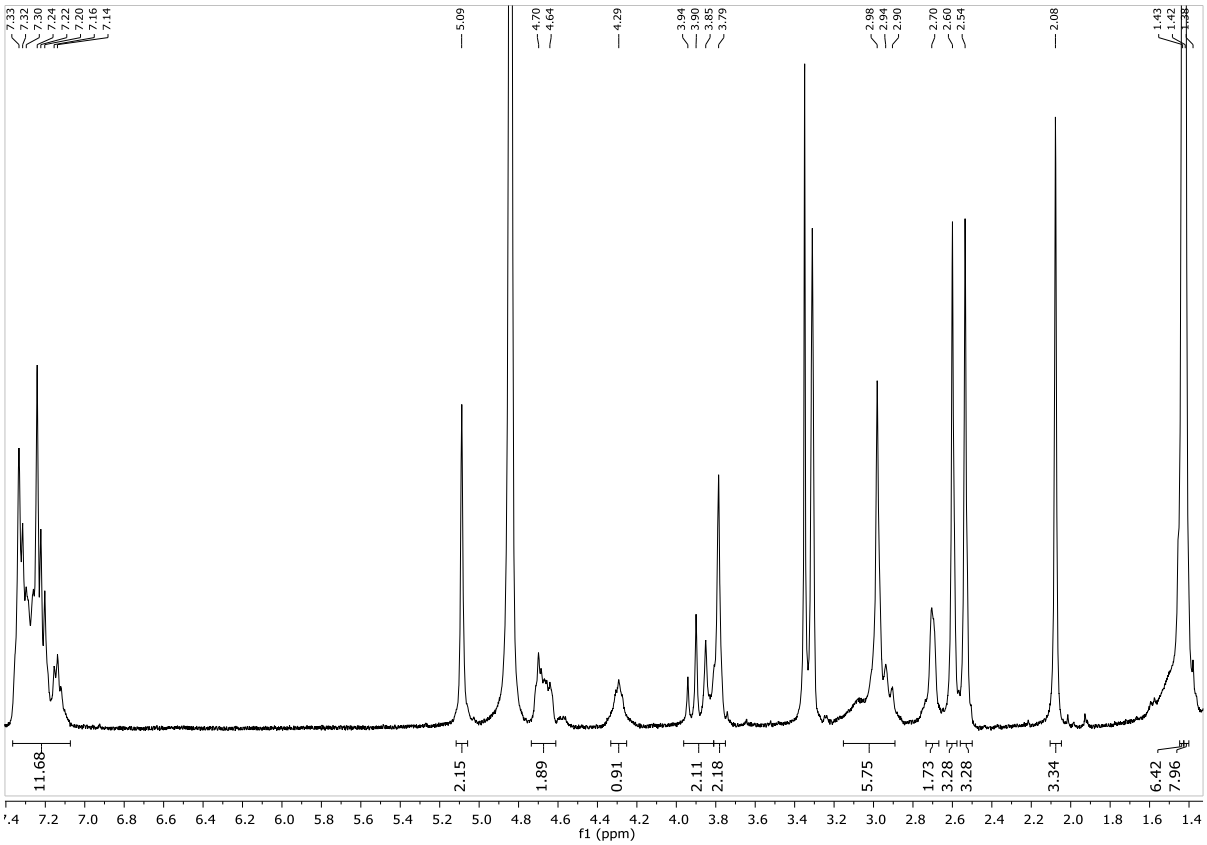

^{13}C-NMR (101 MHz, CD_3OD)

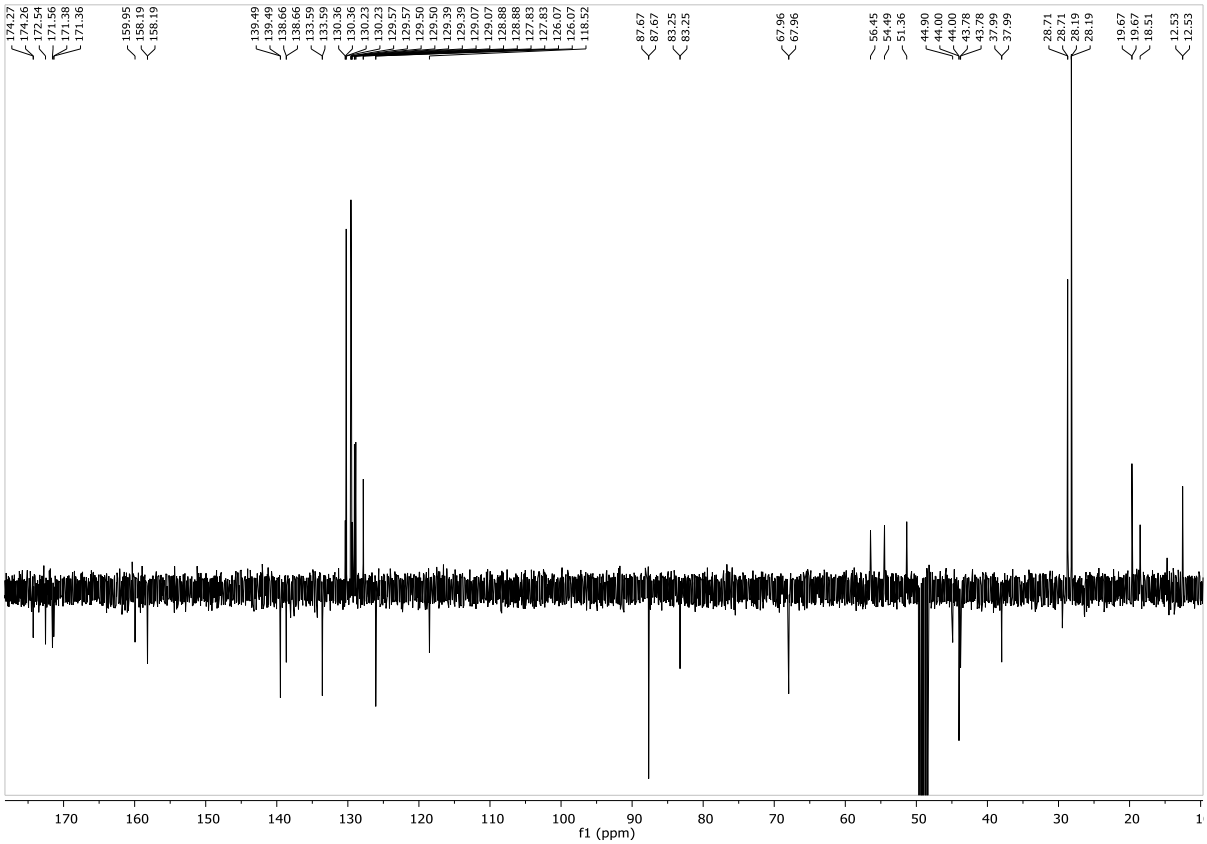

Compound **87**

^{1}H-NMR (600 MHz, CD_3OD)

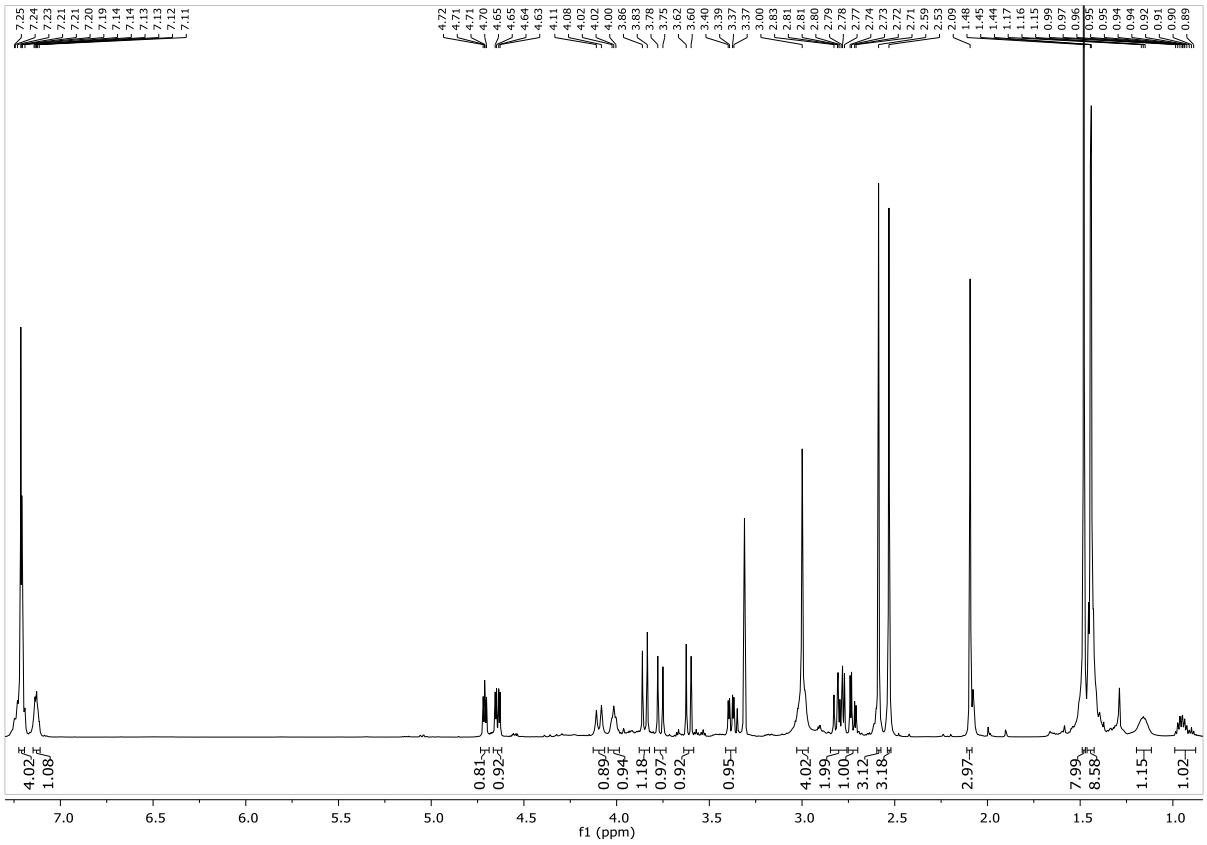

^{13}C-NMR (151 MHz, CD_3OD)

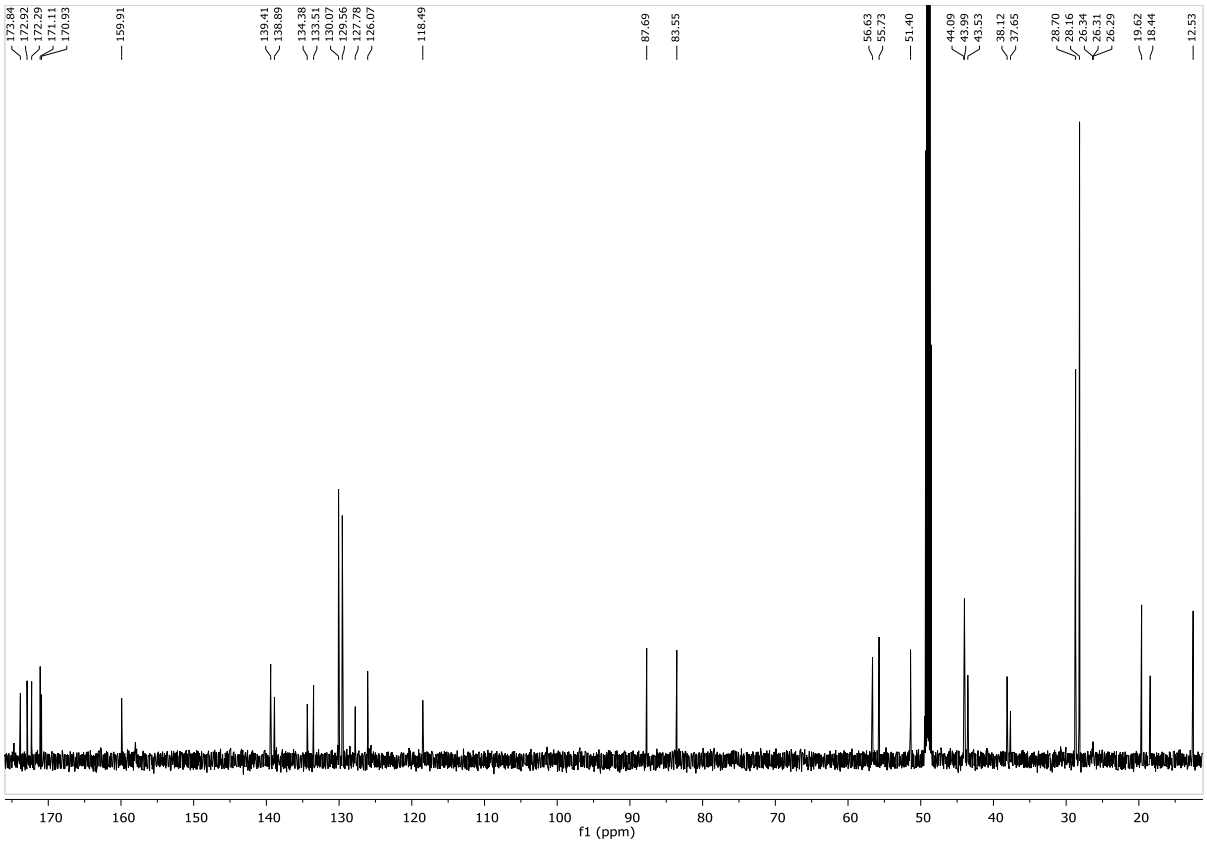

Compound **84**

^{1}H-NMR (400 MHz, D_2O)

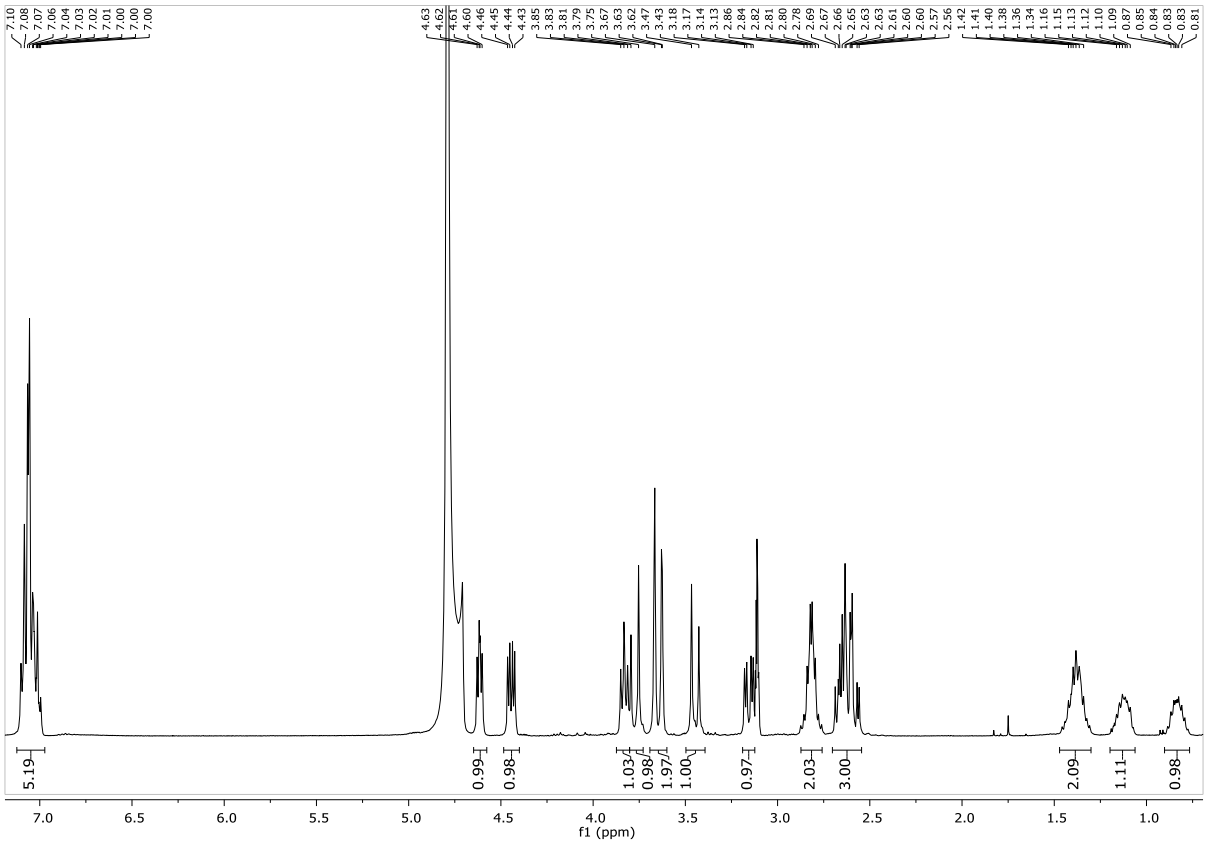

SYNTHESIS OF *CYCLO*[DKP3-RAD] **88A** AND **88B**

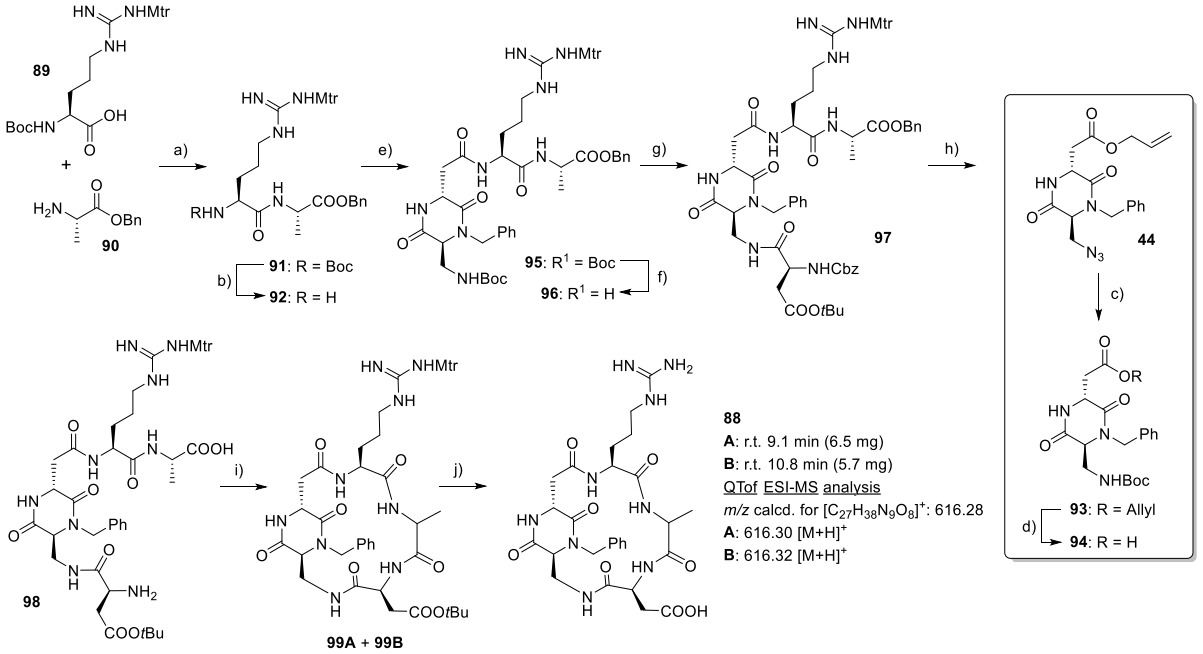

Reagents and conditions. a) HATU, HOAt, *i*Pr$_2$NEt, DMF, 0 °C to r.t., overnight, 84%; b) TFA, CH_2Cl_2, r.t., 2 h; c) PMe_3 in toluene, Boc-ON, THF, -20 °C to r.t., 5 h, 78%; d) [$Pd(PPh_3)_4$], pyrrolidine, PPh_3, CH_2Cl_2, 0 °C, 1 h, quant.; e) **94**, HATU, HOAt, *i*Pr$_2$NEt, DMF, 0 °C to r.t., overnight, 65%; f) TFA, CH_2Cl_2, r.t., 2 h; g) Cbz-L-Asp(O*t*Bu)-OH, HATU, HOAt, *i*Pr$_2$NEt, DMF, 0 °C to r.t., overnight, 83%; h) H_2, 10% Pd/C, THF/H_2O 1:1, overnight, r.t., quant.; i) HATU, HOAt, *i*Pr$_2$NEt, DMF/CH_2Cl_2 1:1 (1.4 mM), 0 °C to r.t., overnight, 82%; j) TFA/thioanisole/EDT/anisole 90:5:3:2, 2 h, rt, 30%.

Compound **91**

^{1}H-NMR (400 MHz, $CDCl_3$)

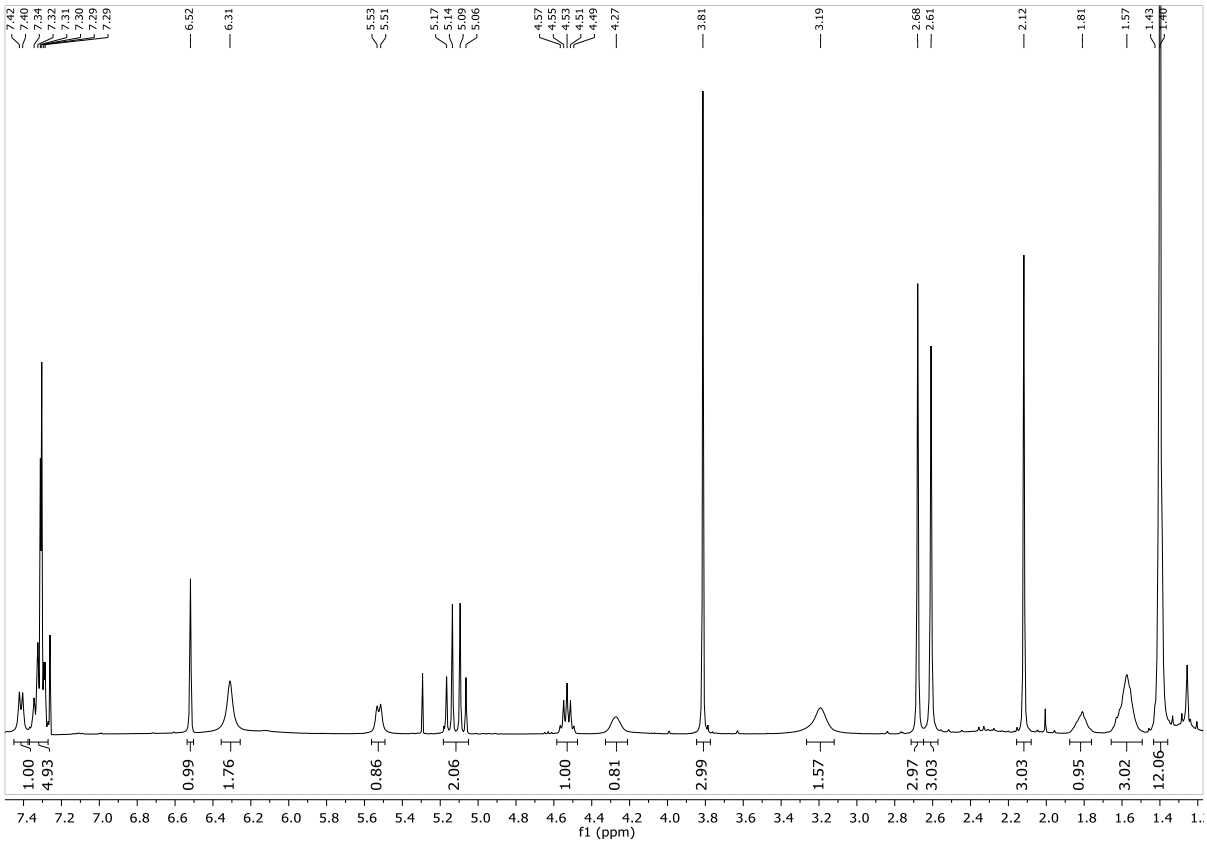

^{13}C-NMR (101 MHz, $CDCl_3$)

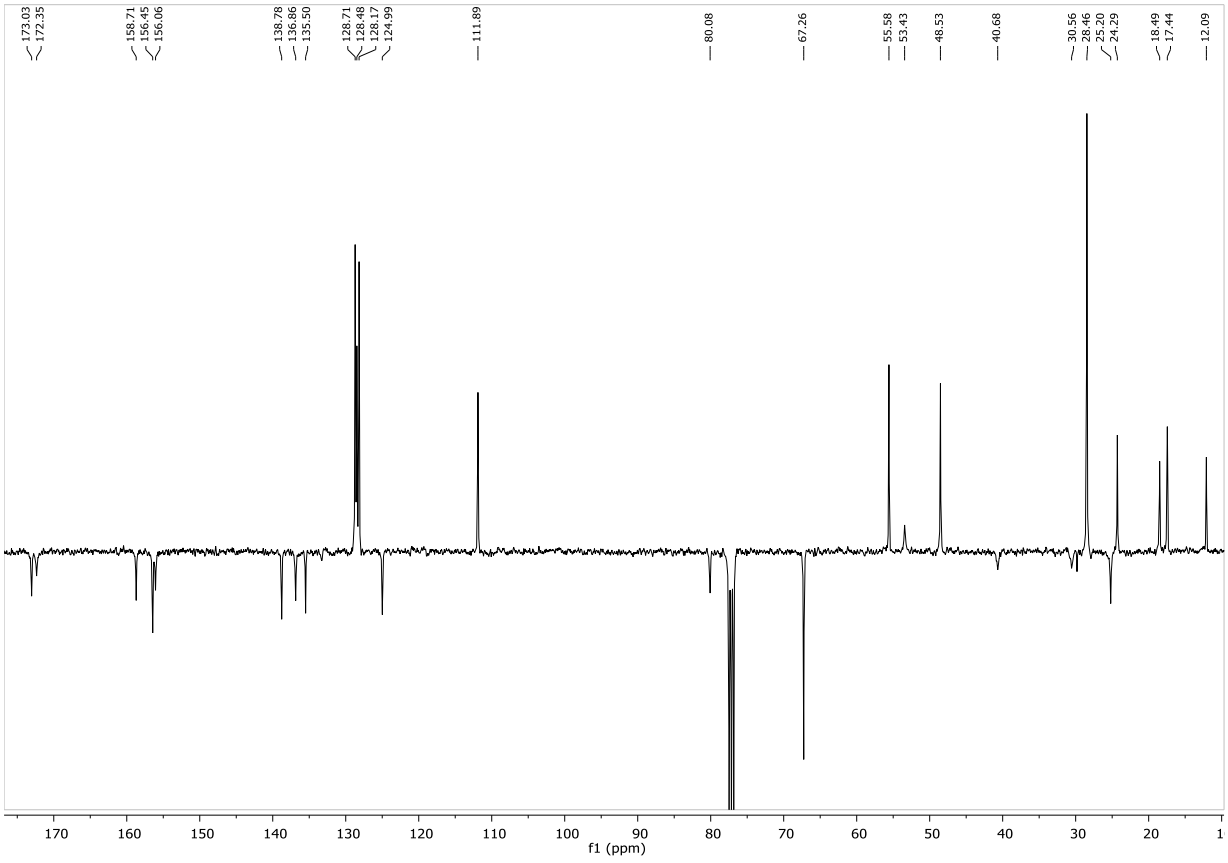

Compound **95**

^{1}H-NMR (400 MHz, CD_2Cl_2)

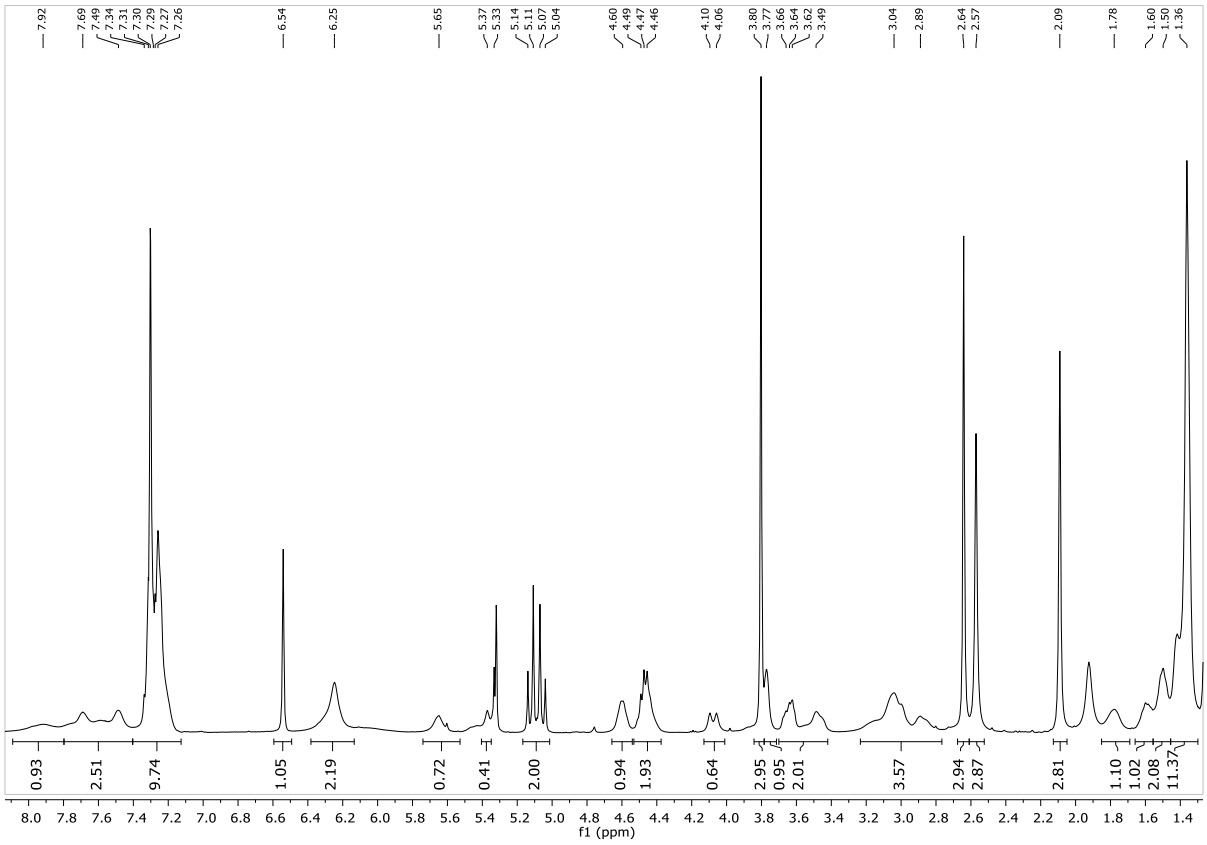

^{13}C-NMR (101 MHz, CD_2Cl_2)

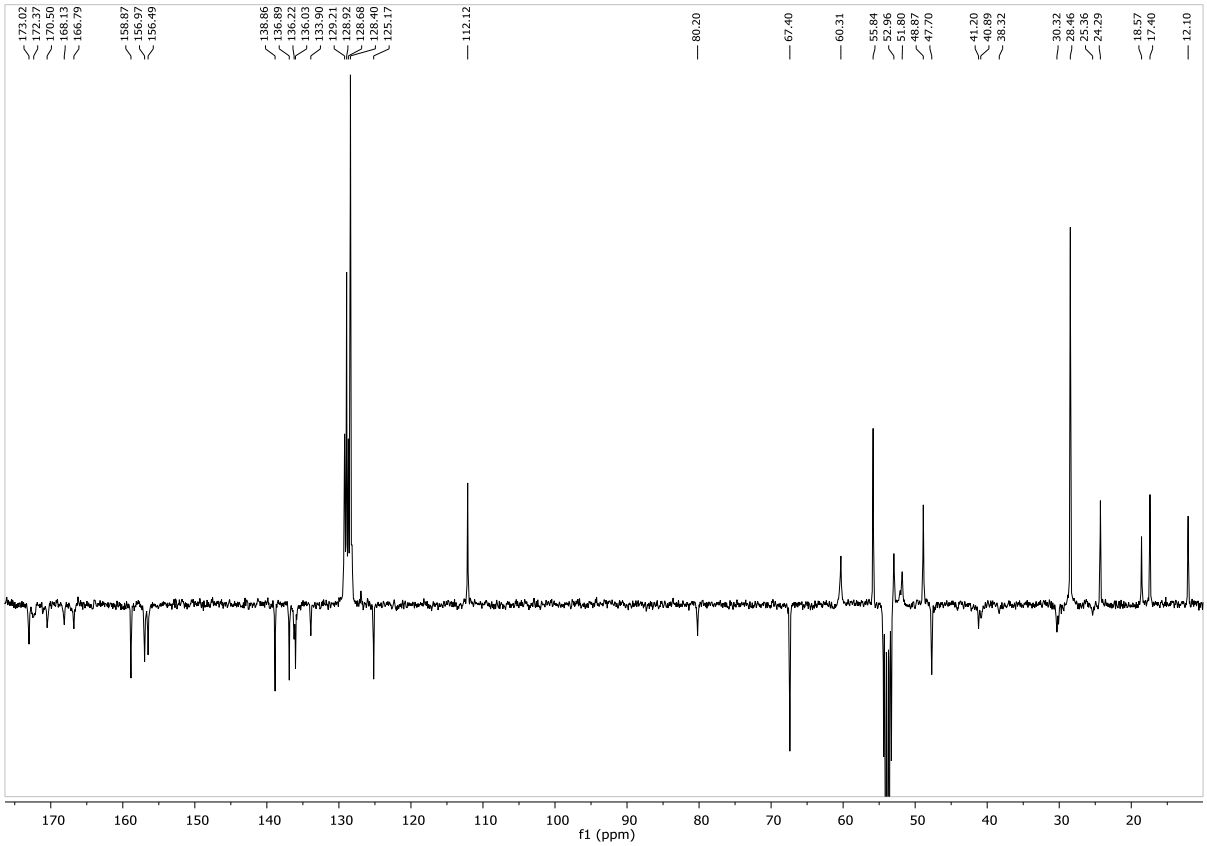

Compound **97**

^{1}H-NMR (400 MHz, CD_2Cl_2)

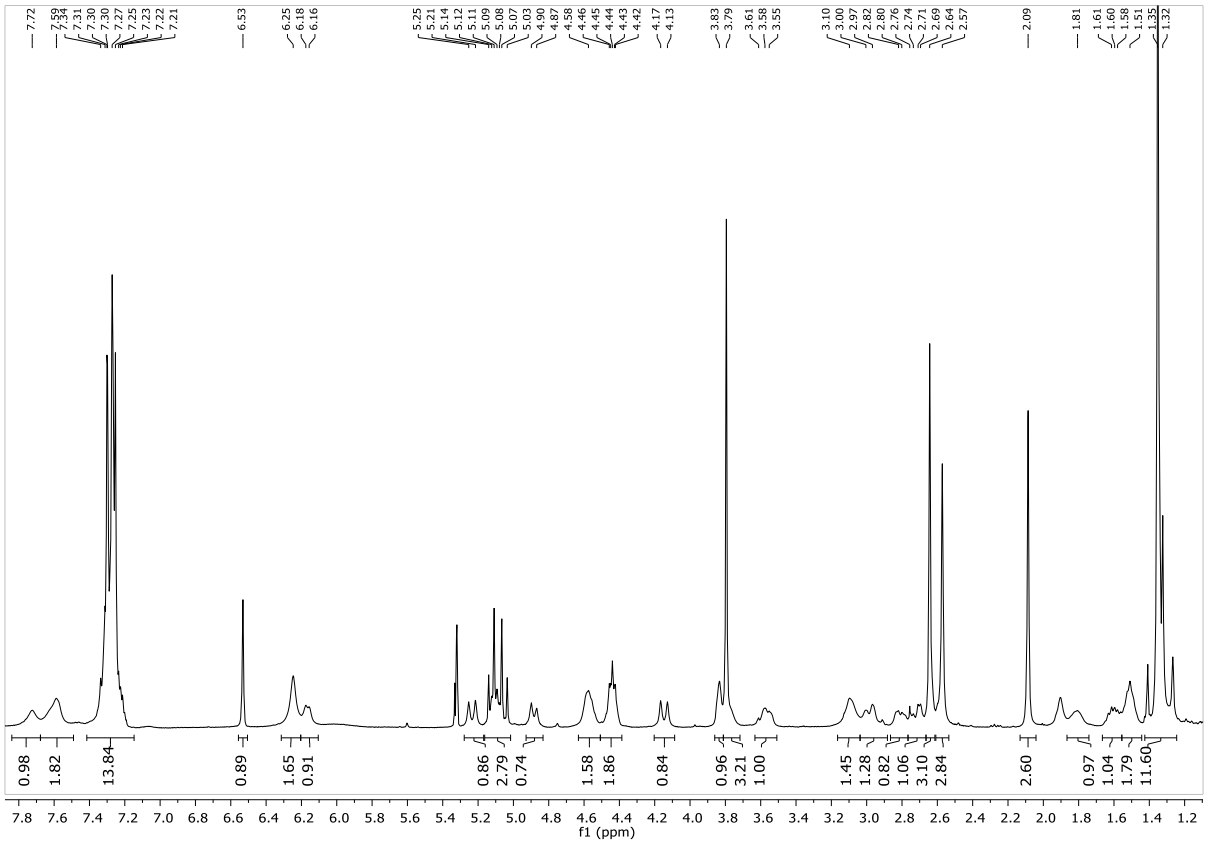

^{13}C-NMR (101 MHz, CD_2Cl_2)

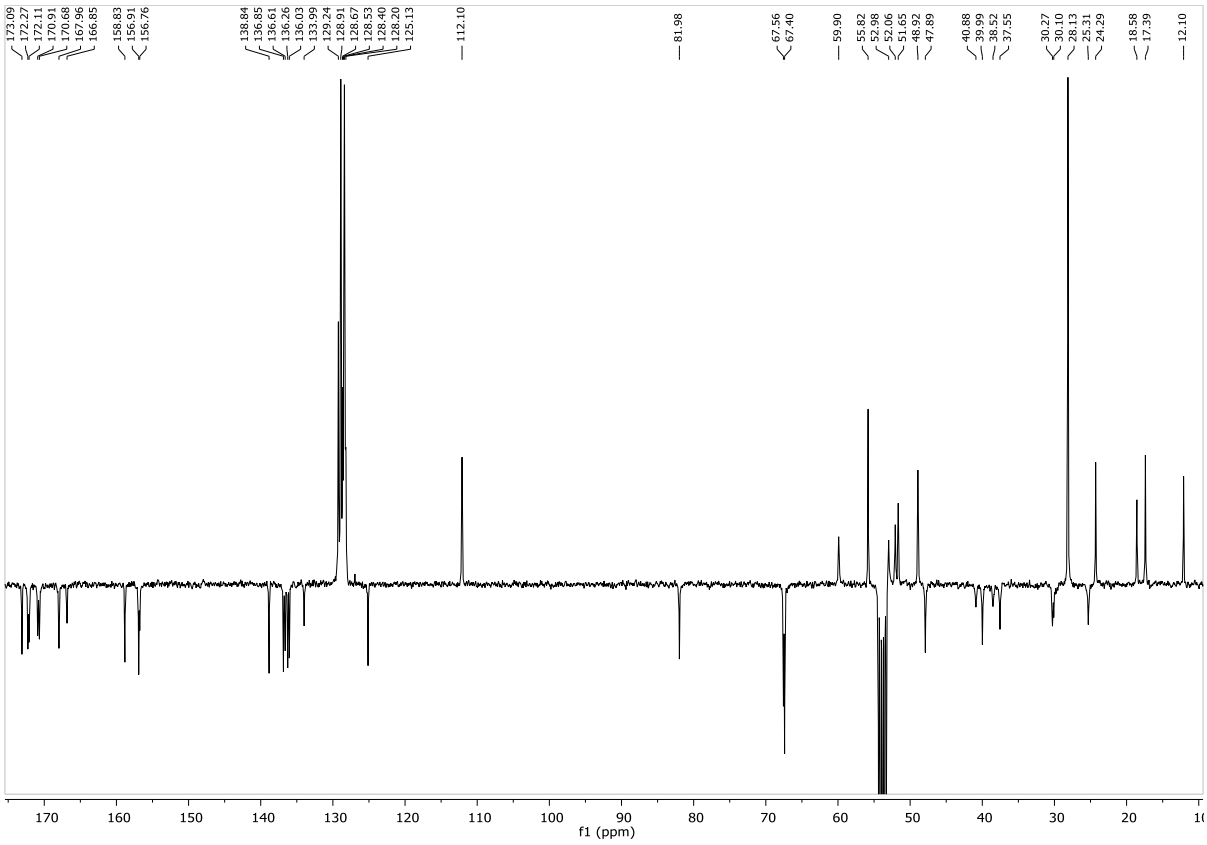

Compound mixture **99A** + **99B**

^{1}H-NMR (400 MHz, CD_3OD)

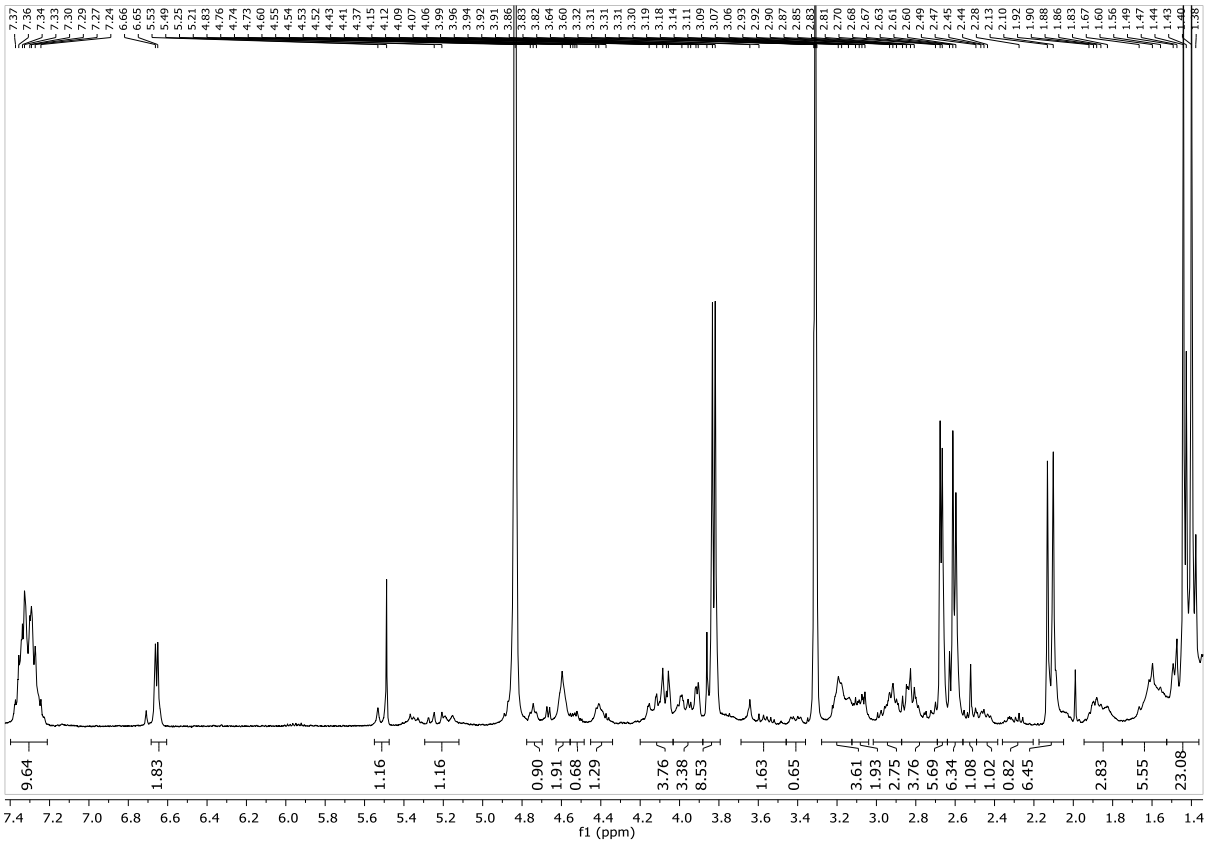

^{13}C-NMR (101 MHz, CD_3OD)

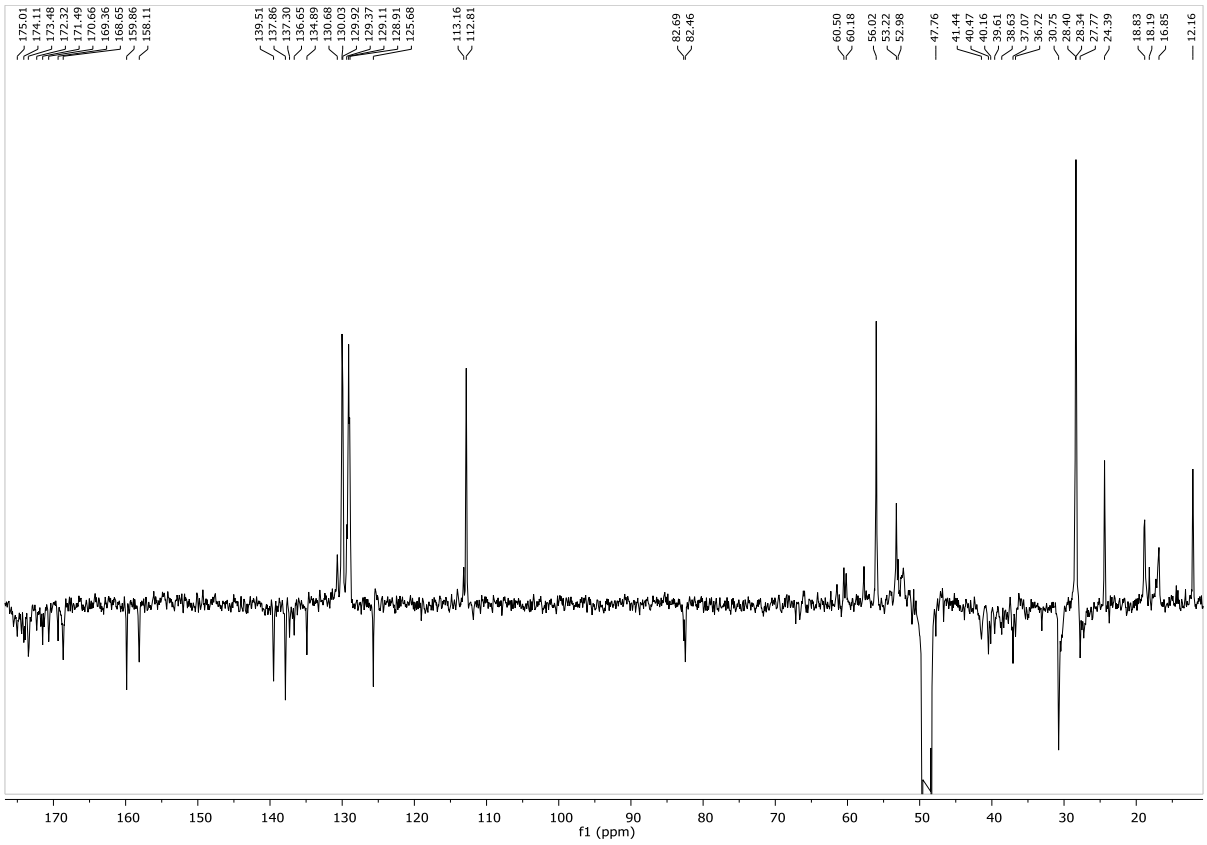

Compound **88A**

^{1}H-NMR (400 MHz, D_2O)

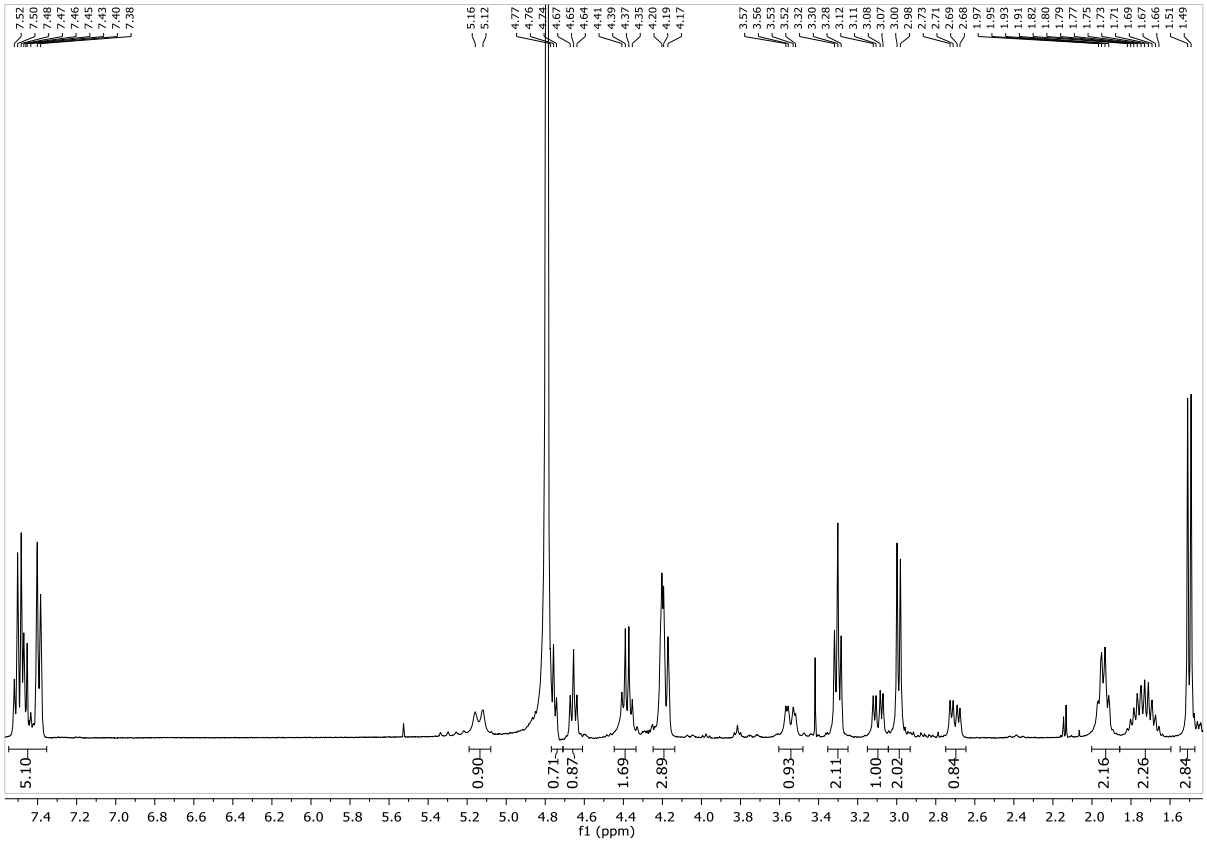

^{13}C-NMR (101 MHz, D_2O)

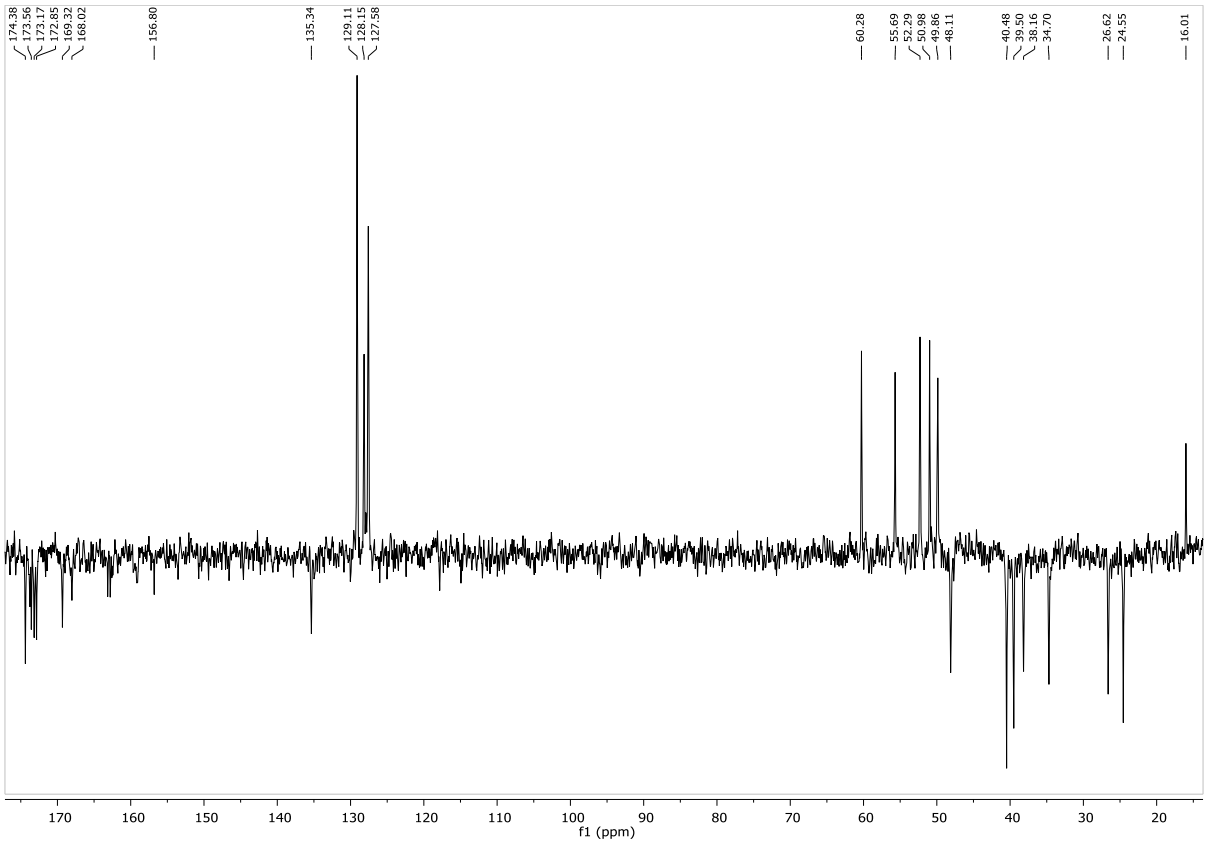

Compound **88B**

^{1}H-NMR (400 MHz, D_2O)

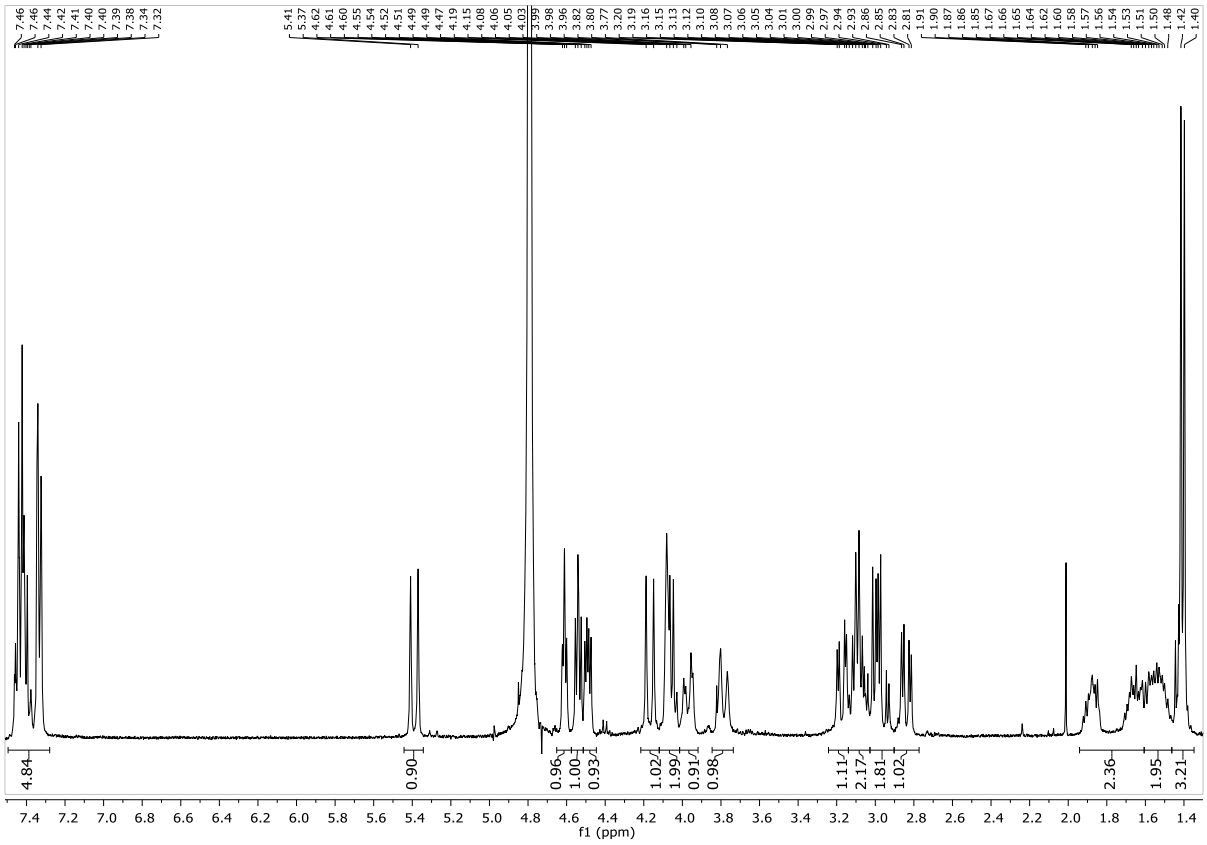

^{13}C-NMR (101 MHz, D_2O)

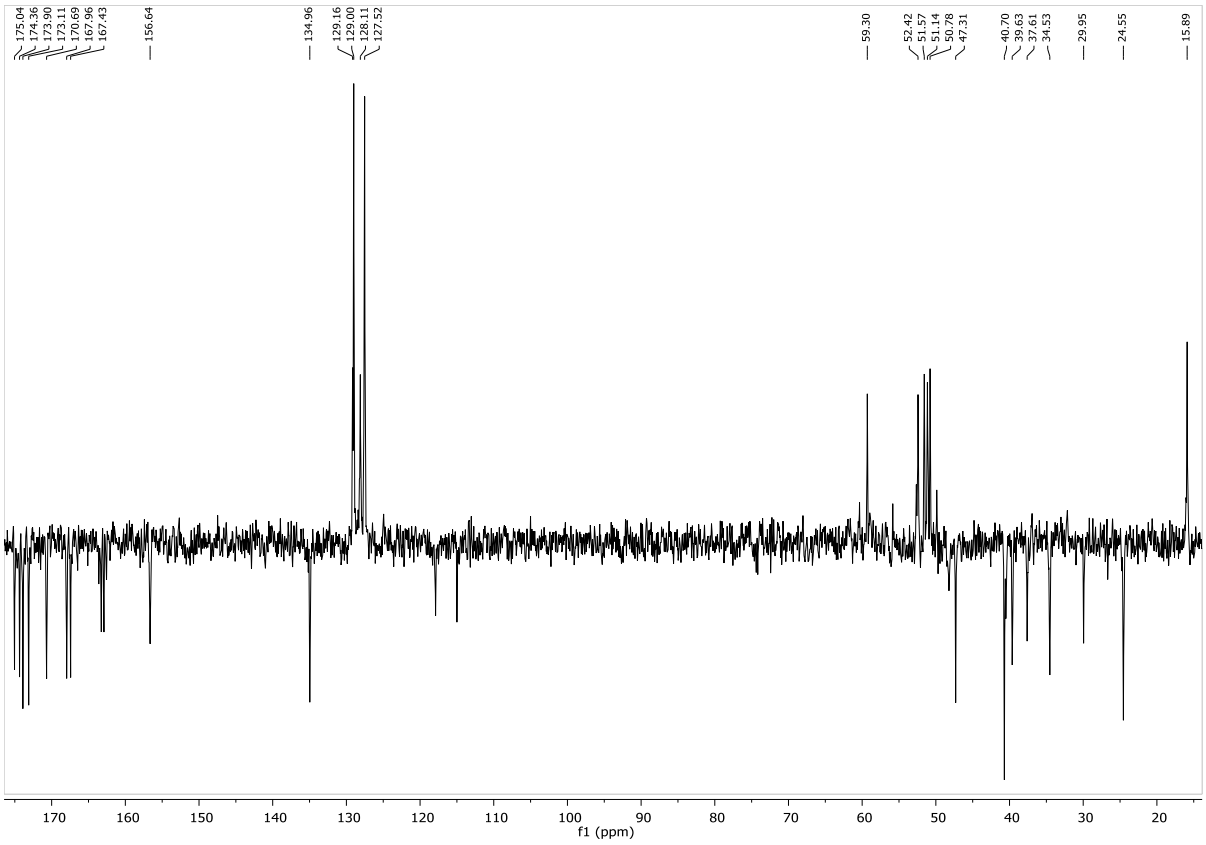

REFERENCES

1 Johannessen, T. C.; Wagner, M.; Straume, O.; Bjerkvig, R.; Eikesdal, H. P. *Expert Opin. Ther. Targets* **2013**, *17*, 7.

2 Qian, C.-N.; Tan, M.-H.; Yang, J.-P.; Cao, Y. *Chin J Cancer* **2016**, *35*:10.

3 Folkman, J. *Annu. Rev. Med.* **2006**, *57*, 1.

4 Danhier, F.; Le Breton, A.; Préat, V. *Mol. Pharmaceutics* **2012**, *9*, 2961.

5 Hanahan, D.; Folkman, J. *Cell* **1996**, *86*, 353.

6 Sund, M.; Nyberg, P.; Eikesdal, H. P. *Pharmaceuticals* **2010**, *3*, 3021.

7 Furugaki, K.; Fukumura, J.; Iwai, T.; Yorozu, K.; Kurasawa, M.; Yanagisawa, M.; Moriya Y.; Yamamoto, K.; Suda, K.; Mizuuchi, H.; Mitsudomi, T.; Harada N. *Int. J. Cancer* **2016**, *138*, 1024, and references therein.

8 Satchi-Fainaro, R.; Mamluk, R.; Wang, L.; Short, S. M.; Nagy, J. A.; Feng, D.; Dvorak, A. M.; Dvorak, H. F.; Puder, M.; Mukhopadhyay, D.; Folkman, J. *Cancer Cell* **2005**, *7*, 251.

9 a) Nussenbaum, F.; Herman, I. M. *J. Oncol.* **2010**, *2010*, 132641; b) Bergers, G.; Hanahan, D. *Nature Reviews Cancer* **2008**, *8*, 592.

10 a) Keibel, A.; Singh, V.; Sharma, M.C. *Curr. Pharm. Des.* **2009**, *15*, 1949; b) Pavalko, F. M.; Otey, C. A. *Proc. Soc. Exp. Biol. Med.* **1994**, *205*, 282.

11 Wang, Z.; Chui, W. -C., Ho, P. C. *Expert Opin. Drug Deliv.* **2010**, *7*, 159, and references therein.

12 a) Cox, D.; Brennan, M.; Moran, N. *Nat. Rev. Drug Disc.* **2010**, *9*, 804; b) Moser, M., Legate, K. R.; Zent, R.; Fässler, R. *Science* **2009**, *324*, 895.

13 a) Wang, H.; Jin, H.; Beauvais, D. M.; Rapraeger, A. C. *J. Biol. Chem.* **2014**, *289*, 30318; b) Zhang, H.; Ozaki, I.; Mizuta, T.; Yoshimura, T.; Matsuhashi, S.; Hisatomi, A.; Tadano, J.; Sakai, T.; Yamamoto K. *Hepatology* **2003**, *38*, 305; c) Akiyama, S. K. *Hum. Cell* **1996**, *9*, 181.

14 a) Askari, J. A.; Buckley, P. A.; Mould, A. P.; Humphries, M. J. *J. Cell Sci.* **2009**, *122*, 165; b) Hantgan, R. R.; Stahle, M. C.; Connor, J. H.; Horita, D. A.; Rocco, M.; Mclane, M. A.; Yakovlev, S.; Medved, L. *Protein Sci.* **2006**, *15*, 1893; c) Takagi, J.; Springer, T. A. *Immunol Rev.* **2002**, *186*, 141; d) Hato, T.; Pampori, N.; Shattil, S. J. *J. Cell Biol.* **1998**, *141*, 1685.

15 a) Ruoslahti, E.; Pierschbacher, M. D. *Science* **1987**, *238*, 491; b) Pierschbacher, M. D.; Ruoslahti, E. *Nature* **1984**, *309*, 30.

16 a) Giancotti, F. G.; Tarone, G. *Annu. Rev. Cell Dev. Biol.* **2003**, *19*, 173; b) Miranti, C. K.; Brugge, J. S. *Nat. Cell. Biol.* **2002**, *4*, E83.

17 Desgrosellier, J. S.; Cheresh, D. A. *Nat. Rev. Cancer* **2010**, *10*, 9.

18 Guo, W.; Giancotti, F. G. *Nat. Rev. Mol. Cell Biol.* **2004**, *5*, 816.

19 a) Ruoslahti, E.; Pierschbacher, M. D. *Science* **1987**, *238*, 491; b) Pierschbacher, M. D.; Ruoslahti, E. *Nature* **1984**, *309*, 30.

20 a) Mas-Moruno, C.; Beck, J. G.; Doedens, L.; Frank, A. O.; Marinelli, L.; Cosconati, S.; Novellino, E.; Kessler, H. *Angew. Chem. Int. Ed.* **2011**, *50*, 9496; *Angew. Chem.* **2011**, *123*, 9668; b) Gottschalk, K. E.; Kessler, H. *Angew. Chem. Int. Ed.* **2002**, *41*, 3767; *Angew. Chem.* **2002**, *114*, 3919.

21 Xiong, J. -P.; Stehle, T.; Zhang, R.; Joachimiak, A.; Frech, M.; Goodman, S. L.; Arnaout, M. A *Science* **2002**, *296*, 151.

22 Auzzas, L.; Zanardi, F.; Battistini, L.; Burreddu, P.; Carta, P.; Rassu, G.; Curti, C.; Casiraghi, G. *Curr. Med. Chem.* **2010**, *17*, 1255.

23 Compounds **5**-**7**: a) Manzoni, L.; Belvisi, L.; Arosio, D.; Civera, M.; Pilkington-Miksa, M.; Potenza, D.; Caprini, A.; Araldi, E. M. V.; Monferrini, E.; Mancino, M.; Podestà, F.; Scolastico, C. *ChemMedChem.* **2009**, *4*, 615; b) Belvisi, L.; Bernardi, A.; Colombo, M.; Manzoni, L.; Potenza, D.; Scolastico, C.; Giannini, G.; Marcellini, M.; Riccioni, T.; Castorina, M.; LoGiudice, P.; Pisano, C. *Bioorg. Med. Chem.* **2006**, *14*, 169. Compound **8**: Haubner, R.; Schmitt, W.; Hölzemann, G.; Goodman, S. L.; Jonczyk, A.; Kessler, H. *J. Am.*

Chem. Soc. **1996**, *118*, 7881. Compound **9**: Sladojevich, F.; Trabocchi, A.; Guarna, A. *J. Org. Chem.* **2007**, *72*, 4254. Compounds **10-11**: a) van Well, R. M.; Marinelli, L.; Altona, C.; Erkelens, K.; Siegal, G.; van Raaij, M.; Llamas-Saiz, A. L.; Kessler, H.; Novellino, E.; Lavecchia, A.; van Boom, J. H.; Overhand, M. *J. Am. Chem. Soc.* **2003**, *125*, 10822; b) van Well, R. M.; Overkleeft, H. S.; van der Marel, G. A.; Bruss, D.; Thibault, G.; de Groot, P. G.; van Boom, J. H.; Overhand, M. *Bioorg. Med. Chem. Lett*. **2003**, *13*, 331. Compounds **12-14**: a) Zanardi, F.; Burreddu, P.; Rassu, G.; Auzzas, L.; Battistini, L.; Curti, C.; Sartori, A.; Nicastro, G.; Menchi, G.; Cini, N.; Bottoncetti, A.; Raspanti, S.; Casiraghi, G. *J. Med. Chem.* **2008**, *51*, 1771; b) Casiraghi, G.; Rassu, G.; Auzzas, L.; Burreddu, P.; Gaetani, E.; Battistini, L.; Zanardi, F.; Curti, C.; Nicastro, G.; Belvisi, L.; Motto, I.; Castorina, M.; Giannini, G.; Pisano, C. *J. Med. Chem.* **2005**, *48*, 7675.

24 a) Reynolds, A. R.; Hart, I. R.; Watson, A. R.; Welti, J. C.; Silva, R. G.; Robinson, S. D.; Da Violante, G.; Gourlaouen, M.; Salih, M.; Jones, M. C.; Jones, D. T.; Saunders, G.; Kostourou, V.; Perron-Sierra, F.; Norman, J. C.; Tucker, G. C.; Hodivala-Dilke, K. M. *Nat. Med.* **2009**, *15*, 392; b) Alghisi, G. C.; Ponsonnet, L.; Rüegg, C. *PLoS ONE* **2009**, *4*, e4449.

25 Selected examples: a) Dal Corso, A.; Caruso, M.; Belvisi, L.; Arosio, D.; Piarulli, U.; Albanese, C.; Gasparri, F.; Marsiglio, A.; Sola, F.; Troiani, S.; Valsasina, B.; Pignataro, L.; Donati, D.; Gennari, C. *Chem. Eur. J.* **2015**, *21*, 6921; b) Bianchi, A.; Arosio, D.; Perego, P.; De Cesare, M.; Carenini, N.; Zaffaroni, N.; De Matteo, M.; Manzoni, L. *Org. Biomol. Chem.* **2015**, *13*, 7530; c) Crisp, J. L.; Savariar, E. N.; Glasgow, H. L.; Ellies, L. G.; Whitney, M. A.; Tsien, R. Y. *Mol. Cancer Ther.* **2014**, *13*, 1514; d) Lee, M. H.; Kim, J. Y.; Han, J. H.; Bhuniya, S.; Sessler, J. L.; Kang, C.; Kim, J. S. *J. Am. Chem. Soc.* **2012**, *134*, 12668.

26 Selected examples: a) Cheng, K.; Kothapalli, S. -R.; Liu, H.; Koh, A. L.; Jokerst, J. V.; Jiang, H.; Yang, M.; Li, J.; Levi, J.; Wu, J. C.; Gambhir, S. S.; Cheng, Z. *J. Am. Chem. Soc.* **2014**, *136*, 3560; b) Lanzardo, S.; Conti, L.; Brioschi, C.; Bartolomeo, M. P.; Arosio, D.; Belvisi, L.; Manzoni, L.; Maiocchi, A.; Maisano, F.; Forni G. *Contrast Media Mol. Imaging* **2011**, *6*, 449; c) Shi, J.; Wang, L.; Kim, Y. -S.; Zhai, S.; Liu, Z.; Chen, X.; Liu, S. *J. Med. Chem.* **2008**, *51*, 7980.

27 a) Marchini, M.; Mingozzi, M.; Colombo, R.; Guzzetti, I.; Belvisi, L.; Vasile, F.; Potenza, D.; Piarulli, U.; Arosio, D.; Gennari, C. *Chem. Eur. J.* **2012**, *18*, 6195; b) Marchini, M.; Mingozzi, M.; Colombo, R.; Gennari, C.; Durini, M.; Piarulli, U. *Tetrahedron* **2010**, *66*, 9528; c) Ressurreição, A. S. M.; Vidu, A.; Civera, M.; Belvisi, L.; Potenza, D.; Manzoni, L.; Ongeri, S.; Gennari, C.; Piarulli, U. *Chem. Eur. J.* **2009**, *15*, 12184.

28 Fanelli, R.; Schembri, L.; Piarulli, U.; Pinoli, M.; Rasini, E.; Paolillo, M.; Galiazzo, M. C.; Cosentino, M.; Marino, F. *Vascular Cell* **2014**, *6*, 11.

29 *Cyclo*[DKP3-RGD] **17** significantly decreased the network formation promoted by pro-angiogenic growth factors, such as VEGF, EGF, FGF, and IGF-I, or by pro-inflammatory inrteleukin-8 (IL-8).

30 a) Corti, A.; Curnis, F. *J. Cell Sci.* **2011**, *124*, 515; b) Curnis, F.; Longhi, R.; Crippa, L.; Cattaneo, A.; Dondossola, E.; Bachi, A.; Corti, A. *J. Biol. Chem.* **2006**, *281*, 36466.

31 Spitaleri, A.; Mari, S.; Curnis, F.; Traversari, C.; Longhi, R.; Bordignon, C.; Corti, A.; Rizzardi, G. P.; Musco, G. *J. Biol. Chem.* **2008**, *283*, 19757.

32 Frank, A. O.; Otto, E.; Mas-Moruno, C.; Schiller, H. B.; Marinelli, L.; Cosconati, S.; Bochen, A.; Vossmeyer, D.; Zahn, G.; Stragies, R.; Novellino, E.; Kessler, H. *Angew. Chem. Int. Ed.* **2010**, *49*, 9278.

33 Ghitti, M.; Spitaleri, A.; Valentinis, B.; Mari, S.; Asperti, C.; Traversari, C.; Rizzardi, G. P.; Musco, G. *Angew. Chem. Int. Ed.* **2012**, *51*, 7702.

34 Mingozzi, M.; Dal Corso, A.; Marchini, M.; Guzzetti, I.; Civera, M.; Piarulli, U.; Arosio, D.; Belvisi, L.; Potenza, D.; Pignataro, L.; Gennari, C. *Chem. Eur. J.* **2013**, *19*, 3563.

35 Selected examples of integrin-targeted imaging agents: a) Yu, C.; Pan, D.; Mi, B.; Xu, Y.; Lang, L.; Niu, G.; Yang, M.; Wan, W.; Chen, X. *Eur. J. Nucl. Med. Mol. Imaging* **2015**, 42, 2021 b) Mozida, A. M.; Holstenssonb, M.; Choudhurya, T.; Ben-Haimb, S.; Allieb, R.; Martinc, J.; Sinusasd, A. J.; Huttonb, B. F.; Mathura, A. *Nucl. Med. Commun.* **2014**, *35*, 839; c) Zhou, Y.; Chakraborty, S.; Liu, S. *Theranostics* **2011**, *1*, 58.

36 Caswell, P.; Norman, J. *Trends Cell Biol.* **2008**, *18*, 257.

37 Caswell, P. T.; Vadrevu, S.; Norman, J. C. *Nat. Rev. Mol. Cell Biol.* **2009**, *10*, 843.

38 a) Pilkington-Miksa, M.; Arosio, D.; Battistini, L.; Belvisi, L.; De Matteo, M.; Vasile, F.; Burreddu, P.; Carta, P.; Rassu, G.; Perego, P.; Carenini, N.; Zunino, F.; De Cesare, M.; Castiglioni, V.; Scanziani, E.; Scolastico,

C.; Casiraghi, G.; Zanardi, F.; Manzoni, L. *Bioconjugate Chem.* **2012**, *23*, 1610; b) Chen, X.; Plasencia, C.; Hou, Y.; Neamati, N. *J. Med. Chem.* **2005**, *48*, 1098; Additions and Corrections **2005**, *48*, 5874.

39 Ryppa, C.; Mann-Steinberg, H.; Fichtner, I.; Weber, H.; Satchi-Fainaro, R.; Biniossek, M. L.; Kratz, F. *Bioconjugate Chem.* **2008**, *19*, 1414.

40 Colombo, R.; Mingozzi, M.; Belvisi, L.; Arosio, D.; Piarulli, U.; Carenini, N.; Perego, P.; Zaffaroni, N.; De Cesare, M.; Castiglioni, V.; Scanziani, E.; Gennari, C. *J. Med. Chem.* **2012**, *55*, 10460.

41 Dal Corso, A.; Pignataro, L.; Belvisi, L.; Gennari, C. *Curr. Top. Med. Chem.* **2016**, *16*, 314.

42 Krall, N.; Scheuermann, J.; Neri, D. *Angew. Chem. Int. Ed.* **2013**, *52*, 1384.

43 a) de Groot, F. M. H.; van Berkom, L. W. A.; Scheeren, H. W. *J. Med. Chem.* **2000**, *43*, 3093; b) de Groot, F. M. H.; Loos, W. J.; Koekkoek, R.; van Berkom, L. W. A.; Busscher, G. F.; Seelen, A. E.; Albrecht, C.; de Bruijn, P.; Scheeren, H. W. *J. Org. Chem.* **2001**, *66*, 8815.

44 Pfaff, M.; Tangemann, K.; Muller, B.; Gurrath, M.; Miiller, G.; Kessler, H.; Timpl, R.; Engel, J. *J. Biol. Chem.* **1994**, *269*, 20233.

45 Selected examples of RAD sequence exploited as negative control in drug targeting and imaging: a) Morlieras, J.; Dufort, S.; Sancey, L.; Truillet, C.; Mignot, A.; Rossetti, F.; Dentamaro, M.; Laurent, S; Vander Elst, L.; Muller, R. N.; Antoine, R.; Dugourd, P.; Roux, S.; Perriat, P.; Lux, F.; Coll, J.-L.; Tillement, O. *Bioconjugate Chem.* **2013**, *24*, 1584; b) Guo, Y.; Yuan, H.; Rice, W. L.; Kumar, A. T. N.; Goergen, C. J.; Jokivarsi, K.; Josephson, L. *J. Am. Chem. Soc.* **2012**, *134*, 19338; c) Eldar-Boock, A.; Miller, K.; Sanchis, J.; Lupu, R.; Vicent, M. J.; Satchi-Fainaro, R. *Biomaterials* **2011**, *32*, 3862; d) Polyak, D.; Ryppa, C.; Eldar-Boock, A.; Ofek, P.; Many, A.; Licha, K.; Kratz, F.; Satchi-Fainaro, R. *Polym. Adv. Technol.* **2011**, *22* 103; e) Kessinger, C. W.; Khemtong, C.; Togao, O.; Takahashi, M.; Sumer, B. D., Gao, J. *Exp Biol Med* **2010**, *235*, 957; f) Ryppa, C.; Mann-Steinberg, H.; Biniossek, M. L.; Satchi-Fainaro, R.; Kratz, F. *Int J Pharm* **2009**, *368*, 89.

46 Panzeri, S.; Zanella, S.; Arosio, D.; Vahdati, L.; Dal Corso, A.; Pignataro, L.; Paolillo, M.; Schinelli, S.; Belvisi, L.; Gennari, C.; Piarulli, U. *Chem. Eur. J.* **2015**, *21*, 6265.

47 a) Sulzmaier, F. J.; Jean, C.; Schlaepfer, D. D. *Nat. Rev. Cancer* **2014**, *14*, 598; b) Frame, M. C.; Patel, H.; Serrels, B.; Lietha, D.; Eck, and M. J. *Nat. Rev. Mol. Cell Biol* **2010**, *11*, 802.

48 Meyer, Y.; Richard, J. -A.; Delest, B.; Noack, P.; Renard, P. -Y.; Romieu, A. *Org. Biomol. Chem.* **2010**, *8*, 1777.

49 Kirchner, M., Schneider, S. *Angew. Chem. Int. Ed.* **2015**, *54*, 13508.

50 Choi, K. Y.; Swierczewska, M.; Lee, S.; Chen, X. *Theranostics* **2012**, *2*, 156.

51 Olsson, A. K.; Dimberg, A.; Kreuger, J.; Claesson-Welsh, L. *Nat. Rev. Mol. Cell Biol.* **2006**, *7*, 359.

52 Takahashi, H.; Shibuya, M. *Clin. Sci.* **2005**, *109*, 241.

53 a) Hoeben, A.; Landuyt, B.; Highley, M. S.; WIldiers, H.; van Oosterom, A.; De Bruijin, E. *Pharmacol. Rev.* **2004**, *56*, 549; b) Muller, Y. A.; Li, B.; Christinger, H. W.; Wells, J. A.; Cunningham, B. C.; de Vos, A. M. *PNAS* **1997**, *94*, 7192.

54 Christinger, H. W.; Fuh, G.; de Vos, A. M.; Wiesmann, C. *J. Biol. Chem.* **2004**, *279*, 10382.

55 Fuh, G.; Li, B.; Crowley, C.; Cunningham, B.; Wells, J. A. *J. Biol. Chem.* **1998**, *273*, 11197.

56 Hughes, D. C. *J. Mol. Evol.* **2001**, *53*, 77.

57 Shibuya, M. J. *Biochem.* **2013**, *153*, 13.

58 Musumeci, F.; Radi, M.; Brullo, C.; Schenone, S. *J. Med. Chem.* **2012**, *55*, 10797.

59 Schenone, S.; Brullo, C.; Botta, M. *Curr. Med. Chem.* **2008**, *15*, 3113.

60 Roskoski, R. Jr. *Biochem. Biophys. Res. Commun.* **2007**, *356*, 323.

61 Woo, H. Y.; Heo, J. *Exp. Opin. Pharmacother.* **2012**, *13*, 1059.

62 Udugamasooriya, D. G.; Dineen, S. P.; Brekken, R. A.; Kodadek, T. *J. Am. Chem. Soc.* **2008**, *130*, 5744.

63 García-Aranda, M. I.; González-López, S.; Santiveri, C. M.; Gagey-Eilstein, N.; Reille-Seroussi, M.; Martín-Martínez, M.; Inguimbert, N.; Vidal, M.; García-López, M. T.; Jiménez, M. A.; González-Muñiza, R.; Pérez de Vega, M. *J. Org. Biomol. Chem.* **2013**, *11*, 1896.

64 Zilberberg, L.; Shinkaruk, S.; Lequin, O.; Rousseau, B.; Hagedorn, M.; Costa, F.; Caronzolo, D.; Balke, M.; Canron, X.; Convert, O.; Laïn, G.; Gionnet, K.; Gonçalvès, M.; Bayle, M.; Bello, L.; Chassaing, G.; Deleris, G.; Bikfalvi, A. *J. Biol. Chem.* **2003**, *278*, 35564.

65 Haase, H. S.; Peterson-Kaufman, K. J.; Lan Levengood, S. K.; Checco, J. W.; Murphy, W. L.; Gellman S. H. *J. Am. Chem. Soc.* **2012**, *134*, 7652.

66 a) Diana, D.; Di Stasi, R.; De Rosa, L.; Isernia, C.; D'Andrea, L.; Fattorusso, R. *J. Pept. Sci.* **2013**, *19*, 214; b) Basile, A.; Del Gatto, A.; Diana, D.; Di Stasi, R.; Falco, A.; Festa, M.; Rosati, A.; Barbieri, A.; Franco, R.; Arra, C.; Pedone, C.; Fattorusso, R.; Turco, M. C.; D'Andrea, L. D. *J. Med. Chem.* **2011**, *54*, 1391.

67 D'Andrea, L. D.; Iaccarino, G.; Fattorusso, R.; Sorriento, D.; Carannante, C.; Capasso, D.; Trimarco, B.; Pedone, C. *PNAS* **2005**, *102*, 14215.

68 a) Desgrosellier, J. S.; Cheresh, D. A. *Nature Reviews Cancer* **2010**, *10*, 9; b) Somanath, P. R.; Malinin, N. L.; Byzova T. V. *Angiogenesis* **2009**, *12*, 177.

69 Borges, E.; Jan, Y.; Ruoslahti, E. *J. Biol. Chem.* **2000,** *275*, 39867.

70 a) West, X. Z.; Meller, N.; Malinin, N. L.; Deshmukh, L.; Meller, J.; Mahabeleshwar, G. H.; Weber, M. E.; Kerr, B. A.; Vinogradova, O.; Byzova, T. V. *PLOS One* **2012,** *7*, e31071; b) Mahabeleshwar, G. H.; Chen, J.; Feng, W.; Somanath, P. R.; Razorenova, O. V.; Byzova, T. V. *Cell Cycle* **2008**, *7*, 335; c) Mahabeleshwar, G. H.; Feng, W.; Reddy, K.; Plow, E. F.; Byzova, T. V. *Circ Res.* **2007**, *101*, 570; d) Mahabeleshwar, G. H.; Feng, W.; Phillips, D. R.; Byzova, T. V. *J. Exp. Med.* **2006**, *203*, 2495; e) De, S.; Chen, J.; Narizhneva, N. V.; Heston, W.; Brainard, J.; Sage, E. H.; Byzova, T. V. *J. Biol. Chem.* **2003**, *278*, 39044.

71 Papo, N.; Silverman, A. P.; Lahti, J. L.; Cochran, J. R. *PNAS* **2011**, *108*, 14067.

72 Zanella, S.; Mingozzi, M.; Dal Corso, A.; Fanelli, R.; Arosio, D.; Cosentino, M.; Schembri, L.; Marino, F.; De Zotti, M.; Formaggio, F.; Pignataro, L.; Belvisi, L.; Piarulli, U.; Gennari, C. *ChemistryOpen* ***2015***, *4*, 633.

73 Acetylation of Lys13 side chain did not substantially affect the conformational and biological properties of compound **110** compared to the parent peptide **108**. See ref. 72.

74 Brozzo, M. S.; Bjelic, S.; Kisko, K.; Schleier, T.; Leppänen, V.; Alitalo, K.; Winkler, F. K.; Ballmer-Hofer, K. *BLOOD* **2012**, *119*, 1781.

75 Leppänen, V.; Tvorogov, D.; Kisko, K.; Prota, A. E.; Jeltsch, M.; Anisimov, A.; Markovic-Muller, S.; Stuttfeld, E.; Goldie, K. N.; Ballmer-Hofer, K.; Alitalo, K. *PNAS* **2013**, *110*, 12960.

76 Leppänen, V. M.; Prota, A. E.; Jeltsch, M.; Anisimov, A.; Kalkkinen, N.; Strandin, T.; Lankinen, H.; Goldman, A.; Ballmer-Hofer, K.; Alitalo, K. *PNAS* **2010**, *107*, 2425.

77 Still, W. C.; Kahn, M.; Mitra, A. *J. Org. Chem.* **1978**, *43*, 2923.

78 Griesinger, C.; Otting, G.; Wîthrich, K.; Ernst, R. R. *J. Am. Chem. Soc.* **1988**, *110*, 7870.